1.

Imperial College Science and Technology

University of London

Friction and Heat Transfer in a

Compressible Turbulent Boundary Layer on a Smooth Flat Plate

BY

Shih Wei Chi, B.Sc.(Eng.) Lond., G.I.Mech.E.

A thesis submitted for the

Degree of Doctor of Philosophy of the University of London.

1965.

ACKNOWLEDGEMENTS

ABSTRACT

This thesis is intended to recommend a simple and reliable method for the prediction of frictional drag and heat transfer in a turbulent boundary layer of air on a smooth flat plate. Particular emphasis has been placed upon the correlation of local and overall frictional drag and heat-transfer data at various values of Reynolds number, Mach number and wall-to-mainstream temperature ratio.

The frictional drag theories given by earlier authors are classified, reviewed and where necessary extended; then the predictions of twenty of these theories are evaluated and compared with all available experimental data, the root-mean-square error being computed for each theory. The theory of van Driest-II gives the lowest root-mean-square error (11.0%).

A new calculation procedure is developed from the postulate that a unique relation exists between $c_f F_c$ and $Re F_R$, where c_f is the drag coefficient and Re is the Reynolds number and F_c and F_R are functions of Mach number and temperature ratio alone. The experimental data are found to be too scanty for both F_c and F_R to be deduced empirically, so F_c is calculated by means of mixing-length theory and F_R is found semi-empirically. Tables and charts of values of F_c and F_R are presented for a wide range of Mach number and temperature ratio. When compared with all experimental data, the predictions of the new procedure give a root-mean-square error of 9.9%; and when compared with the theory of van Driest-II, the present method improves the correlation at

large heat-transfer rates and is easier to use.

The frictional drag coefficient derived is then used as a basis for the prediction of the heat-transfer coefficient (St). The experimental St data giving the Reynolds-analogy factor (S) are too scanty to reveal the small influence of Reynolds number, Mach number and heat transfer on the value of S. A constant value of S which represents the empirical mean of all published experimental data is recommended.

Finally, to give confidence in the use of the constant value of Reynolds-analogy factor beyond the range of heat-transfer conditions for which the experimental data are available in the other literature, heat-transfer rates at T_{ad}, S/T_S up to 2.7 were measured by the transient technique. The present data confirm that the use of the constant value of S is adequate for the evaluation of the heat-transfer coefficient so long as the drag coefficient is calculated by the present procedure.

NOMENCLATURE

1. Introduction

M_G	Mach number of mainstream
Re_x	Reynolds number based upon x and mainstream fluid properties
$T_{ad,S}$	Adiabatic wall temperature, ($^{\circ}$R)
T_G	Mainstream temperature, ($^{\circ}$R)
T_S	Wall temperature, ($^{\circ}$R)
x	Distance measured along mainstream direction from effective start of turbulent boundary layer

2. Frictional Drag

a,b	See Eqs. (2.55) and (2.56)
c_f	Local frictional drag coefficient based upon mainstream fluid properties, Eqs. (2.20) and (2.59)
$\bar{c}_f$	Overall frictional drag coefficient based upon mainstream fluid properties, Eq. (2.68)
C	A constant, Eq. (2.11)
E	A constant, Eq. (2.2)
F_c	Function multiplying c_f in universal drag law, Eqs. (2.53) and (2.61)
$F_{\bar{c}}$	Function multiplying $\bar{c}_f$ in universal drag law, Eq. (2.53)
$F_{R\delta}$	Function multiplying $Re_{\delta 2}$ in universal drag law, Eqs. (2.54) and (2.62)
F_{Rx}	Function multiplying Re_x in universal drag law, Eqs. (2.54) and (2.67)
h	Specific enthalpy, Eq. (2.79), (Btu/lb)
h°	Stagnation enthalpy, Eq. (2.79), (Btu/lb)

K	A constant (≈ 0.4), Eq. (2.2)
M_G	Mach number of mainstream, Eqs. (2.52) and (2.55)
n	Exponent, Eq. (2.14)
p,q	Exponents, Eqs. (2.93) and (2.94)
Pr	Prandtl number, Eq. (2.83)
r	Recovery factor, Eq. (2.82)
Re	Reynolds number in general
$Re_{\delta 2}$	Reynolds number based upon momentum thickness and mainstream fluid properties, Eq. (2.3)
Re_x	Reynolds number based upon x and mainstream fluid properties, Eq. (2.63)
T	Temperature, Eqs. (2.22) and (2.55), (°R)
u	Velocity in x-direction, Eq. (2.1), (ft/h)
u^+	Non-dimensional value of u, Eq. (2.2)
v	Velocity in y-direction, Eq. (2.26), (ft/h)
x	Distance measured along mainstream direction from effective start of turbulent boundary layer, implied in the definition of Re_x, (ft)
y	Distance from wall, Eq. (2.1), (ft)
y^+	Non-dimensional value of y, Eq. (2.2)
z	A different non-dimensional value of u, Eq. (2.3)
β	Exponent, Eq. (2.87)
σ, ϵ, η	Functions of x, Eqs. (2.29), (2.30) and (2.32)
δ	Boundary layer thickness, Eq. (2.14), (ft)
δ_2	Momentum thickness, Eq. (2.3), (ft)
γ	Specific heat ratio, Eq. (2.55)

ϕ	Function appearing in Eqs. (2.2), (2.5) etc.
$\psi, \bar{\psi}$ }	Functions appearing in the generalised
ψ_x	drag law, Eqs. (2.60), (2.66) and (2.69)
ψ	Stream function, Eq. (2.31), (lb /ft h)
ν	Kinematic viscosity, (2.15), (ft^2/h)
ρ	Density, Eq. (2.1) (lb/ft^3).
μ	Viscosity, Eq. (2.3), (lb/ft h)
τ	Shear stress in boundary layer, Eq. (2.1), (lb/ft h^2)

Subscripts and superscripts.

ad	Adiabatic condition, Eq. (2.22)
av	Average conditions in laminar sublayer, Table 2.1
G	Mainstream fluid state, Eq. (2.3)
i	Uniform property flow, Eq. (2.87)
ℓ	State in laminar sublayer, Eq. (2.11)
S	State at the wall, Eq. (2.3)
t	State in turbulent region, Eq. (2.11)
tot	Referring to total, Eq. (2.24)
1	Outer edge of laminar sublayer, Eq. (2.11)
$\ast$	Transformed quantity, Eq. (2.27)
—	Average value, Fig. 2.10

3. Heat Transfer.

a	A constant, Table 3.1
c_f	Local frictional drag coefficient based upon mainstream fluid properties, Eq. (3.1)
$\bar{c}_f$	Overall frictional drag coefficient based upon mainstream fluid properties, appearing in text

c_p Specific heat at constant pressure, Eq. (3.3), (Btu/lb°F)

E A constant, Table 3.1

$\left.\begin{array}{l} F_c \\ F_{R\delta} \\ F_{Rx} \end{array}\right\}$ Functions multiplying c_f, $Re_{\delta 2}$, and Re_x in universal drag law, appearing in text

K A constant (≈ 0.4), Table 3.1

M_G Mach number of mainstream, Eq. (3.8)

Pr Molecular Prandtl number, Eq. (3.4)

Pr_t Turbulent Prandlt number, Eq. (3.4)

Pr_{tot} Total Prandtl number, Eq. (3.2)

Re Reynolds number in general, Eq. (3.8)

$Re_{\delta 2}$ Reynolds number based upon momentum thickness and mainstream fluid properties, appearing in text

Re_x Reynolds number based upon x and mainstream fluid properties, appearing in text

S Reynolds-analogy factor, Eq. (3.1)

St Stanton number based upon mainstream fluid properties, Eq.(3.1)

$\overline{St}$ Overall Stanton number based upon mainstream fluid properties, appearing in text.

T Temperature, Eq. (3.8), (°R)

u Velocity in x-direction, Eq. (3.4), (ft/h)

u^+ Non-dimension value of u, Eq. (3.4)

y Distance from wall, Eq. (3.4), (ft)

y^+ Non-dimensional value of y, Eq. (3.4)

ρ Density, Eq. (3.1), (lb/ft^3)

ε_u Eddy thermal conductivity, Eq. (3.3), (Btu/ft h °R)

ε_h Eddy viscosity, Eq. (3.3), (lb/ft h)

η A different non-dimensional value of y, Table 3.1

k Molecular thermal conductivity, Eq. (3.3), (Btu/ft h °F)

μ Viscosity, Eq. (3.3), (lb/ft h)

τ Shear stress in boundary layer, Eq. (3.1), (lb/ft h^2)

Subscripts.

ad   Adiabatic condition, Eq. (3.8)

exp   Reference to experiment, Eq. (3.6)

G   Mainstream fluid state, Eq. (3.7)

R   Reference state, Table 3.1

S   State at the wall, Eq. (3.2)

t   Turbulent condition, Eq. (3.4)

th   Reference to theory, Eq. (s.6)

tot   Referring to total, Eq. (3.2)

1   Outer edge of laminar sublayer, Table 3.1

2   Outer edge of intermediate layer, Table 3.1

4. Experiments.

B   A constant, Eq. (4.11); or dimensionless driving force, Eq. (4C.5)

c_f Local frictional drag coefficient based upon mainstream fluid properties, Eq. (4.1)

c_p Specific heat at constant pressure, Eq. (4.9), (Btu/lb °F)

C   Velocity coefficient, Eq. (4.2)

$(c\rho\tau)_S$ Product of specific heat, density and thickness of the test plate, Eq. (4.8), (see text)

d   Diameter of sphere, Eq. (4D.3), (ft)

E   e.m.f. of thermocouple, (mv); or a constant Eq. (4.12)

$\left.\begin{array}{l} F_c \\ F_{R\delta} \\ F_{Rx} \end{array}\right\}$ Multiplying functions as defined in §§2 and 3

g Surface conductance for mass transfer, Eq. (4C.5), $(lb/ft^2 h)$

m'' Mass per unit area, Eq. (4D.1), (lb/ft^2)

$\dot{m}''$ Mass transfer rate per unit area, Eq. (4C.5), $(lb/ft^2 h)$

M_G Mainstream Mach number, appearing in text

P Static pressure, Eq. (4.2), (mm of H_2O, or mm of Hg as is clear in the text)

ΔP Difference between the total and the static pressure, Eq. (4.4), (mm of H_2O, unless otherwise stated)

q Heat-transfer rate per unit area, Eq. (4C.1), $(Btu/ft^2 h)$

Re_1 Reynolds number per in of x based upon the mainstream fluid properties, Eq. (4.7), (in^{-1})

S Reynolds-analogy factor, Eq. (4.1)

St Stanton number, Eq. (4.1)

t Time, Eq. (4.9) (h or s)

T Temperature, Eq. (4.3), ($^{\circ}R$, unless otherwise stated)

u Mainstream velocity at x, (ft/s or ft/h)

u_G Average velocity of mainstream velocity, Eq. (4.2), (ft/s or ft/h as it is clear in text)

x Distance measured along mainstream direction from leading edge of test plate, (in or ft)

σ Stefan Boltzman constant, Eq. (4C.1), $(Btu/ft^2 h \ ^{\circ}R^4)$

ε Thermal emissivity, Eq. (4C.1)

ρ Density, Eq. (4.6), (lb/ft^3)

μ Viscosity, Eq. (4.6), (lb/ft h or lb/ft s)

| τ | Test-plate thickness, Eq. (4.9),(units as stated in the text) |

τ Test-plate thickness, Eq. (4.9),(units as stated

in the text)

Subscripts

ad   Adiabatic condition, Eq. (4.4)

c   Reference to STP, Eq. (4.2)

r   Reference to radiation, Eq. (4C.1)

S   State at the wall, Eq. (4.9)

STP   Standard temperature and pressure, ($520°R$ and 760 mm.Hg)

G   State in the mainstream, Eq. (4.9)

0,X,I
II,III   Reference to the positions indicated in Fig.4.9
IV

tot   Reference to total, Eq. (4.10)

5. Conclusions

c_f Local frictional drag coefficients based upon

mainstream fluid properties, Eq. (5.2)

$\bar{c}_f$ Overall frictional drag coefficient based upon

mainstream fluid properties, Eq. (5.3)

F_c Function multiplying c_f in universal drag law, Eq.(5.1)

$F_{R\delta}$ Function multiplying $Re_{\delta 2}$ in universal drag law, Eq.(5.1)

F_{Rx} Function multiplying Re_x in universal drag law, Eq. (5.1)

M_G Mach number of mainstream

Re   Reynolds number in general

Re_x Reynolds number based upon length measured along

mainstream direction from effective start of turbulent

boundary layer and mainstream fluid properties

$Re_{\delta 2}$ — Reynolds number based upon momentum thickness and mainstream fluid properties

S — Reynolds-analogy factor, Eq. (5.2)

St — Stanton number based mainstream fluid properties

$\overline{St}$ — Overall Stanton number based mainstream fluid properties

$T_{ad,S}$ — Adiabatic wall temperature, (°R)

T_G — Temperature of mainstream, (°R)

T_S — Wall temperature, (°R)

6. Suggestions for Further Work

F_c, F_R — Multiplying function for universal drag law

E — A constant in Law of Wall

H_{12} — Shape parameter, Eq. (6.1)

$T_{ad,S}$ — Adiabatic wall temperature

T_S — Wall temperature

δ_1 — Displacement thickness, Eq. (6.1), (ft)

δ_2 — Momentum thickness, Eq. (6.1), (ft)

13.

CONTENTS

LIST OF FIGURES

| <u>Fig No.</u> | <u>Title</u> | <u>Page No.</u> |

Fig. No.	Title	Page No.

24.

LIST OF TABLES.

LIST OF APPENDICES

CHAPTER I

INTRODUCTION

1.1. Problem Investigated.

The designer of high-speed vehicles, combustion chambers, turbine blades, hypersonic ram-jet intakes, rocket-motor nozzles etc. wants to know the values of friction-drag and heat transfer at various Reynolds numbers, Mach numbers, wall temperatures and mainstream temperatures; so the problem of the predictions of frictional drag and heat transfer at a surface along which gas is flowing at high speed and through which heat is being transferred at high rate interests aeronautical and mechanical engineers in many circumstances.

Often the mainstream pressure is not uniform; and sometimes the mainstream fluid is not air; and the surface may be film or transpiration cooled. Despite these facts, it is necessary to restrict attention of the present research to the case in which the pressure gradient is zero, the mainstream fluid is air and no coolant is forced towards the mainstream; that is, to that of the boundary layer of air on a solid flat plate. The reasons are that this is the case for which a large number of experimental data are available and that this is the simplest case which must be understood first. For the same reasons, the effect of roughness and the effect of wall temperature variations are also excluded from the present investigation. Thus, the problem investigated is the frictional drag and convective heat transfer in a compressible turbulent boundary layer of air on a smooth solid flat plate at uniform temperature.

1.2. Outline of Present State of Knowledge.

There have been numerous investigations of the problem both theoretical and experimental; these will be described in some details in the following Chapters ($\S\S$ 2 and 3). Nevertheless, as will appear below, present knowledge of the subject is defective in several respects. First, there is considerable uncertainty as to which of the various theories gives the best predictions; for each theory contains fairly drastic simplifications and has usually been compared with only a small section of experimental data. Secondly, some of the methods of prediction (including unfortunately those which give the most accurate predictions) are difficult to use; the prospective user of the method has to carry out extensive numerical work, because the necessary auxiliary functions have not been computed and tabulated once for all. Thirdly, the experimental heat-transfer measurements at large temperature ratios, (say, at $T_{ad,S}/T_S$ greater than 1.6) are scarce and conflicting; consequently the confidence in checking the validity of the theoretical predictions at the conditions of large $T_{ad,S}/T_S$ is insufficiently adequate.

1.3. Purpose and Scope of Present Research.

This research was intended to remedy the above defects. Its main purposes were: (i) to eliminate the uncertainty of the theory, (ii) to simplify the calculation procedure, and (iii) to extend the range of conditions for which experimental data are available.

As far as possible, uncertainty was eliminated by comparing the existing theories with all published experimental data and developing a new calculation procedure based upon accumulated theoretical and experimental knowledge of the compressible

turbulent boundary layer; tables and graphs are presented which permit frictional drag and heat transfer to be calculated as a result of merely a few minutes' work; and measurements of heat-transfer at conditions of slow-speed flow and various temperature ratios ($T_{ad,S}/T_S$ from about one to three) were made to provide heat-transfer data over a range of heat-transfer conditions wider than so far available in the literature.

Tables and graphs of auxiliary functions, presented below, cover the range of Reynolds number (Re_x) between 1×10^4 and 1×10^9, Mach number (M_G) between 0 and 15, and temperature ratio (T_S/T_G) between 0.05 and 30. The validity of these functions has been confirmed by the published and the present experiments over the range of conditions of Re_x from 1×10^5 to 1×10^8, M_G up to 10 and $T_{ad,S}/T_S$ between 0.5 and 5 for frictional drag and between 0.5 and 3 for heat transfer.

Chapters 2 and 3 are mainly devoted to review of the earlier work and the development of the present calculation procedures. The present experiments and the data therefrom are reported in Chapter 4. In Chapter 5, conclusions and the recommended procedures are summarised. Suggestions for further work are proposed in Chapter 6.

CHAPTER 2

FRICTIONAL DRAG

2.1. Introduction.

A considerable amount of analytical work on turbulent boundary layers has been carried out (2.1-2.26). However, all the theoretical analyses are based upon arbitrary and simplified models or sets of assumptions. The results of the various analyses disagree markedly because of the different assumptions made by the various authors (2.27). The confidence in the theoretical predictions of the frictional drag in a compressible turbulent boundary layer can therefore only be gained, after the theories have been checked by experimental data over a wide range of conditions.

Several earlier authors, for example, Rubesin et al (2.8), Monaghan (2.16), Sommer and Short (2.20), Winkler (2.25), Peterson (2.26) etc., have compared some theories with the experiments; but they used a qualitative method of comparison in the form of numerous figures, so their conclusions are still rather indecisive. The present author has first reviewed the previous theories with an emphasis on the principal assumptions used by the various authors and then evaluated a quantitative measure of the agreement of each theory with all the published experimental frictional-drag-coefficient data available to the author (§§2.2 and 2.3).

The review of the previous theoretical and experimental work described in §§2.2 and 2.3 below leads to an argument for the development of a new calculation procedure semi-empirically (§2.4). This procedure is easy to use and is entirely satisfactory in

correlating all experimental data available in the literature as will be seen below.

In §2.5, results of this chapter are summarised and discussed and the recommended prediction procedure is stated. §2.6 contains conclusions for this chapter.

2.2. Survey of the Previous Theoretical Work.

2.2.1. General characteristics of analyses.

According to the nature of the principal assumptions used by the various authors, many of the theories [2.1-2.26], which are concerned with the derivation of the "drag law", can be grouped into five types, namely:- (i) theories based upon the Prandtl differential equation, (ii) theories based upon the von Karman differential equation, (iii) theories based upon other differential equations, (iv) theories based upon a fixed velocity profile, and (v) theories based upon incompressible formulae with fluid properties inserted at a 'reference' state.

The main features of the analyses for each of those groups will be summarised in the following five sections (§§2.2.2.-2.2.6), and the characteristics of individual theories belonging to those groups will be indicated in Tables 2.1-2.5. §2.2.7 includes descriptions of some miscellaneous analyses [2.22-2.26] which do not belong to any of the five groups mentioned above.

2.2.2. Theories based upon the Prandtl differential equation.

By "the Prandtl differential equation" is meant that postulated by Prandtl [2.29, p.477] relating the shear stress in the turbulent part of the boundary layer to the velocity gradient and

other properties, namely[*],

$$\gamma = \rho K^2 y^2 (du/dy)^2 \quad \dots \quad (2.1).$$

With the assumption $\gamma = \gamma_S$, the velocity distribution in the turbulent boundary layer is derived,

$$y^+ = E^{-1} \exp(K \int_0^{u^+} \phi \, du^+) \quad \dots \quad (2.2).$$

where $y^+ \equiv y(\rho_S \gamma_S)^{\frac{1}{2}}/\mu_S$, $u^+ \equiv u/(\gamma_S/\rho_S)^{\frac{1}{2}}$, $\phi \equiv (\rho/\rho_S)^{\frac{1}{2}}$, $K = a$ mixing length constant, $E =$ an integrating constant, and subscript G refers to the mainstream, i.e., the outer 'edge' of the boundary layer, subscript S refers to the fluid conditions immediately adjacent to the wall, i.e., to the inner 'edge' of the boundary layer.

Eq. (2.2) leads to the integral for $Re_{\delta 2}$:

$$Re_{\delta 2} = (\mu_S/\mu_G)(K/E)(u_G^+)^2 \int_0^1 \phi^3 z(1-z) \exp(K u_G^+ \int_0^z \phi \, dz) dz \quad \dots \quad (2.3.)$$

where $Re_{\delta 2} \equiv (\rho_G u_G \delta_2)/\mu_G$, $\delta_2 \equiv \int_0^\delta (\rho/\rho_G) z(1-z) dy$, $z \equiv u/u_G$.

The above features are common to all analyses of this group. The differences between them are in either: (i) an hypothesis for E (or the method of determining the integration constant), (ii) the nature of the ϕ function, or (iii) the method of evaluating the $Re_{\delta 2}$ integral. Accordingly, the individual members [2.1-2.5] of the group are distinguished by the nature of these items in Table 2.1.

---

[*] All symbols are defined on pp. 5-12.

2.2.3. Theories based upon the von Karman differential equation.

The differential equation postulated by von Karman [2.29, p.485] as the connexion between τ, du/dy and other quantities is

$$\tau = \rho K^2 (du/dy)^4 / (d^2 u/dy^2)^2 \quad \ldots \quad (2.4)$$

The assumption, $\tau = \tau_S$, leads to the velocity distribution

$$y^+ = (K/E) \int_0^{u^+} \exp(K \int_0^{u^+} \phi \, du^+) \, du^+ \quad \ldots \quad (2.5)$$

This leads further to the $Re_{\delta 2}$ integral,

$$Re_{\delta 2} = (\mu_S/\mu_G)(K/E)(v_G^+)^2 \int_0^1 \phi^2 z(1-z) \exp(Ku_G \int_0^z \phi \, dz) \, dz \quad \ldots$$

$$(2.6)$$

Eqs. (2.4)-(2.6) are common to all the methods of this group; individual methods [2.6 - 2.10] are classified in Table 2.2 by reference to either (i) their hypotheses for E, (ii) the nature of the ϕ function, or (iii) the method of evaluating the $Re_{\delta 2}$ integral.

2.2.4. Theories based upon other differential equations.

Analyses of this group start from various differential equations but the assumption of $\tau = \tau_S$ is also made as in the above two groups (§§2.2.2 and 2.2.3). Generally speaking, all proposed differential equations lead to equations for the velocity distribution which are identical in form with Eq. (2.2) or (2.5). However, the nature of ϕ in this expression differs from that in §§2.2.2 and 2.2.3, that is, ϕ here is no longer equal to $(\tau/\tau_S)^{\frac{1}{2}}$. The Reynolds number integral for the analyses of this group is either

$$Re_{\delta 2} = (\mu_S/\mu_G)(K/E)(u_G^+)^2 \int_0^1 \phi(\tau/\tau_S) z(1-z) \exp(Ku_G \int_0^z \phi \, dz) \, dz$$

$$\ldots \quad (2.7)$$

or

$$Re_{\delta 2} = (\mu_S/\mu_G)(K/E)(u_G^+)^2 \int_0^1 (\rho/\rho_S)z(1-z)\exp(Ku_G\int_0^z \phi\,dz)\,dz$$

$$\ldots \qquad (2.8)$$

depending on whether the velocity distribution of Eq. (2.2) or that of Eq. (2.5) is appropriate. Methods [2.11-2.14] of this group are distinguished in Table 2.3 by reference to either (i) the nature of the differential equation, or (ii) the method of evaluating the $Re_{\delta 2}$ integral.

2.2.5. Theories based upon a fixed velocity profile.

In this group it is assumed that the velocity profile is independent of compressibility, for example,

$$y^+ = E^{-1}\exp(Ku^+) \qquad \ldots \qquad (2.9)$$

for which the $Re_{\delta 2}$ integral becomes

$$Re_{\delta 2} = (\mu_S/\mu_G)(K/E)(u_G^+)^2 \int_0^1 (\rho/\rho_S)z(1-z)\exp(Ku_G^+ z)\,dz \ldots \quad (2.10)$$

Methods [2.15-2.16] of this group are distinguished in Table 2.4 by reference to (i) the assumed fixed velocity profile, (ii) the expression for ρ/ρ_S, and (iii) the method of evaluating the $Re_{\delta 2}$ integral.

2.2.6. Theories based upon incompressible formulae with
    reference properties.

Methods [2.17-2.21] of this group imply the existence of a universal relationship between frictional-drag coefficient and Reynolds number, if properties are evaluated at a reference temperature (or reference enthalpy). They are distinguished in Table 2.5 by reference to the expression for T_R/T_G or h_R/h_G.

2.2.7. Miscellaneous other methods.

Some methods [2.22-2.26] which do not belong to those groups discussed in §§2.2.2-2.2.6 include the use of various transformations, the use of empirical data etc. They are individually described below.

(i) <u>C. duP Donaldson [2.22]</u> This author assumed that at the edge of a laminar sub-layer the ratio of the total shear stress to the laminar shear stress was constant (C), ie.

$$C = 1 + (\tau_{t,1}/\tau_{\ell,1}) \quad \cdots \qquad (2.11)$$

and expressed $\tau_{\ell,1}$ and $\tau_{t,1}$ in the following forms:

$$\tau_{\ell,1} = \mu_1 (du/dy)_1 \quad \cdots \qquad (2.12)$$

and
$$\tau_{t,1} = \rho_1 K^2 y_1^2 (du/dy)_1^2 \quad \cdots \qquad (2.13)$$

where $(du/dy)_1$ was obtained from the power-law of velocity,

$$u/u_G = (y/\delta)^{1/n} \quad \cdots \qquad (2.14)$$

With the aid of Eqs. (2.12)-(2.14), Eq. (2.11) can be written as:

$$C = 1 + \frac{u_G K^2 y_1^{(n+1)/n}}{n \mu_1 \delta^{1/n}} \quad \cdots \qquad (2.15)$$

The thickness of the laminar sub-layer (y_1) and the velocity at the outer edge of the laminar sub-layer (u_1) derived from Eqs. (2.14) and (2.15) are:

$$\frac{y_1}{\delta} = \left[\frac{n(C-1)}{K^2} \frac{\mu_1}{u_G \delta} \right]^{n/(n+1)} \quad \cdots \qquad (2.16)$$

where u_1/u_G is from Eq. (2.16) with the values of K,n,C etc.
as previously stated, that is,

$$\frac{u_1}{u_G} = 0.5\left(\frac{T_1}{T_G}\right)^{0.22}(Re_\delta)^{-\frac{1}{8}} \qquad \ldots \qquad (2.23)$$

(ii) <u>Winkler [2.23]</u>. This author used the experimental
data of c_f vs $Re_{\delta 2}$ from Refs. 2.8, 2.23, 2.34, 2.37, 2.43 and 2.48
and obtained an empirical formula:

$$c_f = 0.0246(T_{tot}/T_G)^{\frac{1}{2}}(T_{ad,S}/T_S)^{\frac{1}{4}}Re_{\delta 2}^{-0.251} \qquad \ldots \qquad (2.24)$$

(iii) <u>Spence [2.24] , Burggraf [2.25] and Coles [2.26]</u>.
These authors started from the 2-dimensional uniform-pressure
continuity and momentum equations of mean motion for a compressible
fluid of variable density (x,y) in the form [2.30, pp.82-87],

$$\frac{\partial \rho u}{\partial x} + \frac{\partial \rho v}{\partial y} = 0 \qquad \ldots \qquad (2.25)$$

$$\rho u \frac{\partial u}{\partial x} + \rho v \frac{\partial u}{\partial y} = \frac{\partial \tau}{\partial y} \qquad \ldots \qquad (2.26)$$

and used various transformations to reduce Eqs. (2.25) and
(2.26) to the form[†] :

$$\frac{\partial u_*}{\partial x_*} + \frac{\partial v_*}{\partial y_*} = 0 \qquad \ldots \qquad (2.27)$$

$$\rho_* u_* \frac{\partial u_*}{\partial x_*} + \rho_* v_* \frac{\partial u_*}{\partial y_*} = \frac{\partial \tau_*}{\partial y_*} \qquad \ldots \qquad (2.28)$$

where the parameter ρ_* has the dimension of density and is
independent of position in the x_* and y_* co-ordinates. In this
form the momentum equation is uncoupled from the energy equation.
Thus in the transformed co-ordinates (x_*, y_*) the u_*, v_* and τ_*
relations are independent of the compressibility of air.

[†] Starred quantities below stand for the transformed quantities.

In the above transformation, the definition of x_* and y_* used by the various authors [2.24-2.26] can be written in a general form:

$$x_* \equiv \int_0^x \epsilon(x)\,dx \qquad \ldots \qquad (2.29)$$

$$y_* \equiv \int_0^y \frac{\rho}{\rho_*} \eta(y)\,dy \qquad \ldots \qquad (2.30)$$

and the definition of the stream function introduced by them to satisfy the continuity Eqs. (2.25) - (2.28) can be written as:

$$\rho u \equiv \frac{\partial \psi}{\partial y} \quad ; \qquad \rho v \equiv -\frac{\partial \psi}{\partial x} \qquad \ldots \qquad (2.31)$$

$$\rho_* u_* \equiv \frac{\partial \sigma(x)\psi}{\partial y_*} \quad ; \qquad \rho_* v_* \equiv -\frac{\partial \sigma(x)\psi}{\partial x_*} \quad \ldots \quad (2.32)$$

On the application of Eqs. (2.29) - (2.32), it can be shown [2.26] that the transformed quantity τ_* of Eq. (2.28) has to be defined by

$$\frac{\partial \tau_*}{\partial y_*} \equiv \frac{\rho_* \sigma^2}{\epsilon \eta^2} \left[\frac{1}{\rho} \left(\frac{\partial \tau}{\partial y} - \frac{\psi}{\sigma} \frac{\partial u}{\partial y} \frac{d\sigma}{dx} \right) \right] \ldots \qquad (2.33)$$

and it follows from Eqs. (2.30) and (2.32) that

$$u_* = \frac{\sigma}{\eta} u \qquad \ldots \qquad (2.34)$$

So far the transformation of the momentum and energy equations has been discussed in a general way without reference to boundary layers and there is no need to define τ, τ_*, ϵ, η and σ explicitly. In order to derive frictional-drag coefficient in a compressible turbulent boundary layer, these quantities have been defined or assumed in various ways by the different authors.

(a) Spence [2.24] and Burggraf [2.25]. These authors assumed that ϵ, η and σ were unity. This assumption reduces the shear-stress equation (Eq. 2.33) to

$$\frac{\partial \tau_{\divideontimes}}{\partial y_{\divideontimes}} = \frac{\rho_{\divideontimes}}{\rho} \frac{\partial \tau}{\partial y} \qquad \ldots \qquad (2.35)$$

i.e. $\quad \tau_{\divideontimes} = \tau \qquad \ldots \qquad (2.36)$

It follows that the assumption of ϵ, η and σ being unity together with $\tau_{\divideontimes}$ being defined by Eq. (2.33) is equivalent to the assumption that τ is invariant under transformation.

Now the local frictional-drag coefficients, c_f and $c_{f\divideontimes}$, are defined by

$$c_f \equiv 2 \tau_s / (\rho_G u_G^2) \qquad \ldots \qquad (2.37)$$

and $\quad c_{f\divideontimes} \equiv 2 \tau_{s\divideontimes} / (\rho_{\divideontimes} u_G^2) \qquad \ldots \qquad (2.38)$

Eqs. (2.34) and (2.36) require c_f and $c_{f\divideontimes}$ related by

$$c_{f\divideontimes} = \frac{\rho_G}{\rho_{\divideontimes}} c_f \qquad \ldots \qquad (2.39)$$

Upon introducing the definition of Reynolds number

$$Re_x \equiv \frac{\rho_G u_G x}{\mu_G} \qquad \ldots \qquad (2.40)$$

and the corresponding Reynolds number

$$Re_{x\divideontimes} \equiv \frac{\rho_{\divideontimes} u_{G\divideontimes} x_{\divideontimes}}{\mu_{\divideontimes}}$$

$$= \frac{\rho_{\divideontimes} \mu_G}{\rho_G \mu_{\divideontimes}} Re_x \qquad \ldots \qquad (2.41)$$

where the viscosity $\mu_{\divideontimes}$ is a certain artificial parameter.

Eq. (2.28) implies the existence of a unique relation between $c_{f\divideontimes}$ and $Re_{x\divideontimes}$, and Eq. (2.35) or (2.36) implies that for the uniform-property flow the transformed momentum equation is identical to the original momentum equation; so $c_{f\divideontimes}$ vs $Re_{x\divideontimes}$ relation is identical to the uniform-property c_f vs Re_x relation. Furthermore, Eqs. (2.39) and (2.41) require $c_f(\rho_G/\rho_{\divideontimes})$ vs Re_x $(\rho_{\divideontimes}\mu_G/\rho_G\mu_{\divideontimes})$ relation being the same as $c_{f\divideontimes}$ vs $Re_{x\divideontimes}$ relation.

It follows that $c_f(\rho_G/\rho_*)$ vs $Re_x(\rho_*\mu_G/\rho_G\mu_*)$ is the same as the uniform-property c_f vs Re_x relation.

Finally, Spence [2.24] recommended the evaluation of ρ_* and μ_* at the Eckert's reference temperature, so Spence method is similar to the Eckert's "reference-temperature method" [2.21] , although different uniform-property c_f vs Re_x relations were recommended by those two authors. Burggraf [2.25] recommended the values of ρ_* and μ_* to be evaluated at the outer edge of the laminar sub-layer, so his method is essentially similar to the method based upon the incompressible formula with properties evaluated at a reference state.

(b) <u>Coles [2.26]</u> Coles did not assume ϵ, η, σ being unity, so the shear-stress Eqs. (2.35) and (2.36) do not hold in this case. It is assumed in Ref. 2.26 that at $y = 0$

$$y_* = 0 \qquad \cdots \qquad (2.42)$$

$$\tau_S = \mu_S \,(\partial u/\partial y)_S \qquad \cdots \qquad (2.43)$$

$$\tau_{S*} = \mu_{S*} \,(\partial u_*/\partial y_*)_S \qquad \cdots \qquad (2.44)$$

The transformation Eqs. (2.30) for y_* and (2.34) for u_* then require τ_S and τ_{S*} to be related by

$$\tau_{S*} = \frac{\rho_*\mu_*}{\rho_S\mu_S}\frac{\sigma}{\eta^2}\,\tau_S \qquad \cdots \qquad (2.45)$$

i.e. $$c_f = \frac{\sigma\mu_S}{\mu_*}\frac{\rho_S}{\rho_G}\,c_{f*} \qquad \cdots \qquad (2.46)$$

Upon introducing the conventional momentum thickness

$$\delta_2 = \int_0^\infty \frac{\rho u}{\rho_G u_G}\,(1-\frac{u}{u_G})\,dy \qquad \cdots \qquad (2.47)$$

and the corresponding thickness δ_{2*}, it appears that

$$\delta_{2*} \equiv \int_0^\infty \frac{u_*}{u_{G*}} \left(1 - \frac{u_*}{u_{G*}}\right) dy_*$$

$$= \frac{\rho_G}{\rho_*} \delta_2 \qquad \cdots \qquad (2.48)$$

Consequently, Reynolds numbers are related by the equation,

$$Re_{\delta_{2*}} = \frac{\mu_*}{\mu_G \sigma} Re_{\delta_2} \qquad \cdots \qquad (2.49)$$

When σ is eliminated between Eqs. (2.45) and (2.49), it is seen that

$$c_{f*} Re_{\delta_{2*}} = \frac{\rho_G \mu_G}{\rho_S \mu_S} c_f Re_{\delta_2} \qquad \cdots \qquad (2.50)$$

Hence it follows from Eqs. (2.28), (2.46) and (2.50) that

$\dfrac{\mu_*}{\sigma \mu_S} \dfrac{\rho_G}{\rho_S} c_f$ vs $\dfrac{\rho_G \mu_G}{\rho_S \mu_S} c_f Re_{\delta_2}$ relation is the same as the uniform-

property c_f vs $c_f Re_{\delta_2}$ relation. The recommended method for

the evaluation of $\dfrac{\mu_*}{\sigma \mu_S}$ is by the equation

$$\frac{\mu_*}{\sigma \mu_S} = \frac{\mu(T_1)}{\mu(T_S)} \qquad \cdots \qquad (2.51)$$

where T_1 is the laminar sub-layer temperature and T_S is the wall

temperature. The empirically determined sub-layer temperature

(T_1) for the adiabatic-wall case recommended by Coles [2.26] is:

$$\frac{T_1}{T_S} = 1 + 17.2 \left[\frac{1 + \frac{\gamma-1}{2} M_G^2}{(T_S/T_G)} - 1 \right] \sqrt{\frac{c_{f*}}{2}} -$$

$$- 305 \left[\frac{\frac{\gamma-1}{2} M_G^2}{(T_S/T_G)} \right] \frac{c_{f*}}{2} \qquad \cdots \qquad (2.52)$$

where the value of $c_{f*} \left(\equiv \dfrac{\mu_*}{\sigma \mu_S} \dfrac{\rho_G}{\rho_S} c_f \right)$ is evaluated from the

c_{f*} vs $c_{f*}Re_{\delta 2*}$ relation (which is equivalent to uniform-property c_f vs $c_f Re_{\delta 2}$ relation) at the value of $c_{f*} Re_{\delta 2*}$ $\left(\equiv \dfrac{\rho_G \mu_G}{\rho_S \mu_S} c_f Re_{\delta 2} \right)$ in question.

2.2.8. Résumé.

It has been seen in the above review of various theories that all the analyses are based upon different assumptions and simplifications. The validity of the assumptions and simplifications involved in these theories can only be verified by comparison with experiments. This will be done systematically in the next section.

2.3. Comparison between the Theoretically and Experimentally Obtained Data.

2.3.1. Purpose of comparison.

As pointed out above, all theoretical treatments discussed in §2.2 have been based upon assumptions and simplifications. Further, their predictions differ significantly, as has been shown, for example, by Chapman and Kester [2.27] . It is therefore necessary to establish the relative validity of all theories by comparing them with experimental data. Below, the various theories will be compared with all published experimental data of c_f and $\bar{c}_f$ versus $Re_{\delta 2}$ and Re_x at various M_G and T_S/T_G, and for each theory, a quantitative measure of its agreement with experiment will be evaluated.

2.3.2. Experimental data.

If experimental data were accurate, a few sets of data at desired conditions (Mach number and heat-transfer rates) would suffice to test the validity of various theories. Such data are

however, not available [3.31]. For this reason, the greatest

possible number of experimental data have been collected

[2.7, 2.8, 2,20, 2.23, and 2.31-2.48] and are tabulated in

Appendix (2A). They include measurements on a flat plate and on a

cylinder with axis parallel to the stream direction and radius

large in comparison with the boundary-layer thickness. Figs.

2.1-2.3 show the collected data in the form of c_f vs $Re_{\delta 2}$,

c_f vs Re_x, and $\bar{c}_f$ vs Re_x, and Fig. 2.4 shows the conditions (i.e.

values of M_G and T_S/T_G) which have been explored experimentally.

Although it must be expected that the data are not all equally

reliable, no attempt has been made to estimate their accuracy or

to introduce any weighting factors. The reasons are: (i) the

published details of experiments are often insufficient for them

to be made, and (ii) some arbitrary variables, for example, the

variable effects of transition, have not been possible to be

accounted for with accuracy.

2.3.3. Theoretical data.

Theoretical frictional-coefficient data corresponding to

the experimental Reynolds number ($Re_{\delta 2}$ or Re_x), Mach number (M_G)

and temperature ratio (T_S/T_G) have been obtained by the various

methods discussed in §2.2; however, some authors have not dealt

with all the parameters which are required in order to compare their

results with all the collected experimental data. Extensions can,

however, be made to those theories without contradicting the authors'

original argument. The methods used here in making the extensions

are summarised below.

Conversion of Re_x to $Re_{\delta 2}$ and vice versa. The results
of some analyses, viz. Refs. 2.1, 2.2, 2.9, 2.25 and 2.17-2.21,
imply that a unique relation exists between $c_f F_c$ and $Re F_R$
where F_c and F_R are functions of Mach number and temperature
ratio alone. As will be shown in §2.4, the relations between
F_c, $F_{\bar{c}}$, $F_{R\delta}$ and F_{Rx} are such that

$$F_{\bar{c}} = F_c \qquad \dots \qquad (2.53)$$

$$F_{Rx} = F_{R\delta}/F_c \qquad \dots \qquad (2.54)$$

where F_c and $F_{\bar{c}}$ are the functions of M_G and T_S/T_G multiplying
c_f and $\bar{c}_f$ respectively, and $F_{R\delta}$ and F_{Rx} are the functions of
M_G and T_S/T_G multiplying $Re_{\delta 2}$ and Re_x respectively. Hence Eqs.
(2.53) and (2.54) enable the determination of the c_f versus Re_x
relation of one of those theories from the corresponding $\bar{c}_f$ versus
Re_x or c_f versus $Re_{\delta 2}$ relations, and vice versa.

Extension of theories derived for the adiabatic wall to the
case of heat transfer. When only the adiabatic-wall case is
considered and the Reynolds analogy between momentum and energy
is assumed, as in Refs. 2.7, 2.15, 2.18, etc., the temperature-
distribution equation is

$$T/T_S = 1 - a^2 z^2 \qquad \dots \qquad (2.55),$$

where

$$a^2 \equiv \tfrac{1}{2}(\gamma-1)M_G^2 / \left[1+\tfrac{1}{2}(\gamma-1)M_G^2\right], z \equiv u/u_G, T = \text{absolute temperature}$$

($^\circ$R), and suffixes G and S refer to main-stream and surface,
respectively.

Eq. (2.55) is extended to include the effect of heat transfer
as follows:

$$T/T_S = 1 + bz - a^2 z^2 \qquad \dots \qquad (2.56)$$

where $b = \left\{ \left[1 + \frac{1}{2}(\gamma - 1)M_G^2/(T_S/T_G)\right] \right\} - 1$ and $a^2 = \frac{1}{2}(\gamma - 1)M_G^2/(T_S/T_G)$.

Viscosity law . The viscosity law recommended by the

original authors has been used in most cases for applying their

theory to experimental conditions. When this is not possible,

or no law is recommended, the following power law has been used.

$$\mu \propto T^{0.76} \qquad \cdots \qquad (2.57)$$

Although Sutherland's viscosity law, given by

$$\frac{\mu}{\mu_G} = \frac{T(T_G + 198°R)}{T_G(T + 198°R)} \qquad \cdots \qquad (2.58),$$

is more accurate than the power law, the absolute value of T_G was

not reported by most experimenters. Figs. 2.5 shows the viscosity-

temperature relations used in the various theories. Since μ

has only a weak influence on c_f, it is unlikely that the use

of different viscosity laws for different theories has any

appreciable effect on the final conclusions.

Drag law for incompressible flow. Each of the authors

whose works have been studied incorporates in his theory, implicitly

or explicitly a relationship between frictional-drag coefficient

and Reynolds number (either $Re_{\delta 2}$ or Re_x) valid for incompressible

flow. In each case, the relationship recommended by the author

in question has been used without attempting to calculate

separately its effect on the accuracy of the theory.

2.3.4. Comparison between theories and experiments.

Twenty out of twenty-eight collected theories (2.1-2.26)

are compared below; they are believed to include all the essential

assumptions used by various authors. Eight theories (2.3, 2.4,

2.8, 2.10, 2.12, 2.13, 2.14 and 2.26) are not included, either

because they still have indeterminate constants or because they invclve lengthy time-consuming numerical work which is believed not to be profitable at the present state of knowledge of turbulence.

The criterion used for comparison is the root-mean-square of

$$(c_{f,exp} - c_{f,th})/c_f^{\text{x}},th$$

where $c_{f,exp}$ is the experimental local or overall friction coefficient and $c_{f,th}$ is the theoretical local or overall friction coefficient, at the corresponding experimental Reynolds number ($Re_{\delta 2}$ or Re_x), Mach number (M_G), and temperature ratio (T_S/T_G). In evaluating the above root-mean-square value for each of 20 theories, all the experimental data of Appendix (2A), plotted in Figs. 2.1-2.3, have been used.

The evaluation of the root-mean-square values of $(c_{f,exp} - c_{f,th})/c_{f,th}$ was carried out by the Mercury digital computer of London University. A computer program was written for each of the twenty theories. Then each theory was applied to each of 388 experimental conditions for which $c_{f,exp}$ data were available, yielding appropriate values of $c_{f,th}$. The root-mean-square value of $(c_{f,exp} - c_{f,th})/c_{f,th}$ was then computed for each theory in an obvious manner.

The results of the comparison are shown in Fig. 2.6 and Table 2.6. They give a quantitative indication of the accuracy

---

$^{\text{x}}$ For the sake of simplicity, here and on some other occasions, c_f stands for both c_f and $\bar{c}_f$, as is clear in the text.

of the various theories when compared with the present empirical

knowledge of the compressible turbulent boundary layer.

It is seen from Fig.2.6 and Table 2.6 that the three best

theories are those of van Driest-II [2.9] , Wilson [2.7] extended

to include heat transfer, and Kutateladze and Leont'ev [2.5] . They

are all based upon the mixing-length used in the method of §2.2.2

or 2.2.3, that is, Table 2.1 or 2.2. Table 2.6 also reveals that

all theories exhibit a greater error when compared with the data

for finite heat-transfer rates than when compared with data

obtained under adiabatic conditions.

2.4. Development of an Improved Calculation Procedure.

2.4.1. Fundamental Functions.

c_f vs $Re_{\delta 2}$ For the constant-pressure boundary layer,

it may be expected that

$$c_f = c_f(Re_{\delta 2}, M_G, T_S/T_G) \qquad \cdots \qquad (2.59)$$

The nature of the function can be determined either

theoretically (§2.2) or experimentally.

Now many of the theoretical expressions, Refs. 2.1, 2.2,

2.9, 2.17-2.22 etc. can be written in the form:

$$\tfrac{1}{2}c_f F_c = \psi (Re_{\delta 2} F_{R\delta}) \qquad \cdots \qquad (2.60)$$

where the function ψ is independent of Mach number and temperature

ratio, the effects of which are wholly accounted for by the

functions F_c and $F_{R\delta}$. The latter functions are such that

$$F_c = F_c(M_G, T_S/T_G),$$
$$= 1, \text{ for } M_G = 0, T_S/T_G = 1 \qquad \cdots \qquad (2.61).$$
$$F_{R\delta} = F_{R\delta}(M_G, T_S/T_G),$$
$$= 1, \text{ for } M_G = 0, T_S/T_G = 1 \qquad \cdots \qquad (2.62)$$

Some of the other theoretical expressions, for example, those of Refs. 2.5 and 2.25, if expressed in the form of Eq. (2.60), would imply that $F_{R\delta}$ exhibits a weak dependence on c_f; however, this is by no means certain, as is shown by the comparison between theories and experiments (Table 2.6 and Fig. 2.6) and we shall ignore this dependence.

$\underline{c_f}$ vs $\underline{Re}_x$. The integral momentum equation for the boundary layer on a flat plate [2.28, p.292] leads to

$$\tfrac{1}{2}c_f = dRe_{\delta 2}/dRe_x \qquad \ldots \qquad (2.63)$$

Rewriting Eq. (2.63) in integral form, we obtain

$$Re_x = \int_0^{Re_{\delta 2}} \left(\frac{2}{c_f}\right) dRe_{\delta 2} \qquad \ldots \qquad (2.64).$$

By multiplication of Eq. (2.64) by $F_{R\delta}/F_c$, there is obtained

$$\left(\frac{F_{R\delta}}{F_c}\right)Re_x = \int_0^{F_{R\delta}Re_{\delta 2}} \frac{2}{(c_f F_c)} \, d(F_{R\delta}Re_{\delta 2}) \ldots \quad (2.65)$$

The existence of a unique relation between $c_f F_c$ and $Re_{\delta 2}F_{R\delta}$ in Eq. (2.62), which is independent of Mach number and temperature ratio, has already been postulated. With this, Eq. (2.65) yields

$$\tfrac{1}{2}c_f F_c = \psi_x(Re_x F_{Rx}) \qquad \ldots \qquad (2.66)$$

where the function ψ_x is independent of Mach number and temperature ratio, F_c and $R_{R\delta}$ are the same functions as those of Eqs. (2.61) and (2.62), and F_{Rx} is related to $F_{R\delta}$ and F_c by

$$F_{Rx} = F_{R\delta}/F_c$$

$$= 1, \text{ for } M_G = 0, T_S/T_G = 1 \quad \ldots \qquad (2.67)$$

$\underline{\bar{c}_f}$ vs $\underline{Re}_x$. From the definition of $\bar{c}_f$,

$$\tfrac{1}{2}\bar{c}_f = Re_x^{-1} \int_0^{Re_x} (c_f/2) dRe_x \quad \ldots \quad (2.68)$$

it can be shown by the method of the preceding paragraph that

$$\tfrac{1}{2}\bar{c}_f F_c = \bar{\psi}(Re_x F_{Rx}) \quad \ldots \quad (2.69)$$

where the function $\bar{\psi}$ is again independent of Mach number and temperature ratio, and F_c and F_{Rx} are defined by Eqs. (2.61) and (2.67).

To summarize, it has been shown that, if $F_{R\delta}$ is independent of $\tfrac{1}{2}c_f$, the following functions exist:

$$\tfrac{1}{2}c_f F_c = \psi(F_{R\delta} Re_{\delta 2}) \quad \ldots \quad (2.60)$$

$$\tfrac{1}{2}c_f F_c = \psi_x(F_{Rx} Re_x) \quad \ldots \quad (2.66)$$

$$\tfrac{1}{2}\bar{c}_f F_c = \bar{\psi}(F_{Rx} Re_x) \quad \ldots \quad (2.69),$$

where ψ, ψ_x and $\bar{\psi}$ are independent of Mach number and temperature ratio. The problem has now been reduced to the determination of ψ-functions and F_c and $F_{R\delta}$ as functions of Mach number and temperature ratio.

2.4.2. Determination of ψ-functions.

Several formulae and numerous experimental data are offered in the literature for the relations between frictional coefficient and Reynolds number in uniform-property flow. The experimental data of c_f vs $Re_{\delta 2}$, c_f vs Re_x and $\bar{c}_f$ vs Re_x for the uniform-property flow from Refs. 2.34, 2.43 and 2.49-2.61 are plotted in Figs. 2.7-2.9 respectively. Also plotted in Fig. 2.7 are the well-known theoretical curves due to Blasius and Karman-Schoenherr [2.29, p.439]. The agreement between the Karman-Schoenherr formula and the experiments is seen to be good over a wide range of Reynolds number, but at low Reynolds number the formula over-estimates c_f by a few per cent. It is known that in the

derivation of this formula, the velocity distribution in the "sub-layer" was neglected for simplicity.

At present, a single "law of wall" for the whole region of a uniform-property turbulent boundary layer is available [2.62], that is,

$$y^+ = u^+ + \frac{K}{E}\left\{e^{Ku^+} - 1 - Ku^+ - \frac{(Ku^+)^2}{2!} - \frac{(Ku^+)^3}{3!} - \frac{(Ku^+)^4}{4!}\right\}, \ldots \quad (2.70)$$

In Ref. 2.63, the drag functions was analytically derived from Eq. (2.70). These functions are:

$$Re_{\delta 2} = (u_G^+)^2/6 + (1/KE)\left[(1-2Ku_G^+)\exp(Ku_G^+) + 2/Ku_G^+ + 1 - (Ku_G^+)^2/6 - (Ku_G^+)^3/12 - (Ku_G^+)^4/40 - (Ku_G^+)^5/180\right]\ldots \quad (2.71)$$

$$Re_x = (u_G^+)^4/12 + (1/K^3E)\left\{[6-4Ku_G^+ + (Ku_G^+)^2] - 6 - 2Ku_G^+ - (Ku_G^+)^4/12 - (Ku_G^+)^5/20 - (Ku_G^+)^6/60 - (Ku_G^+)^7/252\right\}\ldots(2.72)$$

$$\tfrac{1}{2}\bar{c}_f = Re_{\delta 2}/Re_x \qquad \ldots \qquad (2.73)$$

where $u_G^+ \equiv (2/c_f)^{\frac{1}{2}}$, K and E are constants to be determined to fit the experiments. The present author has used the data of Figs. 2.7 and 2.8 to determine the respective values of K and E in the following manner.

At various values of K, the average values of E and the standard deviations$(\overline{(\bar{E^2} - \bar{E}^2)/\bar{E}^2})^*$ were calculated by using Eqs. (2.71) and (2.72) and the experimental data of Figs. 2.7 and 2.8 [2.43, 2.49-2.61]. It was found that the minimum standard deviation of E occurred at K = 0.4 (see Fig.2.10). At this value of K (=0.4), the average value of E is 12 as can be seen in Fig.2.10.

---

* The bar stands for the average.

To estimate the accuracy of Eqs. (2.71) and (2.72) with
K = 0.4 and E = 12 for the prediction of the uniform-property-
flow-c_f values, we note in Fig.2.10 that at K = 0.4 the standard
deviation of E is less than 4%. Then by Eqs. (2.71) and (2.72),

$$\text{Re} \propto 1/E \quad \text{(approximately at large } u_G^+\text{)} \quad \ldots \quad (2.74)$$

and according to the 1/7th power law of velocity,

$$c_f \propto 1/\text{Re}_{\delta 2}^{\frac{1}{4}} \quad \text{or} \quad 1/\text{Re}_x^{1/5} \quad \ldots \quad (2.75)$$

so $\quad c_f \propto E^{\frac{1}{4}} \quad \text{or} \quad E^{1/5} \quad \text{(approximately)} \quad \ldots \quad (2.76)$

That is, a 4% deviation of E corresponds to about 1% deviation
of c_f. Hence, with K = 0.4 and E = 12, the root-mean-square
error on c_f basis would be less than 1%.

In Figs. (2.7) - (2.9) the theoretical curves of Eqs. (2.71)
to (2.73) with K = 0.4 and E = 12 are plotted. It can be seen
in these figures that the agreement between the theory and
experiments is good throughout the whole range of the Reynolds
number; so the ψ-functions for the present method have been
established, i.e., Eqs. (2.71-2.73) with K = 0.4 and E = 12.

2.4.3.   Determination of F_c-functions.

Since the functions ψ, ψ_x and $\overline{\psi}$ are known Eqs. (2.71), (2.72)
and (2.73), and since numerous data for compressible turbulent
boundary layer (Appendix 2A) have been collected, it might seem
to be possible to deduce the F_c and $F_{R\delta}$ functions solely from
experiments. An attempt to do this, however, soon showed that the
data were too scanty and inaccurate to allow success. Some
theoretical guidance is therefore sought for the determination of
one of the functions.

In §2.3, it was shown that theories based upon the mixing-length hypothesis of Tables 2.1 and 2.2 gave the best prediction of all the previous theories; it was also discovered that the corresponding method led to the following expression for F_c:

$$F_c = \left[\int_0^1 (\rho/\rho_G)^{\frac{1}{2}} dz \right]^{-2} \qquad \ldots \qquad (2.78)$$

The expression for F_{R6}, by contrast, varies considerably from one theory to the next. Eq. (2.78) has been adopted for the F_c function in the present theory.

Evaluation of F_c from Eq. (2.78) requires the density to be expressed as a function of z, where z is defined as u/u_G. This relationship may be derived from the Reynolds analogy between energy and momentum transfer, modified for non-unity Prandtl number in the following manner.

From the Reynolds analogy, we have

$$\frac{h^o-h_S^o}{h_G^o-h_S^o} = \frac{u - u_S}{u_G-u_S} \qquad \ldots \qquad (2.79)$$

where h^o is the stagnation enthalpy, u is the velocity in the x-direction, and subscripts G and S refer to the mainstream and the fluid adjacent to the wall, respectively.

Now $u_S = 0$, $h^o = c \left[T+\frac{1}{2}(\gamma-1)M_G^2 T_G z^2 \right]$ for a perfect gas, $h_S^o = h_S = cT_S$, where c is the specific heat at constant pressure, and T is the temperature in degrees absolute. Eq. (2.79) can then be written as

$$T/T_G = (T_S/T_G)+\left[1 + \frac{1}{2}(\gamma-1)M_G^2-(T_S/T_G) \right] z-\frac{1}{2}(\gamma-1)M_G^2 z^2 \ldots (2.80)$$

For the adiabatic-wall case, the coefficient of z of Eq. (2.80) is zero, and T_S is equal to the adiabatic-wall temperature, $T_{ad,S}$. Hence

$$T_{ad,S}/T_G = 1 + \tfrac{1}{2}(\delta-1)M_G^2 \qquad \cdots \qquad (2.81)$$

This holds for a Prandtl number of unity. For non-unity Prandtl number,

$$T_{ad,S}/T_G = 1+\tfrac{1}{2}r(\delta-1)M_G^2 \qquad \cdots \qquad (2.82)$$

where r is the recovery factor. For gases of $Pr \approx 0.7$, measurements of recovery factor by various investigators [2.64-2.69] showed that the value of recovery factor lies between 0.88 and 0.9; 0.89 is a fair mean of all measurements. Now Eq. (2.80) can be modified to satisfy the boundary condition at the wall for the adiabatic-wall case, by writing

$$T/T_G = (T_S/T_G)+ [1+\tfrac{1}{2}r(\delta-1)M_G^2-(T_S/T_G)] \; z-\tfrac{1}{2}r(\delta-1)M_G^2 z^2 \; \cdots \; (2.83)$$

where $r = 0.89$ for $Pr = 0.7$. For an ideal gas at constant pressure,

$$\rho/\rho_G = (T/T_G)^{-1} \qquad \cdots \qquad (2.84)$$

On substitution of Eq. (2.83) into Eq. (2.84), there is obtained

$$\rho/\rho_G = \left\{ (T_S/T_G)+[1+\tfrac{1}{2}r(\delta-1)M_G^2-(T_S/T_G)] \; z-\tfrac{1}{2}r(\delta-1)M_G^2 z^2 \right\}^{-1}$$
$$\cdots \qquad (2.85)$$

Hence from Eqs. (2.78) and (2.85), we have

$$F_c = \left\{ \int_0^1 \frac{dz}{\left\{ (T_S/T_G)+[1+\tfrac{1}{2}r(\delta-1)M_G^2-(T_S/T_G)] \; z-\tfrac{1}{2}r(\delta-1)M_G^2 z^2 \right\}^{\frac{1}{2}}} \right\}^{-2}$$
$$\cdots \qquad (2.86),$$

where $r = 0.89$. Eq. (2.86) is the F_c function which has been used.

2.4.4. Determination of $F_{R\delta}$ function.

Though the theoretically derived expressions for $F_{R\delta}$ are uncertain, they can generally be written as

$$F_{R\delta} = (\mu_G/\mu_S)(\rho_S/\rho_G)^\beta (E/E_i) \qquad \cdots \qquad (2.87)$$

where E_i is the value of E for uniform-property flow and is a constant. For example,

(a) In the van Driest-I method, $\beta = \frac{1}{2}$, $E = E_i$, hence,

$$F_{R\delta} = (\mu_G/\mu_S)(\rho_S/\rho_G)^{\frac{1}{2}}$$
$$= (T_G/T_S)^{1.26} \text{ for } \mu_G/\mu_S = (T_G/T_S)^{0.76} \quad \ldots \quad (2.88)$$

(b) In the van Driest-II method, $\beta = 0$, $E = E_i$, hence

$$F_{R\delta} = (\mu_G/\mu_S)$$
$$= (T_G/T_S)^{0.76} \text{ for } \mu_G/\mu_S = (T_G/T_S)^{0.76} \quad \ldots \quad (2.89)$$

(c) In other methods, e.g. those of Kalikman [2.3] and Wilson [2.7]

$$E = f(M_G, T_S/T_G) \qquad \ldots \quad (2.90)$$

Such theories commonly derive E from the assumed values of u_1^+ and y_1^+ by the equation

$$E = \exp(K\int_0^{u_i^+} \phi \, du^+)/y_1^+ \qquad \ldots \quad (2.91)$$

or $\quad E = \exp(Ku_1^+)/y_1^+ \qquad \ldots \quad (2.92)$

A widely used assumption for y_1^+ and u_1^+ is that $y_1^+=u_1^+=11.6$ at all M_G and T_S/T_G [2.1, 2.2, 2.7, 2.8 etc.]. An examination of the measured velocity profiles, which have been collected by Hügel [2.70], however, reveals that although for the adiabatic-wall case y_1^+ and u_1^+ are approximately equal to 11.6 yet for the case of the presence of heat transfer the values of u_1^+ and y_1^+ are directly related to $T_{ad,S}/T_S$. In Table 2.7, the approximate values of y_1^+ and u_1^+ from the collected experimental velocity profiles [2.70] are shown. The corresponding values of E evaluated by Eq. (2.92) with the experimental y_1^+ and u_1^+ are plotted in Figs. 2.11 and 2.12 against M_G and $T_{ad,S}/T_S$ respectively.

The nature of the experimental E derived in the above paragraph can be seen in these figures (Figs. 2.11 and 2.12); for the adiabatic-wall case the dependence of E upon M_G is small, whilst for the case of the presence of heat transfer the value of E is related to $T_{ad,S}/T_S$ by the equation

$$E/E_i = (T_{ad,S}/T_S)^q \qquad \ldots \qquad (2.93)$$

where q is a constant and its approximate magnitude has been found to be unity from the data of velocity profiles as shown in Figure 2.12. A more accurate value of q will be determined below from the numerous drag-coefficient data.

After combination of Eqs. (2.87)-(2.93), we can write

$$F_{R\delta} = (T_S/T_G)^p (T_{ad,S}/T_S)^q \qquad \ldots \qquad (2.94)$$

where p and q are still indeterminate and are to be determined from experiments as in the following paragraphs.

For the adiabatic-wall case, the ratio of the adiabatic-wall to wall temperature is unity and so Eq. (2.94) reduces to

$$F_{R\delta} = (T_S/T_G)^p \qquad \ldots \qquad (2.95)$$

Using the functions ψ, ψ_x, and $\bar{\psi}$ and F_c of Eqs. (2.71-2.73) and (2.86) respectively, and all the collected experimental data for the adiabatic-wall case (summarised in Appendix 2A and Figs. 2.7-2.9), the author has determined the value of p which gives the smallest root-mean-square value of $(c_{f exp} - c_{f,th})/c_{f,th}$. This value of p is -0.702. Thus, for the adiabatic-wall case,

$$F_{R\delta} = (T_S/T_G)^{-0.702} \qquad \ldots \qquad (2.95)$$

where T_S is of course the adiabatic-wall temperature which is obtained by Eq. (2.82).

The index q of Eq. (2.94) can now be found empirically from the drag coefficient in the presence of heat transfer. A computer program was written which varied q and minimized the root-mean-square value of $(c_{f,exp} - c_{f,th})/c_{f,th}$ for all the available heat-transfer experiments, p being given the value -0.702 as derived earlier. The minimum root-mean-square error was found when q was 0.772. The recommended $F_{R\delta}$ is accordingly

$$F_{R\delta} = (T_S/T_G)^{-0.702}(T_{ad,S}/T_S)^{0.772} \quad \dots \qquad (2.96)$$

which reduces to Eq. (2.95) for the adiabatic wall.

2.4.5.   <u>Comparison of the present method with other theories</u>
<u>and experiments.</u>

The root-mean-square value of $(c_{f,exp} - c_{f,th})/c_{f,th}$ for the present theory has been calculated and inserted in Fig.2.6 and Table 2.6 in order to compare with the other theories. The present theory gives the lowest root-mean-square value, namely, 9.9%. This is to be expected because we have derived $F_{R\delta}$ directly from the experimental data.

In order to examine the individual effects of Reynolds number, Mach number and heat-transfer rate on the values of c_f predicted by the present method, (i) c_f vs Re_x curves at the conditions of adiabatic wall and M_G from 0-10 are plotted in Fig.2.13, (ii) c_f vs $Re_{\delta 2}$ curves at $T_{ad,S}/T_S = 2$ and M_G from 0-10 are plotted in Fig. 2.14, and (iii) $\bar{c}_f$ vs Re_x curves at $M_G = 7$ and $T_{ad,S}/T_S$ from 1 to 6 are plotted in Fig. 2.15. It can be seen in these figures that (i) for a given M_G and $T_{ad,S}/T_S$, c_f decreases with increasing Re_x (or $Re_{\delta 2}$);(ii)for a given Re_x (or $Re_{\delta 2}$) and $T_{ad,S}/T_S$, c_f decreases with increasing M_G; and (iii)

for a given Re_x (or Re_{δ_2}) and M_G, c_f increases with increasing $T_{ad,S}/T_S$. The effect of heat transfer on the c_f value at a given Mach number and Reynolds number is, however, not large as indicated in Fig. 2.15 by the small difference between the curves for $T_{ad,S}/T_S$ equal to unity and six respectively.

Also plotted in Figs. 2.13-2.15 are some experimental data at the appropriate conditions, and also for the purpose of comparison the well-known theoretical curves of van Driest-II [2.9] and Eckert [2.21]. Apart from small discrepancies such as are always expected to be present in the experimental data, the experiments are seen to be in close agreement with the present theory at all conditions. For the adiabatic-wall case, the van Driest method based on the von Karman mixing length formula [2.9] is about the same as the present theory whilst the Eckert theory appears to underestimate c_f at large M_G (Fig. 2.13). At the condition of large heat-transfer rates (i.e. at large $T_{ad,S}/T_S$) it can be seen in Fig. 2.15 that the theoretical curves due to van Driest and Eckert lie above the experiments and the present theory.

In the above comparison (Figs. 2.13 - 2.15), data at the conditions of M_G up to about 10 and $T_{ad,S}/T_S$ up to about 6 have been included. These conditions are of the largest M_G and $T_{ad,S}/T_S$ which have so far been explored experimentally. The adequacy of the present theory and the improvement of the present method over the theories of van Driest-II and Eckert under those extreme conditions have therefore been seen. The improvement

at the condition of large heat tranfer rates is particularly noticeable (Fig.2.15).

To compare the present method with the experiments at all conditions, the ratios of the experimental c_f to the theoretical c_f evaluated by the present theory are plotted versus M_G for the adiabatic-wall case (Fig.2.16) and versus $T_{ad,S}/T_S$ for the presence of heat transfer (Fig.2.17). In view of the unavoidable discrepancies present among the experiments as mentioned above, the present theory is seen to be satisfactory to correlate all the experiments so far covered.

Finally, the over-all accuracy of the present method and the experiments are summarised by plotting the experimental and theoretical $F_c c_f$ vs $F_{R\delta} Re_{\delta 2}$, $F_c c_f$ vs $F_{Rx} Re_x$ and $\bar{c}_f F_c$ vs $F_{Rx} Re_x$ in Figs. 2.18-2.20 respectively. Values of the theoretical $F_c c_f$ and $F_R Re$ were evaluated from Eqs. (2.71-2.73); and values of the experimental $F_c c_f$ and $F_R Re$ were evaluated by Eqs. (2.86) and (2.96) using experimental values of c_f, Re, M_G and T_S/T_G.

2.5 Results and Recommended Method of Calculation.

2.5.1. Summary of results.

To facilitate calculation, the main results derived in §2.4 are presented in the form of tables and figures. Table 2.8 gives the corresponding values of $F_c c_f$ and $F_c \bar{c}_f$ vs $F_{R\delta} Re_{\delta 2}$ and $F_{Rx} Re_x$, Table 2.9 gives the values of F_c at various M_G and T_S/T_G, and Table 2.10 gives the values of $F_{R\delta}$ at various M_G and T_S/T_G. Values from Tables 2.8-2.10 are plotted in Figs. 2.21 and 2.22 for the convenience of use.

2.5.2. Discussion of results.

The theory presented in §2.4 has been seen to be satisfactory in correlating frictional-drag data for compressible turbulent boundary layers. It also results in a correlation which is very simple to use as will be seen in §2.5.3.

The expression recommended for F_c implies the assumption of one or the other variety of the mixing-length theory (§2.4.3); the expression for $F_{R\delta}$ is entirely empirical. On the comparison of the theoretically derived and the experimentally obtained $F_{R\delta}$ functions,

$$F_{R\delta,\,th} = (\mu_G/\mu_S)(\rho_S/\rho_G)^\beta (E/E_i) \quad \dots \quad (2.87)$$

$$F_{R\delta,\,exp} = (T_S/T_G)^{-0.702}(T_{ad,S}/T_S)^{0.772} \quad \dots \quad (2.96)$$

they enable us to ascribe the $(T_S/T_G)^{0.702}$ component of $F_{R\delta,exp}$ to the viscosity near the wall and the $(T_{ad,S}/T_S)^{0.772}$ component to the E/E_i. This implies that the (ρ_S/ρ_G) component of $F_{R\delta,th}$ should be unity. Hence the present theory supports the use of the von Karman mixing length theory (§2.2.3) with the integration constant, E, expressed in the form

$$E = E_i(T_{ad,S}/T_S)^{0.772} \quad \dots \quad (2.100)$$

This expression for E (Eq. 2.100) indicates that E increases with increasing rate of heat transfer to the wall (the highest rate corresponds to the highest $T_{ad,S}/T_S$).

Now, theoretically, the expression for E is believed to be a function of u^+ and y^+ at the inner edge of the turbulent outer-layer, whose magnitudes are expected to be dependent upon the laminar-sub-layer and the transitional-buffer-layer characteristics. An implication of the present empirically derived

E is therefore as follows. For the adiabatic-wall case, the temperature gradient at the wall is zero and the properties of the fluid close to the wall are essentially uniform. Hence the use of a constant E was found to be sufficiently adequate to correlate the drag data for the adiabatic-wall condition. For the case of the presence of heat transfer, the existence of the temperature gradient at the wall is expected to cause the variation of the properties of the fluid in the region close to the wall. Hence the value of E was found to be dependent upon the heat-transfer rates $(T_{ad,S}/T_S)$.

The above implication indicates that, in order to find a physical hypothesis to fit the empirically derived E, heat-transfer effects on the values of u^+ and y^+ in the laminar sub-layer and the transitional buffer-layer should be studied. Such data are still lacking; it is not as yet possible to formulate a reliable analysis for the region close to the wall and in particular for the transitional region. Under this circumstance, it is thought better at the present stage to recommend the empirically derived functions than to advance speculative hypotheses. It should however be mentioned that a large amount of information about the hypothesis for the E function can be obtained at low speeds without a supersonic wind tunnel as it is clear in the above discussion.

2.5.3. Recommended method of calculation.

In most common cases, the problem is to find the drag coefficient when the Reynolds number, Mach number and temperature

61.

ratio are known. The procedure for solving this problem by use of the present method is as follows. First, the value of F_c is determined from Table 2.9 or figure 2.22. Then the value of $F_{R\delta}$ is determined from Eq. (2.96), Table 2.10 or Fig. 2.22, and where necessary the value of F_{Rx} is obtained from the equation

$$F_{Rx} = F_{R\delta}/F_c \qquad \ldots \qquad (2.67)$$

Finally, by using the input value of $Re_{\delta 2}$ (or Re_x) and the values of $F_{R\delta}$ (or F_{Rx}) and F_c above, c_f or $\bar{c}_f$ can be obtained from Table 2.8 or Fig. 2.21.

The above calculation can be performed in a few minutes with an accuracy of 1%. The latter is, of course, well within the limit of experimental accuracy at present.

2.6 Conclusions.

In conclusion, the results of the present chapter can be summarised as follows.

A procedure has been developed semi-empirically for predicting the drag coefficient on a smooth surface of zero streamwise pressure gradient at various Reynolds numbers, Mach numbers and ratios of surface temperature to stream temperature.

The extent to which the procedure correlates the existing experimental data can be judged by the inspection of Figs. 2.18-2.20, whereby it must be remembered that the experiments have been carried out in several entirely different pieces of apparatus and are not of high accuracy. The correlation is better than that given by any of the other existing theories as can be seen from Table 2.6 and Fig. 2.6. The value of the present

procedure is that it does not make use of the more arbitrary assumptions of earlier theories; it lets the data speak for themselves.

The procedure is simple and quick to use in engineering calculations and its accuracy is only limited (at the present time) by accuracy of experimental data from which it is in part derived.

The necessary auxiliary functions have been tabulated (Tables 2.8-2.10) and plotted in Figs. 2.21 and 2.22 for ready reference. However, it must be remembered that experiments have not yet been carried out over the whole range of conditions covered by the tables and figures. Figs. 2.1-2.4 show how remarkably restricted has been the range of experimental conditions so far.

The procedure is capable of greater refinement when more accurate experimental data are available, say, by modification of the $F_{R\delta}$ function.

As a point of academic interest, it was shown in §2.5.2 that the present theory could be built on a model based upon the von Karman mixing length theory with an empirical expression for E. The nature of the E was discussed in §2.5.2.

CHAPTER 3

HEAT TRANSFER

3.1. Introduction.

A simple way to calculate heat transfer in turbulent flow
is to derive it from the frictional drag coefficient (c_f) with an
equation

$$St = S.c_f/2 \qquad \ldots \qquad (3.1)$$

where St is the Stanton number and S is the "Reynolds-analogy
factor". A procedure for the calculation of the frictional-drag
coefficient at various Reynolds numbers, Mach numbers, and wall-
to-mainstream temperature ratios has been developed in the previous
chapter. A recommendation for an adequate Reynolds-analogy factor
for the turbulent flow of air will be made below.

There are several theories in the literature, for example,
see Refs. 3.1-3.9, which are concerned with the derivation of the
Reynolds-analogy factor. They are reviewed and compared in §3.2.

In order to check the theoretical predictions, extensive
heat transfer measurements available in the literature (3.11-3.22)
are collected and examined in §3.3.

The value of the Reynolds-analogy factor which is
recommended for use is given in §3.4. Results of this chapter
are summarised and discussed in §3.5. Conclusions are given in
§3.6.

3.2. Survey of Previous Theoretical Work.

3.2.1. Natures of analyses.

The modes of derivation of twelve theoretical Reynolds-analogy
factors (3.1-3.9) are indicated in Table 3.1. The significance

of the contents of this table will be described below. It was
found that the theories have much in common with one another.

One reason for the similarities is that they can all be
derived from the equation

$$S = \left[\int_0^1 Pr_{tot} \left(\frac{\tau}{\tau_S}\right)^{Pr_{tot}-1} d\frac{u}{u_G} \right]^{-1} \quad \ldots \quad (3.2)$$

where Pr_{tot} is the total Prandtl number and is defined as

$$Pr_{tot} = \frac{c_p(\mu+\epsilon_u)}{(k+\epsilon_h)} \quad \ldots \quad (3.3)$$

Eq. (3.2) was derived from the 2-dimensional boundary layer
continuity, momentum and energy equations with the assumption of
τ, q and T distributions in the boundary layer being functions
of u only, (e.g. see Ref. 3.8)

To evaluate the S-integral of Eq. (3.2), the distribution
of the shear stress (τ) and the total Prandtl number (Pr_{tot})
in boundary layers are required to be known. For the former,
with the exception of van Driest [3.8] and Spence [3.9] all the
other authors of the theories of Table 3.1 have assumed τ/τ_S
to be unity. For the Pr_{tot} distribution, several different
assumptions have been used by the various authors.

The assumptions about Pr_{tot} can, however, be divided into
three categories, namely, (i) the turbulent transport is
assumed to be negligibly small in comparison with the molecular
transport (i.e. $Pr_{tot} = Pr = c_p\mu/k$); (ii) the molecular
transport is assumed to be small in comparison with the turbulent
transport, (i.e. $Pr_{tot} = Pr_t = c_p\epsilon_u/\epsilon_h$); and (iii) the

turbulent and the molecular transports are of comparable sizes, the Pr_{tot} is then derived from Eq. (3.3) with the assumption that a "Law of Wall" ($u^+ = u^+(y^+)$) exists. In the last category the expression for Pr_{tot} is:

$$\text{Pr}_{tot} = \frac{dy^+/du^+}{\frac{1}{\text{Pr}}\frac{\mu}{\mu_S} + \frac{1}{\text{Pr}_t}(\frac{dy^+}{du^+} - \frac{\mu}{\mu_S})} \quad \ldots \quad (3.4)$$

For the uniform-property boundary layer, Eq. (3.4) reduces to

$$\text{Pr}_{tot} = \frac{dy^+/du^+}{\frac{1}{\text{Pr}} + \frac{1}{\text{Pr}_t}(\frac{dy^+}{du^+} - 1)} \quad \ldots \quad (3.5)$$

In Table 3.1, the individual theories based upon Eq. (3.2) are distinguished by the assumed γ and Pr_{tot} distributions, and the assumed Pr_t value. The values of S predicted by the various theories will be compared in the following sections (§§3.2.2 and 3.2.3).

3.2.2. <u>Theoretical Reynolds-analogy factor for the uniform-property turbulent boundary layer of air.</u>

It can be seen in Table 3.1 that most of the theories have not taken the boundary-layer property variations into account. In order to examine the fundamental assumptions made by the various authors, the values of S for the uniform-property turbulent boundary layer are first compared. For this purpose, the S values predicted by the various theories (Table 3.1 and Ref. 10) at Re_x equal to 1×10^6 and $\text{Pr} = 0.7$ are shown in Fig.3.1 and the variation of the S values for Re_x from 1×10^5 to 1×10^8 is shown in Table 3.2.

It can be seen from Table 3.2 that the variation of the S value versus Reynolds number predicted by the different theories

depends essentially on the assumed value of the turbulent Prandtl number (Pr_t); that is, on the assumption of Pr_t being unity the S values at Ro_x equal to 1×10^5 and 1×10^8 are respectively about 3% above and below the mean S value over the stated Re_x range, whilst on the assumption of Pr_t being in the range of 0.85 to 0.9 the S values *are* about 1.5% about the mean S value.

For the theoretically predicted S value at a given Reynolds number, (say, Re_x equal to 1×10^6) it can be seen in Fig. 3.1 that the difference of one theory from the other can be as great as 20%. This difference appears due mainly to the assumed "Law of Wall" and/or its associated parameters such as u_1^+, u_2^+ etc. It is indicated in Fig. 3.1 by the fact that different values of S are predicted by those theories which used the same assumptions for γ distribution ($\gamma/\gamma_S = 1$) and the Pr_t value ($Pr_t = 1$).

With regard to the influence of the shear-stress distribution, though the required shear-stress law is by no means certain at the present, for the boundary layer of air its influence on the S value appears to be small. It can be seen in Fig. 3.1 that when the van Driest [3.8] and the Spence [3.9] theories are modified to γ/γ_S being unity and Pr_t being 0.9, the predicted S values are about the same as those predicted by the original van Driest and Spence theories [3.8 and 3.9] with variable shear-stress distributions.

Comparison between various theories has been made above; the accuracy of the individual methods will be checked against experiments in §3.3.

3.2.3. Theoretically predicted influence of the

compressibility of air.

When the stream velocity and/or the temperature difference between the wall and the mainstream are large, the air properties in boundary layers will be non-uniform. The influence of the property variation has been considered by the authors of Refs. 3.2, 3.5, 3.6, 3.8 and 3.9.

The ratios of the variable-property to the uniform-property S predicted by those theories (3.2, 3.6, 3.8 and 3.9)[*], which have considered the property variation, are plotted versus M_G (at $T_{ad,S}/T_S = 1$) and $T_{ad,S}/T_S$ (at $M_G = 0$) in Figs. 3.2 and 3.3 respectively. These figures show the qualitative agreement between the various theories, that is, the value of S is directly related to M_G (Fig. 3.2) and inversely related to $T_{ad,S}/T_S$ (Fig. 3.3). The validity of these theoretically predicted trends is still left to be checked by experiments.

3.2.4. Résumé.

The natures of analyses of the various theories have been discussed and the comparison between those theories have been made above. In the following section (§ 3.3), the experimental-S data will be collected and compared with the theories in order to check the accuracy of those theories.

---

[*]The theories of Ref. 3.5 is not included, because the "reference station" at which the properties are recommended for use is still indeterminate.

68.

3.3. <u>Survey of the Experimentally Obtained Reynolds-Analogy-Factor Data.</u>

3.3.1. <u>Collection of experimental-Reynolds-analogy-factor data.</u>

As very few investigators made the simultaneous heat-transfer and frictional-drag measurements, the experimental Reynolds-analogy factor (S_{exp}) will be derived from the measured heat-transfer coefficient (St_{exp}) by the equation,

$$S_{exp} = 2St_{exp}/c_{f,th}^{*} \qquad \ldots \qquad (3.6)$$

where $c_{f,th}$ is calculated by the method of §2.5.3.

All published experimental St data available to the author [3.11-3.22] have been collected and tabulated in Appendices 3A and 3B together with the derived S values (by Eq. 3.6). Fig. 3.4 shows the collected St vs Re_x data for the uniform-property flow of air (i.e. data obtained at small M_G and small $|T_G-T_S|$). Figs. 3.5-3.7 show the collected variable-property-turbulent-boundary-layer data in the form of St vs Re_{δ_2}, St vs Re_x and $\overline{St}$ vs Re_x, and Fig. 3.8 shows the conditions (i.e. values of M_G, T_S/T_G and $T_{ad,S}/T_S$) which have been explored experimentally.

3.3.2. <u>Examination of the experimental-Reynolds-analogy factor data for the uniform-property flow of air.</u>

The collected experimental data for the uniform-property

---

* The suffices "exp" and "th" stand for experimental and theoretical, respectively; but on some occasions below these suffices are omitted for sake of simplicity as is clear in the text.

flow of air (Appendix 3A) are at the conditions of $T_G = 90^\circ F$.
(i.e. $Pr = 0.7$), $T_S/T_G = 1.03$, and $M_G = 0.08$ and Re_x from 2×10^5
to 3×10^6 (average $Re_x = 1 \times 10^6$). The corresponding experimental
value of S at these conditions is 1.162 on the average. On
comparison of this empirical-S value with the various theoretically
predicted S values at the same conditions (Fig. 3.1), it is
found that several theories (i.e. theories of Prandtl-Taylor
and Refs. 3.3 and 3.7) are in close agreement with the
experiments.

The comparison above has been restricted to a particular
Reynolds number ($Re_x = 1 \times 10^6$). In order to check the accuracy
of the theories at other Reynolds numbers, the range of Re_x
covered by the experiments is too small to allow a direct
comparison. However, it was shown in §3.2.2 that the theories
which use Pr_t equal to unity predict greater variation of S
versus Re_x than those theories which use $Pr_t = 0.9$. Johnson
[3.23] measured the mean as well as the fluctuating velocity
and temperature in turbulent boundary layers on a flat plate
and found that the average turbulent Prandtl number was at the order
0.9. This Pr_t value is the same as that used by Spalding and
Jayatillaka [3.7] ; but Prandtl-Taylor [3.1, p.206] and von
Karman [3.3] used Pr_t equal to unity which is not in agreement
with the measured Pr_t [3.23] . The variation of S versus Re_x
is therefore expected to agree closer with the theory of Ref.
3.7 than with the theory of Prandtl-Taylor or Ref. 3.3.

From the above comparison, it appears that the theory of
Ref. 3.7:

$$S = 1 / \left[Pr_t \left\{ 1 + \frac{8.32}{u_G^+} \left(\left(\frac{Pr}{Pr_t} \right)^{\frac{3}{4}} - 1 \right) \right\} \right] \quad \cdots \quad (3.7)$$

where $Pr_t = 0.9$, gives the best agreement with the experiments

for the uniform-property turbulent boundary layer of air.

Now the variation of S vs Re_x calculated by Eq. (3.7)

is only 1.4% about the mean over the Re_x range from 1×10^5

to 1×10^8 (see Table 3.2). Hence for the uniform-property flow

of air a constant value of S (say, equal to 1.162) is sufficiently

adequate. Fig. 3.4 shows the experimental and theoretical

St vs Re_x, where the theoretical St vs Re_x curve was calculated

by Eq. (3.1) with S = 1.162 and c_f being evaluated by Eq. (2.72).

The agreement between the theory and the experiments is seen to

be good.

3.3.3. Examination of the experimental-S data for the

influence of the compressibility of air.

The theoretically predicted influence of the compressibility

of air was examined in §3.2.3. It was found that (i) for the

adiabatic-wall case, the S increases with increasing M_G (Fig.3.2)

and (ii) for the case of the presence of heat transfer, the S

decreases with increasing $T_{ad,S}/T_S$ (Fig.3.3). The collected

experimental data of Appendix 3B will be examined below for the

trends predicted by the theories.

(i) "Adiabatic-wall case" By the adiabatic-wall case here

is meant that the heat-transfer rate is small so that $T_{ad,S}/T_S$

is approximately equal to unity (say, $0.9 \leqslant T_{ad,S}/T_S \leqslant 1.1$).

S data of Appendix 3B with $T_{ad,S}/T_S$ between 0.9 and 1.1 are

plotted against Mach number (M_G) in Fig. 3.9 and Fig. 3.10 where Fig. 3.9 shows the data for Re_x equal to 1×10^6 (approximately) only, whilst Fig. 3.10 includes data at all Re_x.

On comparison of Fig. 3.9 with the theoretically predicted influence of M_G (Fig. 3.2), it is seen that the experimental data do not show the trends indicated by the theories. It appears that the discrepancies between the experiments are too great to check the small influence of M_G; because at M_G, say, equal to 5, the theories indicate a deviation of only 4% from the S value for the uniform-property flow, whilst the experimental-S data fluctuate at about 10% about the value of S equal to 1.162. Fig. 3.10, which includes S data at all Reynolds number, shows that the experimental-S data are still within about $\pm$ 10% of the constant 1.162. Hence the value of S being 1.162 represents a good mean for the experimental data at all Mach numbers and Reynolds numbers which have so far been explored experimentally.

(ii) <u>Case of the presence of heat transfer.</u> All the S data of Appendix 3B are plotted against $T_{ad,S}/T_S$ in Figs. 3.11 and 3.12, where Fig. 3.11 includes the data for Re_x equal to 1×10^6 (approximately) and Fig. 3.12 includes the data at all Reynolds-number values. Fig. 3.11 indicates that the S data are again too scanty to detect the small effect of heat transfer on the value of S predicted by the various theories (Fig. 3.3). Fig. 3.12 indicates that the value of S being 1.162 represents a good mean for all the data at $T_{ad,S}/T_S$ between 0.5 and 1.6 regardless of the difference in the value of Re_x (or $Re_{\delta 2}$).

For the value of $T_{ad,S}/T_S$ greater than 1.6, the data are however scarce and conflicting.

3.4. <u>Determination of Reynolds-Analogy Factor (S)</u>.

In general S can be written as:

$$S = S(M_G, T_{ad,S}/T_S, Re, Pr) \quad \cdots \qquad (3.8)$$

Although the wall and /or the mainstream temperatures are often not reported so that the exact value of Pr is not known in many cases, yet most wind-tunnel tests have been carried out at a mainstream temperature of around $100^{\circ}F$ [3.24]. When the mainstream total temperature is at $100^{\circ}F$. and $T_{ad,S}/T_S$ is not greatly different from unity, the wall temperature will remain at about $100^{\circ}F$. Hence the value of Pr of air in the region close to the wall, where the molecular transport is important, remains substantially constant in most cases and an average value of 0.7 can be assumed for the present investigation. This simplifies the S-function of Eq. (3.8) to

$$S = S(M_G, T_{ad,S}/T_S, Re) \quad \cdots \qquad (3.9)$$

Now, experimental data giving S can be used to determine the dependence of S on M_G, $T_{ad,S}/T_S$ and Re. The drag is calculated for the same condition as the Stanton number measurements using the method of §2.5.3. It was, however, seen in the above section (§3.3) that there is no ordered dependence of S on either of these parameters, whilst a constant S equal to 1.162 for the uniform-property turbulent boundary *layer* of air at Pr equal to 0.7 can be taken as a good mean for the compressible turbulent boundary layer.

For want of more conclusive experimental evidence, the empirical constant (S = 1.162), which fits the data well, is recommended for use. A better estimate of S can be made when better experimental results become available.

3.5. Results and Discussion.

The theoretically and experimentally obtained heat-transfer data for the flow of air have been reviewed in §§3.2 and 3.3 respectively. It was found that the theories predict (i) a small variation of S vs Reynolds number (Table 3.2) and (ii) a small influence of the compressibility of air on the value of S (Figs. 3.2 and 3.3). The experimental data giving S were found to be too scanty for checking the small influence of the compressibility of air on the value of S (Figs. 3.10 and 3.12).

This situation has also been recognised by several previous authors, for example, those of Refs. 3.22 and 3.24. For this reason, a simple analogy factor, such as the Colburn's Analogy $(S = Pr^{-2/3})$ [3.10] , has often been recommended for use (e.g. see Refs. 3.12 and 3.24). The degree of correlation achieved by the use of Colburn analogy had not, however, been able to be shown, because the drag coefficient (c_f) was not often measured simultaneously with the heat transfer coefficient (St) and the reliability of the theoretically predicted c_f was still rather uncertain.

As a suitable procedure for the prediction of c_f has now been developed (§2) the present author has obtained S from the experimental St data using c_f for the same condition as the

St measurements by the method of §2.5.3 and found that the empirical S value (= 1.162) from the uniform-property flow of air at Pr = 0.7 satisfactorily correlates the S data for the variable-property turbulent boundary layer of air and it is much better than the commonly used Colburn analogy (see Figs. 3.1, 3.10 and 3.12).

The recommended procedure for the evaluation of the Stanton number (St) is therefore to calculate the drag coefficient (c_f) by the method of §2.5.3 and then to obtain the required St by multiplying $c_f/2$ by 1.162.

The recommendation of a constant value of S for the flow of air implies that the influence of the compressibility of air on the heat-transfer coefficient (St) is entirely taken care of by the F_c and F_R functions which were developed in §2.4. Stanton-number values at several different Reynolds numbers, Mach numbers and heat-transfer conditions have been computed by the presently recommended procedure and are plotted in Figs. 3.13 and 3.14. As shown in these Figs. (3.13 and 3.14), (i) for a given M_G and $T_{ad,S}/T_S$, St decreases with increasing Re_x, (ii) for a given Re_x and $T_{ad,S}/T_S$, St decreases with increasing M_G, (iii) for a given Re_x and M_G, St increases with increasing $T_{ad,S}/T_S$.

The extent to which the recommended method correlates all the existing experimental data can be judged by inspection of Figs. 3.15 to 3.17, where the theoretical and the experimental values of F_cSt (or $F_c\overline{St}$) are plotted against $F_{R\delta}\,Re_{\delta 2}$ (or $F_{Rx}Re_x$). It is

75.

seen in these figures that the present method correlates all the data within about $\pm 10\%$ with the exception of the data of Ref: 3.21. On comparison of the data of Ref: 3.21 with the data of Ref: 3.22 and the recommended theory as shown in Fig: 3.18, it is seen that the data of Ref: 3.21 are about 20% above the data of Ref. 3.22 and the theory for the same conditions (i.e. Re_x, M_G and $T_{ad,S}/T_S$). It is therefore believed that the accuracy of the data of Ref: 3.21 is doubtful. On the exclusion of the data of Ref. 3.21, the present method correlates the existing Stanton-number data within an error which is about the accuracy of the data from different sources.

Finally, it must be mentioned that the recommended S equal to 1.162 is entirely empirical. From Figs. 3.2 to 3.8 it can be seen that the ranges of conditions at which experimental data are available are Re_x from 1×10^5 to 1×10^8, M_G up to 10 and $T_{ad,S}/T_S$ from 0.5 to 1.6 (excluding the doubtful data of Ref. 3.21). The scarcity of data at large $T_{ad,S}/T_S$ is obvious. However, it was seen in §2.5.2 that the $T_{ad,S}/T_S$ is an important parameter of the Law of Wall; and it was seen in §3.2 that the theoretically derived S expressions are dependent of the assumed Law of Wall. In order to give sufficient confidence in the use of a constant S for large $T_{ad,S}/T_S$, it is desirable to extend the range of $T_{ad,S}/T_S$ for which data are available.

3.6. Conclusions.

In conclusion, the results of the present chapter can be summarised as follows.

All existing theories predict small influence of Re, M_G and T_S/T_G on the value of the Reynolds-analogy factor (S), but the exising experimental data are too scanty to reveal this small influence. Under this circumstance, an empirical constant value of the Reynolds-analogy factor is tentatively recommended for use, namely, S = 1.162. The degree of correlation for the existing data achieved by the use of S equal to 1.162 where c_f being evaluated by the method of §2.5.3, is remarkably good (see Figs. 3.15 to 3.17).

The recommended procedure for the evaluation of St at a specified condition (Re, M_G and T_S/T_G) is therefore simply to calculate the frictional-drag coefficient (c_f) by the method of §2.5.3 and then to obtain the required St by multiplying the $c_f/2$ by 1.162.

With regard to the experimental data available in the literature, it was found that the data at large temperature difference (or large $T_{ad,S}/T_S$) are scarce and conflicting. The recommended method has been confirmed by experiments only at $T_{ad,S}/T_S$ up to about 1.6. Additional data at large $T_{ad,S}/T_S$ are desirable in order to increase confidence in the use of the presently recommended method. Experiments at $T_{ad,S}/T_S$ up to 2.7 which have been carried out by the present author are reported in the following chapter.

CHAPTER 4

EXPERIMENTS

4.1. Introduction.

Numerous experimental heat-transfer data in compressible turbulent boundary layers from the literature were reviewed in the previous chapter (§3); the conditions were of Reynolds number (Re_x) from 1×10^5 to 1×10^8, Mach number (M_G) from 0.2 to 10, and temperature ratio ($T_{ad,S}/T_S$) from 0.5 to 1.6. It was found in §3 that experiments are not accurate enough to reveal the effect of the various parameters (Re, M_G and $T_{ad,S}/T_S$) on the value of the Reynolds-analogy factor, $S(\equiv 2St/c_f)$; a simple equation,

$$St = S.c_f/2 \qquad \ldots \qquad (4.1)$$

where $S = 1.162$ and $c_f/2$ is calculated by the method of §2.5.3, correlates all the data at the conditions stated above within an accuracy of about 10% as shown in Figs. 3.10 to 3.12. These figures also show that the greatest uncertainty exists in the region of large heat-transfer conditions, that is, data at large $T_{ad,S}/T_S$ (say greater than 1.6) are scarce and conflicting.

The purposes of the present experiments were (i) to extend the range of heat-transfer conditions beyond those of other publications and (ii) to check the applicability of Eq. (4.1) at large $T_{ad,S}/T_S$. For these purposes, measurements of heat-transfer have been made for Re_x from 1×10^5 to 2×10^6, M_G from 0.05 to 0.25 and $T_{ad,S}/T_S$ ($\approx T_G/T_S$ for the present case) from 1.02 to 2.7.

The experimental method and the calibration of wind tunnel are respectively described in §§4.2 and 4.3 below. Measurements of heat-transfer coefficients are reported in §4.4, and conclusions drawn from the experiments are summarised in §4.5.

4.2 Description of Method, Apparatus and Measurements.

4.2.1. Experiments Method.

The transient technique was used to measure the heat-transfer rate. This technique has been used by a number of earlier investigators, for example, those of Refs. 4.1-4.4. It is particularly suitable for the present purposes, because a wide range of temperature ratio was intended to be explored.

The measurement was carried out in a 18"x12" low-speed wind tunnel. A 12"x24"x3/16" test plate was placed vertically in the centre-line of the tunnel. The plate was precooled by liquid nitrogen to about -300°F. On subsequent exposure of the precooled plate to the tunnel air at known velocity (controllable between 70° and 280°F.), temperature of the plate at 12 positions were recorded against time. From these recorded T (temperature) - t (time) curves, heat-transfer coefficients at various Reynolds numbers and temperature ratios were derived.

Details of various components of the apparatus and instruments are described below.

4.2.2. Apparatus.

The apparatus consisted essentially of a wind tunnel, flat test plate, cooling apparatus and air drying plant. Figs. 4.1 and 4.2 are the respective photograph and sketch of the general layout of the apparatus.

(i) <u>Wind tunnel</u>. The wind tunnel was of the closed circuit type and air was circulated by a fan which was driven by two constant-speed motors of 5 h.p. at 575 r.p.m. for the lower speed range and 120 h.p. at 2950 r.p.m. for the higher speed range through a Vulcan Sinclair Fluidrive Coupling providing infinitely variable speed ratio of 5 to 1. The fan speed was remotely controlled electrically through a handle and a set of switches mounted on a control panel.

A heat exchanger of the secondary surface type was used to obtain a range of temperatures by passing water or steam through the heat exchanger. Steam and water entry was controlled by remotely operated valves.

At the entry to the working section reasonably uniform velocity, temperature and humidity profiles were required. These were achieved by an "egg box" type straightener immediately after the Cascade bend preceding the working section having length/width ratio of 3 to 1 followed by a 30 mesh x 36 S.W.G. wire mesh screen, following by a smooth contraction into the working section.

The tunnel had the following performance:

Size of working section .... 18"wide x 12"high x 36"long.

Size of section before .... 2'-6" square.
   contraction into working
   section.

Velocity in working section .. 2 to 240 ft/s.

Flow Rate .... 22,000 ft^3/m (max).

Temperature   ....   Controllable over the range of
                                       ambient temperature to ambient
                                       plus $200^{\circ}F$.

Humidity   ....   Down to dew point temperature
                                       of $10^{\circ}F$.

Conditions at entry to working

  section   ....   Reasonably uniform velocity,
                                       temperature and humidity
                                       profiles and reasonably low
                                       level of turbulence.

(ii) <u>Test plate</u>.   Design of the test plate is shown in
Fig. 4.3.   The plate was 24" long x 12" high x 3/16" thick
(nominal size) placed vertically in the centre-line of the tunnel
working section.   The mounting of the plate to the tunnel was so
designed as to reduce the heat conduction in the chordwise
direction.   The material of the plate was Monel 400.   It was
chosen, because (i) its physical properties over the whole
interested range of temperatures were known, (ii) it was easily
machined and polished, and (iii) its medium value of thermal
conductivity (e.g. 16 c.f. 222 Btu/h ft $^{\circ}F$ for coper at room
temperature) gave a compromise between the uniform temperature
across the thickness of the plate and the low heat conduction
along the plate.

Twelve calibrated copper-constantan thermocouples of 0.0048"
(40 S.W.G.) were electrically welded and then soft soldered into
twelve 0.020" diameter (No. 76 drill) small holes in the surface
of the plate.   Electrically insulated thermocouple leads were

imbedded in 1/32" grooves. Details of the thermocouple fixing
is shown in Fig. 4.3a.

Six of these thermocouple beads were placed along the
centre-line of the plate and the other six were placed alternately
at one inch above and below the centre-line; this arrangement
enables the effect of chordwise heat conduction to be observed
during the test. Positions of the thermocouples are indicated
in Fig. 4.3.

The plate was polished and lapped by a portable electrical
sander. The finished surface was smooth and its thickness was
found to be $0.186" \pm 0.001"$. The front part of the plate was
tapered at 5° on each side; the leading edge of the plate was
sharp so as to eliminate the uncertainty of the effect of
bluntness (4.4) .

(iii) <u>Cooling apparatus</u>. Fig. 4.4 shows the general layout
of the cooling apparatus. Its main component was the "Cooling
Jacket" which was divided into three compartments. At the top
of the middle compartment, there was a 2'-0" by 3/16" slot in
which the plate was placed. The plate was separated from the main
body of the cooling jacket by a Teflon sliding seal which also
acted as a thermal insulator. Three holes at the bottom of the
middle compartment were the liquid-nitrogen-inlet holes; eight
holes at the bottom of the side compartments were the outlet holes
for the gasified liquid nitrogen.

Two pneumatic rams synchronised by two air-flow regulators
were used for moving the cooling jacket up or down as desired.

Bottled nitrogen gas was used to apply a pressure of 15 lb / in ^{2} on the surface of the liquid nitrogen in the container so as to pump the liquid nitrogen through the cooling jacket. Two Valves A and B (Fig. 4.4) were for shutting off the nitrogen supply and for quick release of the residue nitrogen in the cooling jacket at the end of each cooling operation.

The cooling operation was performed by pushing the cooling jacket to the uppermost position, closing the valve B, opening the valve A, adjusting the gaseous-nitrogen pumping pressure to 15 lb /in ^{2}, opening the valve D and closing the valve C. When the plate temperature had reached the required temperature, the supply of liquid nitrogen was stopped by closing the valve D, opening the valve C, closing the valve A, opening the valve B, and lowering the cooling jacket. The recording of the plate T-t history then began.

(iv) _Air drying plant._ The air drying plant consisted essentially of a 12" diameter x 5'-0" high mild-steel vessel and a 3 h.p. air blower as shown in Fig. 4.5. The vessel was packed with a bed of $\frac{1}{4}$ to $\frac{1}{2}$" granular "Actal" (Activated Alumina). The top of the vessel was connected to the air bleeding hole of the tunnel; the lower end of the vessel was connected to the inlet of the blower, the outlet of the blower was connected to the air inlet port of the tunnel.

The plant was operated as follows: When the blower was running at full speed and the tunnel fan was running at 500 r.p.m. part of the tunnel air by-passed the drying plant at a rate of

1.2 ft $^3/s$, where the water vapour was absorbed by the packed "Actal". It was possible to reduce humidity of tunnel air to a dew point of about 10^OF after 2 hours.

4.2.3. Measurements and instruments.

Figs. 4.6 and 4.7 are the respective photographs of the layout of the instruments for the measurements of thermocouple e.m.f.'s and for the measurements of tunnel air pressures. Details of the instruments are described below.

(i) Thermocouples. All thermocouples used were of BS 1828 (1961) copper-constantan wires of 40 S.W.G. (0.0048" diameter) supplied by the Saxonic Wire Company Limited.

A set of Standard Thermometers (from -120 to 260^OF.) having absolute accuracy of 0.2^OF. were used to calibrate the thermocouples. A thermocouple was tied to a standard thermometer and immersed in water or in a mixture of Methanol and Cardice. The corresponding thermocouple e.m.f.'s and thermometer readings were noted over the range of temperatures from -120 to 212^OF. The e.m.f.'s of the thermocouple at the boiling points of liquid oxygen and liquid nitrogen were also measured. The differences between the measured e.m.f.'s and the reference e.m.f.'s from BS 1828 (1961) [4.5] are plotted against temperatures in Fig.4.8. This figure together with Table 4.1 (from Ref. 4.5) gives an accurate relationship between e.m.f. and temperature of the thermocouple.

(ii) Total temperature measurements. The total temperatures at the centre of the cross-sections at positions O and X, that is

the upstream and the downstream of the contraction at the entry
into the working section of the wind tunnel as shown in Fig. 4.9,
were respectively measured by placing a thermocouple in a
stainless steel tube of 0.125" O.D. The design of the total
temperature probe was in accordance with Ref. 4.6. The e.m.f.
of the thermocouple was measured by a Tinsley Potentiometer. The
thermocouple circuit is shown in Fig. 4.10.

(iii) <u>Tunnel-air static pressures</u>. The tunnel-air static
pressures at positions 0 and X were tapped from two $\frac{1}{8}$"-diameter
holes drilled on a side wall of the tunnel. Each of these holes
was connected by a rubber tube through a cock to one of the two
manifolds which were in turn connected to the two limbs of a
Casella Vernier Reading Manometer. The manifolds were also
connected to an inclined manometer (30°), this was used to give
a quick rough reading so as to facilitate the adjustment of the
height of the Vernier reading manometer. Fig. 4.11 is a sketch
of the connections of the tubings, manometers and manifolds.

The range of the Vernier Reading Manometer was 300 mm with
verniers reading to 0.01 mm. There were glass wool filters and
Actal driers fitted in the pipe-lines as shown in Fig. 4.11.

(iv) <u>Mainstream pressure and temperature measurements</u>.
A pitot-static-thermocouple mounted on a 2-dimensional traversing
gear was used to measure the temperature, static pressure and
velocity head of the tunnel air at various positions in the working
section. The traversing gear was fixed in the horizontal centre-
plane of the tunnel. Details of the pitot-static-thermocouple
are shown in Fig. 4.12.

The thermocouple e.m.f. and the pitot-static pressure were respectively measured by the Tinsley Potentiometer (Fig. 4.10) and the Cassela Vernier Reading Manometer (Fig. 4.11) as previously described.

(v) Test-plate temperature measurements. A Honeywell Multipoint Recording Potentiometer was used to record six of the twelve test-plate thermocouples at each run. The thermocouple circuit was as follows: The six pairs of potentiometer terminals were connected to the six reference junctions and a 12-point socket, whilst the No.1-6 thermocouple leads were connected to a 12 point plug and the No. 7-12 thermocouple leads were connected to another plug. Thus, by plugging the appropriate plug into the socket, either the first six or the second six plate-thermocouple e.m.f.'s were recorded as desired. The described circuit is sketched in Fig. 4.13. Numbering of the thermocouples is shown in Fig. 4.3.

The recording potentiometer had: (i) ranges of 0-3 mv DC and 0-7.5 mv DC on a full scale travel of 11 inches, (ii) chart speeds of 120 in/h and multiples of 2,3 and 4 of 120 in/h, (iii) intervals between consecutive print of 1.25 and 2.5 seconds. The 0-3 mv range, 240 in/h chart speed, and 2.5 second printing speed were used for tests at small temperature differences (i.e. small T_G-T_S); the 0.-7.5 mv, 480 in /h and 1.25 second were used for tests at large temperature difference (i.e. large T_G-T_S).

(vi) Tunnel-air humidity measurement. The humidity of the tunnel air was measured by an AEI-Birlec dewpointer. An air-flow

regulator and a simple air flow-meter were fitted in series with the dewpointer as shown in Fig. 4.14. The tunnel air was tapped from a hole in wall at position O (Fig. 4.8). The required flow rate through the dewpointer was 2 ft^3/h. The temperature of the dewpointer surface was reduced by bubbling air through ether in the centre-reservoir of the dewpointer.

4.3. Calibration of Wind Tunnel.

4.3.1. Purpose and method of calibration.

Wind-tunnel velocity is often calibrated in terms of the difference between the reservoir pressure (or the pressure before the contraction) and the pressure after the contraction at the entry into the working section, for example, see Refs. 4.7 and 4.8. The reason is that once the relationship between the said pressure difference and the air velocity at the working section is determined, the latter can afterwards be gauged without excessive manipulation of instruments and without the obstruction of excessive instruments in the stream. The main theory implied in the calibration of a low-speed wind tunnel is the "uni-directional incompressible flow theory".

On application of this theory (e.g. see Ref. 4.9), we can obtain the equation,

$$u_G = C \sqrt{(P_0 - P_X)_c} \quad \ldots \quad (4.2),$$

where $(P_0 - P_X)_c = (P_0 - P_X) \times (760/P_0) \times (T_0/520) \quad \ldots \quad (4.3),$

C is a constant dependent on the density of air at STP (520^0R and 760 mm Hg), the cross-sectional area of the tunnel at positions O and X (Fig. 4.8), and the unit of the pressure difference.

When the pressure difference is measured in mm of water and the velocity is measured in ft/s , the theoretical value of C for the present tunnel is 13.94.

In practice, the compressibility of air and the presence of tunnel-wall boundary layers make the value of C be a certain unknown function of Mach number and Reynolds number which in turn depend on the temperature, pressure and velocity of the tunnel air. However, for a given low-speed tunnel, the absolute air pressure at the working section does not change greatly, both Mach number and Reynolds number at a given temperature are functions of velocity (u_G) only. Moreover, as a first approximation, u_G is proportional to $\sqrt{(P_0-P_X)_c}$. Hence it is seen that the value of C is a function of $(P_0-P_X)_c$ at a given temperature.

From the above deduction, it is seen that it is possible to obtain a family of experimental C ($\cong u_G/\sqrt{(P_0-P_X)_c}$) versus $\sqrt{(P_0-P_X)_c}$ curves at various T_0 for the present tunnel. Tests have been carried out at T_0 equal to 80 and 280°F, for the purpose of obtaining these calibration curves.

The measurements of pressure, temperature and velocity are to be described in §4.3.2 and the results of the calibration are summarised in §4.3.3.

4.3.2. Description of experiments and derivation of results.

(i) Measurements and observations. Measurements of T_0, P_0 and (P_0-P_X) at various tunnel fan speeds and air temperatures were made in accordance with the method described in sub-sections (ii)

and (iii) of §4.2.3.

u_G was derived from the average values of u_I, u_{II}, u_{III} and u_{IV}; and the latters were in turn derived from the pitot-static-thermocouple readings (sub-section iv of §4.2.3) at positions I, II, III and IV (Fig. 4.9). The traversing of the pitot-static-thermocouple was made in the horizontal centre-plane of the tunnel working section as described in sub-section (iv) of §4.2.3 for finding the mainstream velocity outside the test-plate boundary layer. It was justified by the facts that the tunnel velocity and temperature profiles were reasonably uniform (i of §4.2.2) and that all the test-plate thermocouples were fixed close to the centre-line of the plate (Fig. 4.3).

Observations of (a) T_0, P_0 and (P_0-P_X), and (b) the mainstream velocity head (ΔP) (which was found by traversing the pitot-static-thermocouple away from the plate until the maximum value of ΔP was observed), the static pressure (P), and the temperature (T) at positions I, II, III and IV were made. Readings (a) were used to derive the value of $(P_0-P_X)_c$; and readings (b) were used to derive the corresponding values of u_I, u_{II}, u_{III} and u_{IV} and hence the value of u_G.

Table 4.2a shows the readings obtained at the nominal T_0 equal to $80^{\circ}F$; and Table 4.2b shows the readings obtained at the nominal T_0 equal to $280^{\circ}F$.

(ii) <u>Derivations.</u> From the recorded values of T_0, P_0 and (P_0-P_X) of Tables 4.2a and 4.2b, the value of $(P_0-P_X)_c$ was calculated by Eq. (4.3) in a simple manner.

From the recorded values of P_I, ΔP_I and T_I, the value of u_I was derived in the following manner: With the aid of the tabulated "one-dimensional Isentropic Compressible Flow Functions" (Table 30 of Ref. 4.10), the Mach number was derived from the P_I and ΔP_I readings, and the value of u_I was then calculated by the equation,

$$u_I = \sqrt{\frac{2\Delta P_I}{\sqrt{(1+\frac{1}{4}M_1^2)}\, \rho_{STP}(\frac{520}{T_I})(\frac{P_I}{720})}} \quad \cdots \quad (4.4)$$

with the appropriate units (that is, if ΔP_I is in lb/ft^2 and ρ_{STP} is in $slugs/ft^3$, u_I will be in ft/s).

Similarly, u_{II}, u_{III} and u_{IV} were derived from the observed data of the pressure and temperature at the respective positions II, III and IV.

Thence, by the equation,

$$u_G \equiv (u_I + u_{II} + u_{III} + u_{IV})/4 \quad \cdots \quad (4.5)$$

the value of u_G was derived.

At the bottom of Tables 4.2a and 4.2b the calculated values of u_G, $\sqrt{(P_0-P_X)_c}$ and C ($\equiv u_G/\sqrt{(P_0-P_X)_c}$) are tabulated. In Fig. 4.15, values of C are plotted against $\sqrt{(P_0-P_X)_c}$ with different symbols to indicate whether the point was derived from the test condition of T_0 equal to 80 or $280^{\circ}F$.

Fig. 4.16 shows the plotting of the percentage increase of the mainstream velocity per foot length of x. It was derived from the values of u_I, u_{II}, u_{III} and u_{IV} (i.e. the velocities at x equal to 3", 9", 15" and 21" respectively).

(iii) <u>Correlation of experimental data.</u> It can be seen from Fig. 4.15 that the values of C are not affected greatly by the temperature, and that the "C-function" can be represented by a straight line in C vs $\sqrt{(P_0-P_X)_c}$ plane.

From Fig. 4.16 it can be seen that the average rate of the increase of the mainstream velocity in the x-direction is 0.475% of u_G per foot length of x.

The values of E_I, E_{II}, E_{III} and E_{IV} (the thermocouple e.m.f.'s at positions I, II, III and IV respectively) shown in Tables 4.2a and 4.2b indicate that the heat loss through the tunnel wall at the working section was small. The maximum difference of the E's is 0.008 mv which corresponds to less than 0.5^OF.

The values of P_X, P_I, P_{II}, P_{III} and P_{IV} (the mainstream static pressures) of Tables 4.2a and 4.2b indicate that the static pressure variation along x is small. It is less than 0.05% of P_G (absolute).

4.3.3. Summary of results of calibration.

Results of the calibration are summarised below:

(i) Tunnel average mainstream velocity can be derived from the measurements of P_0, T_0 and (P_0-P_X) with the aid of Eqs. (4.2) and (4.3) and Fig. 4.15.

The procedure is as follows:

(a) The value of $(P_0-P_X)_c$ is calculated by substituting P_0, T_0 and (P_0-P_X) into Eq. (4.3).

(b) The value of C is then obtained from Fig. 4.15.

(c) u_G can now be calculated by Eq. (4.2).

(ii) The mean total temperature of the tunnel air can be measured by placing a total temperature probe (Fig. 4.17) at x equal to 12"; the accuracy of this measurement is within $\pm 0.3^{\circ}$F.

(iii) The mainstream static pressure can be gauged by a hole in wall at X.

(iv) The mainstream air velocity increases along the plate at the rate of 0.475% of u_G per foot of the plate length (x) (Fig. 4.16); so the velocity distribution along the plate is satisfactory for the presently intended flat-plate tests.

4.4. Measurements of Heat-transfer Coefficient.

Although the purpose of the measurements was to obtain heat-transfer in compressible turbulent boundary layers at large temperature ratios $(T_{ad,S}/T_S)$, in order to examine the adequacy of the present setting-up and the influence of some factors, e.g. the smoothness of the plate, the shape of the plate leading edge and the turbulence level of the tunnel air, the first experiments were carried out at small temperature ratios (i.e. $1 < T_G/T_S < 1.1$). The reasons are that at slow speeds and small temperature ratios the boundary-layer-fluid properties are essentially uniform and the well confirmed experiments and theories (§3.3.2) are available.

These tests will be reported in §4.4.1; tests with large temperature ratios will be reported in §4.4.2. The difference between those two sets of tests was in the method used to precool the test plate, that is, shop-air instead of liquid nitrogen was used as the coolant for the uniform-property tests. Conclusions from the experiments will be stated in §4.5.

4.4.1. <u>Tests at small temperature ratios.</u>

(i) <u>Procedure and observation.</u> The tunnel-air dewpoint was first checked. The mainstream velocity and temperature were set at suitable values. When the cooling jacket was in the raised position, shop-air was supplied to its middle compartment to cool the test-plate to a required temperature. The cooling jacket was then lowered. On the exposure of the precooled plate to the preset hot air stream, the subsequent plate temperature was recorded against time in terms of the thermocouple e.m.f. versus time. Meanwhile P_0, T_0 and (P_0-P_X) readings were taken. Four tests have been run at the following conditions:

Test No.	1	2	3	4
Re_1	7.80×10^4	7.79×10^4	1.113×10^4	1.174×10^4
T_G °F	183.29	183.18	249.40	236.64
$T_{S,i}$ °F	137.38	139.53	171.56	161.63
TCN	1-6	7-12	1-6	7-12

where Re_1 indicates the Reynolds number per inch, T_G the mainstream-air temperature, T_S the initial plate temperature and TCN the thermocouple number.

The data which were observed during these tests are listed and tabulated in Appendix 4A. 24 T-t curves were obtained from those tabulated data with the aid of Table 3.1 and Fig. 4.8 for the conversion of the thermocouple e.m.f. readings to temperatures. Fig. 4.18 is an example of the typical T-t curves.

(ii) <u>Derivations.</u> From the readings of (P_0-P_X), P_0, E_0 and E_G, the mainstream velocity (u_G), temperature (T_G) and pressure (P_G) were derived by the method of §4.3.3. Reynolds

number per inch (Re_1) was then calculated by the equation:

$$Re_1 = (u_G \rho_G)/(12 \mu_G) \quad \ldots \quad (4.6)$$

where u_G, ρ_G and μ_G are the mainstream velocity in ft/s, density in lb/ft^3, and viscosity in lb/ft s respectively. The relation between μ and T is shown in Fig. 4.19 $\left(4.11, \text{p.504}\right)$. The Reynolds number ($Re_x$) at x" from the leading edge of the plate is then obtained from the equation:

$$Re_x = xRe_1 \quad \ldots \quad (4.7)$$

Heat transfer to a given point at distance x" from the leading edge of the plate was computed from the transient-heat-capacity equation,

$$q = (c \rho \tau)_S (dT/dt)_S \quad \ldots \quad (4.8)$$

where q is the total (convected, conducted, radiated etc.) heat-transfer rate per unit area of the test surface; $c=c(T_S)$ is the specific heat of the plate material (monel) obtained from Refs. 4.12-4.14 (Fig. 4.20); ρ is the density of the wall material (= 0.319 lb/in^3); τ is the wall thickness (= 0.186); and $(dT/dt)_S$ is the time derivative of the wall temperature which was obtained from T-t curves (e.g. Fig. 4.18) with the aid of a mirror, that is, a normal to a point on a curve was first drawn by placing a mirror on the point so that part of the curve and its image in the mirror forms a continuous curve, the slope of the curve was then derived from the slope of the normal. If q is considered to be only convected heat, then the dimensionless heat-transfer coefficient, Stanton number, may be written as:

$$St = \frac{(c \rho r)_S (dT/dt)_S}{(c_p \rho_G u_G)(T_{ad,S} - T_S)} \quad \ldots \quad (4.9)$$

At slow speeds, $T_{ad,S} \approx T_G \approx T_{tot,G}$, so

$$St = \frac{(c \rho r)_S (dT/dt)_S}{(c_p \rho_G u_G)(T_G - T_S)} \quad \ldots \quad (4.10)$$

where $c_p \rho_G u_G$ represents the product of constant pressure specific heat, density and velocity of the mainstream air; T_G is the mainstream temperature; T_S is the wall temperature at the point where the time derivative of temperature was determined.

72 values of Stanton number at conditions of Reynolds number (Re_x) from 1.7×10^4 to 1.7×10^6 and temperature ratio (T_G/T_S) from 1.02 to 1.09 have been calculated and are tabulated in Table 4.3.

(iii) <u>Results and conclusions</u>.   The above calculated Stanton numbers are plotted against Reynolds number in Fig. 4.21. For the purpose of comparison, theoretical curves (a,b and c) are also drawn in the Fig. 4.21. The curves (a) and (b) were derived from the exact solutions of uniform-property-laminar-boundary-layer equations at the conditions of zero pressure gradient, Prandtl number equal to 0.7, and temperature difference $(T_G - T_S)$ respectively equal to constant (4.15) and proportional to x (4.16); the curve (c) was derived from Eq. 4.1 with $S = 1.162$ and c_f being calculated by Eq. 2.72.

Fig. 4.21 reveals that (i) the boundary layer was kept laminar

state till Reynolds number got to about 8×10^4 and the transition completed at Reynolds number equal to about 1.2×10^5, (ii) in the laminar region, the present data agree with the curve (b) and (iii) in the turbulent region, the data agree with the curve (c) which is also in agreement with the other experimental results for the uniform-property turbulent boundary layer as previously shown (see Fig. 3.4).

Fig. 4.22 shows the typical wall temperature variations along the test plate. It can be seen from this figure that the variation of the wall temperature is much greater in the laminar region than it is in the turbulent region. Theoretically, in the laminar region [4.16] .

$$St = B/Re_x^{\frac{1}{2}} \qquad \dots \qquad (4.11)$$

where B is a constant;   so the temperature difference $(T_G - T_S)$ is proportional to $\sqrt{x}$. This is consistent with the present results as shown in Fig. 4.21 by the curve (b) and the experimental data lying in the laminar region.

The conclusions are therefore that the present method of measurements is reliable and that the setting-up of the apparatus is satisfactory for the purpose of obtaining the data for the turbulent boundary layer on a smooth solid flat plate at uniform temperature.

4.4.2.. Tests at large temperature ratios.

(i) Procedure and observations. The procedure for the tests at large temperature ratios was essentially the same as that previously described for the tests at the small temperature ratios

($4.4.1.), except that liquid nitrogen instead of shop-air

was used as the coolant in order to obtain large property

variations in the boundary layer: The method of cooling the

test plate with liquid nitrogen has been described in sub-

section (iii) of §4.2.2. 8 tests (No. 8 to 12) have been run

at the following conditions.

Test No.	5	6	7	8
Re_1	6.92×10^4	9.31×10^4	6.46×10^4	61.5×10^4
$T_G^o F$	77.61	81.30	238.57	238.51
$T_{S,i}{}^o F$	-274.91	-290.33	-301.45	-301.43
TCN	7-12	7-12	1-6	7-12

Test No.	9	10	11	12
Re_1	3.82×10^4	5.60×10^4	4.99×10^4	6.10×10^4
$T_G^o F$	228.50	236.07	245.77	240.69
$T_{S,i}{}^o F$	-277.62	-298.93	-300.21	-299.36
TCN	11	11	11	11

The observed data are listed and tabulated in Appendix 4B.

28 T-t curves were obtained from those tabulated data. An

example of those curves is shown in Fig. 4.23.

(ii) Derivations. The derivation of the mainstream

characteristics (u_G, P_G and T_G) from the observed data of (P_0-P_X),

P_0, E_O and E_G has been described in §4.4.1. The Reynolds number

was then calculated by Eqs. (4.6) and (4.7). Eq. (4.10),

$$St' = \frac{(c\rho\gamma)_S (dT/dt)_S}{(c_p \rho_G u_G)(T_G - T_S)} \qquad \ldots \qquad (4.10)$$

was used to calculate the Stanton number (St'), where the time

derivative of temperature $(dT/dt)_S$ was obtained from the T-t

curves by the method of "mirror and image" as described in

sub-section (ii) of §4.4.1. The symbol St' has been introduced

here for the Stanton number derived from Eq. (4.10). It is

because these values will be corrected for pertinent experimental

errors and the symbol St is reserved for the data after correction

for the experimental errors has been made. The values of St' ,

Re_x and T_G/T_S are given in Table 4.4.

(iii) <u>Experimental errors</u>. The Stanton number (St') derived

above subjects to two basics types of error: (a) error whose

magnitude can be evaluated and (b) error whose magnitude cannot

be accurately calculated.

The first type of error is due to the radiation, condensation

and non-uniform wall temperature. Details of the method of

the evaluation of this type of error are described in Appendix

4C. The correction has been made for the values of St'; the

maximum correction required was not greater than 6.5%. The

corrected Stanton-number data are shown in Table 4.4 as St.

The second type of error contributes to the uncertainty of

the accuracy of the experimental data. It consists of the

effective turbulent starting position, the temperature potential,

the T-t slope measurement, the effect of the increased plate

thickness and surface roughness due to the frost deposition. An

estimate has been made for each of these items. Details of the

estimation are given in Appendix 4D. It was found that the total

uncertainty is about 8%.

(iv) Results and discussion.

(a) Results. Heat transfer through turbulent boundary

layers on a smooth solid flat plate at the slow mainstream speed

($M_G \approx 0.2$) and large temperature ratio has been measured by the

transient technique. Stanton number at seven different temperature

ratios, namely, T_G/T_S = 1.25(0.25)2.5 and 2.7, were evaluated.

Table 4.4 and Fig. 4.24 give a summary of the test conditions and

the evaluated heat-transfer and boundary-layer parameters.

Smoothed experimental data of Stanton number are plotted in

Fig. 4.25. As shown by this figure, for a given value of Re_x,

St increases with increasing rate of heat transfer to the plate

(the highest rate corresponds to the highest T_G/T_S); for a given

T_G/T_S, St decreases with increasing Re_x.

(b) Comparison between theories and experiments.

The experimental Stanton-number data of Table 4.4 will be

compared with theoretical predictions. As the theoretical Stanton

number is evaluated by Eq. (3.1), i.e.,

$$St = S.c_f/2 \qquad \ldots \qquad (3.1)$$

the comparison will first be made on the basis of a fixed Reynolds-

analogy factor (S) with the different c_f theories and then on

the basis of a fixed c_f theory with different S theories.

Comparison based upon a fixed Reynolds-analogy factor. The

theoretical values of Stanton number have been computed by Eq.3.1

with S equal to 1.162 (§ 3.4) and c_f being evaluated by four

different methods, namely, those of van Driest-I [4.21], van Driest-II [4.22] , Eckert [4.23] and §2.5.3. The first three of these four methods are representative examples for a large number of theories based upon (i) the Prandtl differential equation, (ii) the von Karman differential equation and (iii) the incompressible formula with reference properties; and the fourth method is the present semi-empirical method.

Comparison of the computed Stanton-number values and the experimental data is shown in Fig. 4.26. At the moderate rate of heat-transfer (say, at $T_G/T_S = 1.5$), the degrees of correlation achieved by all the four theories are about the same. The agreement between the experiments and the theories of van Driest-II and Eckert, however, becomes less favourable as T_G/T_S increases, whilst the agreement between the experiments and the respective predictions by the method of van Driest-I and the method of §2.5.3 remains good at all the temperature ratios explored.

Although the van Driest-I method and the present method (§2.5.3) give about the same predictions for the present case of low Mach-number flow, the two theories have different implications as discussed in §2.4.4.   That is, the $F_{R\delta}$ function of the van Driest-I theory is:

$$F_{R\delta} = (\mu_G/\mu_S)(\rho_S/\rho_G)^{\frac{1}{2}}$$

$$= (T_G/T_S)^{1.26}, \text{ for low Mach-number flow } \dots \quad (4.11)$$

whilst the $F_{R\delta}$ function of the method of §2.5.3 is:

$$F_{R\delta} = (\mu_G/\mu_S)(E/E_i)$$
$$= (T_G/T_S)^{0.702}(T_{ad,S}/T_S)^{0.772}$$
$$= (T_G/T_S)^{1.472}, \text{ for low Mach-number flow} \ldots (4.12)$$

As c_f is a weak function of $F_{R\delta}$, the small difference in the

indices of (T_G/T_S) of Eqs. (4.11) and (4.12) for the condition

of low Mach-number flow does not give appreciable difference

in the c_f values. However, at large M_G, the difference between

Eqs. (4.11) and (4.12) is great. For example, at the condition

of the adiabatic wall, the two $F_{R\delta}$ functions become:

$$F_{R\delta} = (T_{ad,S}/T_G)^{-1.26} \quad \ldots \quad (4.13)$$

and $\qquad F_{R\delta} = (T_{ad,S}/T_G)^{-0.702} \quad \ldots \quad (4.14)$

respectively. The failure of the Eq. (4.13) to correlate c_f

data at large M_G for the adiabatic wall case has been shown in

§2.3 (see RMS error for the van Driest-I method shown in Table

2.6); so the agreement between the van Driest-I method and the

present experimental results is entirely accidental. The method

of §2.3.5 should therefore be used to evaluate the c_f values.

As it was shown in §3 that the effect of heat-transfer on

the values of S is small, the above comparison has therefore

indirectly confirmed the adequacy of the method of §2.5.3 for

the evaluation of c_f. In order to examine the effect of heat

transfer on the values of S in greater details, the present St

data giving S with c_f being evaluated by the method of §2.5.3 will

be examined below.

Comparison based upon a fixed drag theory. With the experimental

St data of Table 4.4 and the theoretical c_f values of §2.5.3, the

values of S at various Re_x and T_G/T_S have been calculated. They
are plotted in Figs. 4.27 and 4.28 versus Re_x and T_G/T_S respectively.

As the range of Re_x covered by the present experiments is
small, it is expected that there is no appreciable variation of
the value of S at a given T_G/T_S for the present data. This is
confirmed by Fig. 4.27, where the data of S are plotted versus Re_x.

The average values of Re_x and T_G for the present
experiments are at around 1×10^6 and $600^{\circ}R$ respectively. The
theoretical values of S at the average condition (i.e.
$Re_x = 1 \times 10^6$ and $T_G = 600^{\circ}R$ with Pr being the value at the wall,
namely at $T = T_S = 600 T_S/T_G \,^{\circ}R$) have been computed by the methods
of Prandtl-Taylor [4.1, p.206] , Colburn [4.24], Rubesin [4.25],
van Driest [4.22], Spence [4.26] , Deissler and Loeffler [4.27]
and Spalding and Jayatillaka [4.28] ; and they are plotted
against T_G/T_S in Fig. 4.28 in order to compare themselves with
the experiments. It can be seen in this figure that the theories
which give the best agreement with the experiments at the small
temperature ratio still give the best agreement at the large
temperature ratio. It is because the influence of T_G/T_S on the
value of S indicated by the experiments as well as the theories
is small. Hence the use of a constant value of S which is
suitable for the uniform-property turbulent boundary layer is
also adequate for the large temperature ratios.

Fig. 4.29 shows the extent to which the present St data
are correlated by the method using S equal to 1.162 and c_f
from §2.5.3. The degree of correlation achieved is seen to be

provides a qualitative guidance to the law for the transitional region.

It was seen in §2.4.4 (Table 2.7) that the position of the intersection in discussion is mainly a function of $T_{ad,S}/T_S$ regardless of the difference in M_G and Re_x. It is therefore plausible that the law of wall for the transitional region and consequently the S function are also dependent mainly on $T_{ad,S}/T_S$ regardless of the difference in M_G and Re_x. The present experiments have indicated that the effect of $T_{ad,S}/T_S$ up to about 3 imposed on the value of S is negligibly small.

Although the experiments were carried out at low Mach number, from the above discussion it is plausible that the effect of $T_{ad,S}/T_S$ at the other Mach number is also small. Furthermore, the effect of M_G (up to 10) and Re_x (from 10^5 to 10^8) at smaller $T_{ad,S}/T_S$ on the value of S has already been confirmed to be small by the other published results as it was seen in §3. Hence the confidence in the use of S equal to 1.162 for the range of Re_x from 1×10^5 to 1×10^8, M_G up to 10 and $T_{ad,S}/T_S$ up to 3 has now been increased.

4.5. Conclusions.

The heat-transfer rates have been measured on a smooth solid flat plate at slow speed flow of air by the transient technique. The first experiments were carried out at small temperature ratios (i.e. $1 < T_{ad,S}/T_S < 1.1$). The results are found to be in agreement with the other reported data for the incompressible turbulent

boundary layer, so the setting-up of the apparatus is believed to be satisfactory.

The subsequent experiments were carried out at the larger temperature ratios. The values of Stanton number at seven temperature ratios (namely, $T_{ad,S}/T_S$ equal to 1.25(0.25)2.50 and 2.7) have been evaluated. The increase in the value of St for a fixed value of Re_x with decreasing $T_{ad,S}/T_S$ and the decrease in the value of St for a fixed value of $T_{ad,S}/T_S$ with increasing Re_x are consistent with the predictions recommended in §3.

The present experimental results therefore confirm the adequacy of the method recommended for the prediction of c_f and support the applicability of a constant S (= 1.162) for $T_{ad,S}/T_S$ up to about 3. The data reported in other publications (reviewed in §3) have been obtained at smaller $T_{ad,S}/T_S$ than the present data, but at greater M_G and Re_x (or $Re_{\delta 2}$); they also support the applicability of the constant S. It is therefore plausible that the combined effect of Mach number, Reynolds number and temperature ratio is also small; so the use of the prediction:

$$St = S.c_f/2 \qquad \cdots \qquad (4.1)$$

with S = 1.162 and c_f being evaluated by the method of §2.5.3 is believed to be adequate for the range of conditions which have now been explored experimentally, i.e. for Re_x from 1×10^5 to 1×10^8, M_G up to 10 and $T_{ad,S}/T_S$ from 0.5 to 3.

Fig. 4.30 shows the degree of correlation achieved by the

recommended method. The agreement between the predictions and the experiments is seen to be about $\pm10\%$ which is believed to be about the accuracy of the experiments having so far been achieved.

CHAPTER 5

CONCLUSIONS

In conclusion the results of this research can be summarised as follows:

5.1. Frictional Drag.

(i) The theoretical treatments given by earlier authors are classified, reviewed and where necessary extended; then the predictions of twenty of these theories are evaluated and compared with all experimental data, the root-mean-square error being computed for each theory. The theory of van Driest-II [5.1] gives the lowest root-mean-square error (11.0%).

(ii) A new calculation procedure has been developed semi-empirically from the postulate that a unique relation exists between $c_f F_c$ and $Re F_R$ where c_f is the drag coefficient, Re is the Reynolds number and F_c and F_R are functions of Mach number and temperature ratios. When compared with all experimental data, the predictions of the new procedure not only give a low root-mean-square error (9.9%), but also give a better correlation at large $T_{ad,s}/T_s$ than the van Driest-II predictions.

(iii) The extent to which the procedure correlates the existing experimental data can be judged by inspection of Figs. 2.18 to 2.20. In view of the fact that experiments have been carried out in several entirely different pieces of apparatus and are not of high accuracy, the correlation is entirely satisfactory.

(iv) The procedure is simple and quick to use in engineering calculations and its accuracy is only limited (at the present time) by the accuracy of the experimental data from which it is in part derived.

(v) The necessary auxiliary functions have been tabulated in Tables 2.8 to 2.10 and plotted in Figs. 2.21 and 2.22 for ready reference.

(vi) The procedure is capable of greater refinement when more accurate experimental data are available, say, by modification of F_R functions.

5.2. Heat Transfer.

(i) Theoretical treatments for the Reynolds-analogy factor (S) are reviewed, classified and compared. It was found that for the flow of air the effect of Reynolds number, Mach number and temperature ratio on the value of S predicted by all the theories is small.

(ii) Measured Stanton number reported in other publications are collected. Using these, the dependence of S on Mach number, Reynolds number and heat-transfer condition is examined. The drag is calculated for the same conditions as the Stanton-number measurements using the recommended procedure. Experimental St data giving S are too scanty to check the small effect of M_G, Re_x (or $Re_{\delta 2}$) and $T_{ad,S}/T_S$ on the value of S predicted by the various theories. However, it was found that a constant S equal to 1.162 represents a good mean for all the conditions so far explored experimentally.

(iii)   The recommended method for the evaluation of St is simply by multiplying the $c_f/2$ (by the presently recommended procedure) by 1.162. The extent to which this method correlates the data in other publications can be seen in Figs. 3.15 to 3.17. In view of the unavoidable discrepancies existing between the data from different sources, the correlation is satisfactory.

(iv)   With regard to the experimental Stanton-number data available in the other literature, the data at large heat-transfer rates (i.e. at $T_{ad,S}/T_S$ greater than 1.6) are scarce. It is proposed to obtain additional data at large $T_{ad,S}/T_S$ so as to check the applicability of the constant Reynolds-analogy factor (S = 1.162) beyond the range of the heat-transfer conditions for which experimental data are available in the other literature.

5.3. Experiments.

(i)   Heat Transfer through turbulent boundary layer on a smooth flat plate at slow speed flow of air has been measured by the transient technique and the values of Stanton number at $T_{ad,S}/T_S$ up to 2.7 have been evaluated.

(ii)   The present experimental results confirm the applicability of the constant S (= 1.162) for large heat-transfer rates, when the drag is calculated by the recommended procedure. The close agreement between the experiments and the theory can be seen in Fig. 4.29.

5.4. Summary of Recommended Procedure of Calculation. For the turbulent boundary layer of air on a smooth flat solid plate, when the Reynolds number, Mach number and temperature ratio are known, the procedure for the evaluation of the frictional drag

coefficient and Stanton number is as follows:

(i)   The value of F_c is determined from Table 2.9 or Fig. 2.22.

(ii)   The value of $F_{R\delta}$ is determined from Eq. (2.96) or Table 2.10 or Fig. 2.22 and when necessary the value of F_{Rx} is obtained from the equation,

$$F_{Rx} = F_{R\delta}/F_c \qquad \cdots \qquad (5.1)$$

(iii)   By using the input value of $Re_{\delta 2}$ (or Re_x) and the values of $F_{R\delta}$ (or F_{Rx}) and F_c above, c_f or $\bar{c}_f$ can be obtained from Table 2.8 or Fig. 2.21.

(iv)   The value of St (or $\overline{St}$) is then obtained by the equation,

$$St = 0.581(c_f) \qquad \cdots \qquad (5.2)$$

or
$$\overline{St} = 0.581(\bar{c}_f) \qquad \cdots \qquad (5.3)$$

The above calculation can be performed in a few minutes with an accuracy of one per cent, the latter is, of course, within the limit of experimental accuracy at the present time.

CHAPTER 6

SUGGESTIONS FOR FURTHER WORK.

It is suggested that the present theory should be extended and developed in the following ways:

1. There is need for experimental work of greater range and higher accuracy, so that the theory can be further refined. Simultaneous measurements of skin-friction coefficient and Stanton number are required. Data at various Mach number and temperature ratio would be required, but data at large $T_{ad,S}/T_S$ would be of particular interest.

2. In the above development of the method of predictions for flat-plate friction and heat transfer, a formulation has been used which can well be adapted to a later extension to the situation with finite pressure gradient. That is, the drag coefficient has been related to the Reynolds number based upon momentum thickness as well as that based upon distance along the wall.

For the application of the present method to the case with mainstream pressure gradient, the calculation of the shape parameter defined by:

$$H_{12} = \delta_1/\delta_2 \qquad \ldots \qquad (6.1),$$

where δ_1 is the displacement thickness of the boundary layer, would be required. This would then be used with the momentum equation to determine the development of the boundary layer.

3. For the flow of air at high Mach number and/or temperature, the wall is often transpiration cooled. In Ref. 6.1 an extension to include the mass transfer has been made. In that extension the F_R function, for the zero mass-transfer case, was similar to that of the van Driest-II theory. It should now be examined whether the extension based upon the present F_R function would improve the predictions.

4. When the speed of aircraft becomes so great that the temperature of the surrounding air becomes sufficiently high, the air components partially dissociate. The present method should also be extended to include the effect of dissociation imposed on the frictional drag and heat transfer.

5. Finally, it should be mentioned that the present subject could also be approached in a more fundamental manner than that described in the present thesis. For example, it has been seen above that the presently recommended expressions for F_c and F_R imply the existence of a "Law of Wall" based upon the von Karman mixing length and the influence of heat transfer on the value of 'E'. A hypothesis for E should be provided.

For this purpose, initial work confined to the careful measurements and analyses of velocity and temperature profiles at low Mach number and different temperature ratios (T_S/T_G much less than unity would be of particular interest) should be fruitful. The next step would be to find the effect of Mach number, Reynolds number and temperature ratio.

With regard to the analyses of the measured velocity and temperature profiles, particular attention to the effect of Reynolds number, Mach number and temperature ratio on the laminar sub-layer and transitional intermediate-layer should first be given. This might lead to a Law of Wall with a reliable hypothesis for E.

Although a good law of wall is useful in formulating various boundary-layer functions (e.g. drag and heat transfer) which are of great practical interests, it is not expected to be in entire agreement with the experiments. For example, Professor Spalding has accounted for the discrepancy between the Law of Wall and the experiments by an entrainment law [6.2] . The effect of Reynolds number, Mach number and temperature ratio on the entrainment law should also be examined.

REFERENCES

2. Frictional Drag.

2.1. F. Smith and R. Harrop, "The turbulent boundary layer with heat transfer and compressible flow". ARE TN Aero.1759, (1946).

2.2. E. R. van Driest, "Turbulent boundary layer in compressible fluids". J. Aero. Sci., Vol.18,pp.145-160, 216, (1951).

2.3. L. E. Kalikman, "Turbulent boundary layer in gas flow past a flat plate". Doklady Akad. Nauk SSSR, Vol.106, pp. 123-126, (1956).

2.4. W. H. Dorrance, "Dissociation effects upon compressible turbulent *boundary* layer skin friction and heat transfer." Convair Sci.Res.Lab.,Res. Rept.No.6 (1960).

2.5. S. S. Kutateladze and A. I. Leontev, "Drag law in a turbulent flow of a compressible gas and the method of calculation friction and heat transfer." Discussion on Heat and Mass transfer, Akad.Nauk BSSR, Minsk, pp.1-23, (1961, Translation TIL T5258).

2.6. F. Frankl and V. Voishel, "Turbulent friction in the boundary layer of a flat plate in a two dimensional flow of compressible gas at high speeds." NACA TM 1052 (1943).

2.7. R. E. Wilson, "Turbulent boundary layer characteristics at supersonic speed -- theory and experiments." J. Aero.Sci., Vol.17,pp.585-594, (1950).

2.8. M. W. Rubesin, R.C. Meydew and S. A. Varga, "An analytical and experimental investigation of the skin friction of the turbulent boundary layer on a flat plate at supersonic speeds." NACA TN 2305, (1951).

2.9. E. R. van Driest. "The turbulent boundary layer with variable Prandtl number." 50 Years Boundary Layer Theory, Frieder-Vieweg und Sohn, Braunschweig, ed. H. Gortler and W. Tollmien, pp.257-271, (1955).

2.10. R. G. Deissler and A. L. Loeffler, "Analysis of turbulent flow and heat transfer on a flat plate at high Mach number with variable fluid properties." NASA TR R-17, (1959).

2.11. D. H. Clemmow, "The turbulent boundary layer flow of a compressible fluid along a flat plate." ARC 14051, RM 1568, DGWRD Rept. 5016, (1951).

2.12. C. Ferrari, "Study of the boundary layer at supersonic speeds in turbulent flow: Case of flow along a flat plate." Quar. Appl. Math. Vol.8 pp. 33-57, (1950).

2.13. T. Y. Li and H. T. Nagamatsu, "Effect of density fluctuations on the turbulent skin friction of an insulated plate at high supersonic speed." J. Aero. Sci. Vol.18, pp. 696-700, (1951).

2.14. S. I. Kosterin and Y. A. Koshmarrov, "The turbulent boundary layer on a flat plate in a uniform stream of a compressible fluid." Soviet Physics, Vol.4, pp. 819-828 (1960).

2.15. W. G. Cope, "The turbulent boundary layer in compressible flow". ARC R & M 2840, (1943).

2.16. R. J. Monaghan, "Comparison between experimental measurements and a suggested formula for the variation of turbulent skin friction in compressible flow." ARC CP 45, (1950).

2.17. Th. von Karman, "The problem of resistance in compressible fluids." 5th Volta Congress. Rome, pp. 255-264, (1935).

2.18. M. Tucker, "Approximate calculation of turbulent boundary layer development in compressible flow." NACA TN 2337 (1951).

2.19. C. B. M. Young and E. Janssen, "The compressible boundary layer." J. Aero. Sci. Vol. 19, pp. 229-236 (1952).

2.20. S. C. Sommer and B. J. Short, "Free flight measurements of turbulent boundary layer skin friction in the presence of severe aerodynamic heat at Mach number from 2.8-7.0." NACA TN 3391, (1955).

2.21. E. R. G. Eckert, "Engineering relations for friction and heat transfer to surface in high velocity flow." J. Aero. Sci. Vol.22 pp. 585-587, (1955).

2.22. C. duP Donaldson, "On the form of the turbulent skin friction law and its extension to compressible flow". NACA TN 2962,(1952).

2.23. E. M. Winkler, "Investigation of flat plate hypersonic, turbulent boundary layers with and without heat transfer." J. Appl. Mech., Trans. ASME, Vol. 28, Ser.E. pp. 323-329 (1961).

2.24. D. A. Spence, "Distribution of velocity, enthalpy and shear stress in the compressible turbulent layer on a flat plate". RAE Rept. Aero. 2631, (1959).

2.25. O. R. Burggraf, "The compressible transformation and the turbulent boundary layer equations." J. Aero/Sp.Sci., Vol. 29, pp. 434-439, (1962).

2.26. D. E. Coles, "The turbulent boundary layer in a compressible fluid." Rand Corp. Rept. R.403-PR, (1962).

2.27. D. R. Chapman and R. H. Kester, "Measurements of turbulent skin friction on cylinders in axial flow at subsonic and supersonic velocity." J. Aero. Sci., Vol. 20, pp. 441-448, (1953).

2.28. J. B. Peterson, "A comparison of experimental and theoretical results for the compressible turbulent boundary-layer skin friction with zero pressure gradient". NASA TN D-1795, (1963).

2.29. H. Schlichting, "Boundary Layer Theory." Translated by J. Kestin, McGraw Hill Book Co., Inc., London, 4th ed., (1960).

2.30. C. C. Lin , "Turbulent Flows and Heat Transfer." Oxford University Press, London, (1959).

2.31. H.M. Spivak, "Experiments in the turbulent boundary layer of a supersonic flow." Aero. Phys. Lab., Nor. Am. Avia., Rept. GM-615, AL-1052 (1950).

2.32. P. F. Brinich and N. S. Diaconis, "Boundary layer development and skin friction at Mach number 3.05." NACA TN 2742, (1952).

2.33. W. F. Cope, "The measurement of skin friction in turbulent boundary layer at Mach number of 2.5, including the effect of shock wave." Proc. Roy. Soc., Ser. A, No. 1120, Vol. 215, pp. 84-99, (1952).

2.34. S. Dahwan, "Direct measurements of skin friction." NACA TN 2567, (1952).

2.35. R. J. Monaghan and J. E. Johnson, "The measurement of heat transfer and skin friction at supersonic speeds. Part II Boundary layer measurements on a flat plate at M = 2.5 and zero heat transfer". ARC CP 64, (1952).

2.36. R. J. Monaghan and J. R. Cooke, "The measurements of heat transfer and skin friction at supersonic speeds. Part IV Tests on a flat plate at M = 2.82." ARC CP 140, (1953).

2.37. D. R. Chapman and R. H. Kester, "Turbulent boundary layer and skin friction measurements in axial flow along cylinders at Mach number between 0.5 and 3.6". NACA TN 3097, (1954).

2.38. D. Coles, "Measurements of turbulent friction on a smooth flat plate in supersonic flow". J. Aero. Sci., Vol. 21, pp. 433-448, (1954).

2.39. R. M. O'Donnell, "Experimental investigation at a Mach number of 2.41 of average skin-friction coefficients and velocity profiles for laminar and turbulent boundary layers and an assessment of probe effects."
NACA TN 3122, (1954).

2.40. R. J. Hakkinen, "Measurements of Turbulent skin friction on a flat plate at transonic speeds."
NACA TN 3486, (1955).

2.41. R. H. Korkegi, "Transition studies and skin friction measurements on an insulated flat plate at Mach number of 5.8". J. Aero. Sci., Vol. 23, pp. 97-107, 192, (1956).

2.42. F. E. Goddard, "Effect of uniformly distributed roughness on turbulent skin friction drag at supersonic speeds."
J. Aero./Sp. Sci., Vol.26, pp. 1-25,24, (1959).

2.43. F. W. Matting, D. R. Chapman, J. R. Nyholm and A. G. Thomas, "Turbulent skin friction at high Mach numbers and Reynolds numbers in air and helium."
NASA TR R-82, (1961).

2.44. I. H. Abbot, "Some factors contributing to scale effect at supersonic speeds." AGARD Memo. AG8/M4 (1953).

2.45. R. J. Monoghan and J. R. Cooke, "The measurements of heat transfer and skin friction at supersonic speeds. Part III Measurements of overall heat transfer and of the associated boundary layers".

ARC CP 139, (1953).

2.46. C. C. Pappas, "Measurements of heat transfer in the turbulent boundary layer on a flat plate in supersonic flow and comparison with skin friction results."

NACA TN 3222, (1954).

2.47. F. K. Hill, "Boundary layer measurements in hypersonic flow." J. Aero. Sci., Vol.23 pp. 35-42 (1956).

2.48. F. K. Hill, "Turbulent boundary layer measurements at Mach number from 8-10". Phys. of Fluids, Vol. 2., pp. 668-680, (1959).

2.49. G. Kempf, "Neue Ergebnisse der Widerstandsforschung." Werft Reederei, Hafen, Vol. 11., pp. 234-239, (1929).

2.50. K. E. Schoenherr, "Resistance of flat surface moving through a fluid." Trans. Soc.Nav. Arch. Mar. Eng., Vol. 40, pp. 279-297, (1932).

2.51. F. Schults-Grunow, "New frictional resistance law for smooth plates." NACA TM 986, (1941).

2.52. K. Wieghart, "On the turbulent friction layer for rising pressure." NACA TM 1314, (1944).

2.53. F. R. Hama, "The turbulent boundary layer along a flat plate, I. and II." Rept. Inst. Sci. and Tech., Tokyo, Japan, Vol. 1, pp. 13-19, (1947).

2.54. H. Ludwig and W. Tillmann, "Investigation of the
wall-shearing stress in turbulent boundary layers."
NACA TM 1285 (1949).

2.55. P. S. Klebanoff and Z. W. Diehl, "Some features of
artificially thickened fully developed turbulent boundary
layers with zero pressure gradient." NACA TN 2475 (1951).

2.56. T. A. Dutton, "The accuracy of measurement of turbulent
skin friction by means of surface pitot-tubes and the
distribution of skin friction on a flat plate".
ARC R & M 3058, (1957).

2.57. H. S. Mickley and R. S. Davis, "Momentum transfer for
flow over a flat plate". NACA TN 4017, (1957).

2.58. L. Landweber and T. T. Siao, "Comparison of two
analyses of boundary layer data on a flat plate."
J. Ship Res., Vol. 1, pp. 21-33, (1958).

2.59. D. W. Smith and J. H. Walker, "Skin friction measurements
in incompressible flow." NACA TN 4231, (1958).

2.60. V. M. Falkner, "A new law for calculating drag (the
resistance of a smooth flat plate with turbulent boundary
layer)". Aircraft Engineering, Vol. 15, pp. 65-69, (1943).

2.61. G. Hughes, "Frictional resistance of smooth plane surfaces
in turbulent flow – New data and a survey of existing data".
Trans. Inst. Nav. Arch., Vol. 94, pp. 287-322, (1952).

2.62. D. B. Spalding, "A single formula for the law of the wall".
J. Appl. Mech., Trans. ASME, Ser.E., pp. 445-458, (1961.)

2.63.   D. B. Spalding, "A new analytical expression for the drag
        of flat plate valid for both the turbulent£laminar regimes".
        Int. J. Heat Mass Transfer, Vol. 5, pp. 1133-1138, (1962).

2.64.   J. Kaye, "Survey of friction coefficients, recovery factors,
        and heat-transfer coefficients for supersonic flow." J.
        Aero. Sci., Vol. 21, pp. 117-129, (1954).

2.65.   J. R. Stalder, M. W. Rubesin and T. Tendeland, "A
        determination of the laminar-, transitional-, and
        turbulent-boundary-layer temperature-recovery factors on
        a flat plate in supersonic flow".
        NACA TN 2077, (1950).

2.66.   W. F. Hilton, "Wind-tunnel test for temperature recovery
        factors at supersonic velocities." J. Aero. Sci.,
        Vol. 18, pp. 97-100, (1951).

2.67.   E. G. Slack, "Experimental investigation of heat-transfer
        through laminar and turbulent boundary layers on a cooled
        flat plate at a Mach number of 2.4". NACA TN 2686, (1952).

2.68.   M. J. Brevoort and B. D. Arabian, "Summary of experimental
        heat-transfer coefficients for supersonic flow". J. Aero
        Sci., Vol. 21, pp. 117-129, (1954).

2.69.   P. F. Brinich, "Recovery temperature, transition and heat-
        transfer measurements at Mach 5." NASA TN D-1047, (1961).

2.70.   H. E. Hügel, "Velocity profiles in turbulent compressible
        flow". DIC thesis, (1963).

3. Heat Transfer.

3.1. E. R. G. Eckert and R. M. Drake, "Heat and Mass Transfer".
McGraw-Hill, New York, (1959).

3.2. M. W. Rubesin, "A modified Reynolds analogy for the
compressible turbulent boundary layer on a flat plate."
NACA TN 2917, (1953).

3.3. Th. von Karman, "The analogy between fluid friction and
heat transfer." Trans. ASME, Vol. 61, pp. 705-710, (1939).

3.4. H. Reichardt, "The principles of turbulent heat transfer."
NACA TM 1048, (1957).

3.5. F. Smith and R. Harrop, "Turbulent boundary layer with
heat transfer and compressible flow." RAE TN Aero 1559,
(1946).

3.6. R. G. Deissler and A. L. Loeffler, "Analysis of
turbulent flow and heat transfer on a flat plate at high
Mach numbers with variable fluid properties". NASA TR
R-17, (1959).

3.7. D. B. Spalding and C. L. V. Jayatillaka, "A survey of
theoretical and experimental information on the resistance
of the laminar sub-layer to heat and mass transfer." 2nd
All-Union Conference on Heat Mass Transfer, Minsk, BSSR,
Paper No. 2-30, (1964).

3.8. E. R. van Driest, "Turbulent boundary layer with variable
Prandtl number." 50 years boundary layer theories. Frieder-
Vieweg und Sohn, Braunschweig, pp. 257-271, (1955).

123.

3.9. D. A. Spence, "Distribution of velocity, enthalpy and shear stress in the compressible turbulent boundary layer on a flat plate". RAE Rept. Aero. 2631, (1959).

3.10. A. P. Colburn, "A method of correlating forced convection heat-transfer data and a comparison with fluid friction." Trans. Am. Inst. Chem. Eng., Vol. 29, pp. 174-210, (1933).

3.11. W. C. Reynolds, W. H. Kays and J. S. Kline, "Heat transfer in turbulent incompressible boundary layer. — 1. Constant wall temperature." NASA Memo. 12-1-58W, (1958).

3.12. J. E. Johnson and R. J. Monaghan, "Measurement of heat transfer and skin friction at supersonic speeds. – Preliminary results of measurements on flat plate at Mach number of 2.5." ARC CP 59, (1951).

3.13. R. J. Monaghan and J. R. Cooke, "The measurement of heat transfer and skin friction at supersonic speeds – Part III Measurements of overall heat transfer and of the associated boundary". ARC CP 139, (1953).

3.14. R. J. Monaghan and J. R. Cooke. "The measurement of heat transfer and skin friction at supersonic speeds. – Part IV Tests on a flat plate at M = 2.82". ARC CP 140, (1953).

3.15. C. C. Pappas and M. W. Rubesin, "Heat transfer in the compressible turbulent boundary layer on a flat plate". Heat Transfer and Fluid Mech.Inst. Preprint of papers, pp. 19-28, (1953).

3.16. C. C. Pappas, "Measurement of heat transfer in the turbulent boundary layer on a flat plate in supersonic flow and comparison with skin-friction results." NACA TN 3222, (1954).

3.17. J. R. Jack and N. S. Diaconis, "Heat transfer measurements on two bodies of revolution at Mach number of 3.12". NACA TN 3776, (1956).

3.18. M. J. Brevoort and B. D. Arabian, "Summary of experimental heat-transfer measurements in turbulent flow for a Mach number range from 0.87 to 5.05". NACA TN 4248, (1958).

3.19. T. Tendeland, "Effects of Mach number and wall-temperature ratio on turbulent heat transfer at Mach numbers from 3 to 5". NASA TR R-16, (1959).

3.20. F. K. Hill, "Turbulent boundary layer measurements at Mach numbers from 8 to 10." Phys. of Fluids, Vol. 2, pp. 668-680, (1959).

3.21. P. F. Brinich, "Recovery temperature, transition and heat-transfer measurements at Mach 5". NASA TN D-1047, (1961).

3.22. E. M. Winkler, "Investigation of flat plate hypersonic turbulent boundary layer with heat transfer". Trans. ASME, Vol. 28, pp. 323-329, (1961).

3.23. D. S. Johnson, "Velocity and temperature fluctuation measurements in a turbulent boundary layer downstream of a stepwise discontinuity in wall temperature". J. Appl. Mech., Vol. 26, pp. 325-336, (1959).

3.24. E. R. G. Eckert, "Survey on heat transfer at high speeds". ARL 189, (1961).

4. Experiments.

4.1. S. S. Sugawara and T. Sato, "Heat transfer on the surface of a flat plate in the forced flow." Memo. of Faculty of Engineering, Kyoto University, Japan, Vol. 14, No.1, pp. 21-37, (1952).

4.2. J. R. Jack and N. S. Diaconis, "Heat transfer measurements on two bodies of revolution at Mach number of 3.12". NACA TN 3776, (1956).

4.3. M. . Brevoort and B. D. Arabian, "Summary of experimental heat-transfer measurements in turbulent flow for a Mach number range from 0.87 to 5.05". NACA TN 4248, (1958).

4.4. P. F. Brinich, "Recovery temperature, transition, and heat-transfer measurements at Mach 5". NASA TN D-1047, (1961).

4.5. BSI, "Reference tables of thermocouples (copper v. constantant)." BS 1828, (1961).

4.6. R. J. Monaghan and J. R. Cooke, "The measurement of heat transfer and skin friction at supersonic speeds. Part III - Measurements of overall heat transfer and of the associated boundary layers on a flat plate at $M_1 = 2.43$". ARC CP 139, (1953).

4.7. A. F. H. Ali, "Heat transfer from a flat surface to a moving fluid". Ph.D. Thesis, London (1951).

4.8. H. B. Squire and K. G. Winter, "The Royal Aircraft

Establishment 4 ft x 3 ft experimental low turbulence

wind tunnel. Part I – General flow characteristics."

ARC R & M 2690,(1953).

4.9. A. B. Cambel and B. H. Jennings, "Gas Dynamics".

McGraw-Hill, New York, (1958).

4.10. J. H. Keenan and J. Kaye, "Gas Tables". John Wiley,

New York (1957).

4.11. E. R. G. Eckert and R. M. Drake, Jr.,"Heat and Mass

Transfer". McGraw-Hill, New York, (1959).

4.12. W. F. Hampton and J. H. Mennie, "The specific heat of

Monel metal between -183° and $25^{\circ}C$". Canadian J. Res.

Vol. 7, pp. 677-679,(1932).

4.13. T. B. Douglas and J. L. Dever, "Enthalpy and specific

heat of corrosion resistant alloys at high temperatures."

J. Res. NBS Res. Paper 2560, Vol. 54, pp. 15-19, (1950).

4.14. R. J. Corruceini and J. J. Gniewek, "Specific heats and

enthalpies of technical solids at low temperatures, a

compilation from the literature."NBS Mono. 21, (1960).

4.15. D. B. Spalding and H. L. Evans, "Mass transfer through

laminar boundary layers – 3. Similar solutions of b-equation".

Int. J. Heat Mass Transfer, Vol. 2, pp. 314-341, (1961).

4.16. S. Levy, "Heat transfer to constant-property-laminar

boundary layer flows with power-function free-stream velocity

and wall temperature variation". J. Aero. Sci., Vol. 19,

pp. 341-348,(1952).

4.17. W. H. McAdams,"Heat Transmission". 3rd ed., McGraw-Hill, New York, (1954).

4.18. D. B. Spalding, "Convective mass transfer - an introduction". Edward Arnold, London (1963).

4.19. J. Hilsenrath et al. "Tables of Thermodynamic and Transport properties". Pergamon, Oxford,(1960).

4.20. H. Schlichting, "Boundary Layer Theory". 4th ed., McGraw-Hill,London,(1960).

4.21. E. R. van Driest, "Turbulent boundary layer in compressible fluids". J. Aero. Sci., Vol. 18, pp. 145-160, 216,(1951).

4.22. E. R. van Driest, "The turbulent boundary layer with variable Prandtl number". 50 Years Boundary Layer Theory, Frieder-Vieweg und Sohn, Braunschweig, Ed. Gortler and W. Tollmien, pp. 257-271,(1955).

4.23. E. R. G. Eckert, "Survey on heat transfer at high speeds". Aeronautical Research Laboratory, Office of Aerospace Research, United States Air Force, Report No. ARL.189,(1961).

4.24. A. P. Colburn, "A method of correlating forced convection heat-transfer data and a comparison with fluid friction". Trans. Am.Inst. Chem. Eng., Vol. 29, pp. 174-210, (1933).

4.25. M. W. Rubesin, "A modified Reynolds analogy for the compressible turbulent boundary layer on a flat plate". NACA TN 2917, (1953).

4.26. D. A. Spence, "Distribution of velocity, enthalpy and shear stress in the compressible turbulent boundary layer on a flat plate". RAE Rept. Aero. 2631, (1959).

4.27. R. G. Deissler and A. L. Loeffler, "Analysis of turbulent flow and heat transfer on a flat plate at high Mach numbers with variable fluid properties". NASA TR R-17, (1959).

4.28. D. B. Spalding and C. L. V. Jayatillaka, "A survey of theoretical and experimental information on the resistance of the laminar sub-layer to heat and mass transfer". 2nd All-Union Conference on Heat Mass Transfer, Minsk, BSSR, Papaer No. 2-30, (1964).

5. Conclusions.

5.1. E. R. van Driest, "Turbulent boundary layer with variable Prandtl number." 50 Years Boundary Layer Theories. Frieder-Vieweg und Sohn, Braunschweig, Ed. H. Gortler and W. Tollmien, pp. 257-271, (1955).

6. Suggestions for Further Work.

6.1. D. B. Spalding, D. M. Auslander and T. R. Sundarum, "Heat and mass transfer in boundary layers. Part I: Transpiration cooling". Northern Research and Engineering Corporation, Massachusetts, U.S.A., and London, England, Report No. 1058-1, (1962).

6.2. D. B. Spalding, "A unified theory of friction, heat transfer and mass transfer in the turbulent boundary layer wall jet". Imperial College, Mech. Eng. Dept. Rept. April, 1964.
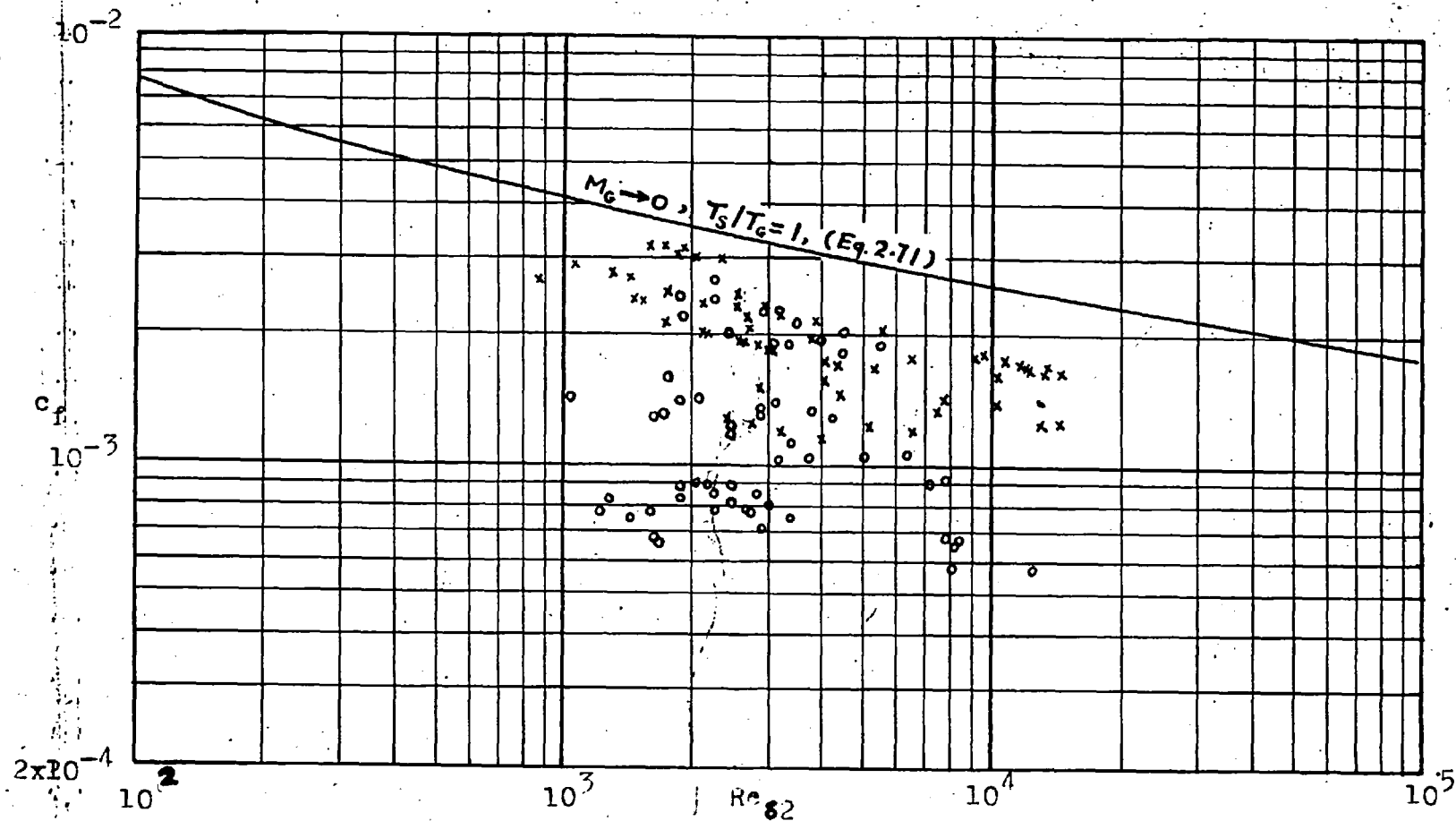
Fig.2.1 Collected experimental data of c_f vs Re_{δ_2} in compressible turbulent boundary layer. ×, adiabatic; o, with heat transfer.
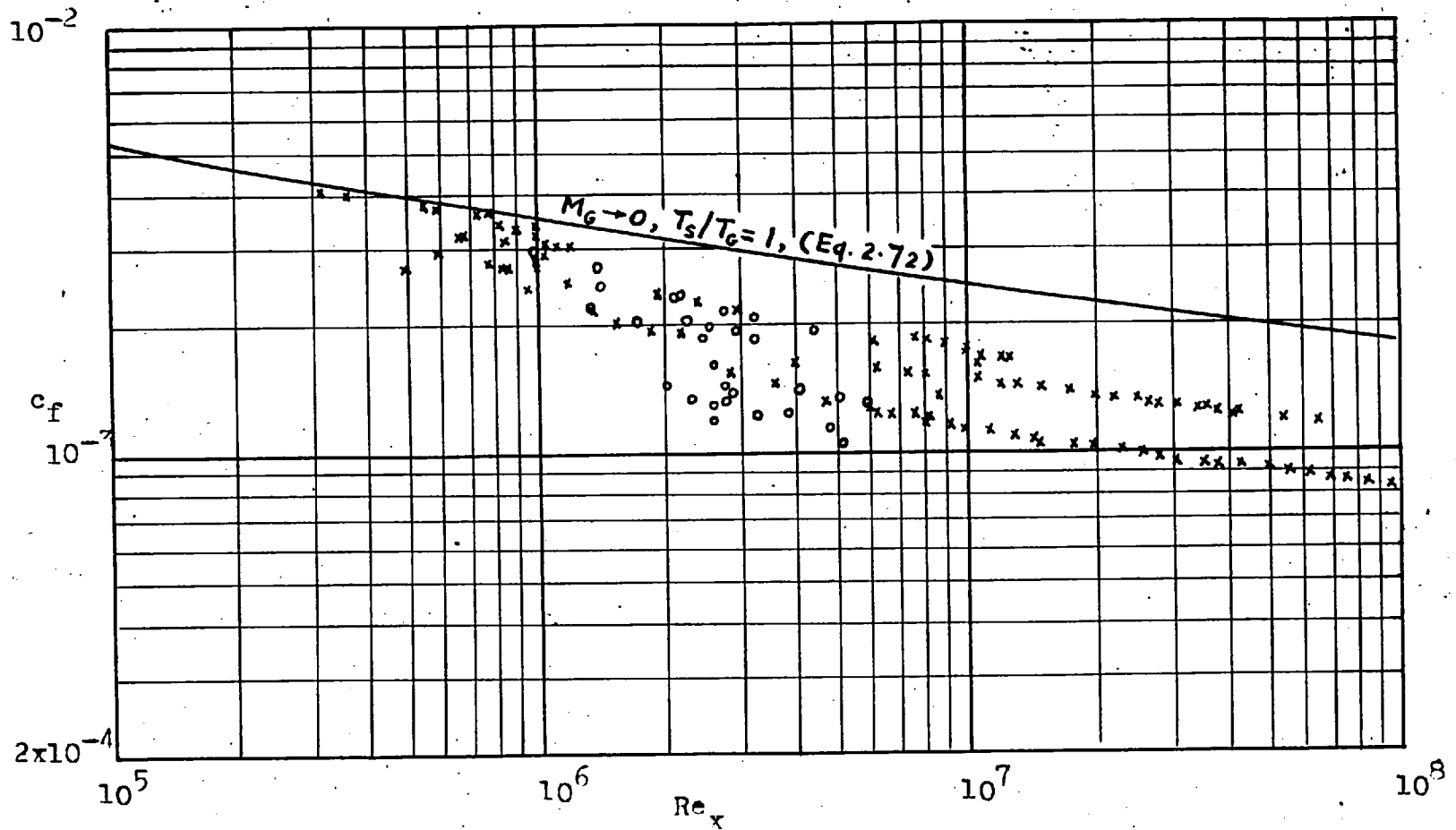
Fig.2.2 Collected experimental data of c_f vs Re_x in compressible
trubulent boundary layer. x, adiabatic: o, with heat transfer.
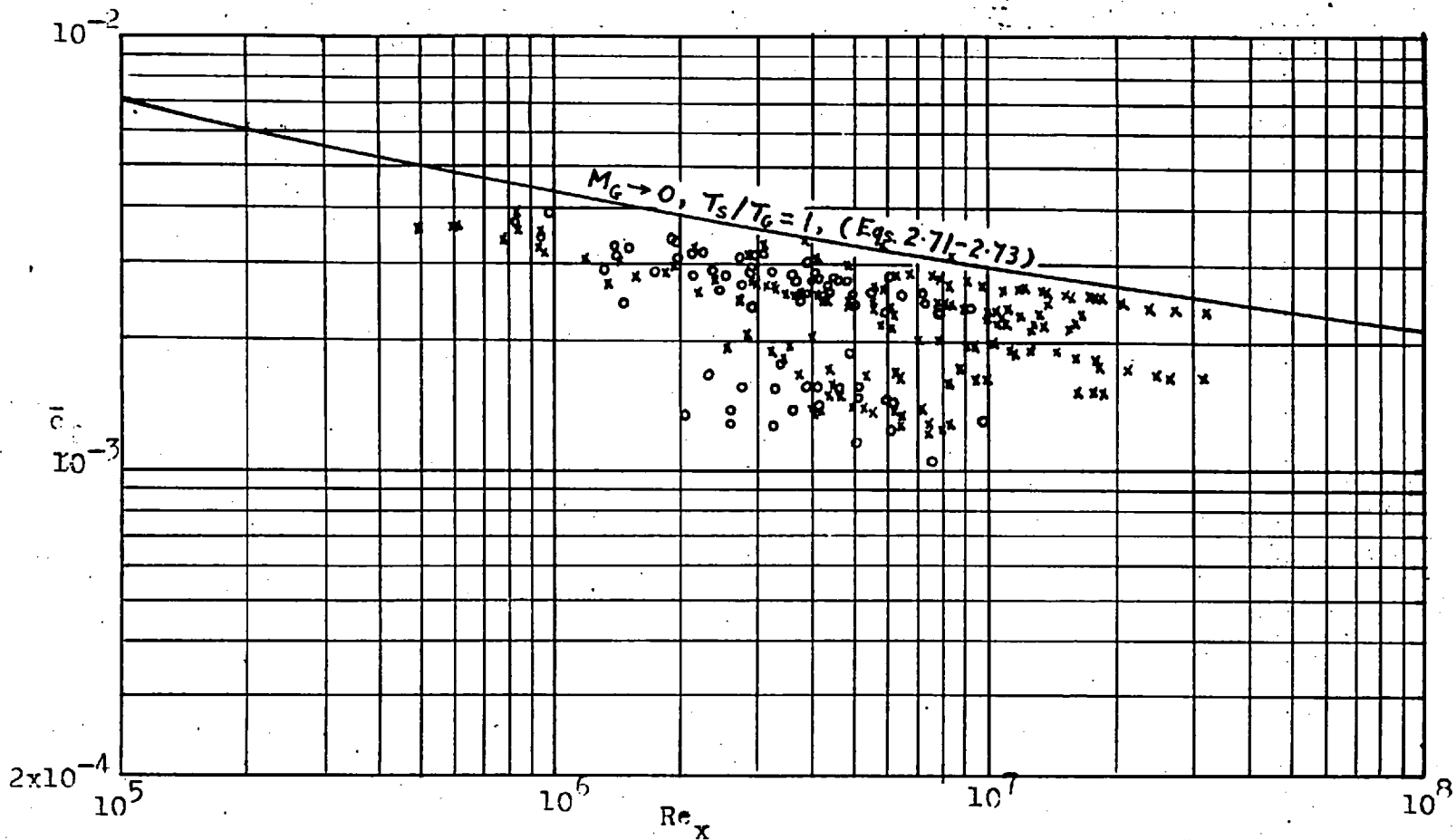
Fig.2.3 **Collected** experimental data of $\bar{c}_f$ vs Re_x in compressible
turbulent boundary layer. x, adiabatic; o, with heat
transfer.
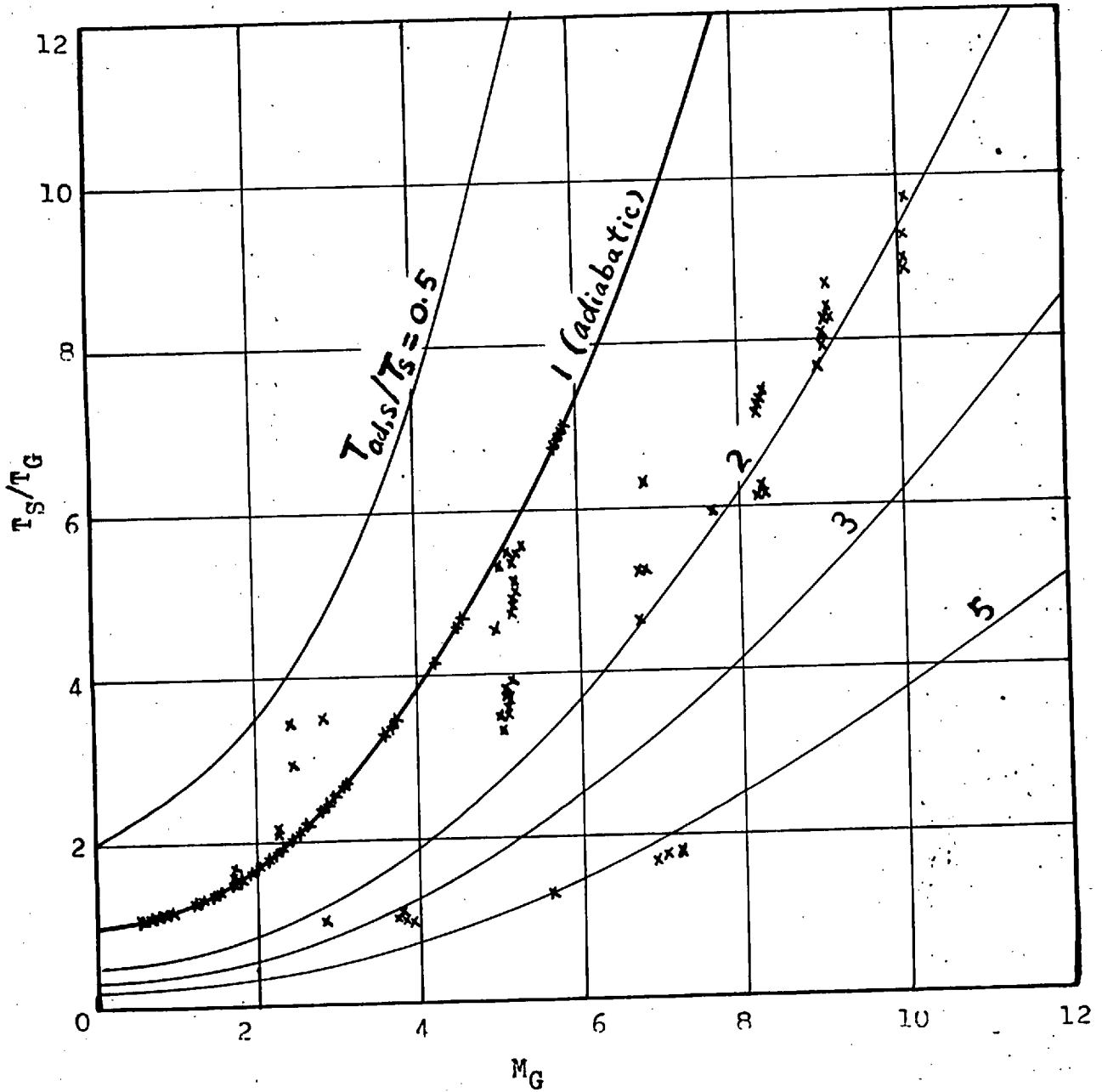
Fig. 2.4 Area of conditions explored experimentally, (for drag).
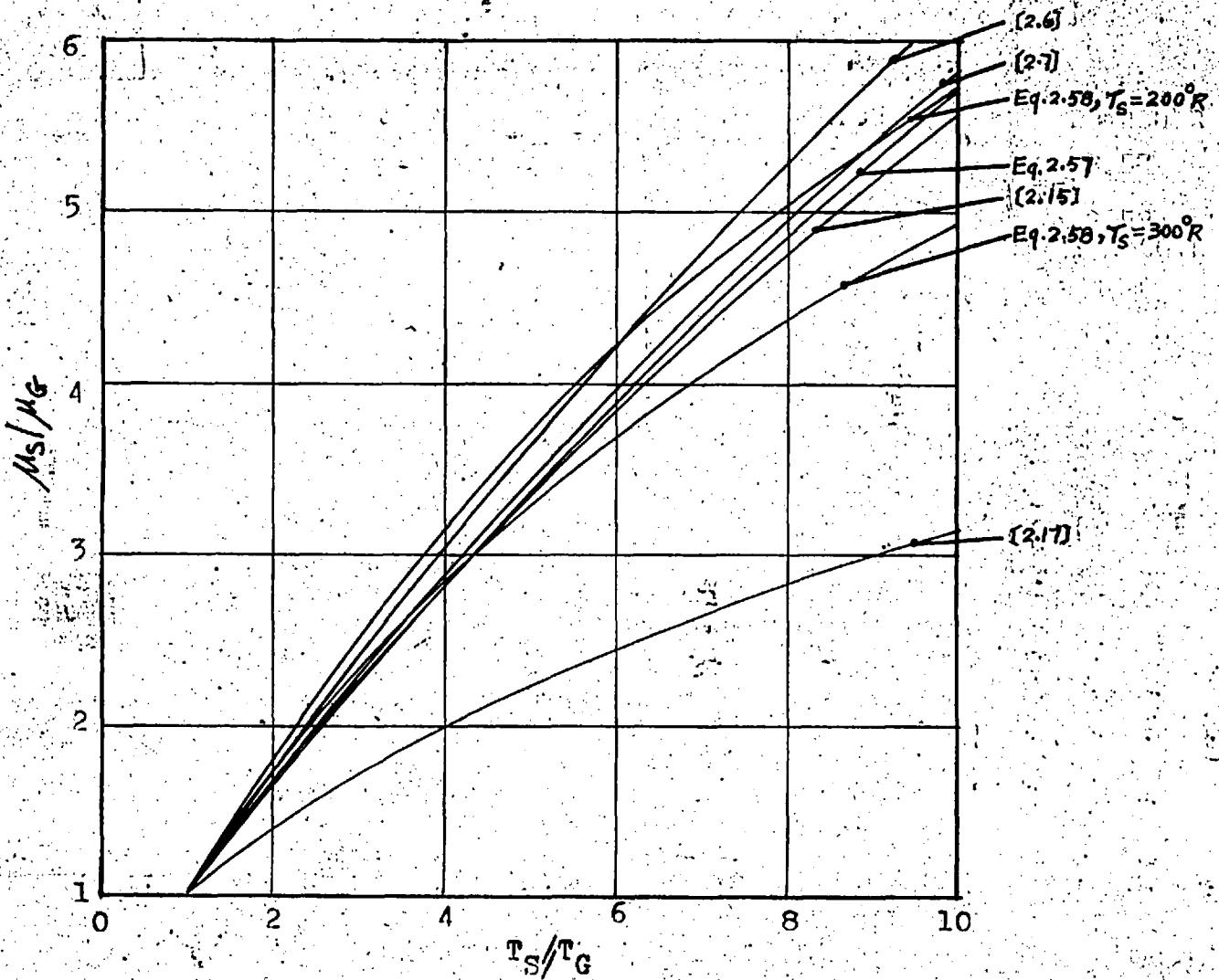
Fig.2.5. Comparison of various viscosity-temperature laws.

Root Mean Square of $(\bar{c}_{f,exp}/c_{f,th} - 1)$ in %

35 — Smith & Harrop [2·1]

Prandtl Differential Equation (§2·2·2)
Von Karman Differential Equation (§2·2·3)
Fixed Velocity Profile (§2·2·5)
Reference Temperature (§2·2·6)
Miscellaneous (§§2·2·4 & 2·2·7)

— Von Karman (2·17)

— Frankl & Voishel [2·6]

— Clemmow-I [2·11]

— Cope-I [2·15]
— Monaghan [2·16]
— Cope-II [2·15]

— Burggraf [2·25]

— Winkler [2·23]

— Young & Janssen [2·19]

— Van Driest-I [2·2]

— Eckert [2·21]
— Tucker [2·18]

— Donaldson [2·22]
— Clemmow-II [
— Spence [2·24]

— Sommer & Short [2·20]

— Kutateladze & Leont'ev [2·5]

— Wilson [2·7]
— Van Driest-II [2·9]

Present Method

Fig. 2.6 Comparison of theories with experimental data.

Fig. 2.7. Comparison of theories with uniform-property data, c_f vs $Re_{\delta2}$.
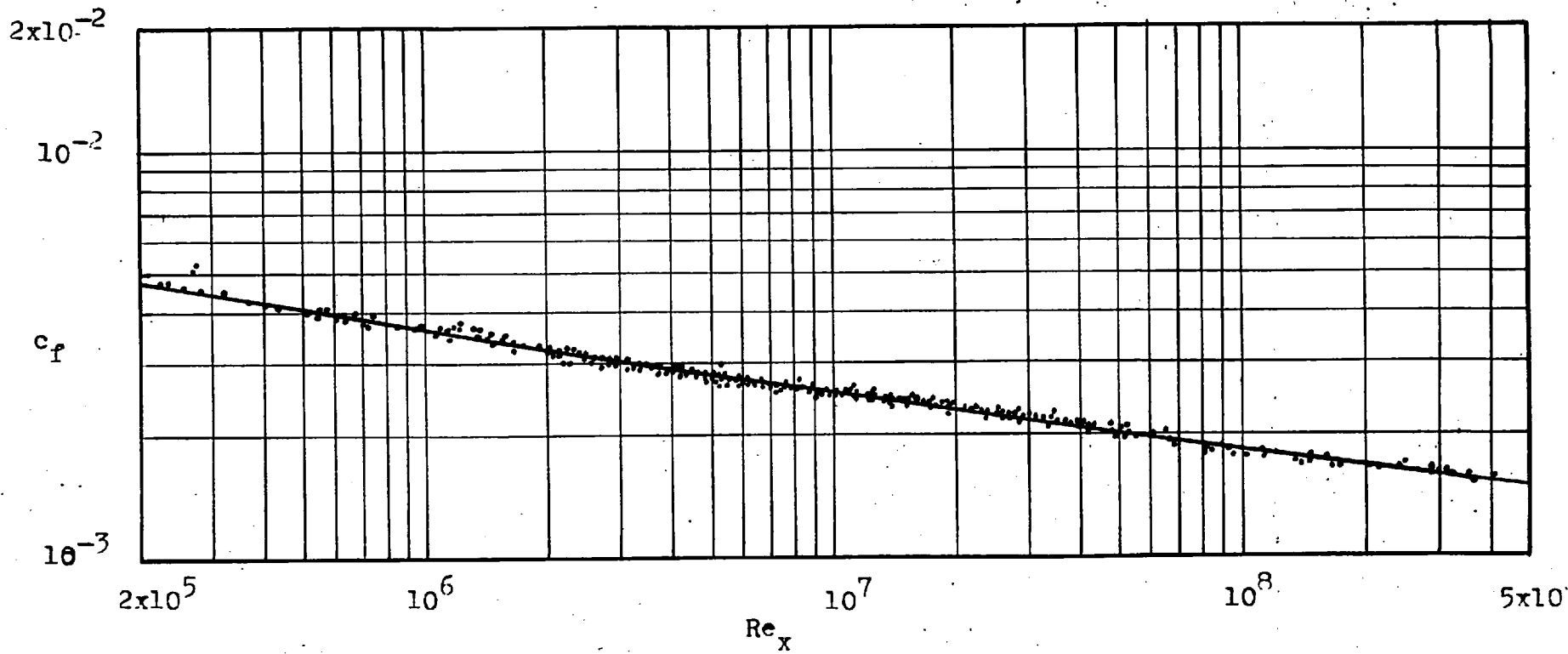
Fig.2.8 Comparison of Eq.(2.72) with uniform-property data,
c_f vs Re_x.
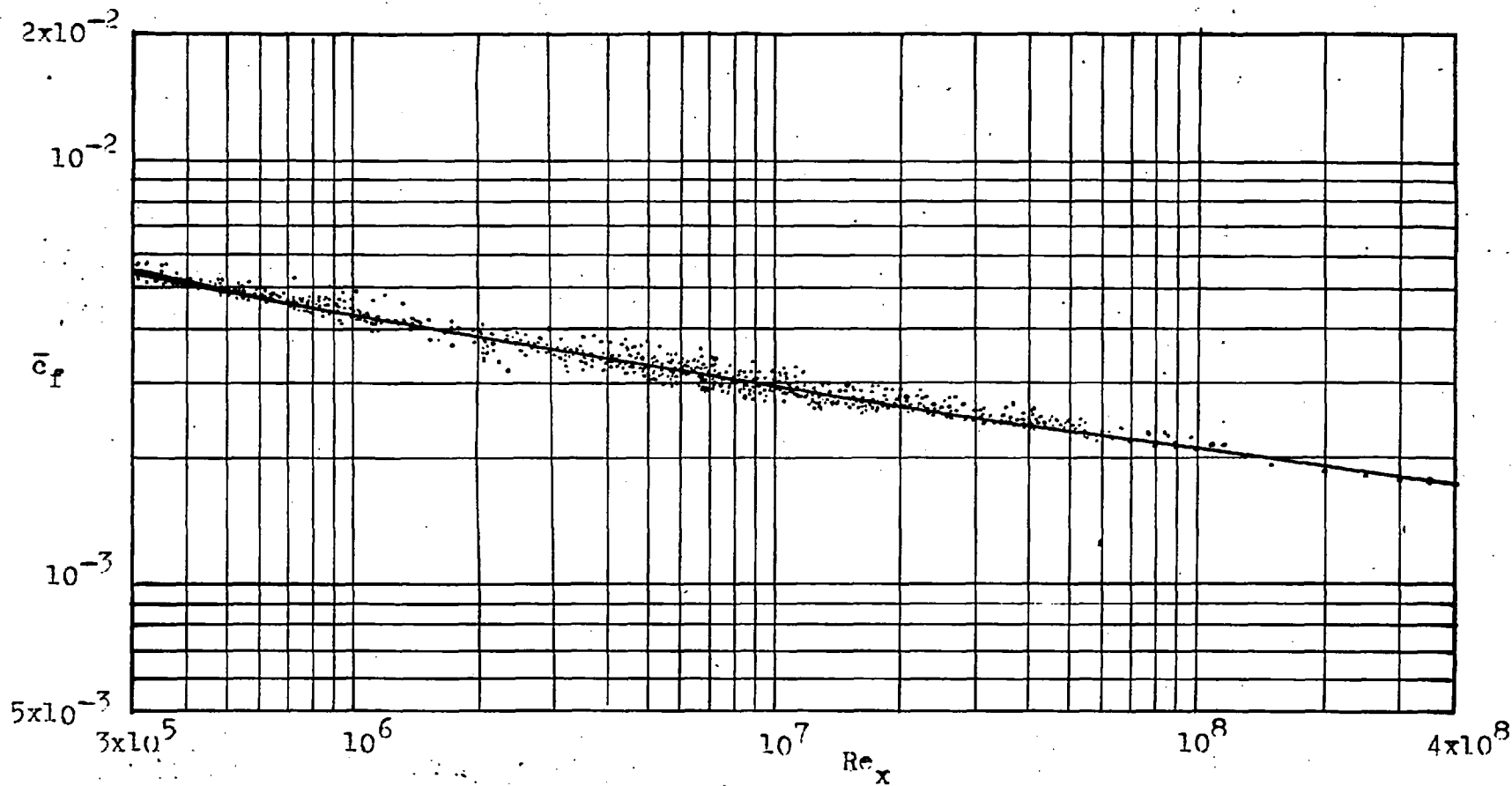
Fig.2.9 Comparison of Eq.(2.73) with uniform-property data,
$\bar{c}_f$ vs Re_x.
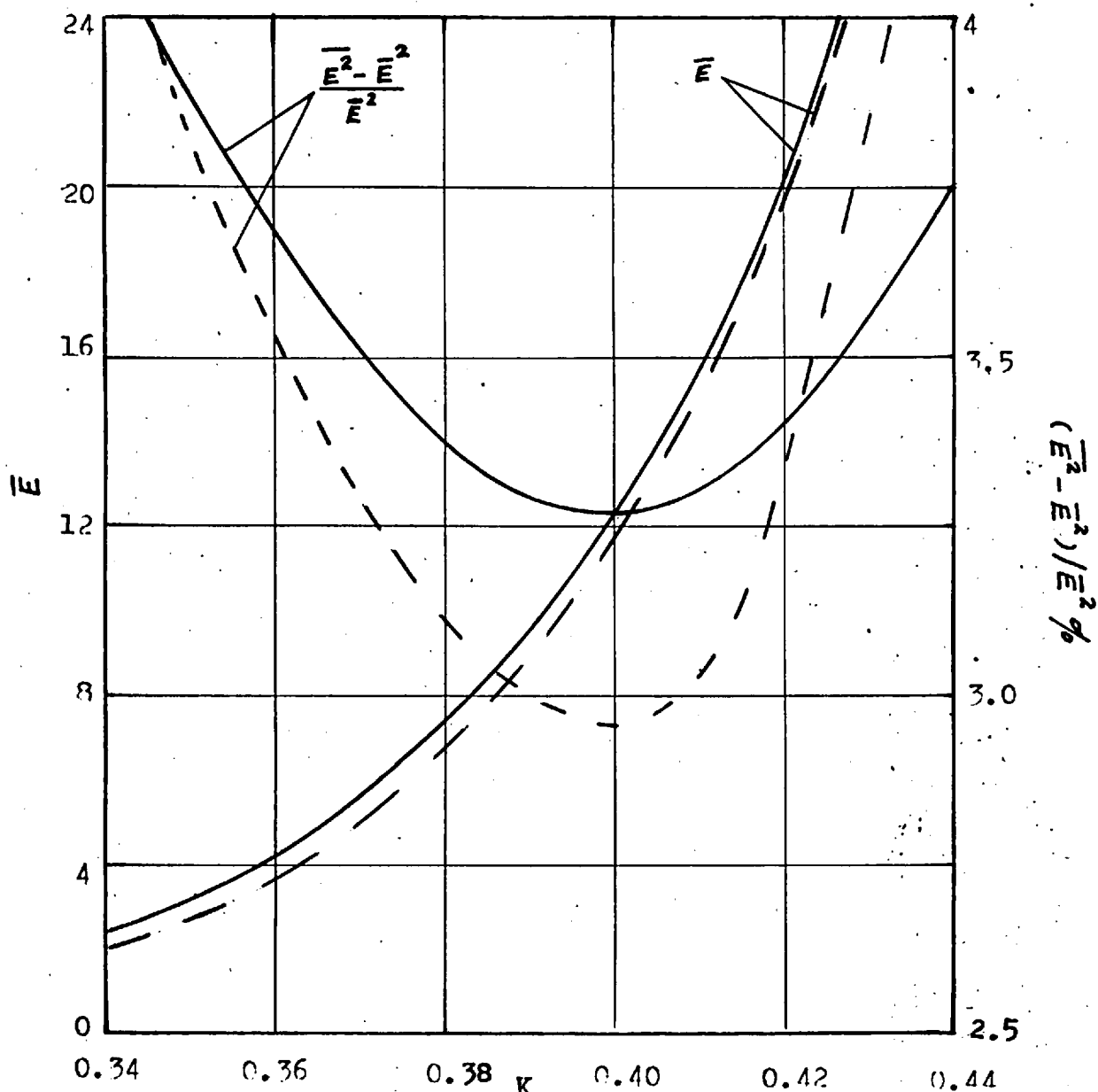
Fig. 2.10 $\overline{E}$ and $(\overline{E^2}-\overline{E}^2)/\overline{E}^2$ vs K from uniform-property data. ——— from c_f vs $Re_{\delta 2}$; - - - from c_f vs Re_x.
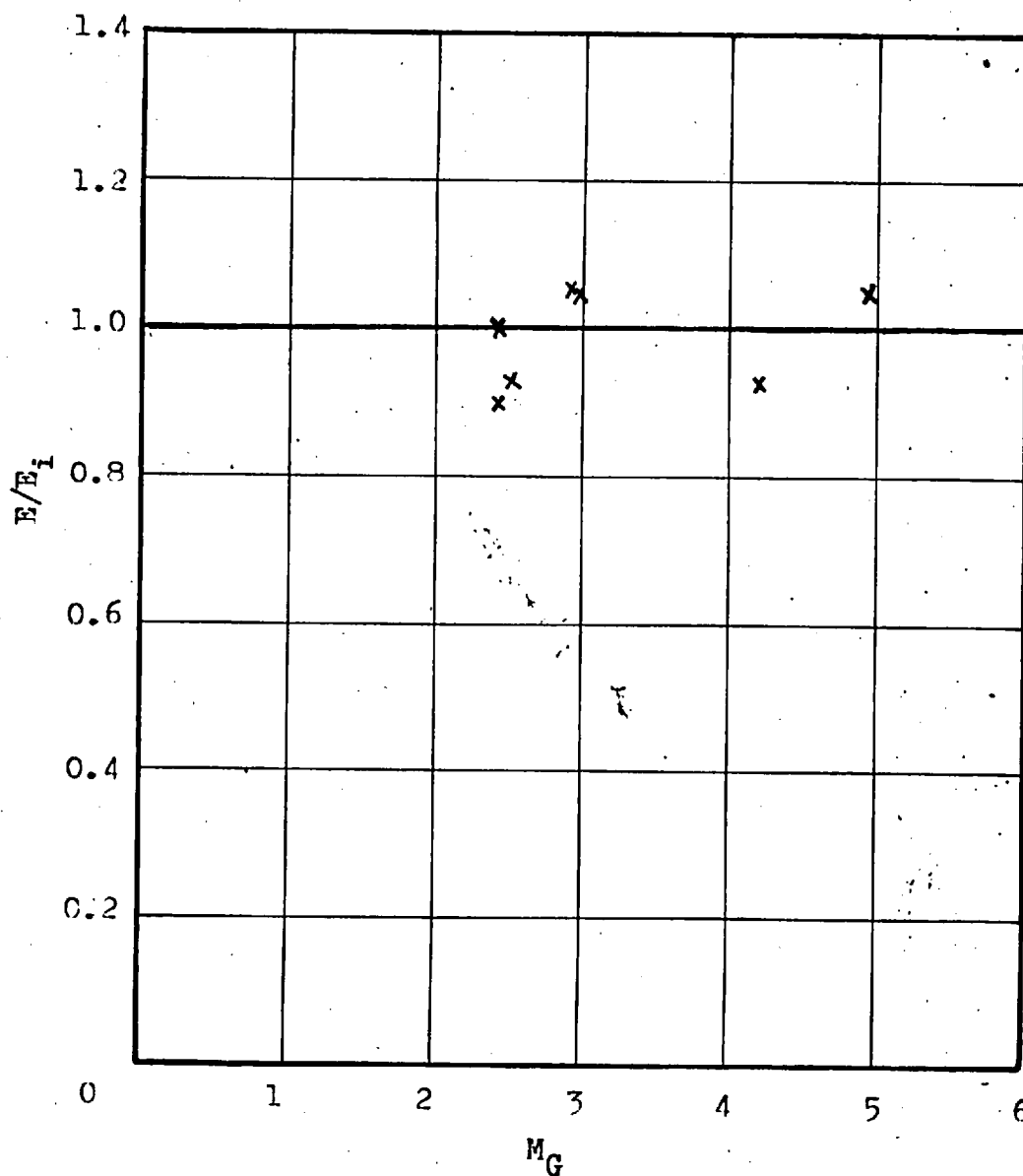
Fig.2.11 E/E_i vs M_G for adiabatic wall case from measured velocity profiles.
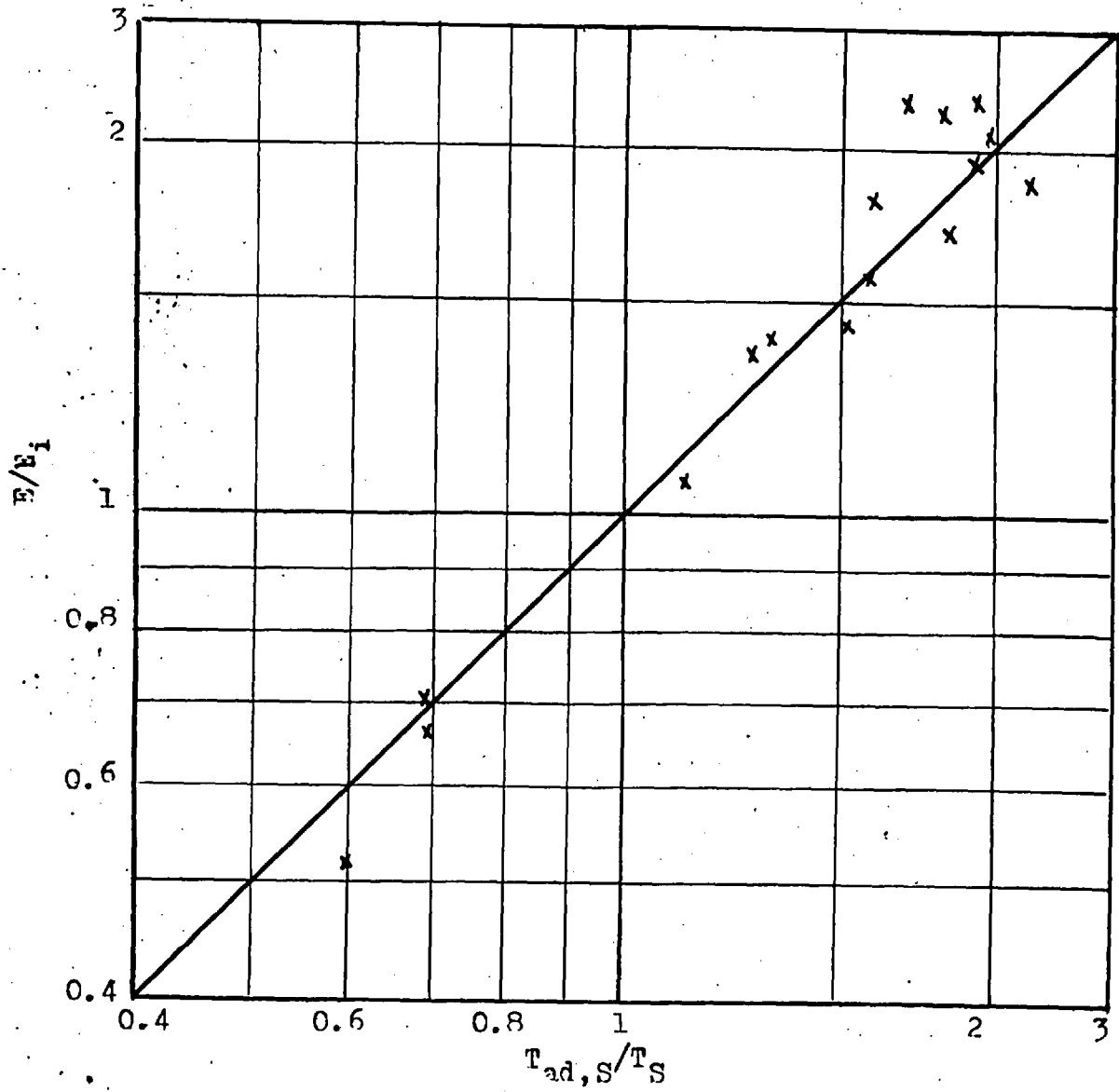
Fig.2.12 E/E_i vs $T_{ad,S}/T_S$ derived from measured velocity profiles.
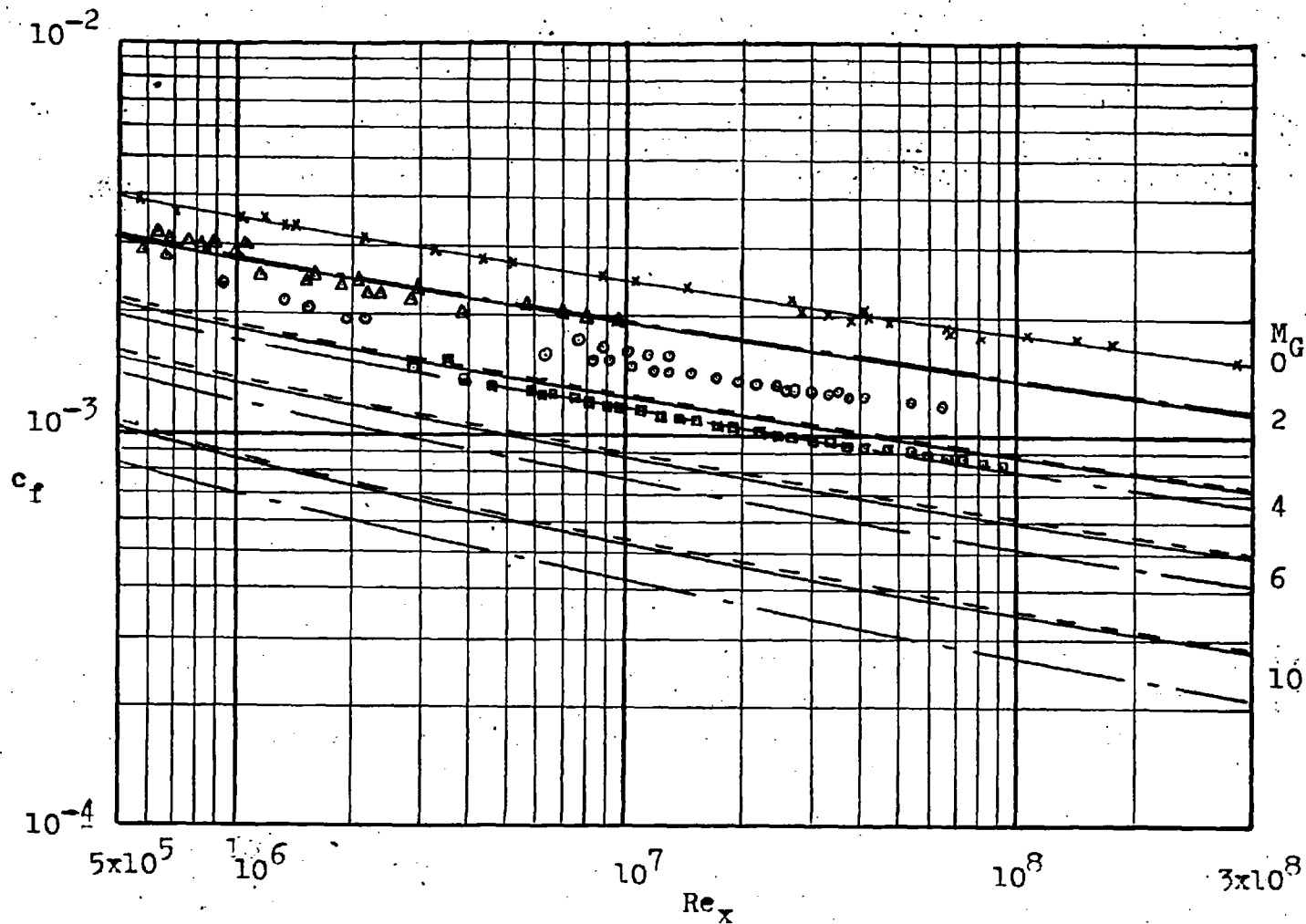
Fig.2.13 Theoretical and experimental c_f vs Re_x, adiabatic wall.
Theoretical Predictions: ——,§2.5.3; — — —,van Driest–II
[2.9]; — · — · —,Eckert [2.21]. Experiments: x, $M_G \approx 0$
[2.35, 2.49, 2.57]; Δ, $M_G = 1.5$–2.5 [2.34, 2.36, 2.41];
o, $M_G = 2.62$–2.95 [2.29, 2.45]; □, $M_G = 4.2$–4.5 [2.29, 2.39].
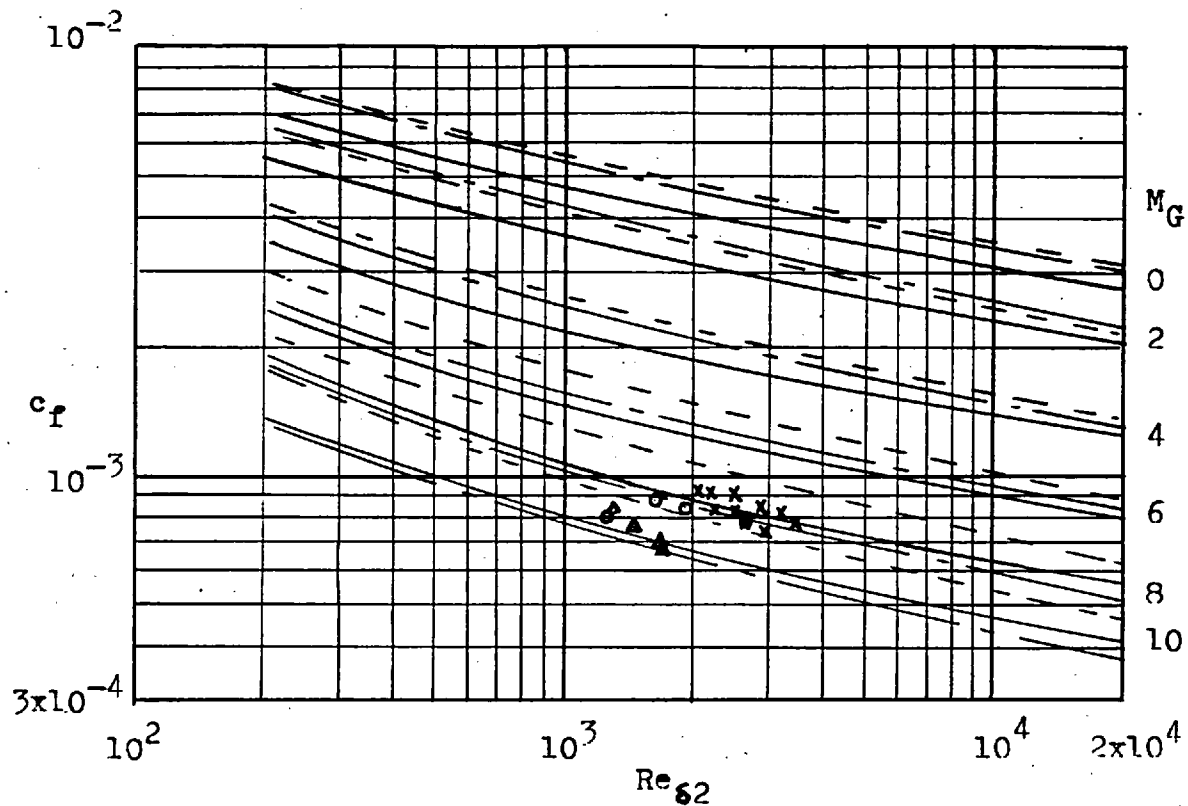
Fig.2.14 Theoretical and experimental c_f vs $Re_{\delta 2}$, at $T_{ad,S}/T_S = 2$.
Theoretical predictions: —— §2.5.3; — — — van Driest-II
[2.9]; — · — · — Eckert [2.21]. Experiments: x, $M_G = 8.22$–
8.29, $T_{ad,S}/T_S = 1.78$–2.14 [2.47, 2.48]; o, $M_G = 8.99$–9.10,
$T_{ad,S}/T_S = 1.82$–2.14 [2.47, 2.48]; ▲, $M_G = 10.03$–10.06,
$T_{ad,S}/T_S = 1.82$–2.11 [2.49].

2.14

10^{-2}

$\bar{c}_f$

$M_G \quad T_{ad,S}/T_S$
$0 \qquad 1$

10^{-3}

$7 \qquad 6$

$7 \qquad 1$

3×10^{-4}

$10^6 \qquad\qquad 10^7 \qquad\qquad 10^8$

Re_x
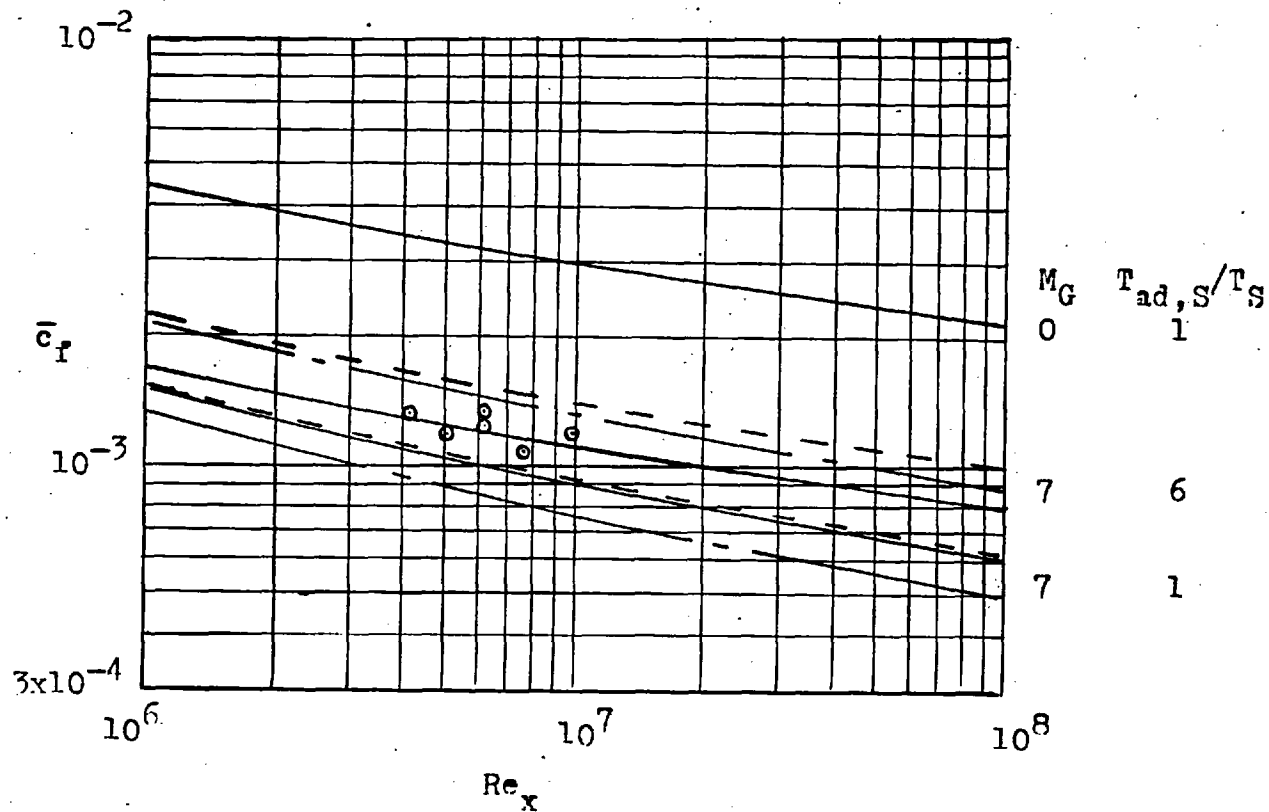
Fig.2.15 Theoretical and experimental $\bar{c}_f$ vs Re_x,
$M_G = 7$. Theoretical predictions: ——
§2.5.3; --- van Driest-II [2.9]; — — —
Eckert [2.21]. Experiments: o, M_G=6.9–
7.25, $T_{ad,S}/T_S$ = 5.55–5.78[2.20].

144
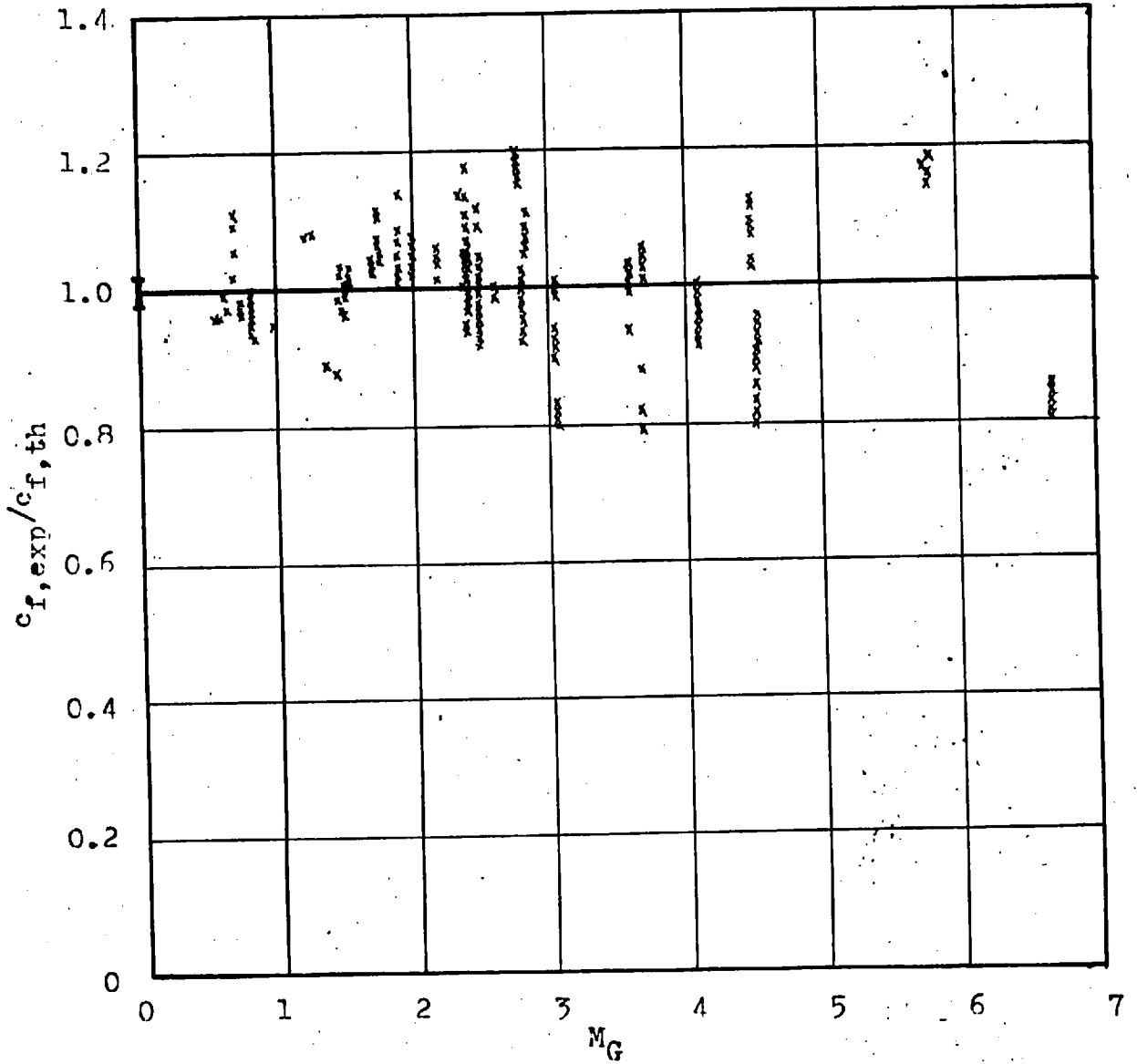
Fig. 2.16 $c_{f,exp}/c_{f,th}$ vs M_G for adiabatic wall, (where $c_{f,th}$ from §2.5.3).
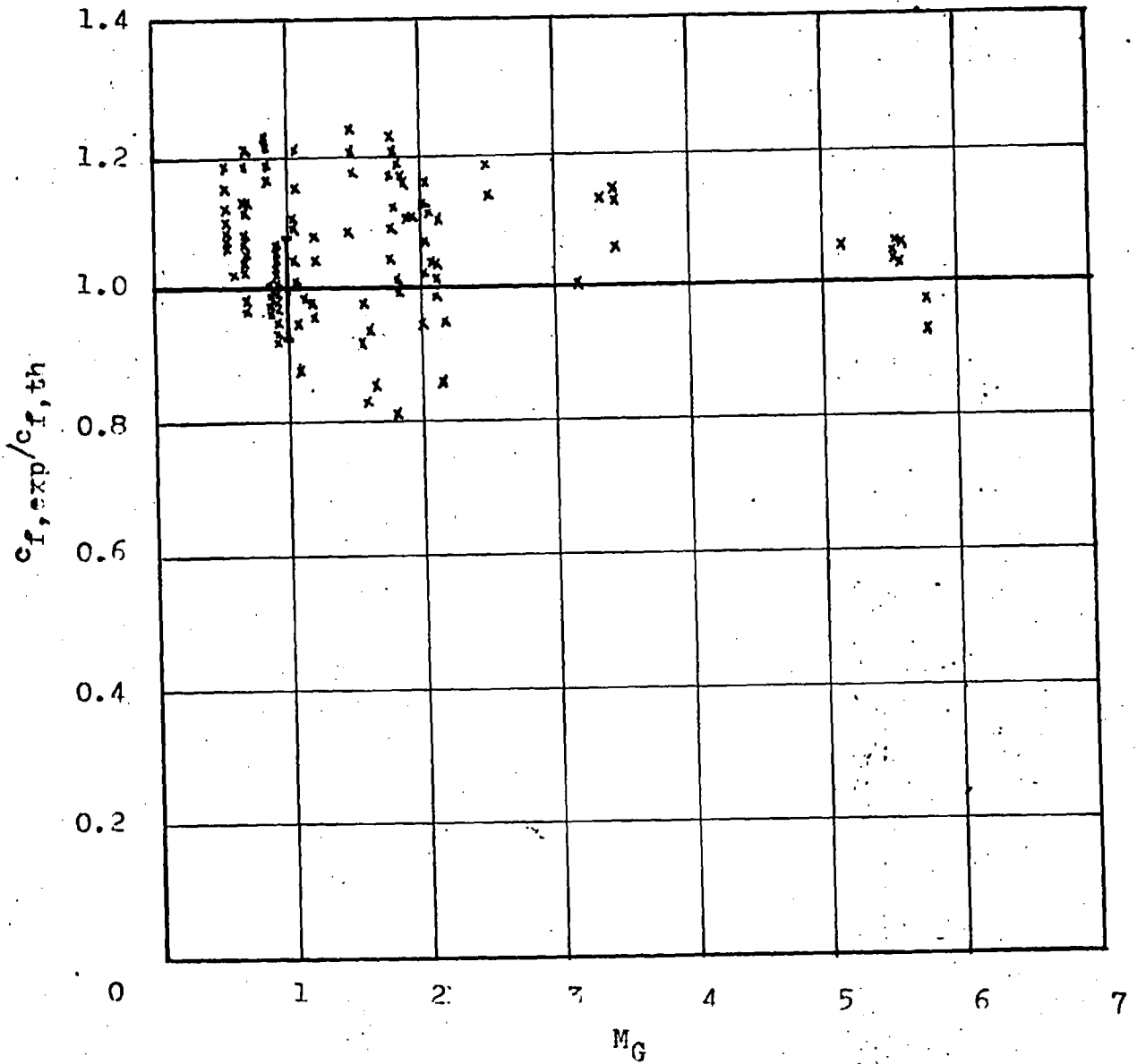
Fig. 2.17 $c_{f,exp}/c_{f,th}$ vs $T_{ad,S}/T_S$ with $c_{f,th}$ by §2.5.3.
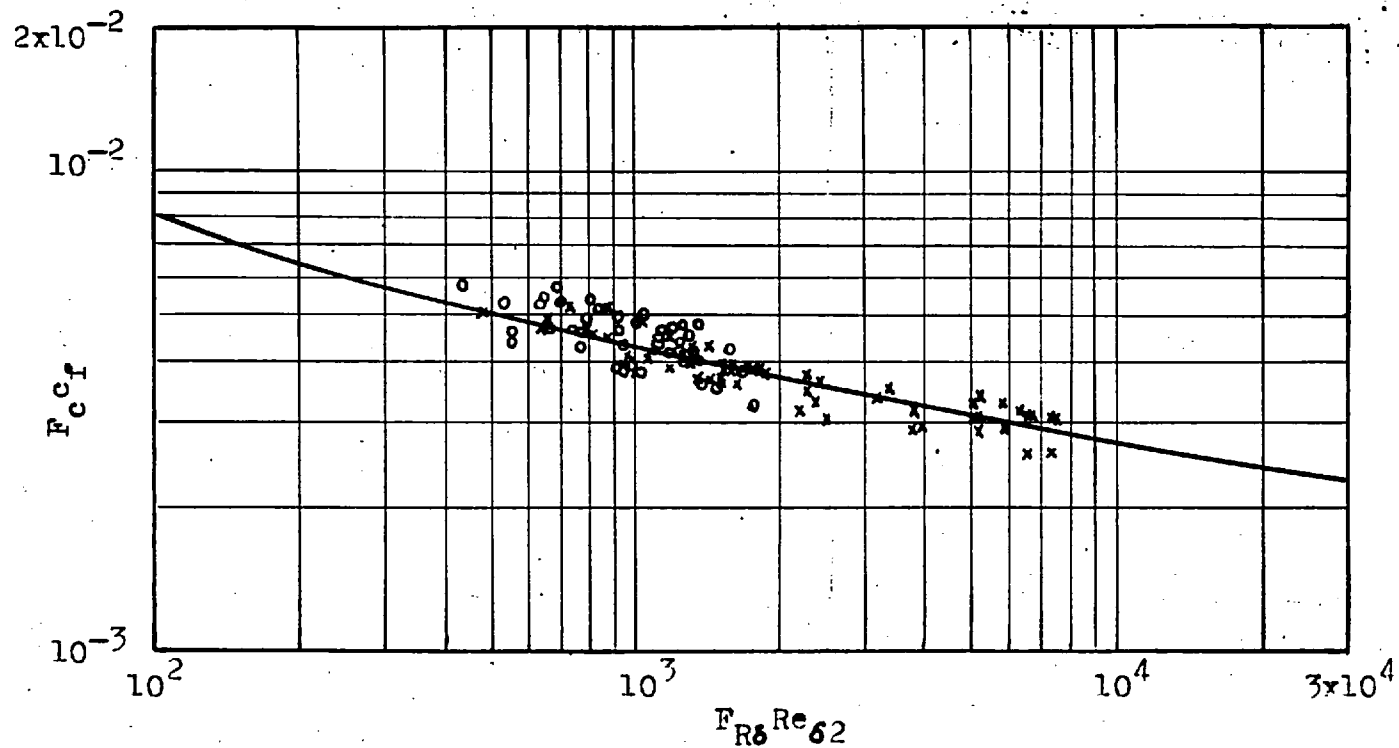
Fig.2.18 Comparison between theoretical and experimental $F_c c_f$
$F_{R\delta} Re_{\delta 2}$. x, experiments, adiabatic; o, experiments,
with heat transfer; ——, theory, Eq.(2.71).
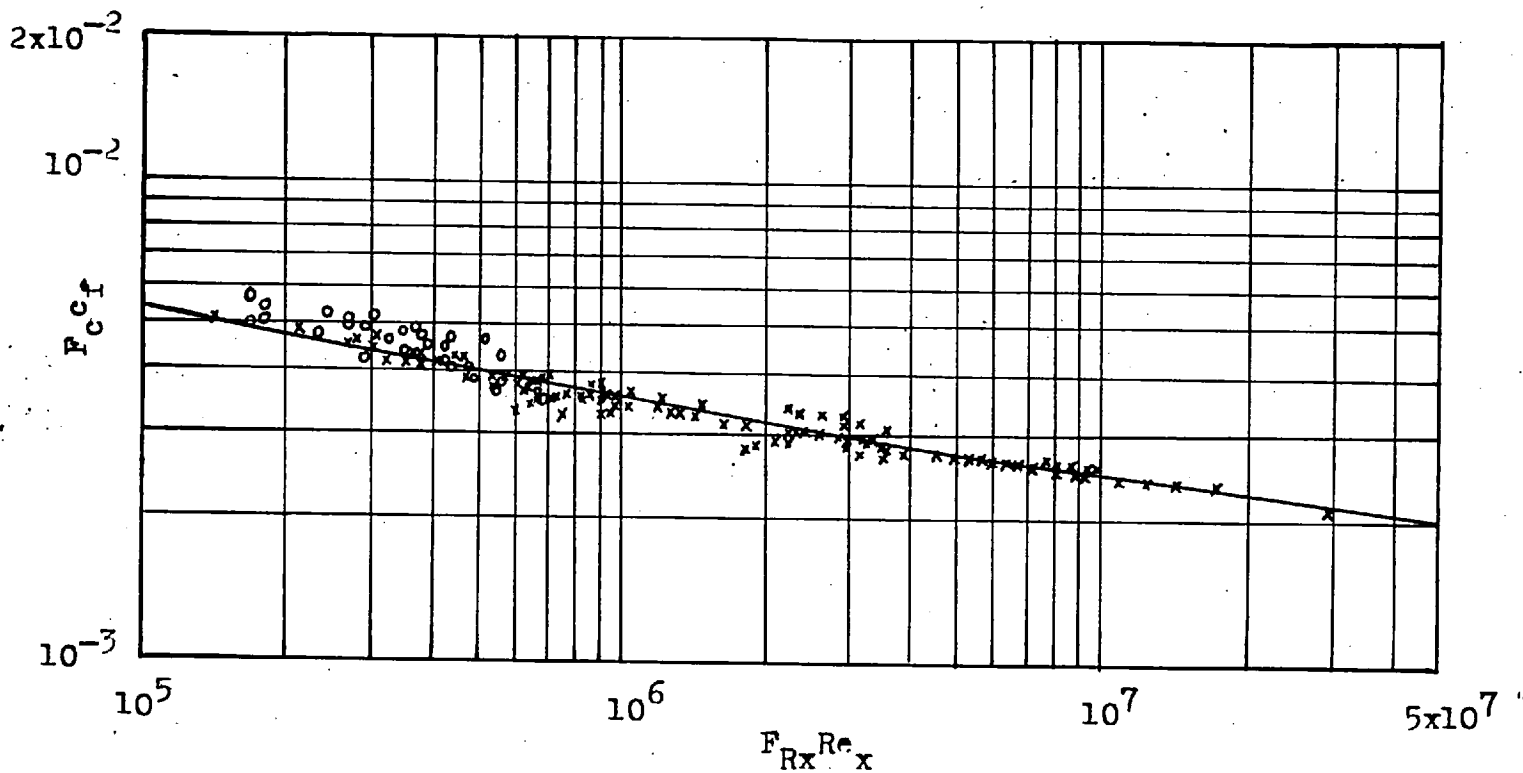
Fig.2.19   Comparison between theoretical and experimental $F_c c_f$ vs
$F_{Rx} Re_x$. x, experiments, adiabatic; o, experiments, with heat
transfer; ——, theory, Eq.(2.72).
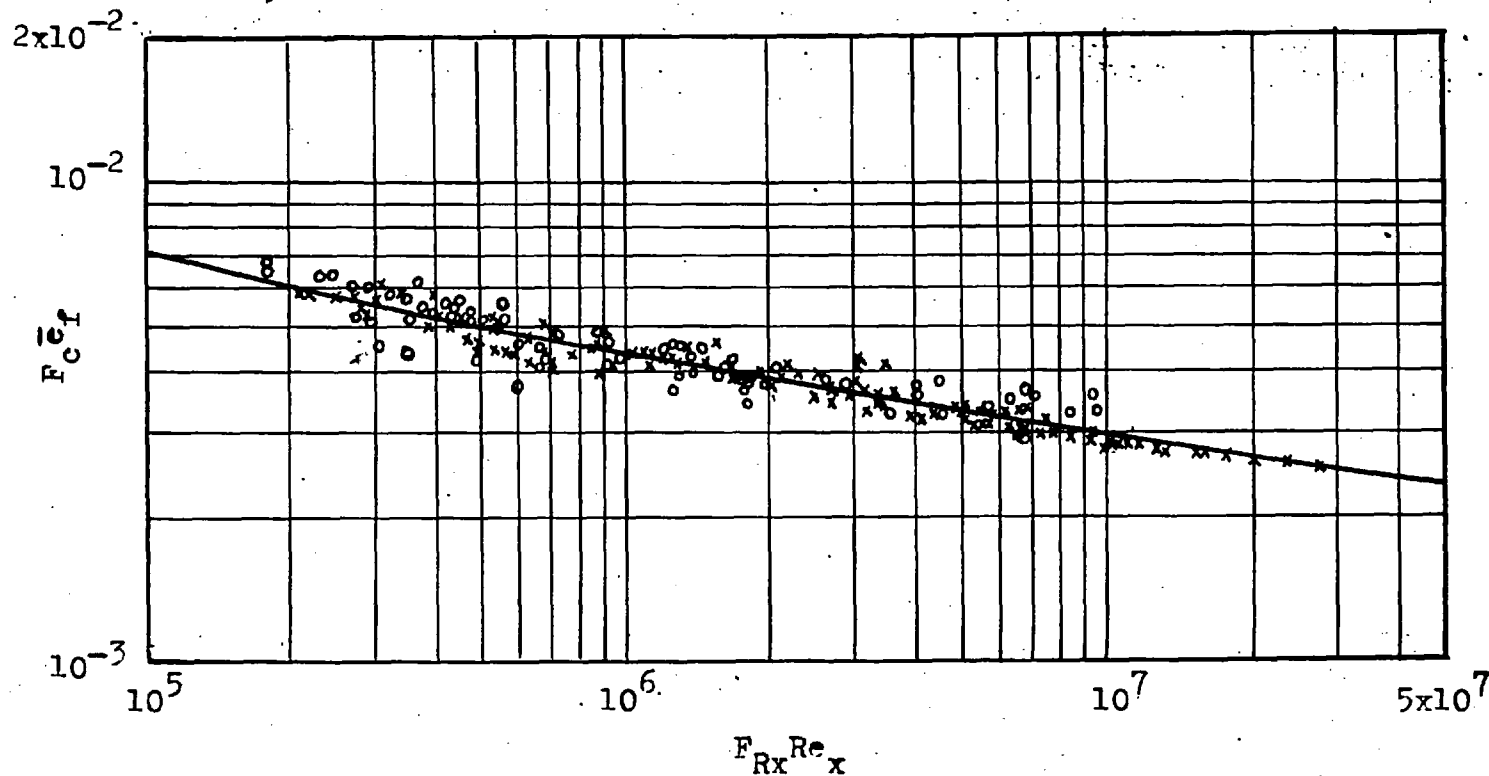
Fig.2.20 Comparison between theoretical and experimental $F_c \bar{c}_f$ vs
$F_{Rx}Re_x$. x, experiments, adiabatic; o, experiments, with
heat transfer; ——, theory, Eq.(2.73).
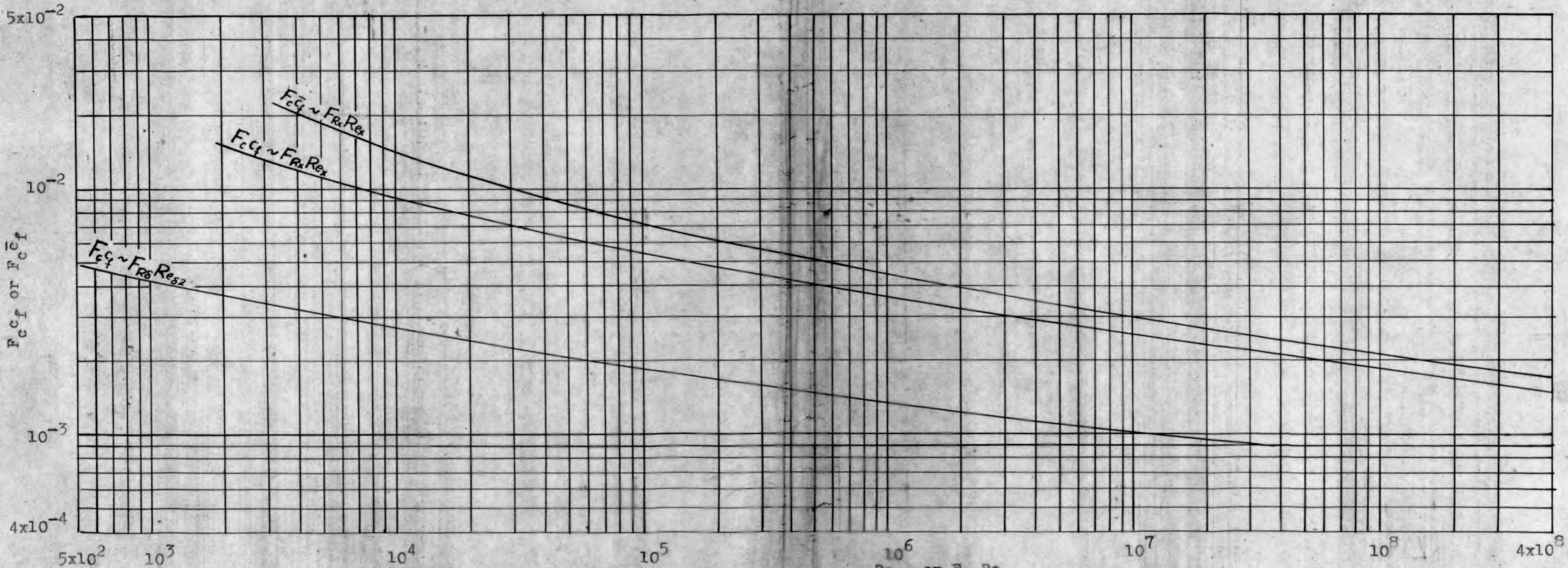
Fig. 2.21 Theoretical $F_c c_f$ and $F_c \bar{c}_f$ vs $F_R Re_{\delta 2}$ and $F_{Rx} Re_x$, Eqs. (2.71-2.73)
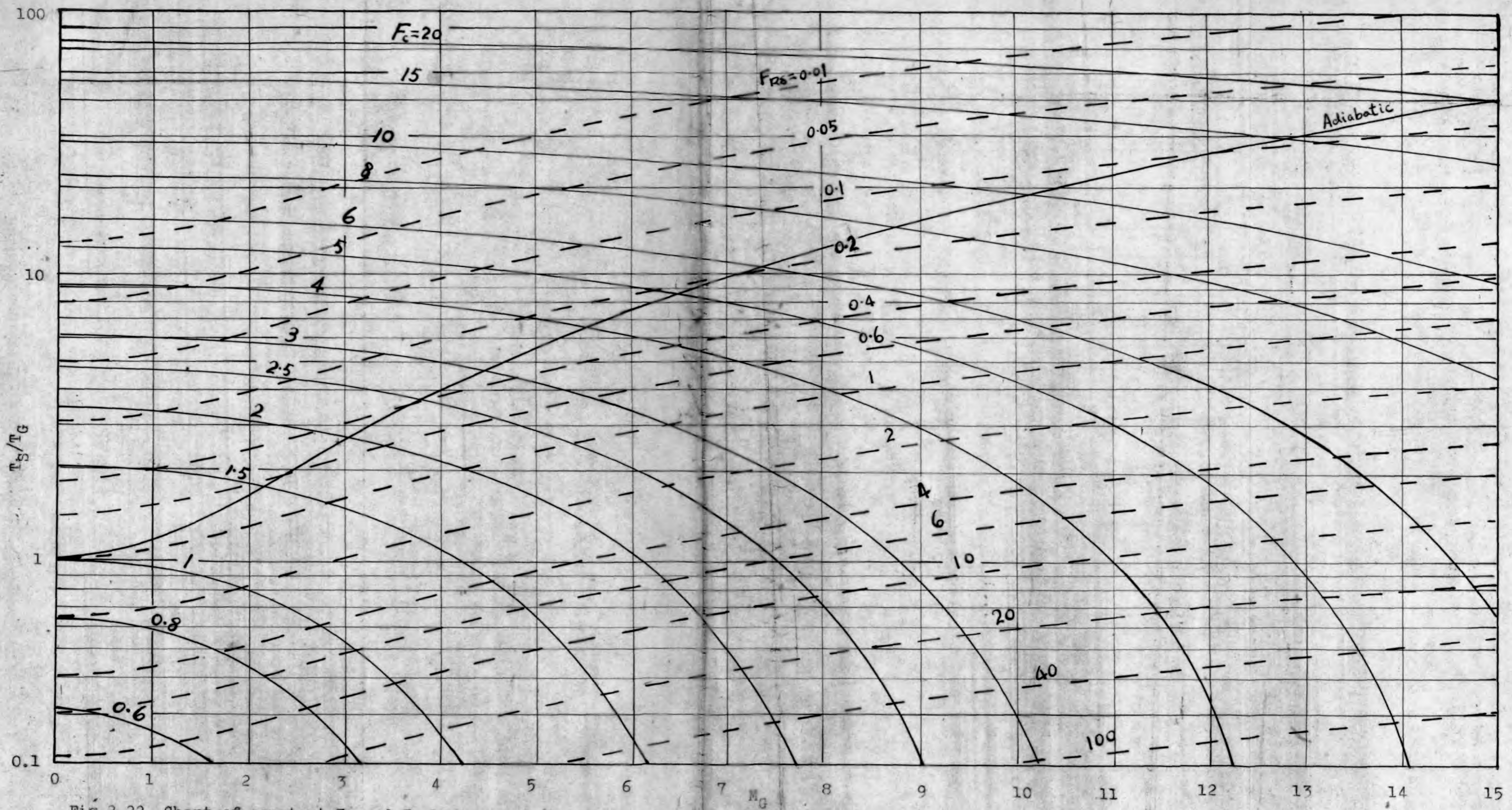
Fig.2.22 Chart of constant F_c and $F_{R\delta}$ lines on T_S/T_G and M_G co-ordinates.
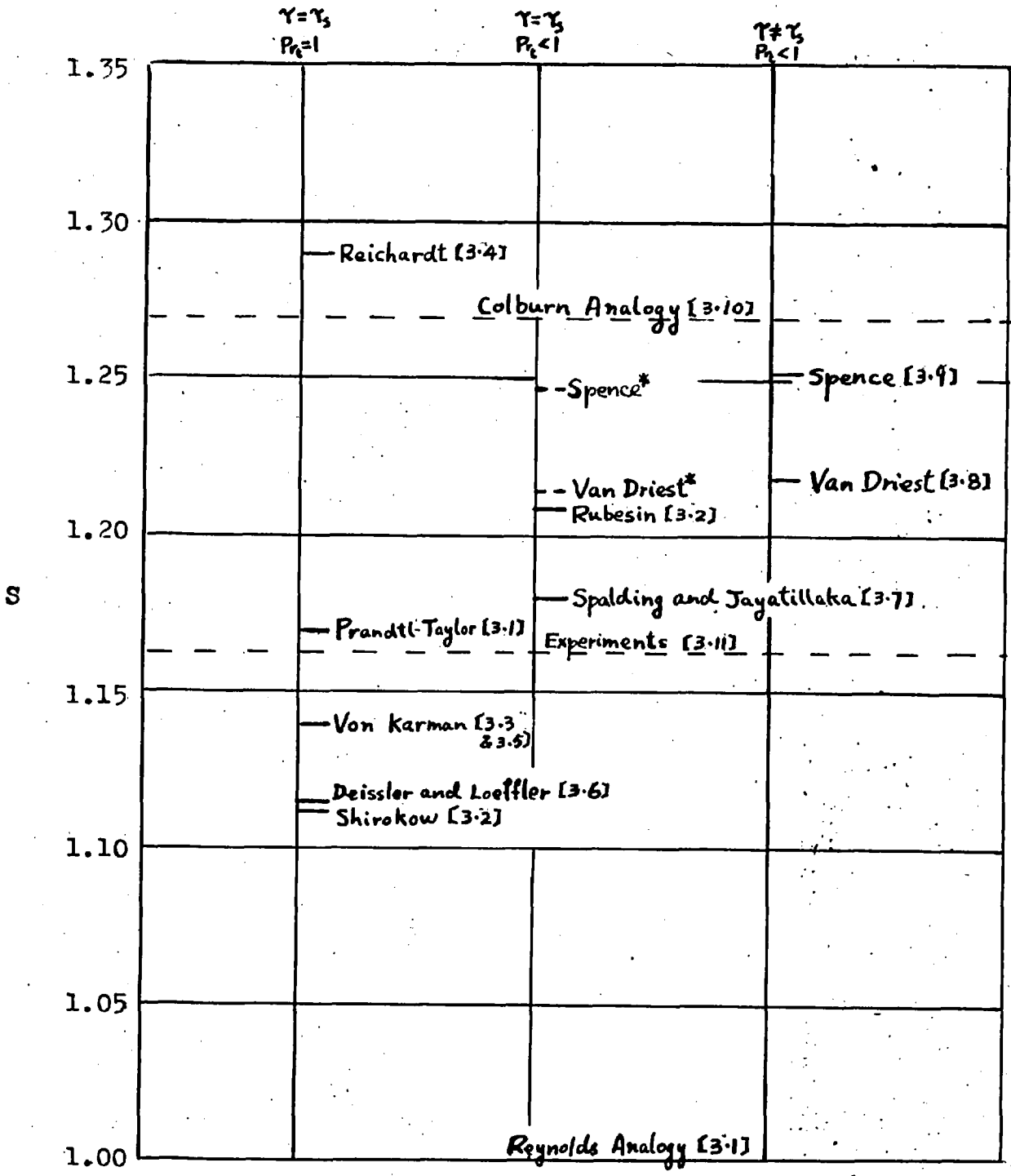
Fig.3.1 Comparison between theories for uniform—property turbulent boundary layer at Pr = 0.7 and $Re_x = 1 \times 10^6$.
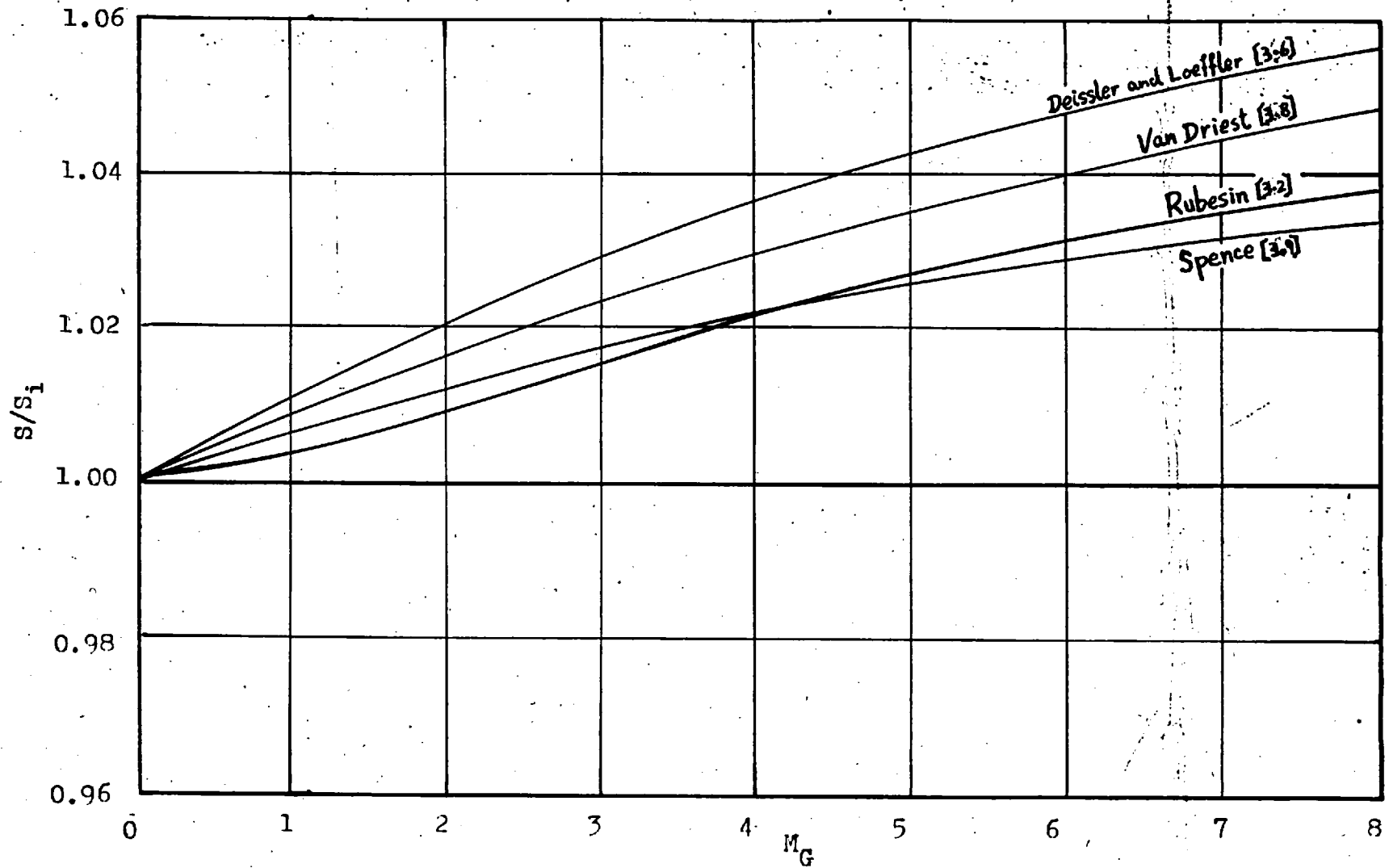
Fig. 3.2   Theoretically predicted influence of Mach number on the value of S, (S/S_i vs M_G at $Pr = 0.7$, $T_{ad,S}/T_S = 1$ and $Re_x = 1 \times 10^6$).
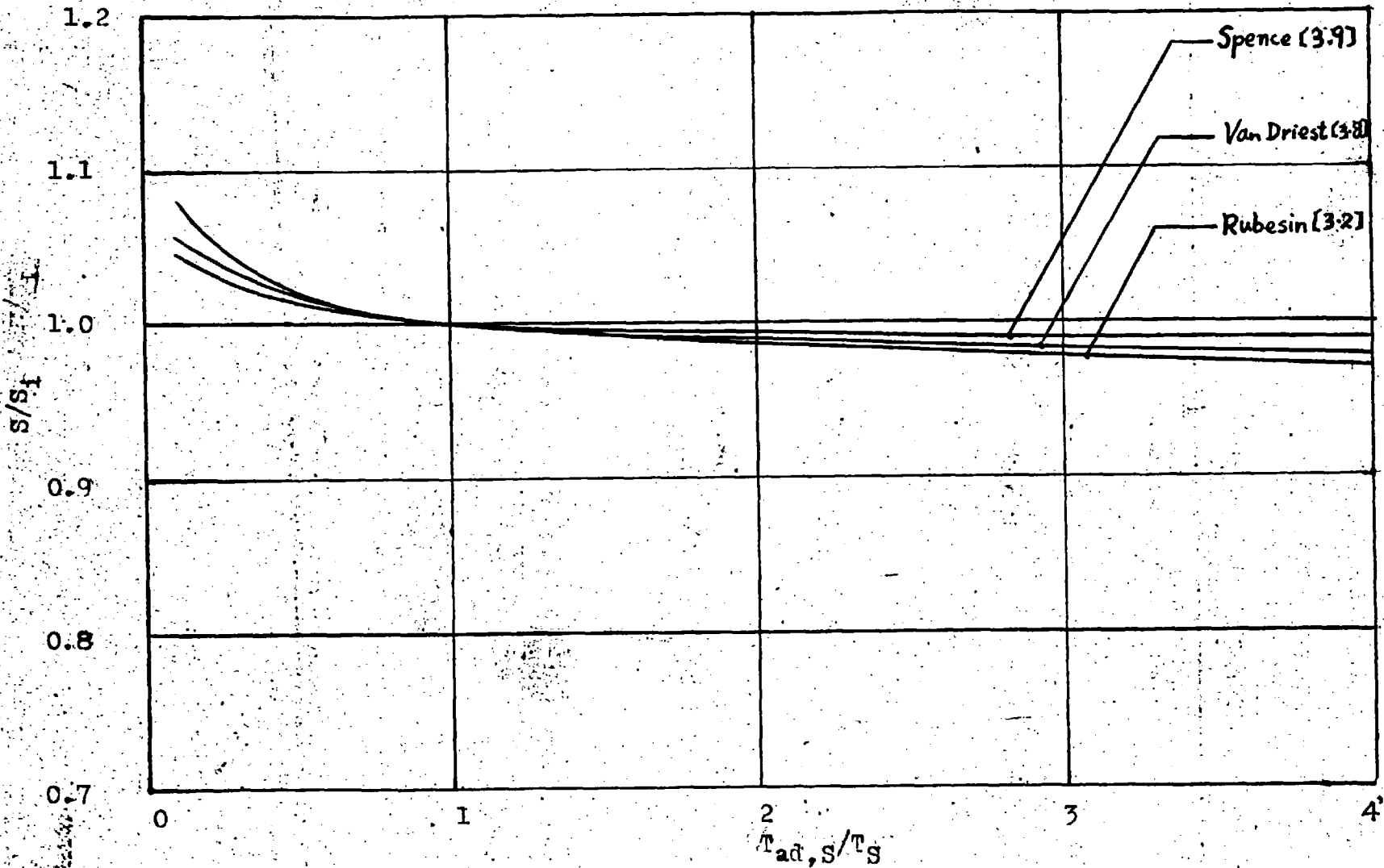
Fig. 3.3 Theoretically predicted influence of heat transfer on the value of S, (S/S$_i$ vs T$_{ad,S}$/T$_S$ at Pr = 0.7, M$_G$ = 0 and Re$_x$ = 1x10^6).
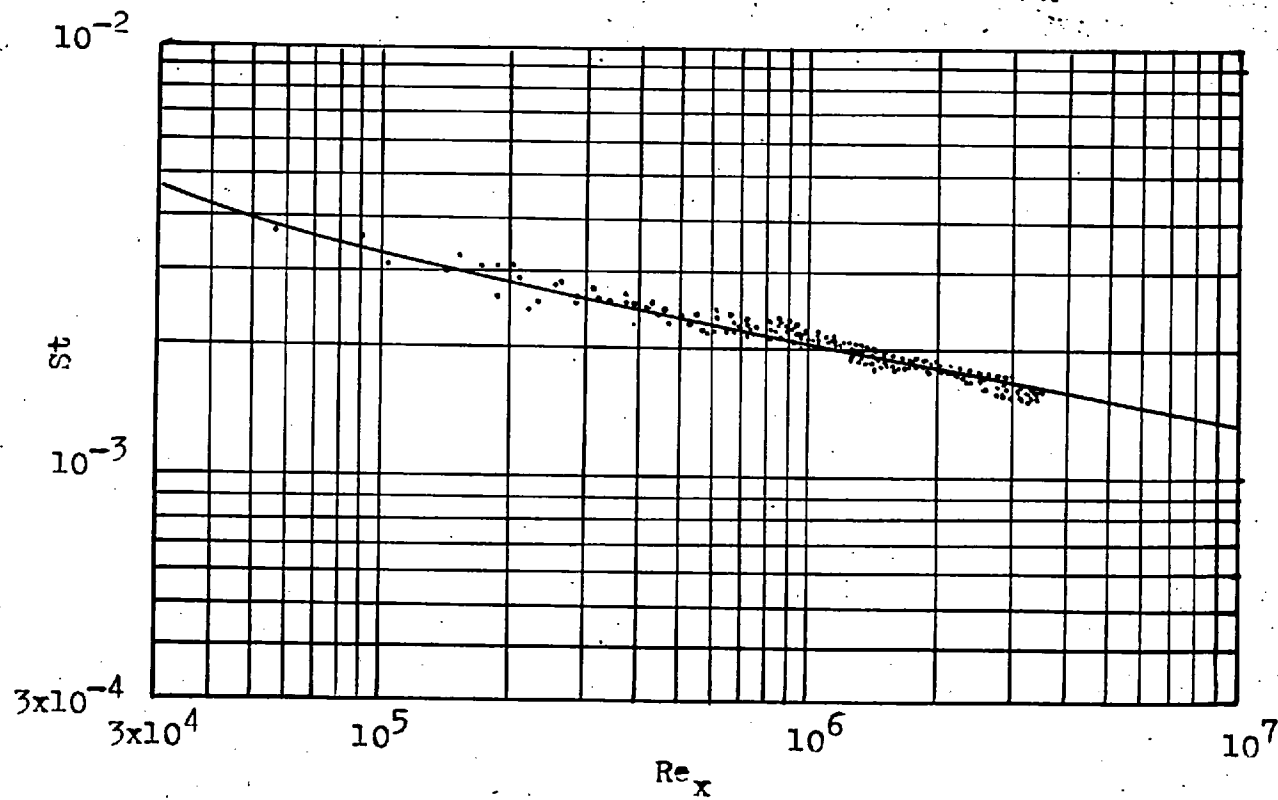
Fig. 3.4 Uniform-property St vs Re_x. x, experiments; ———;
theory with $S = 1.162$ and c_f by §2.5.3.
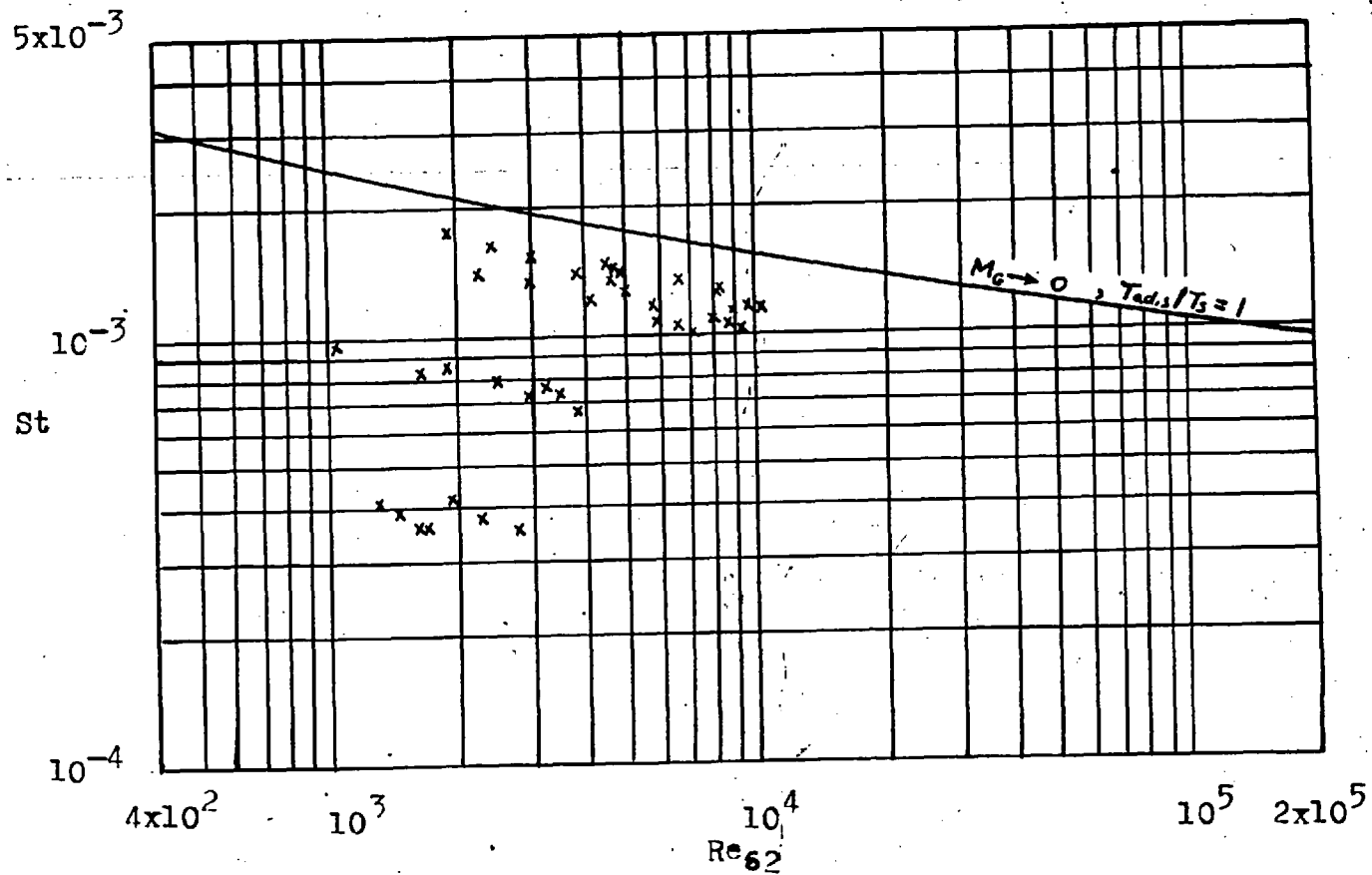
Fig. 3.5   Collected experimental data of St vs $Re_{\delta 2}$ in compressible
turbulent boundary layer.
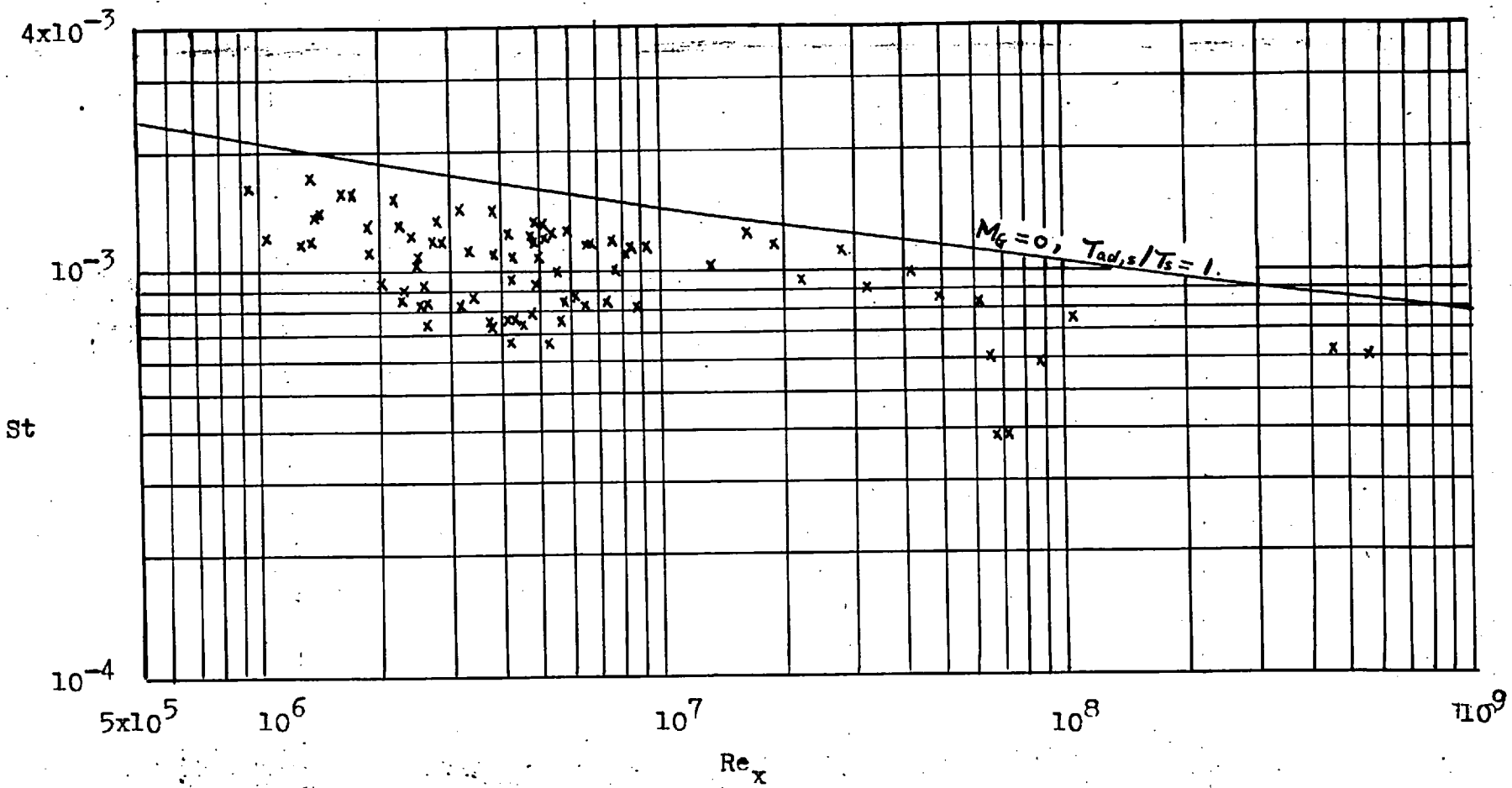
Fig.3.6 Collected experimental data of St vs Re_x in compressible turbulent boundary layer.

6×10^{-3}

$\overline{St}$

10^{-3}

4×10^{-4}

4×10^5 10^6 Re_x 10^7 10^8
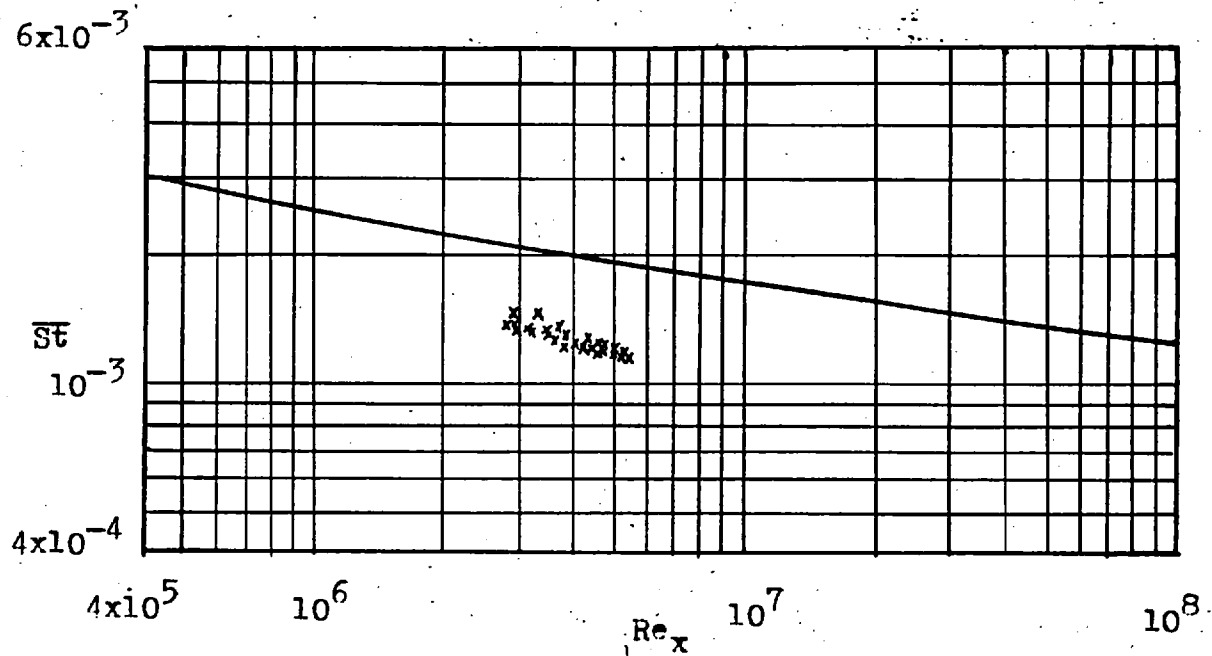
Fig.3.7 Collected experimental data of $\overline{St}$ vs Re_x in
compressible turbulent boundary layer.
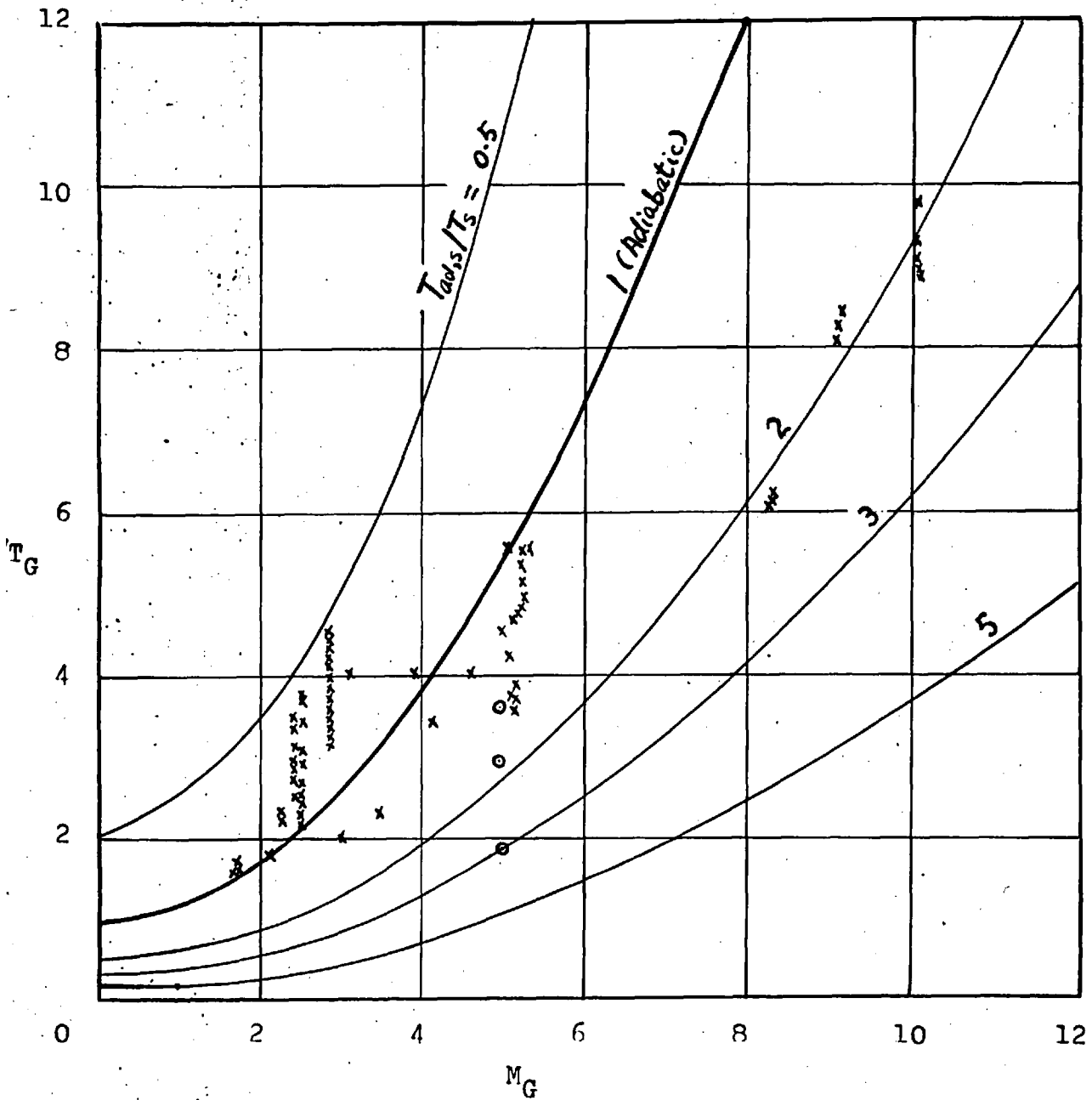
Fig. 3.8 Area of conditions explored experimentally, (for St).
Experiments: x, Refs. 3.11-3.20,3.22; o, Ref. 3.21;
I, §4.

159
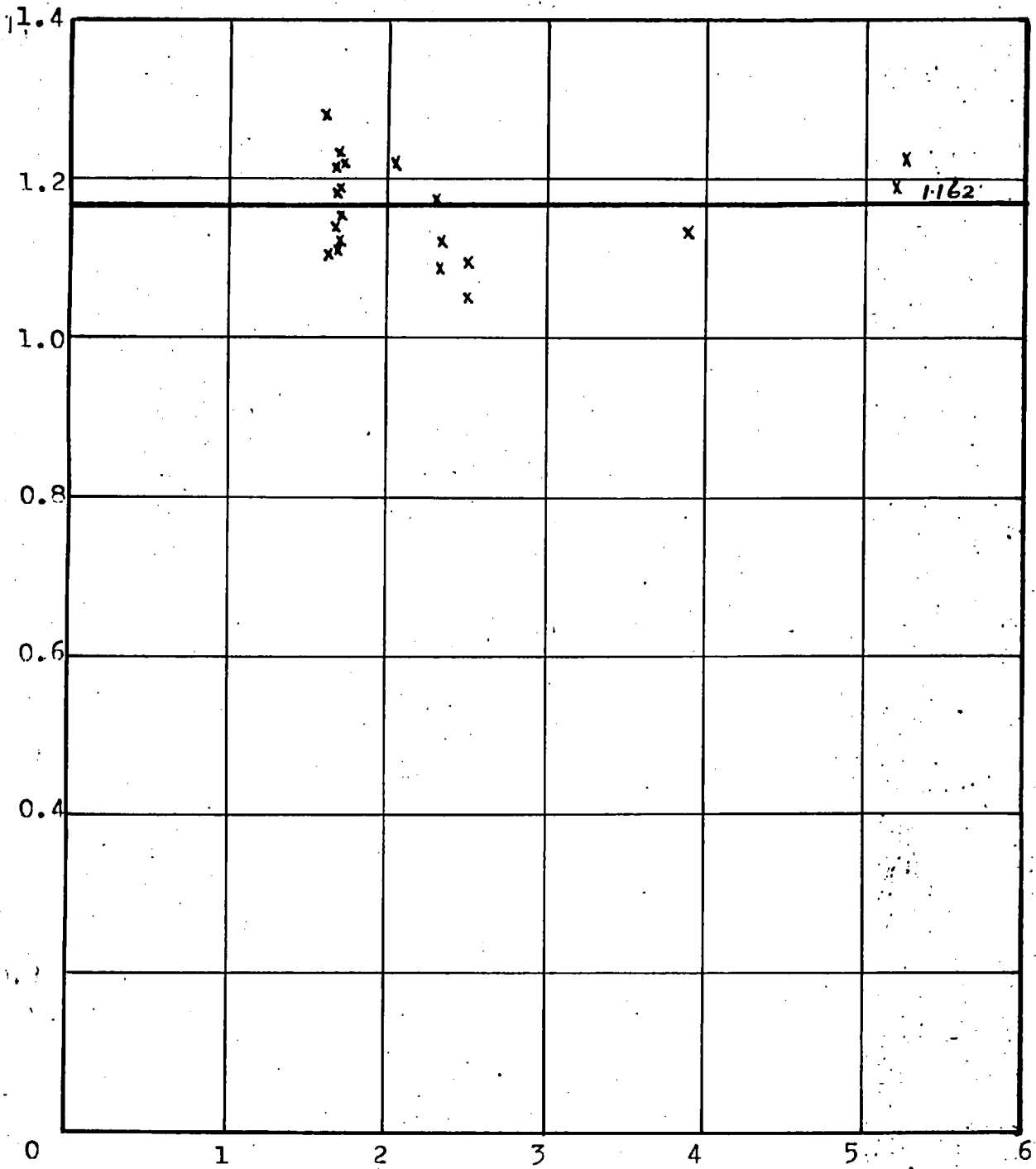
Fig.3.9 Experimental S vs M_G "adiabatic wall", ($T_{ad,S}/T_S$ =0.9 to 1.1), and Re_x from 5×10^5 to 3×10^6.
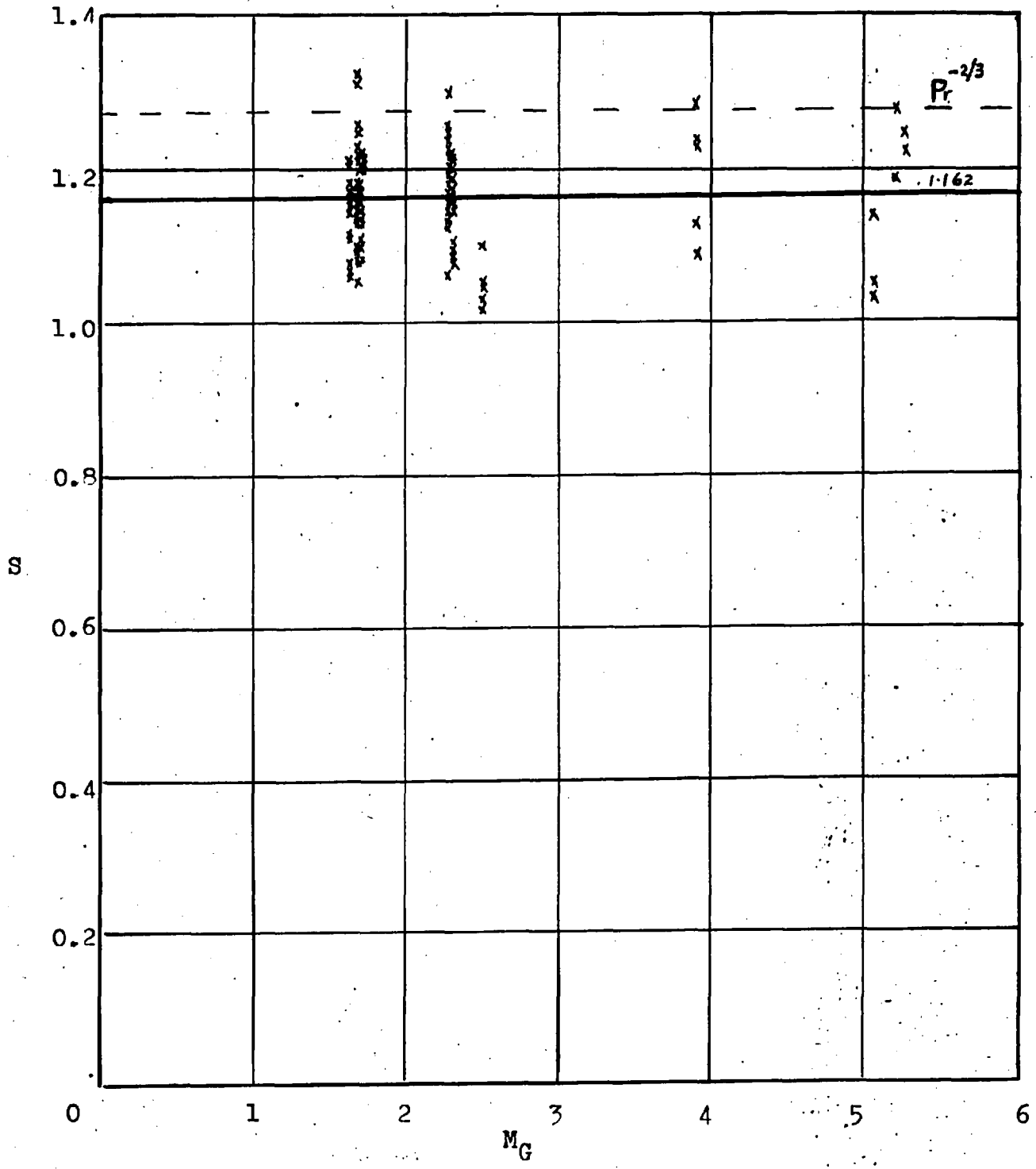
Fig.3.10 Experimental S vs M_G for "adiabatic wall", ($T_{ad,S}/T_S$ =0.9 to 1.1), and all Re_x(or $Re_{\delta 2}$) so far available.
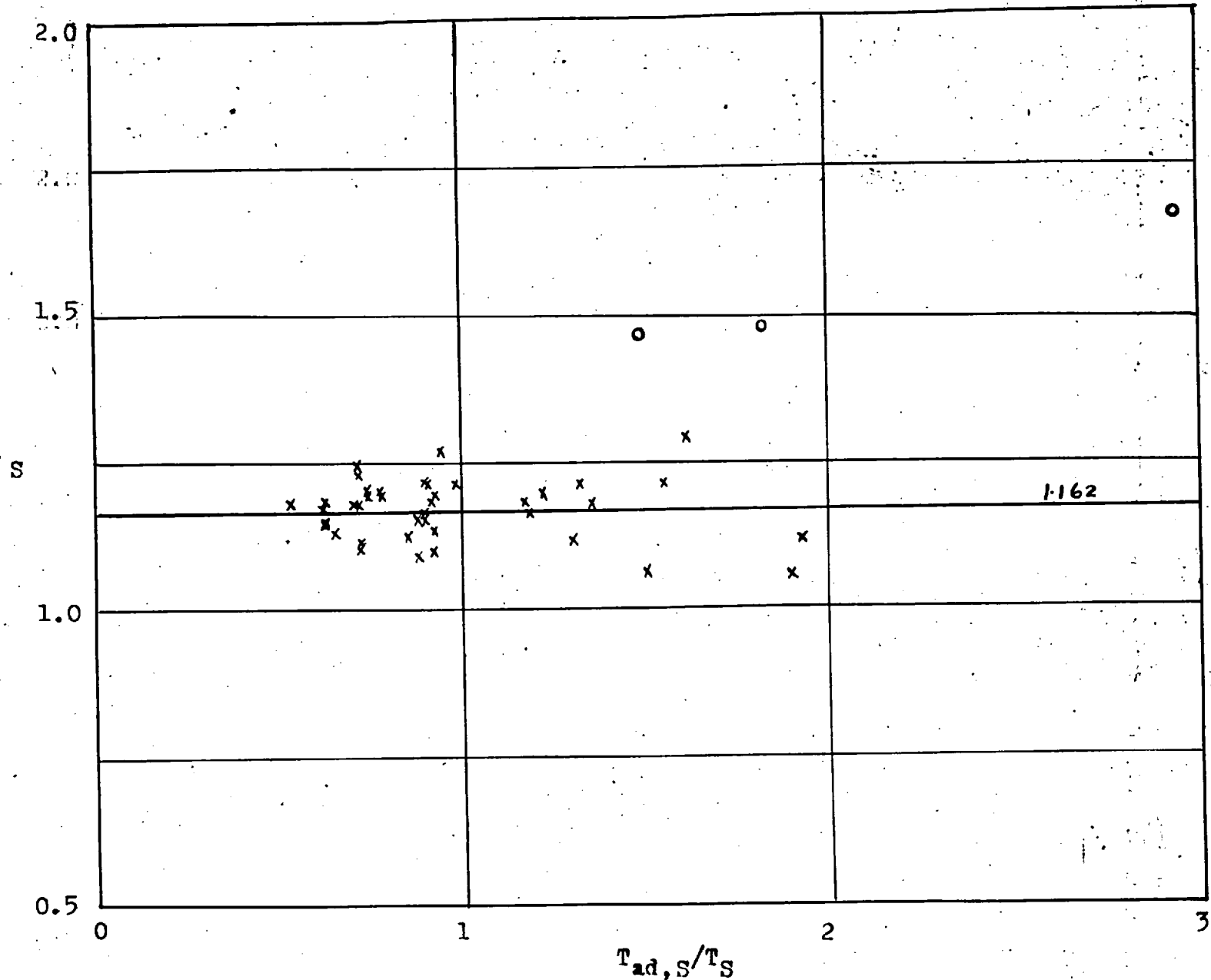
Fig. 3.11 Experimental S vs $T_{ad,S}/T_S$ for Re_x from 5×10^6 to 3×10^6. x, Refs. 3.11 to 3.20, 3.22; o, Ref. 3.21.
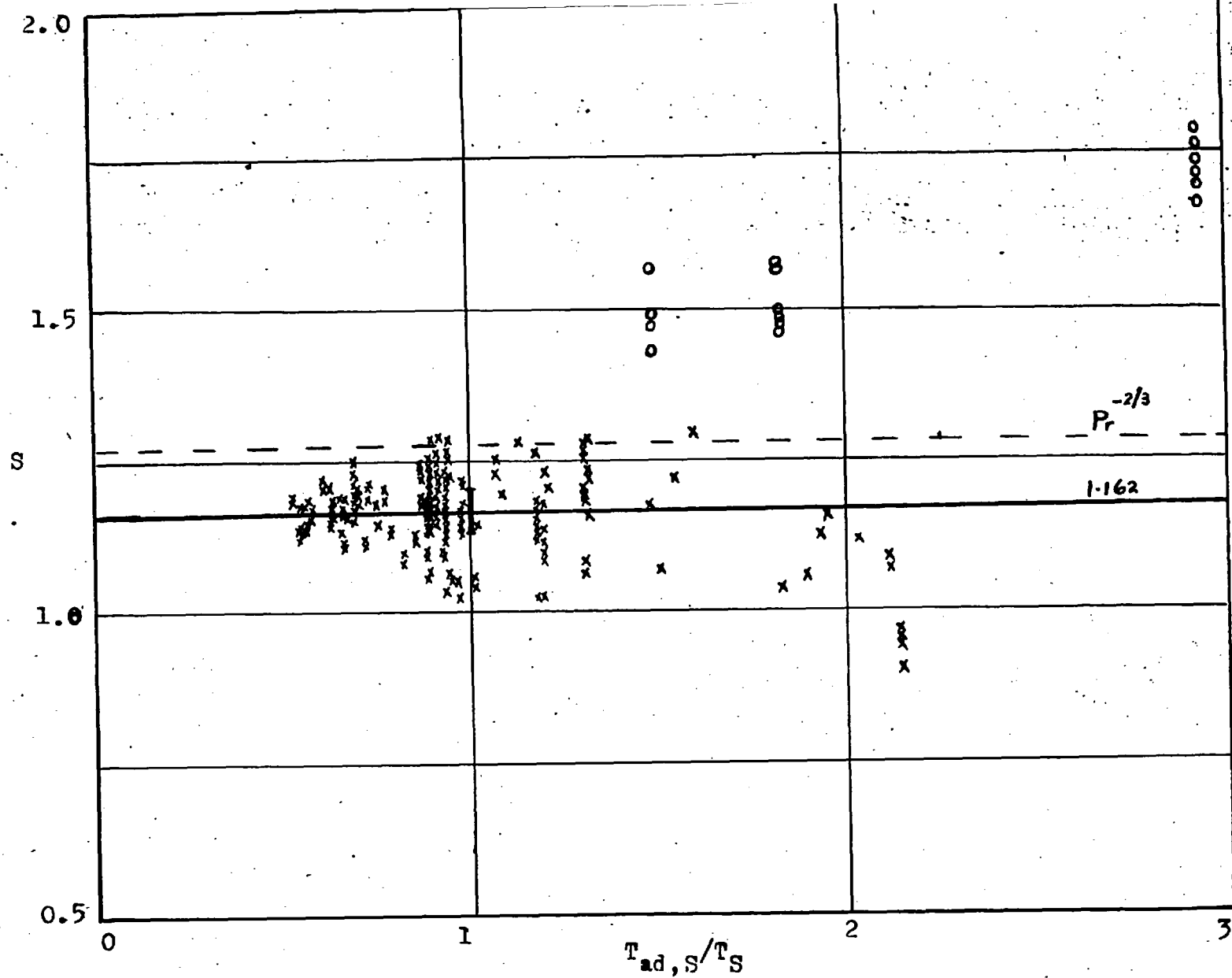
Fig. 3.12 Experimental S vs $T_{ad,S}/T_S$ for all Re_x (or $Re_{\delta 2}$) so far available. x, Refs. 3.11-3.20, 3.22; o, Ref. 3.21.
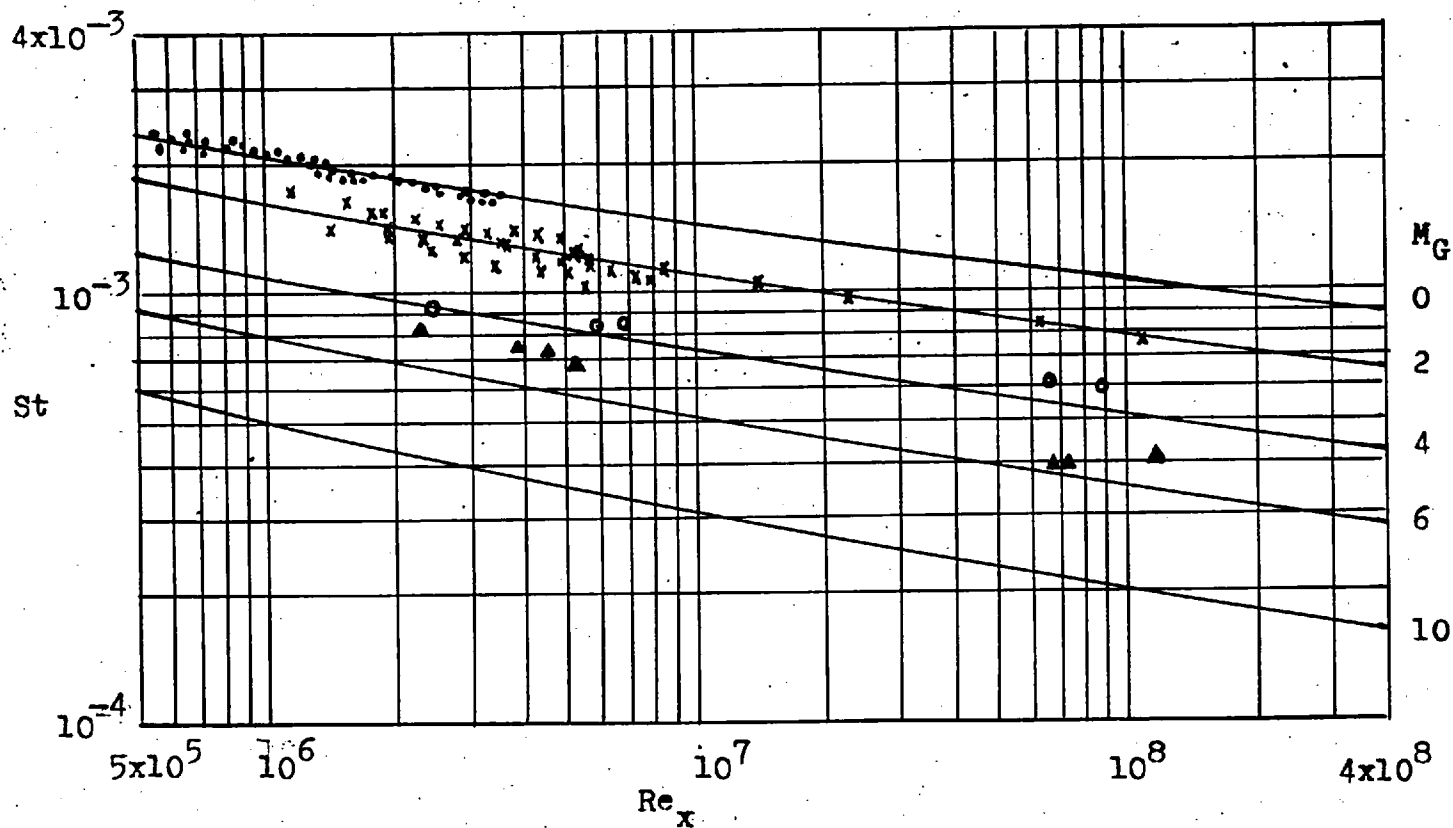
Fig.3.13 Theoretical and experimental St vs Re_x for adiabatic wall.
Theory: $T_{ad,S}/T_S = 1$, Eq.3.1 with $S = 1.162$ and c_f by §2.5.3.
Experiments:(at $T_{ad,S}/T_S$ 0.9 to 1.1): ·, M_G 0.2 3.11 ;
x, $M_G = 1.7-2.3$ [3.16]; o, $M_G = 3.9$ [3.18]; ▲, M_G 4.9-5.2
[3.22].
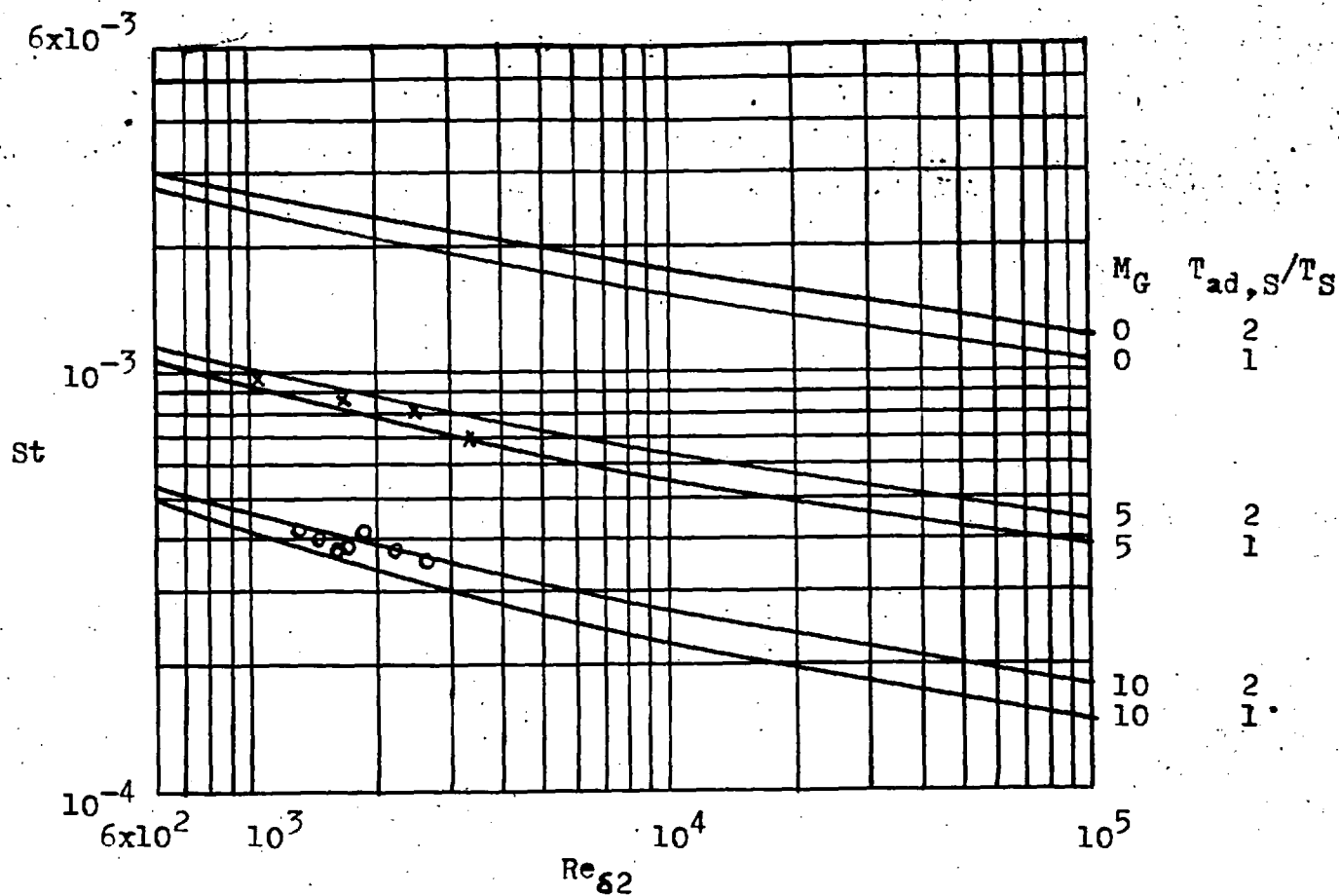
Fig. 3.14 Theoretical and experimental St vs Re$_{\delta 2}$ at various
M_G and $T_{ad,S}/T_S$. Theory: ———, Eq. 3.1 with $S = 1.162$,
c_f by §2.5.3. Experiments: x, $M_G = 5.1-5.2$, $T_{ad,S}/T_S$
$= 1.4-1.6$ [3.22]; ŏ, $M_G = 9-10$, $T_{ad,S}/T_S = 1.8-2.1$ [3.20].

164
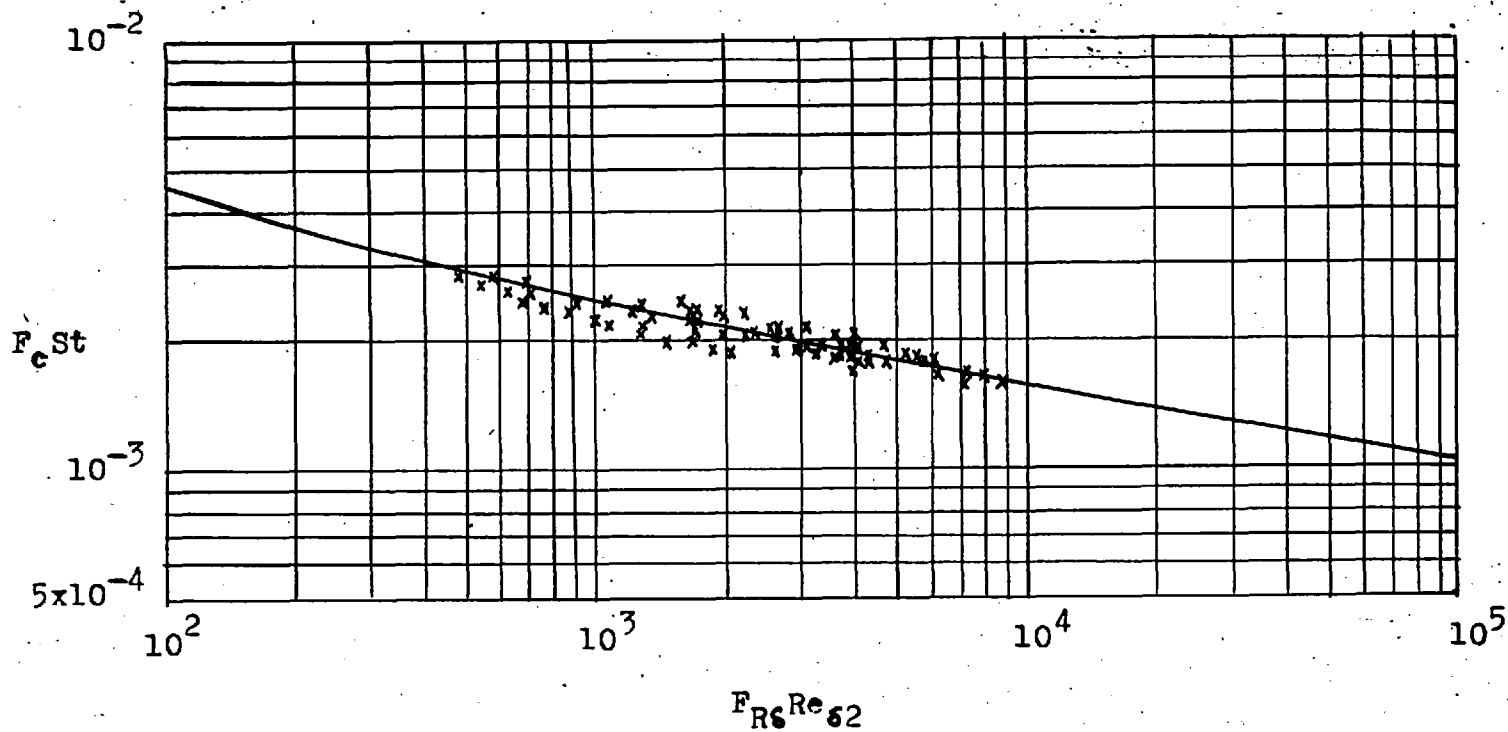
Fig.3.15 Theoretical and experimental $F_c St$ vs $F_{R\delta} Re_{\delta 2}$. ⟶; theory;
x, experiments (Appendix 3B).
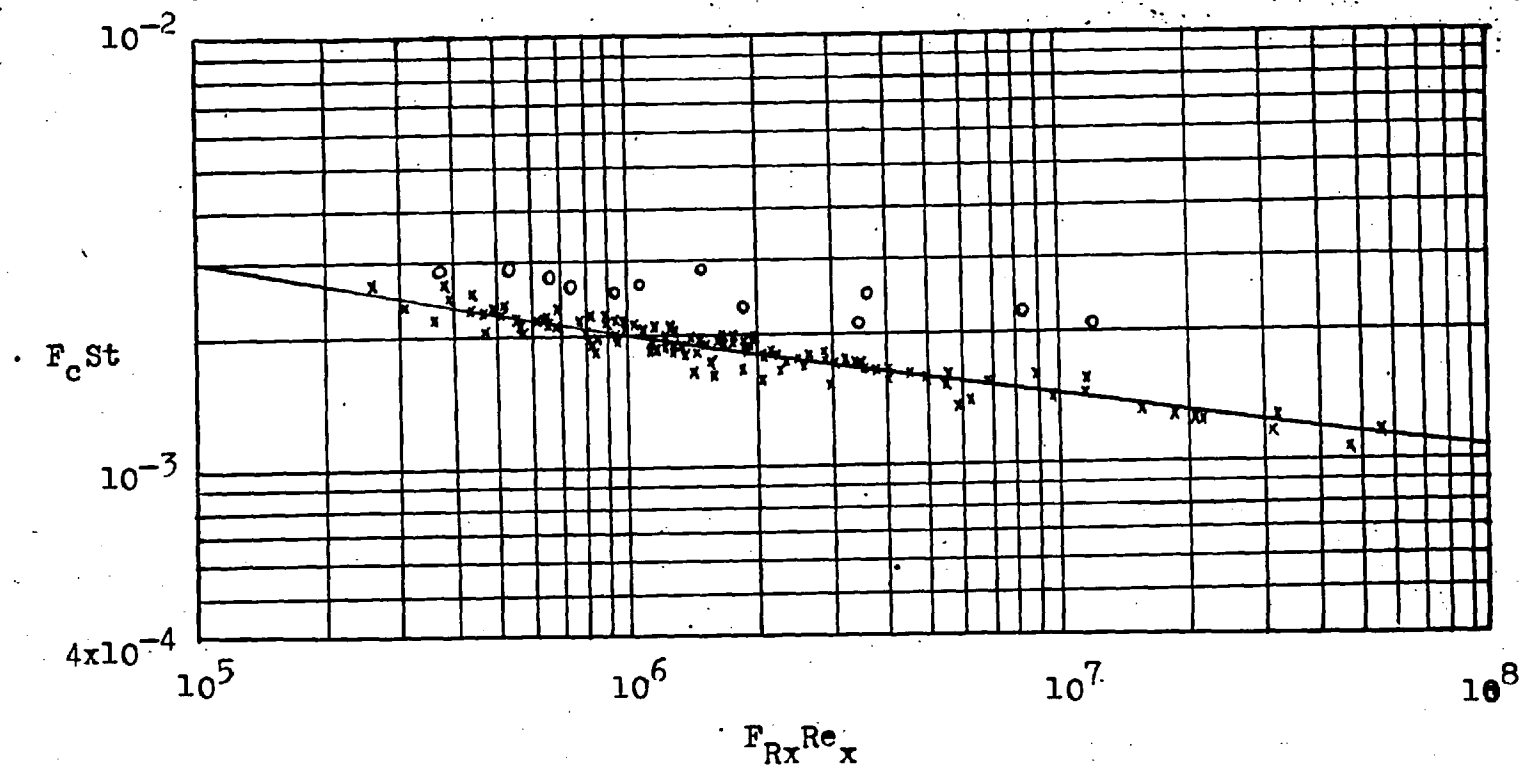
Fig. 3.16 Theoretical and experimental $F_c St$ vs $F_{Rx} Re_x$. ———, theory;

x, experiments [3.12–3.20, 3.22]; o, experiments [3.21]

whose accuracy doubtful.
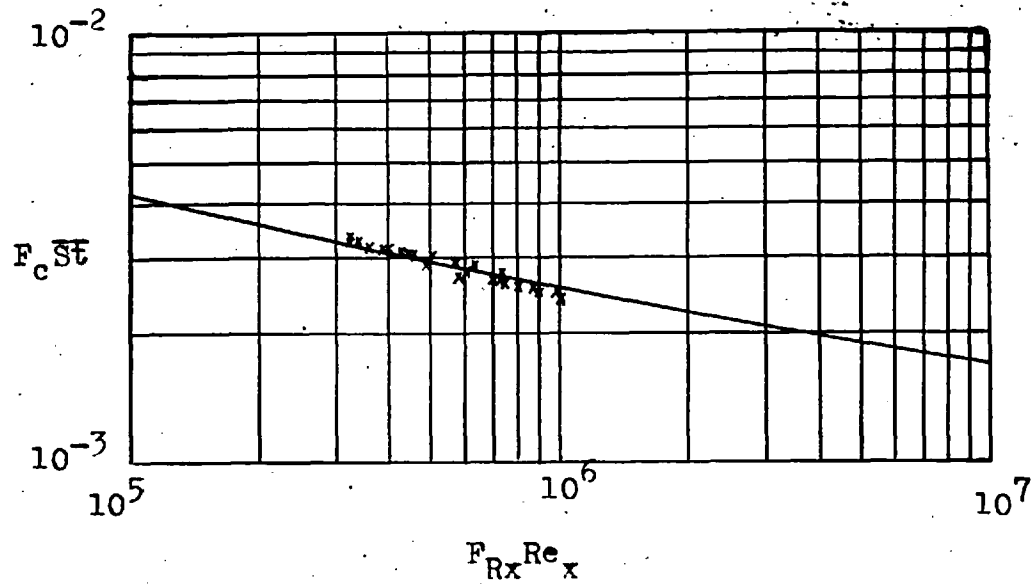
Fig. 3.17 Theoretical and experimental $F_c \overline{St}$ vs $F_{Rx} Re_x$.
———, theory; x, experiments (Appendix 3B).
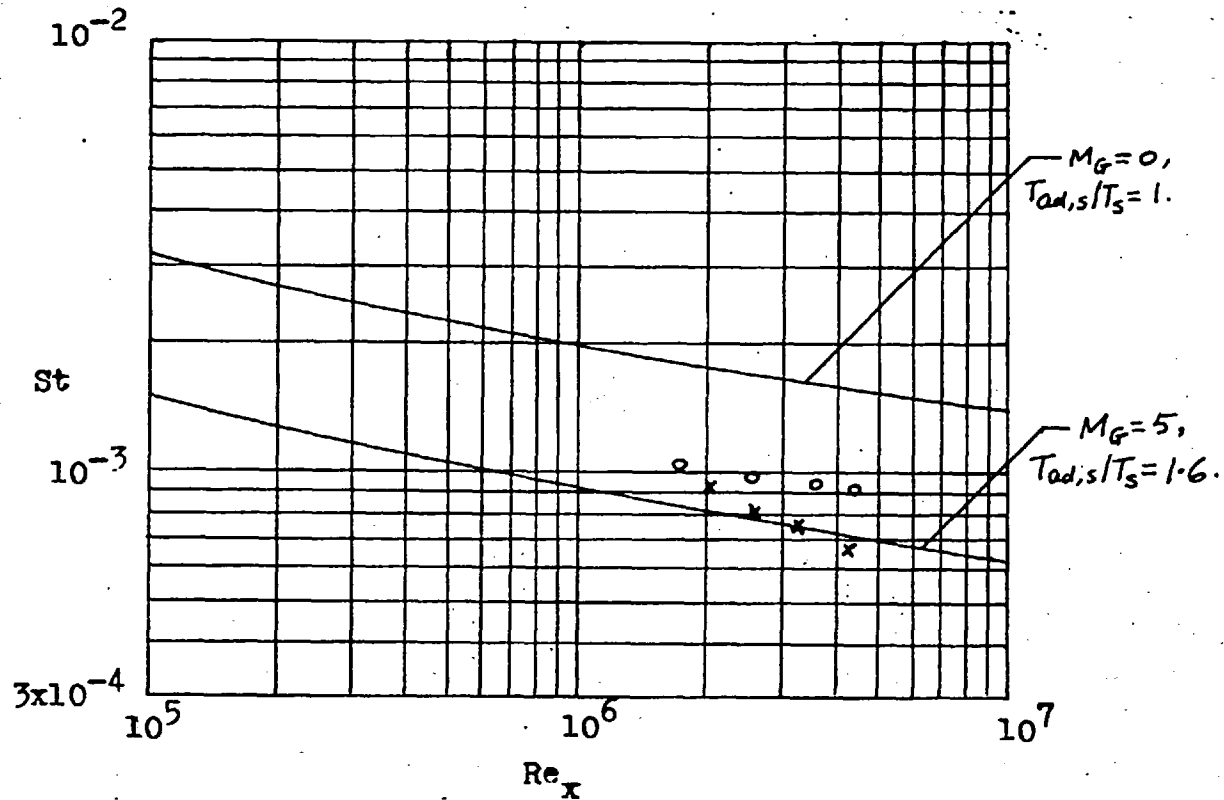
Fig. 3.18 Comparison of data of Ref. 3.21 with the present
theory and data of Ref. 3.22. ———, theory;
o, data of Ref. 3.21; x, data of Ref. 3.22.

169

Fig. 4.1 Photograph of general layout of apparatus.

Fig.4.2   Diagrammatic drawing of general layout of apparatus.

Heat exchanger.

Working section

Gaseous N_2 Bottle

Liquid N_2 container

Flexible tube

Cooling Jacket

Tunnel fan

Fluid Coupling

Electric motor.

Pneumatic rams

Air drying plant
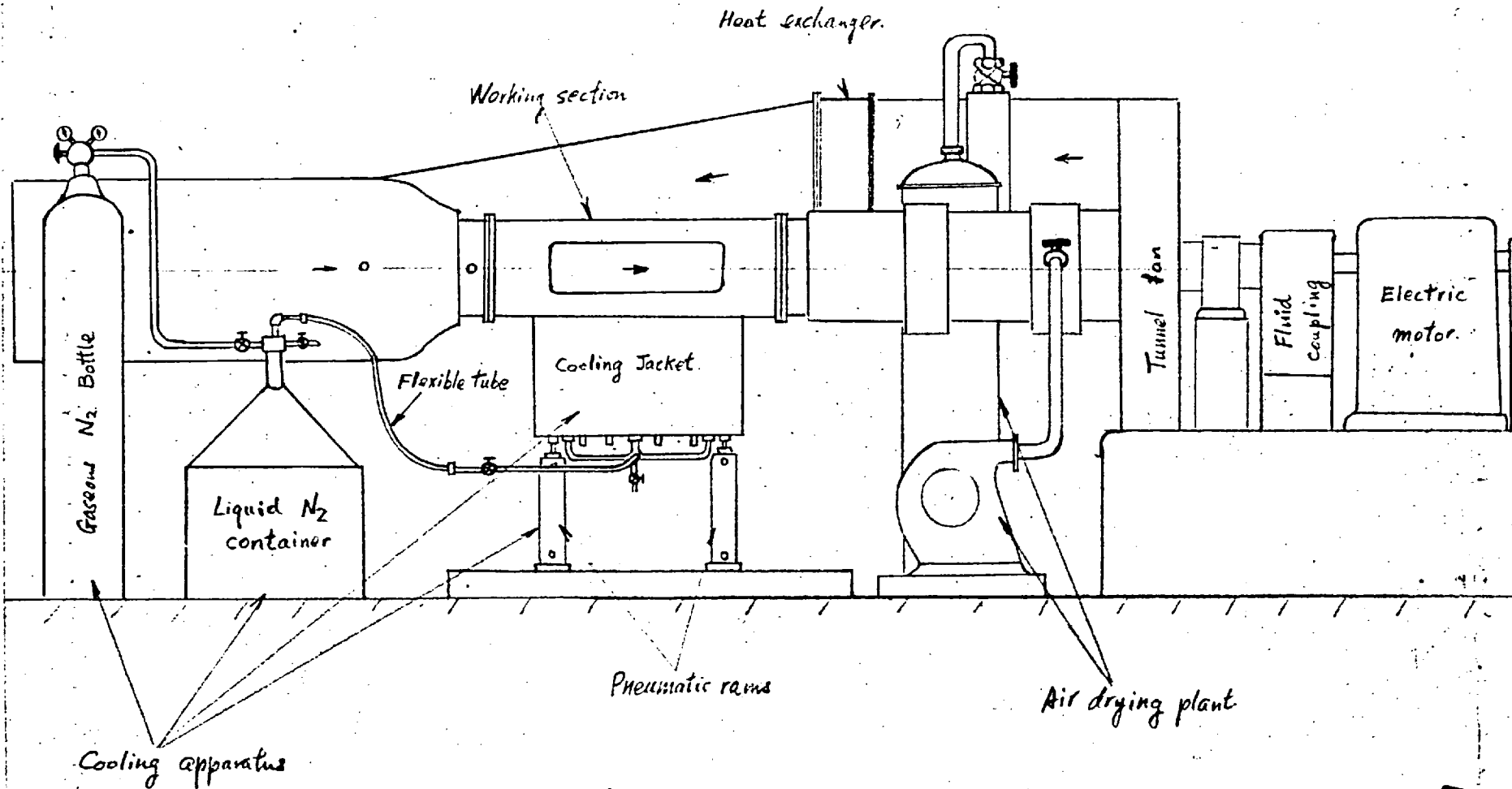
Cooling apparatus

Fig.4.3 Design of 3/16" thick Monel test plate. (Elevation)
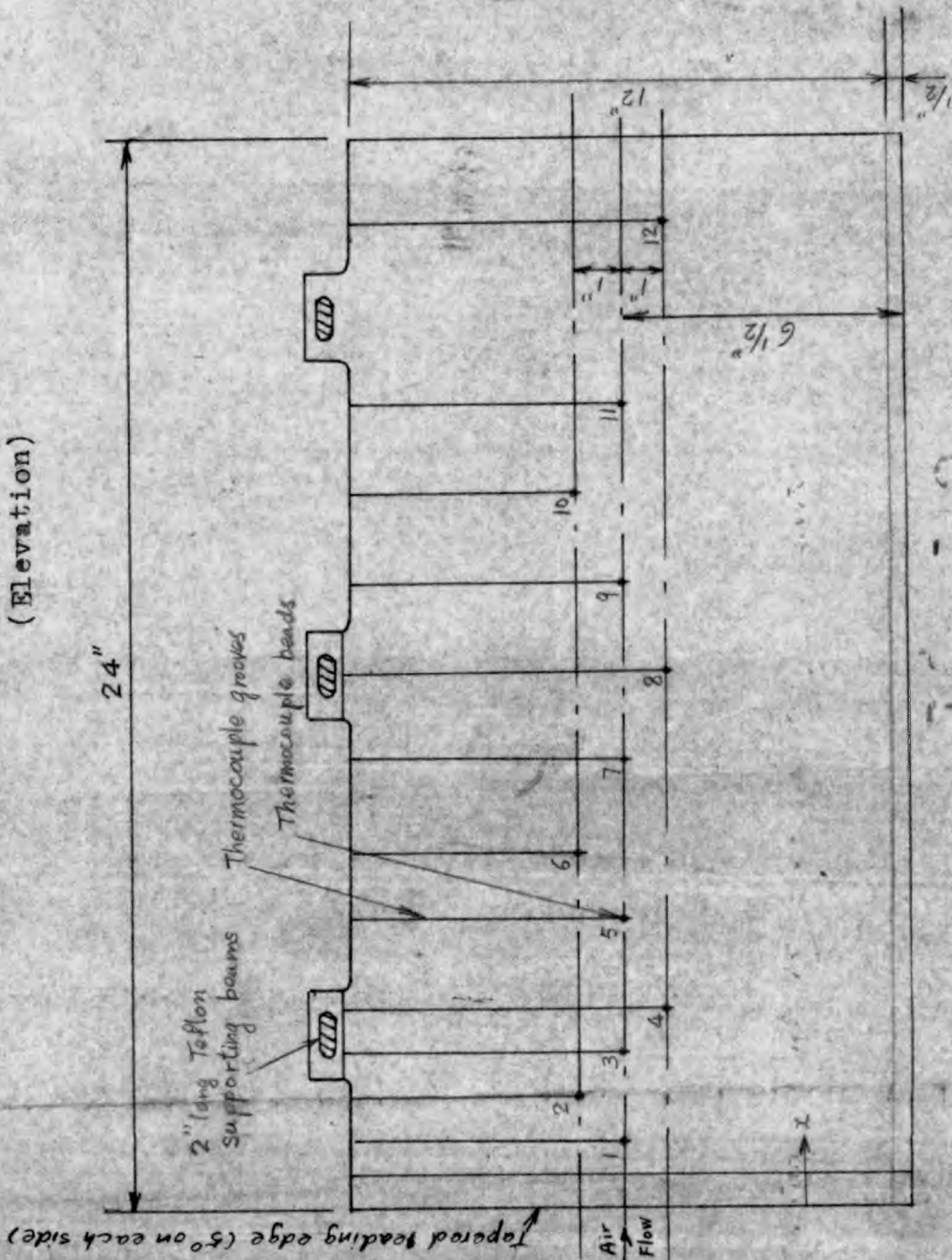
Fig.4.3(a) Details of the thermocouple fixing

Electrically insulate thermocouple leads.

Araldite

22 SWG Monel wire

Thermocouple bead soft soldered to the plate

0.186"

0.030" hole

1/32"

24"

1/2"

12"

6 1/2"

1" 1"

Thermocouple grooves

Thermocouple beads

2" long Teflon supporting beams

Tapered leading edge (5° on each side)

Air Flow

x
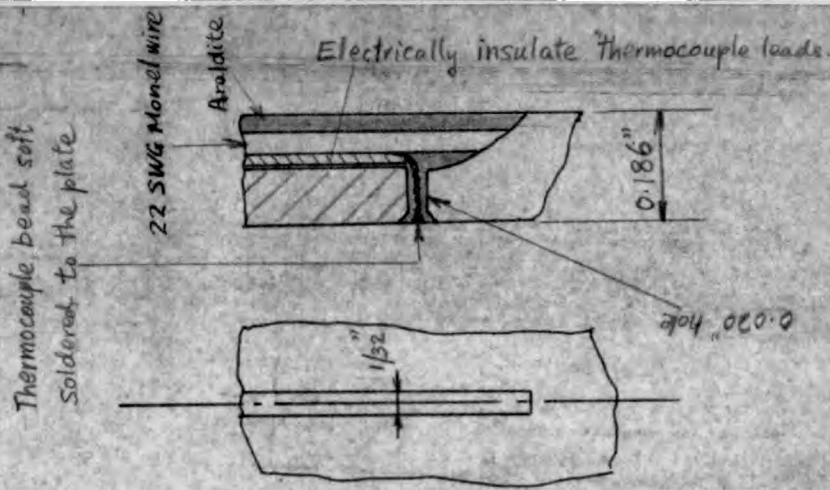
Thermocouple No.	1	2	3	4	5	6	7	8	9	10	11	12
x"	1·5	2·6	3·5	4·5	6·5	8	10	12	14	16	18	22

171

Fig.4.4   Diagrammatic layout of cooling apparatus

Teflon Sliding Seal

Test Plate

X →

Air Flow

Cooling Jacket

27"

12"

D

C

A

B

X

X →

Side Compartments

Middle compartment

Sectional View on XX

Bottled N₂ Gas

5 Gal. Liquid N₂ Container

12" Stroke, 2½" Bore   Pneumatic Rams

Air Flow Regulators.
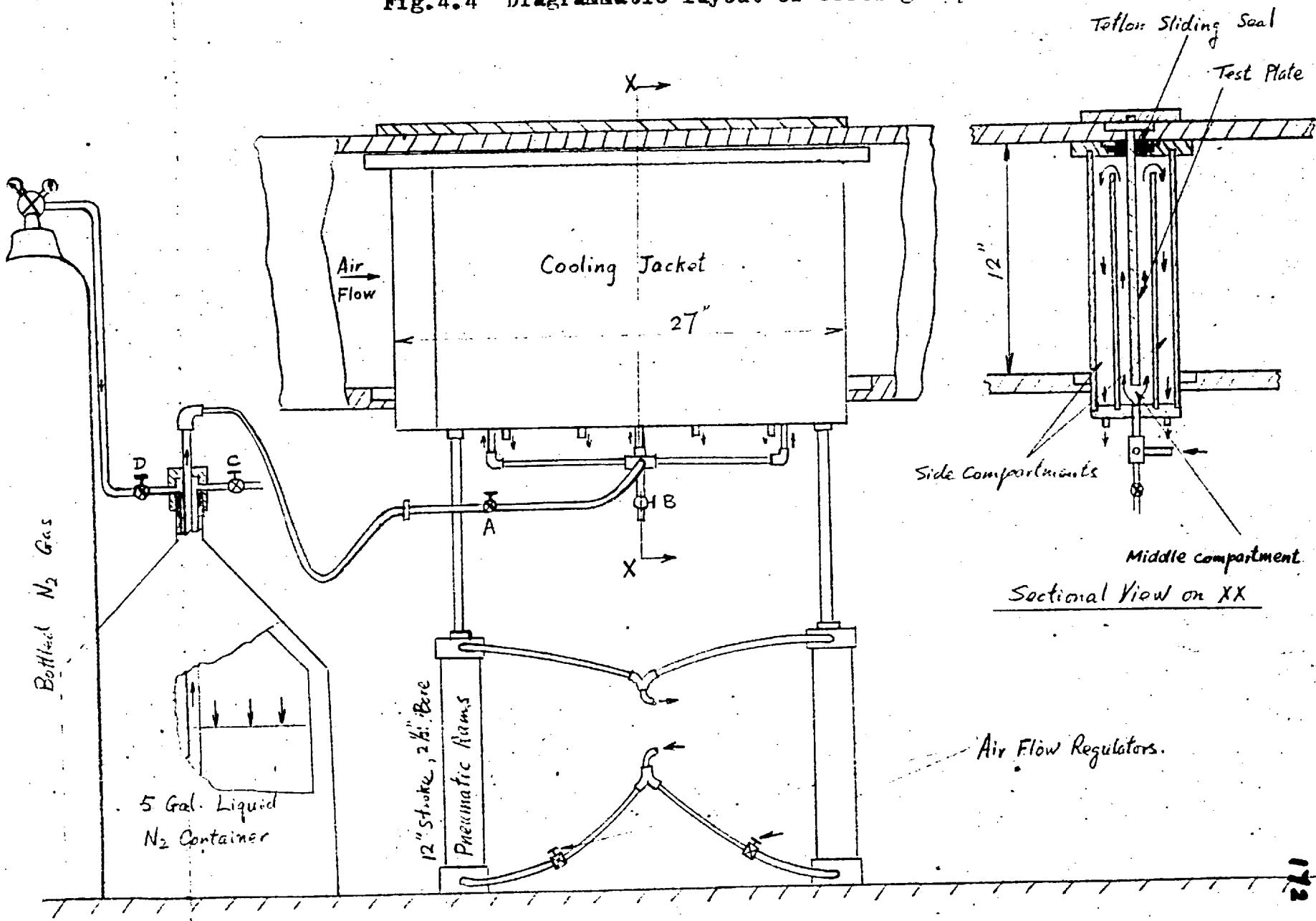
Fig.4.5   Diagrammatic drawing of air drying plant.

From Air Bleeding Hole

2½" BS Pipe

1" Diam. BS Orifice

Pressure Leads to U Tube Manometer

Air Filters

5'-0"

Packed "Actal" 3'-0" High

To Air Inlet Port

Air Blower

3 HP Electric Motor

1'-0"
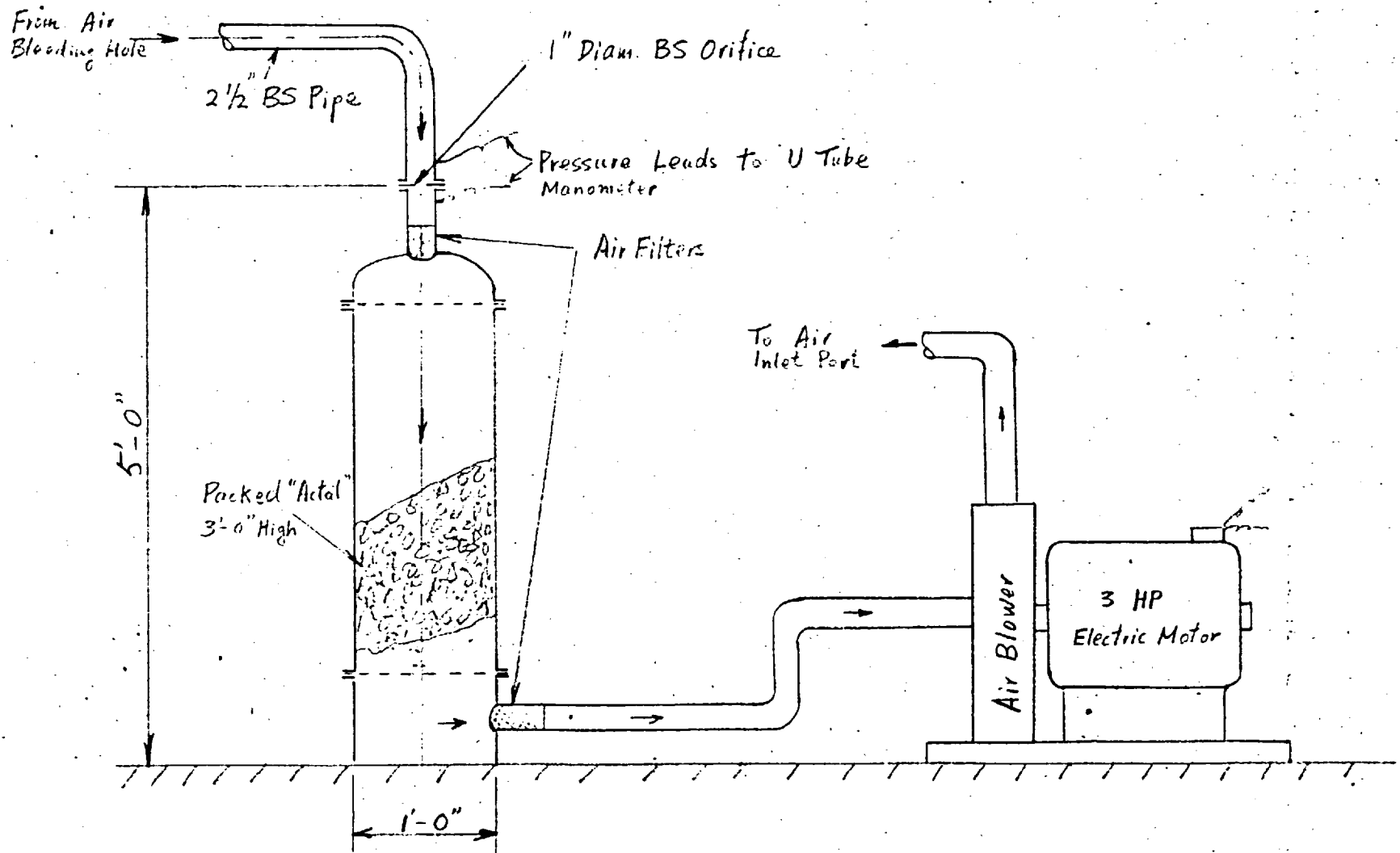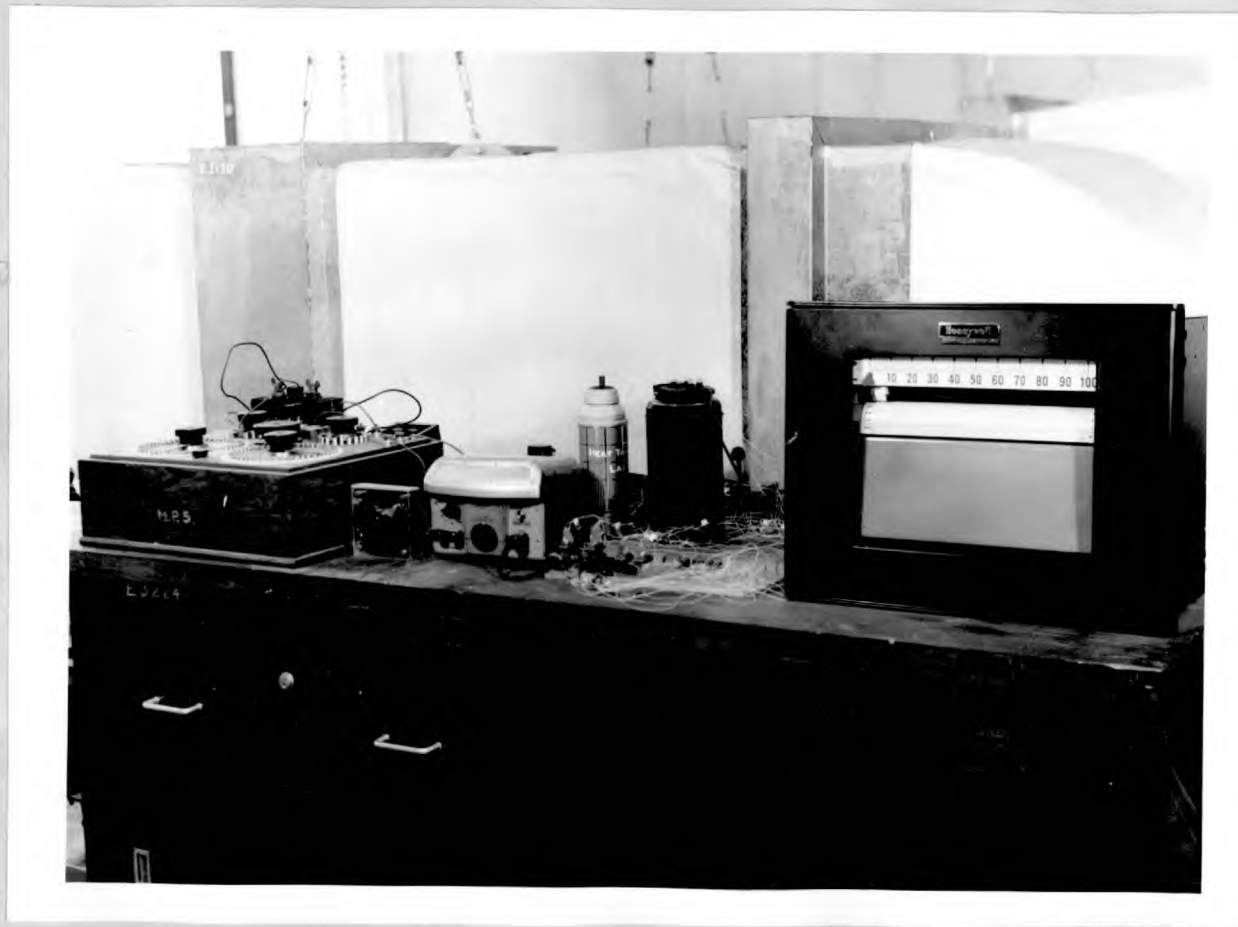
Fig. 4.6   Photograph of thermocouple e.m.f. measureing instruments.
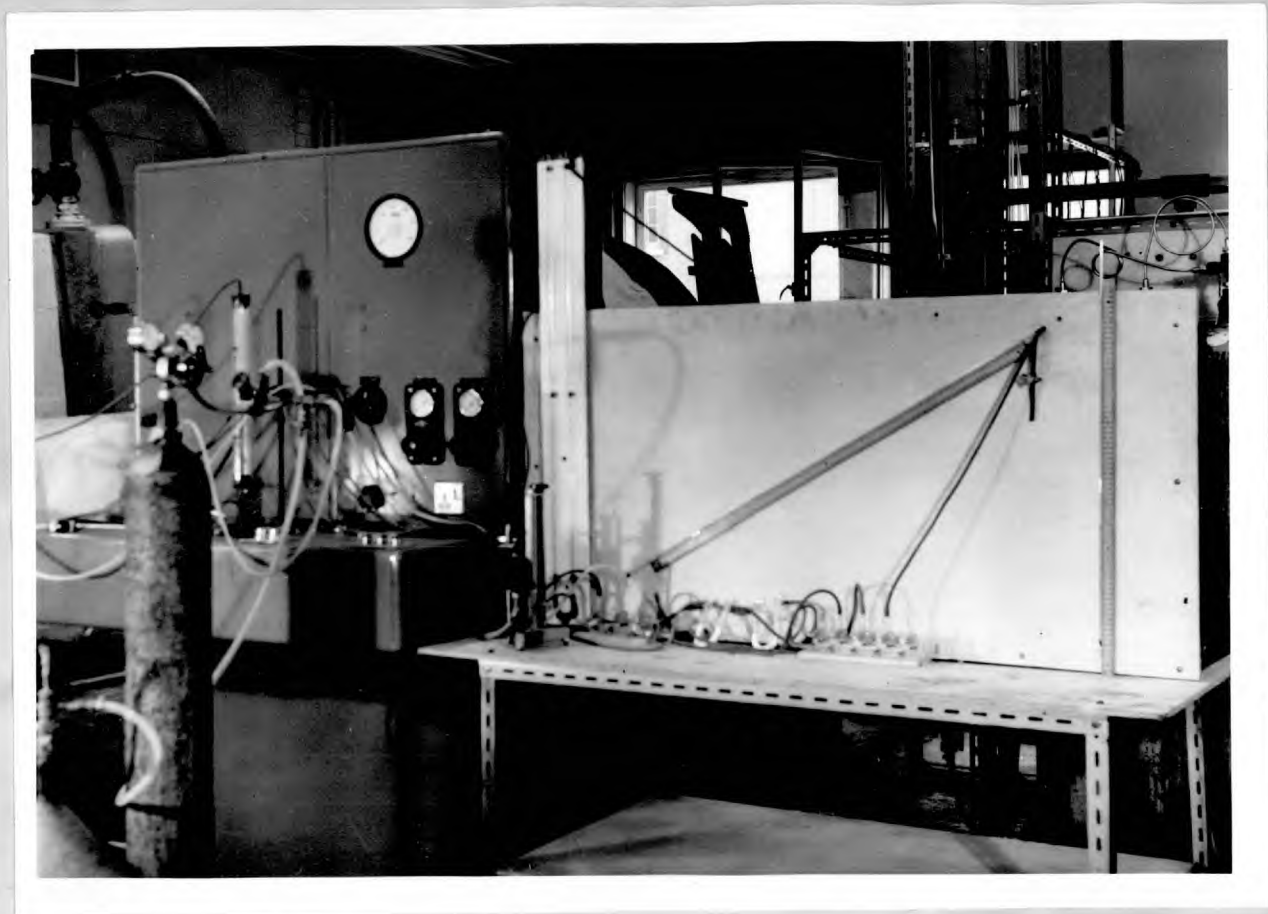
Fig.4.7 Photograph of pressure measuring instruments.

175
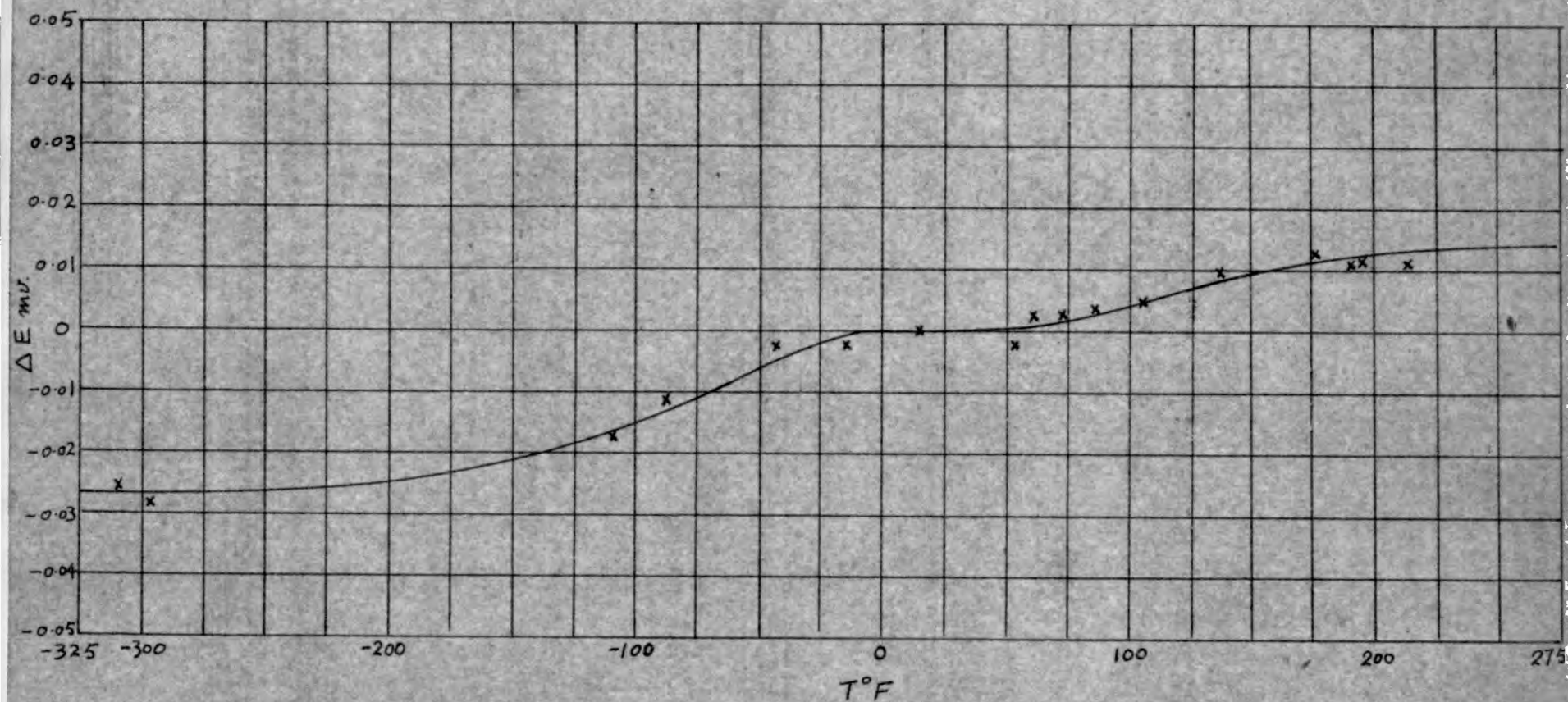
Fig. 4·8 Thermocouple calibration curve, (where
ΔE ≡ Measured e.m.f. - Reference e.m.f. of BS 1828).

176
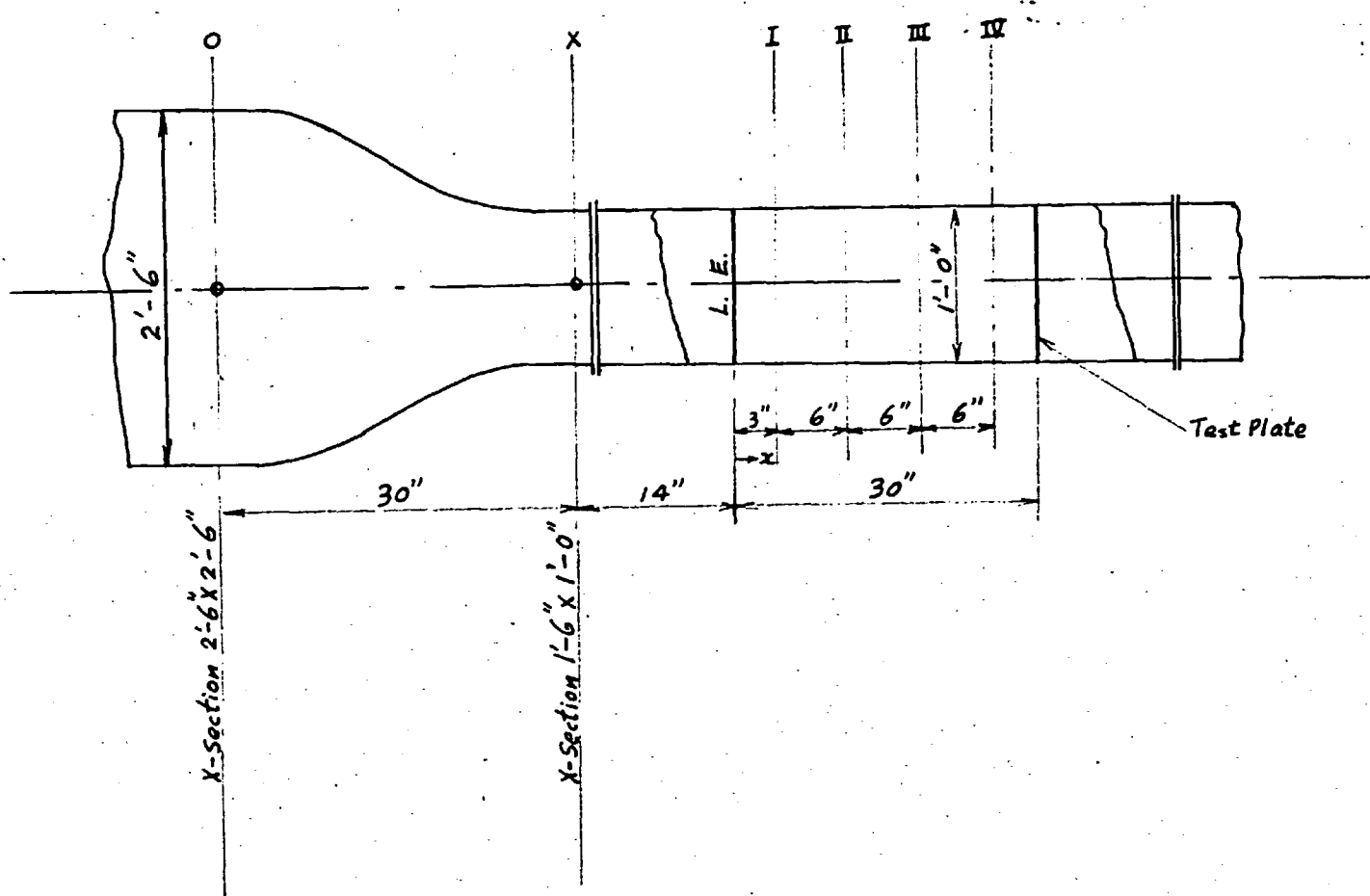
Fig.4.9 Relative wind-tunnel positions.
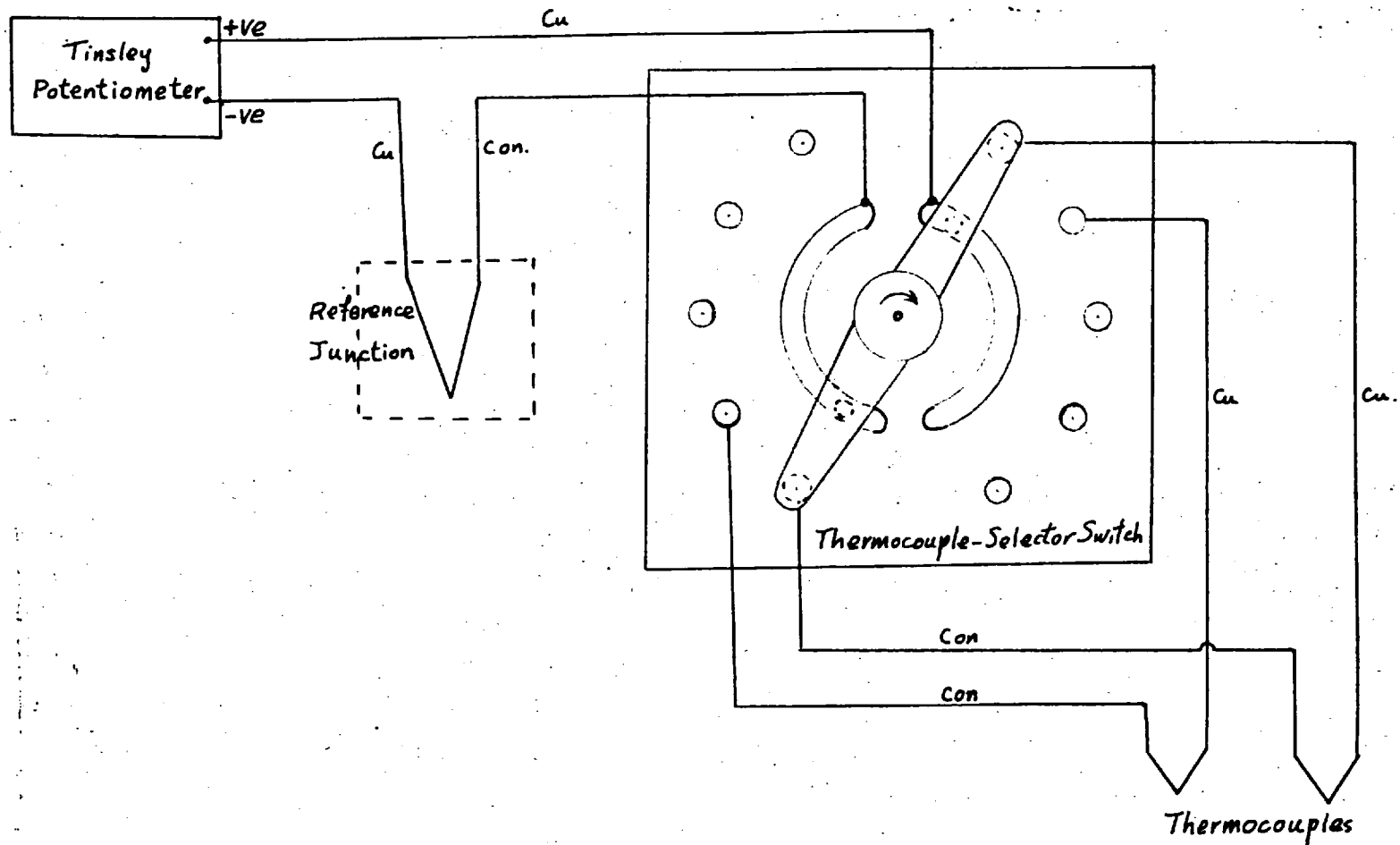
Fig.4.10   Thermocouple circuits.
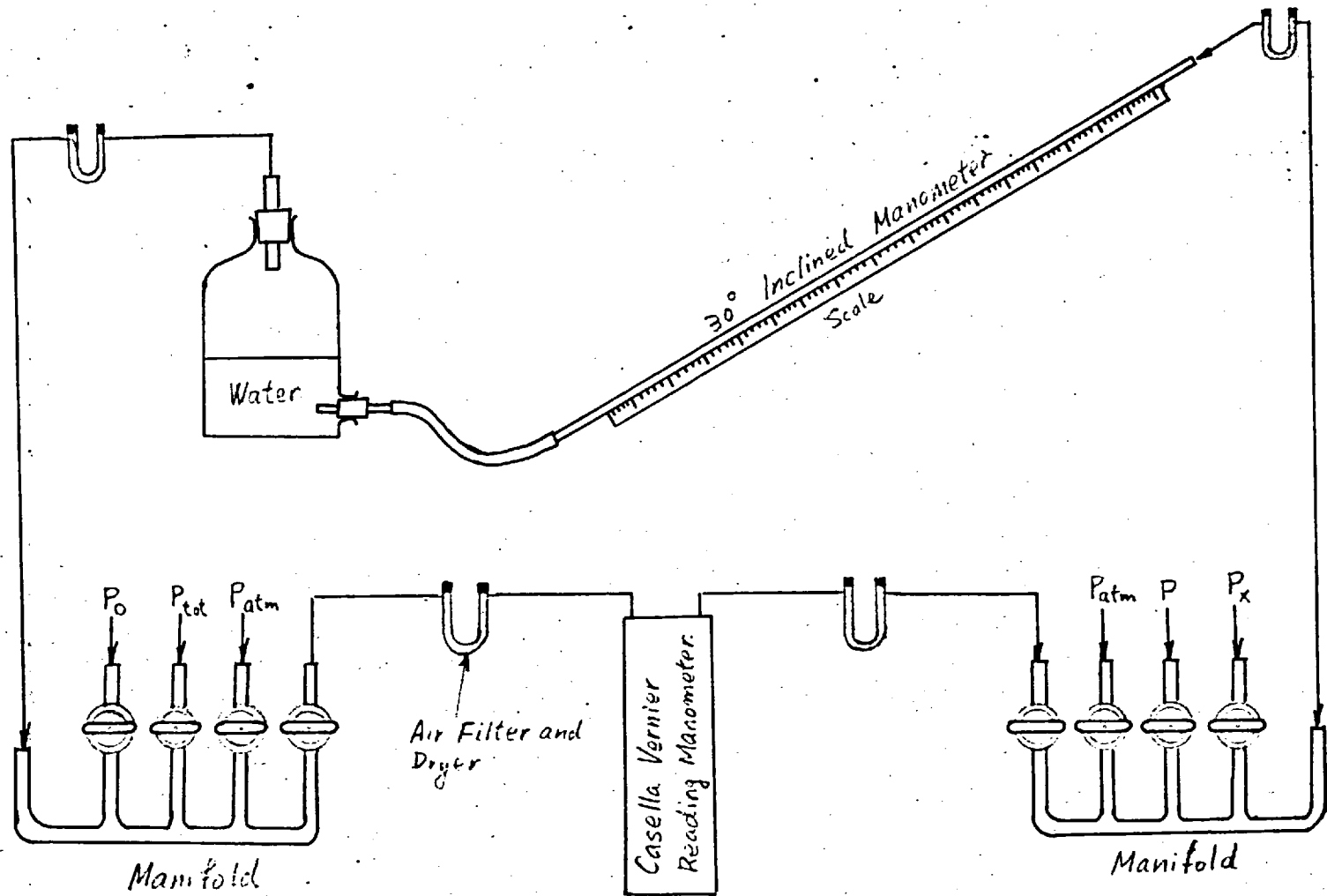
Fig. 4.11   Manometer connections.

Thermocouple Bead.

7 Holes, 0.038"D.

5/8" BSF

7/8

Flow

5/32"

5/16"

2"

5"

1 1/2"

1/4"

7/8

P

P_{tot}
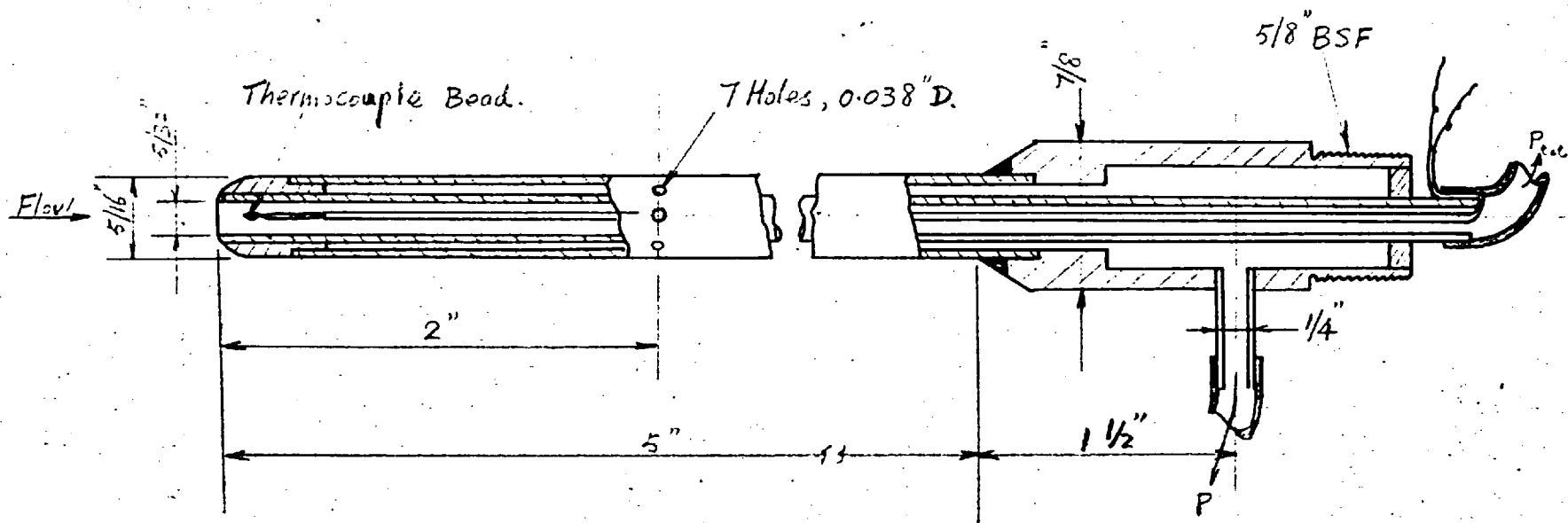
Fig. 4.12   Traversing Pitot-thermocouple.

12 Point Plug (I)

6 Test-Plate Thermo-Couples (No. 1-6)

12 Point Plug (II).

6 Test-Plate Thermo-Couples (No. 7-12)

Honeywell Multipoint Recording Potentiometer

6 Reference Junctions

12 Point Socket

Terminals
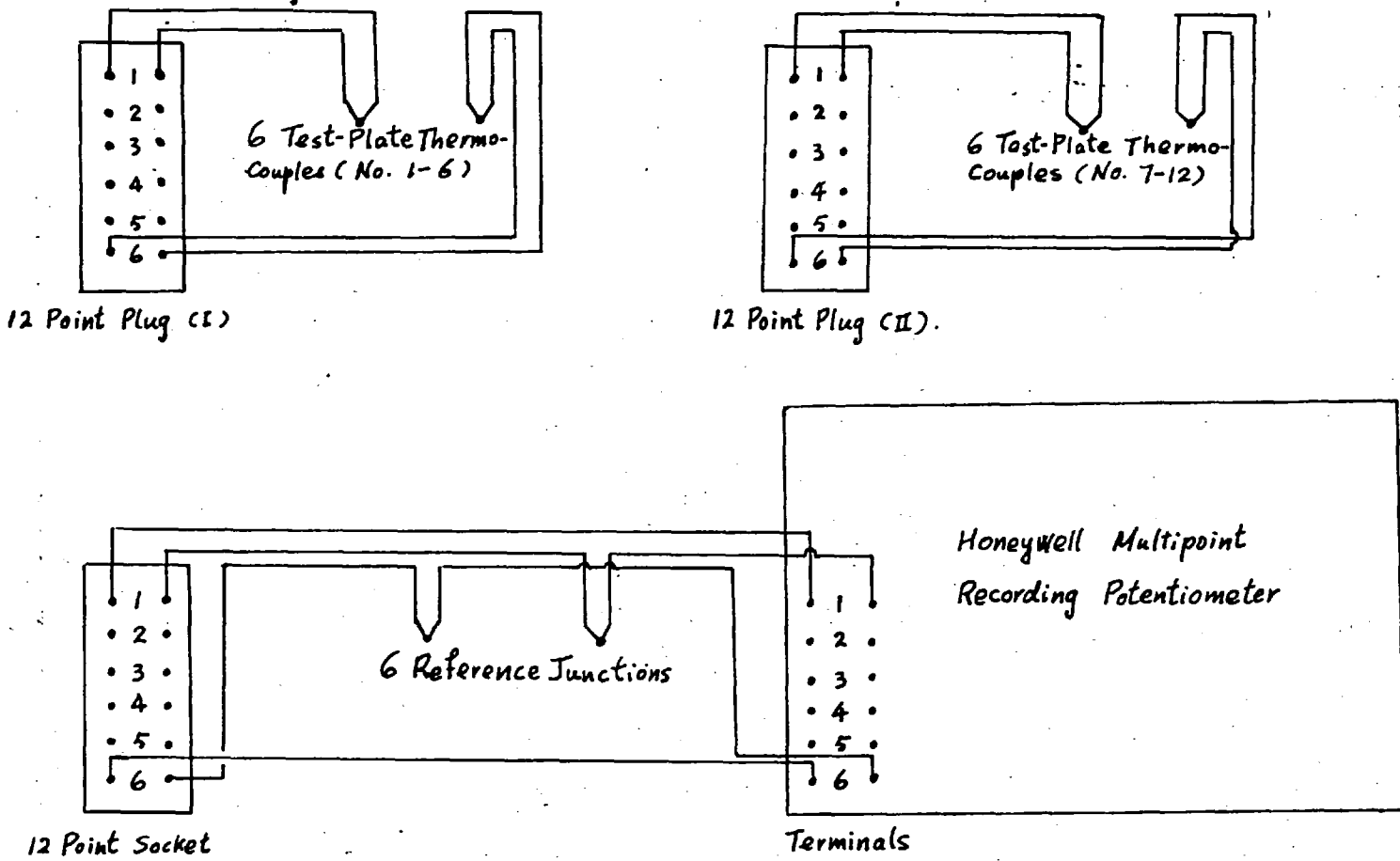
Fig.4.13 Test-plate thermocouple circuit.
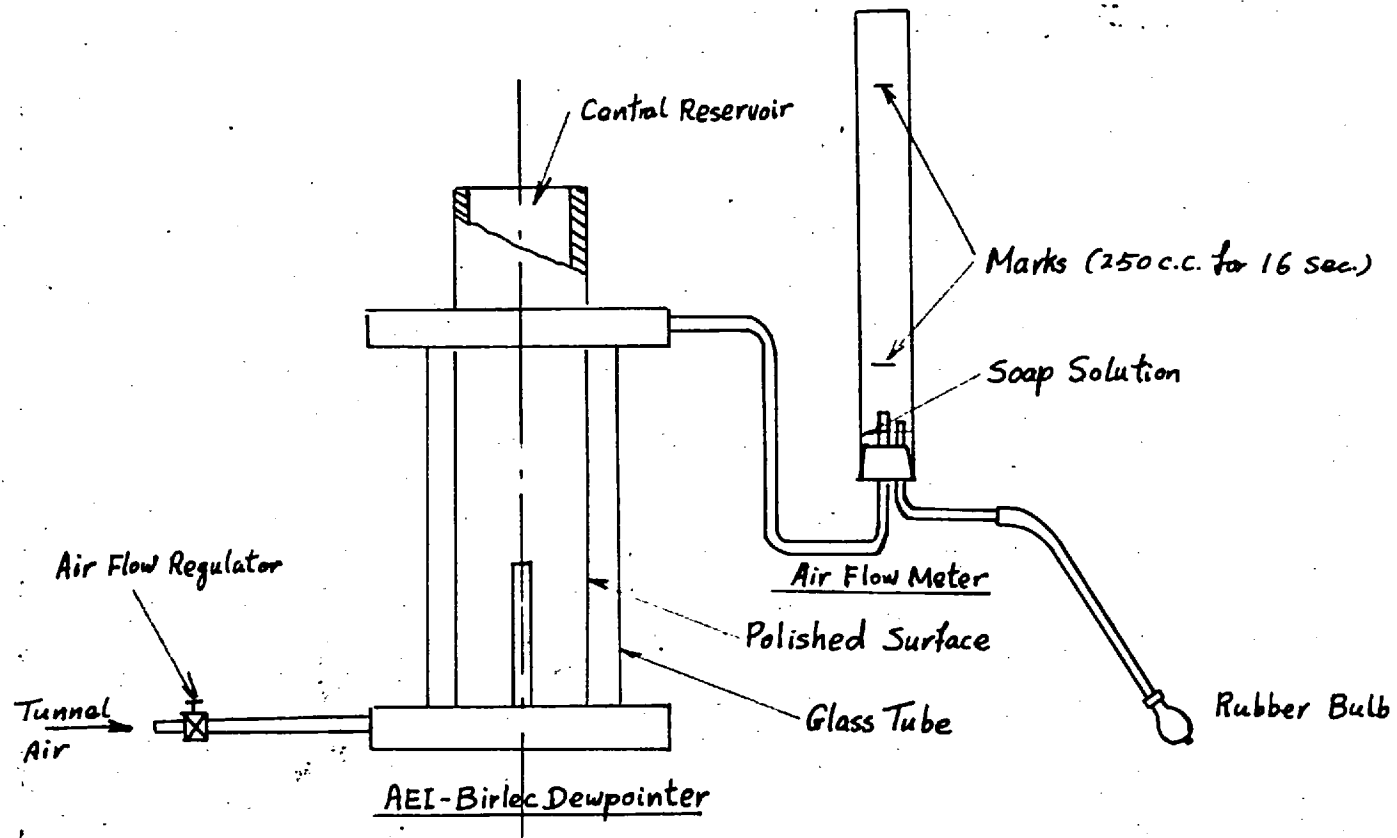
Fig. 4.14 Humidity measuring instruments.
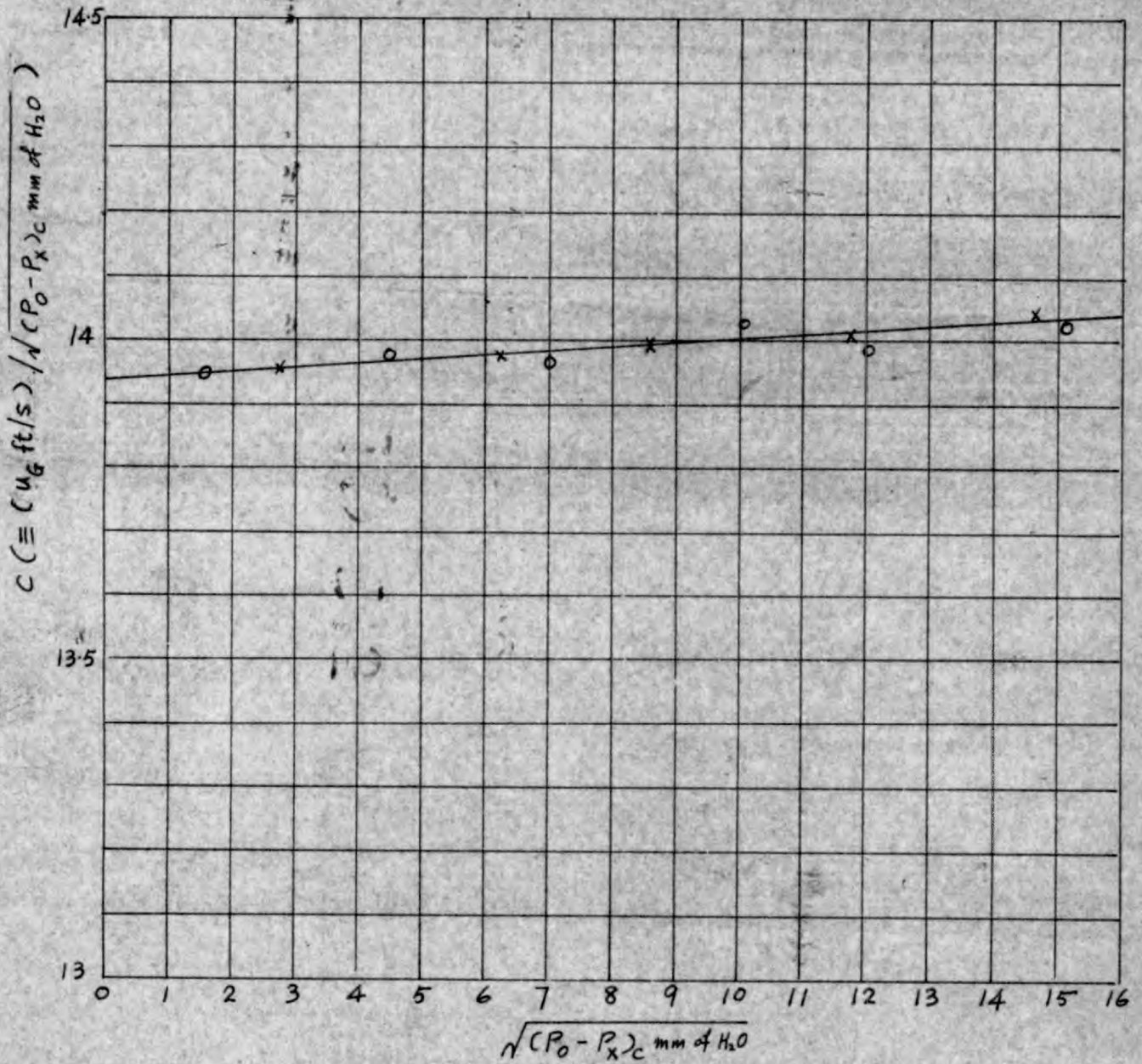
Fig. 4.15 Wind tunnel calibration curve.
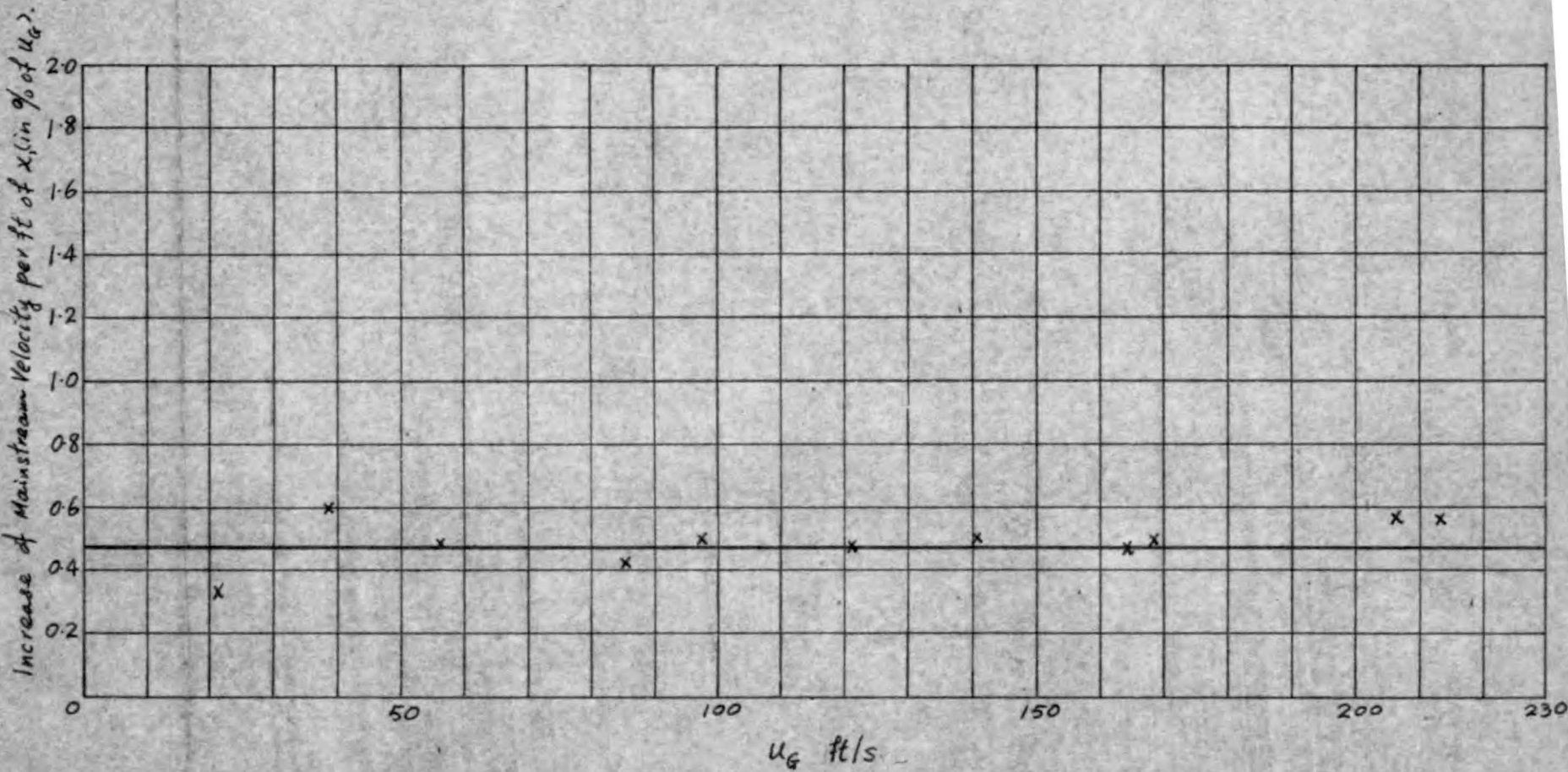
Fig.4.16 Variation of mainstream velocity in x-direction.

184
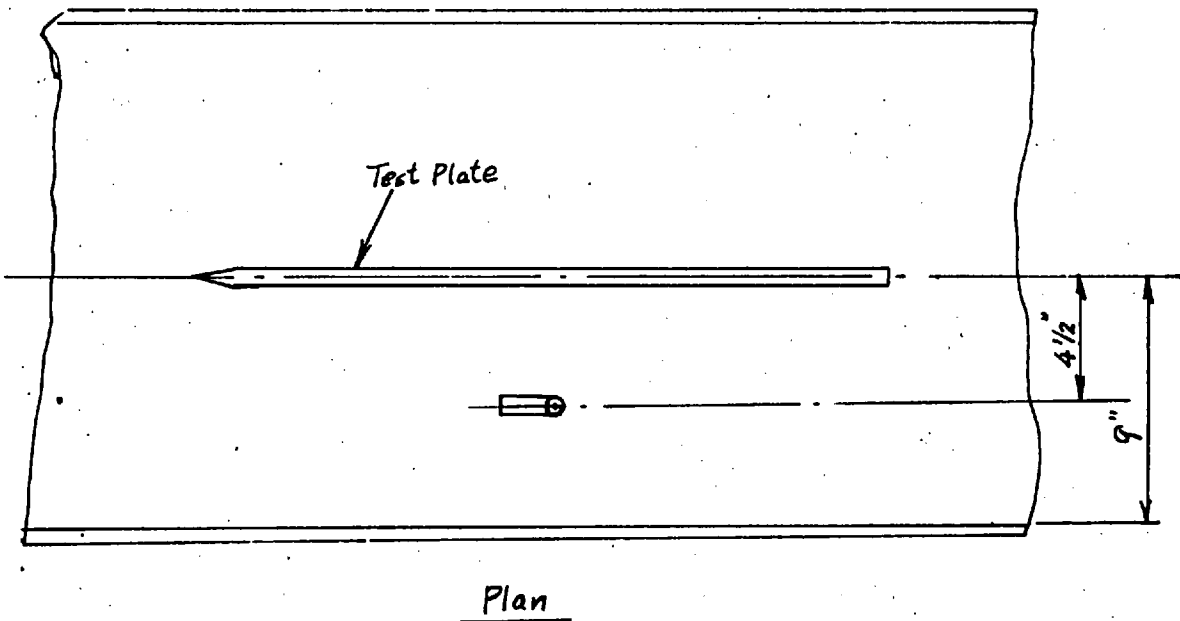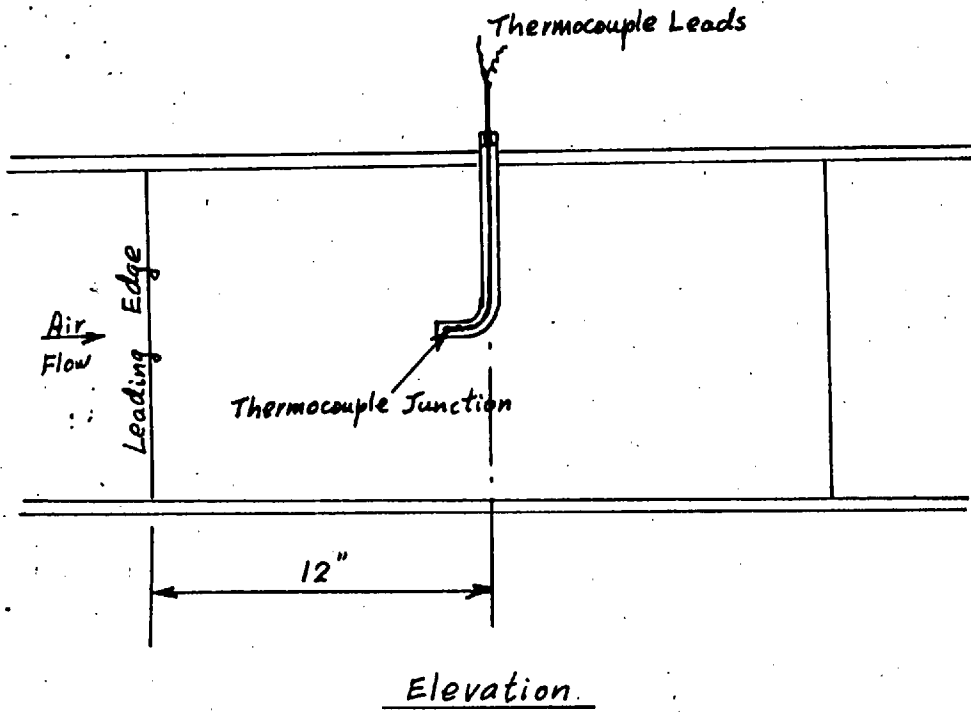
Fig. 4.17   Thermocouple probe for mainstream temperature.

186
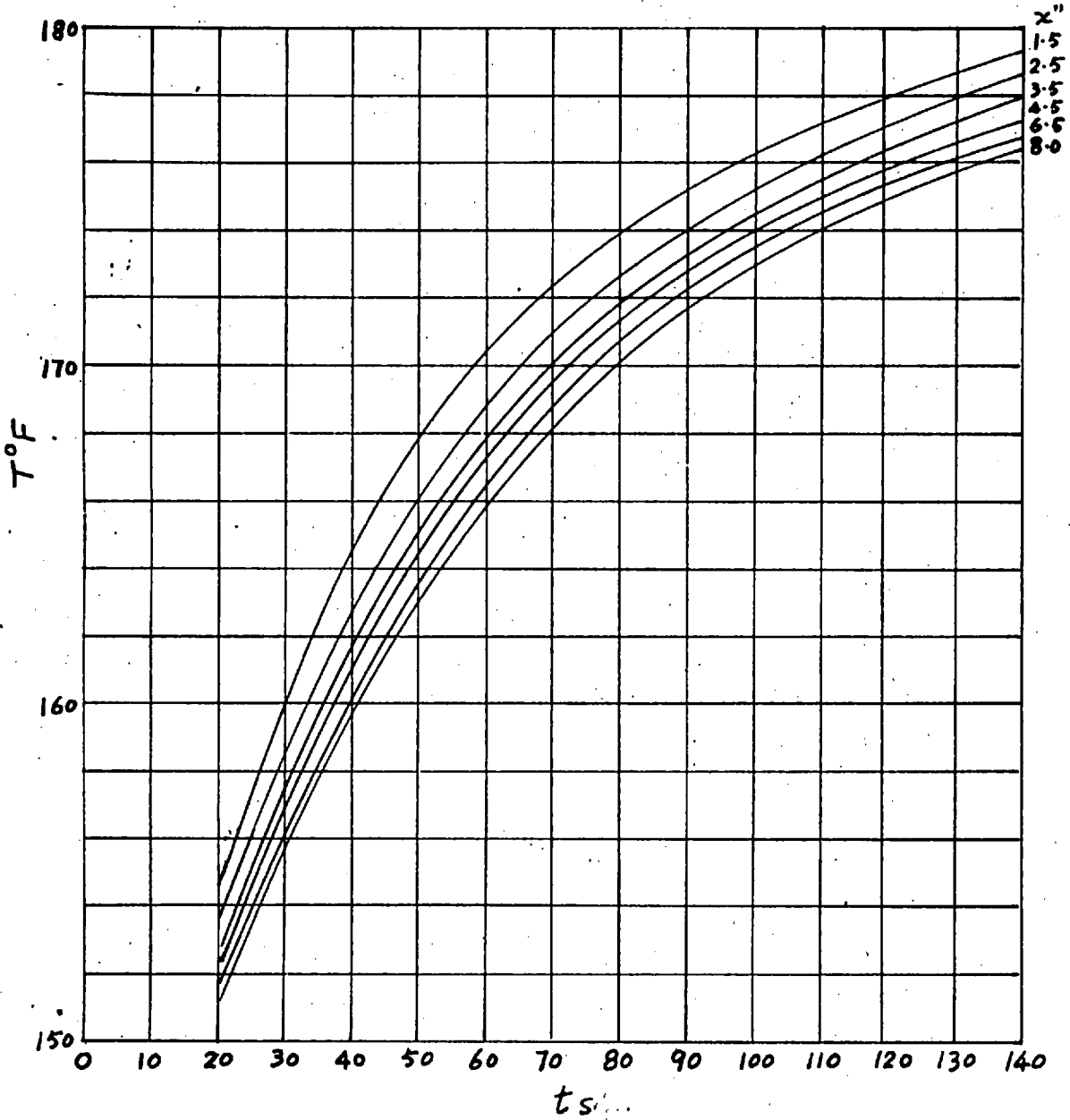
Fig. 4.18   T vs t curves from Test 1.
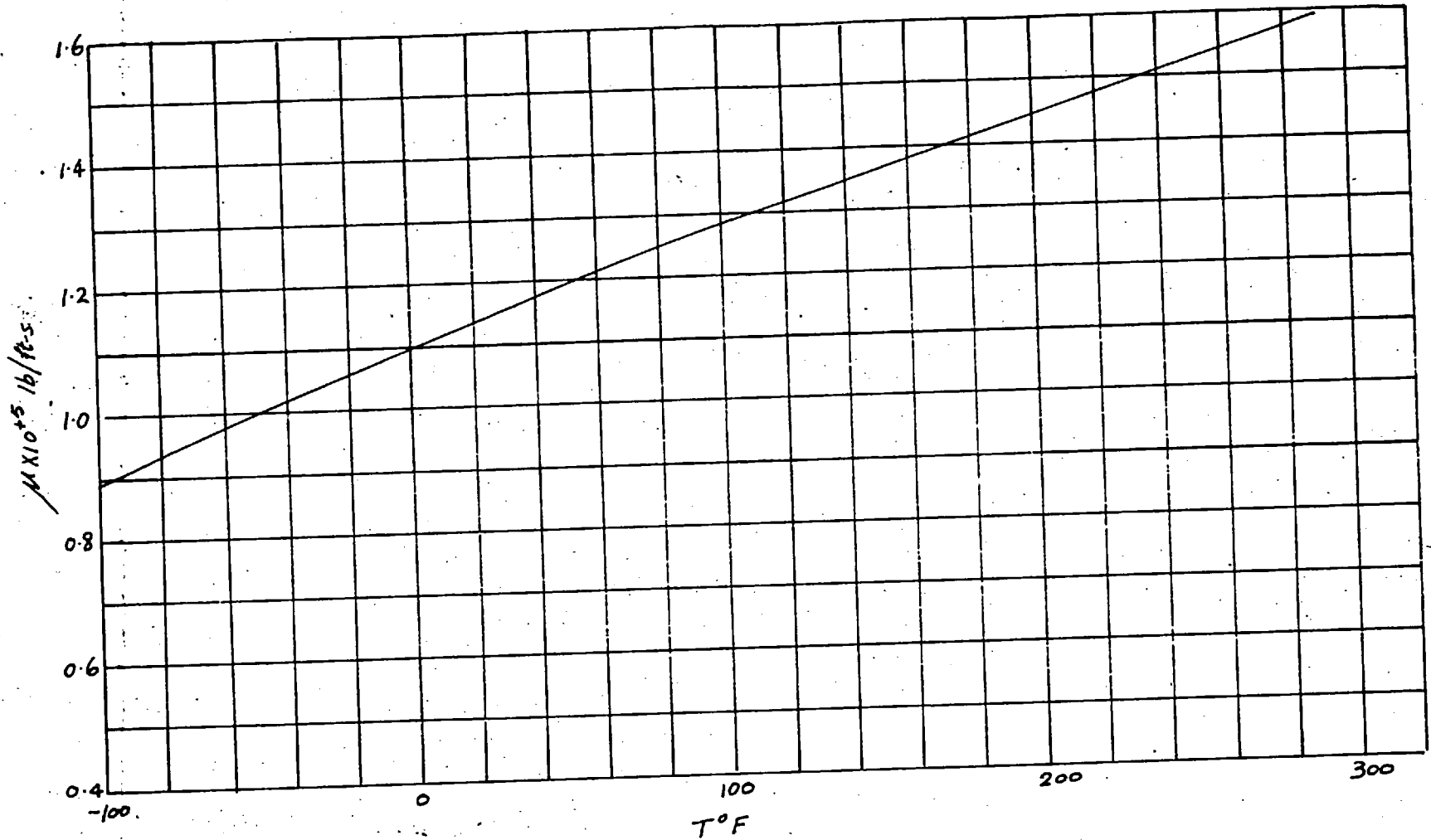
Fig. 4.19 Viscosity of air.
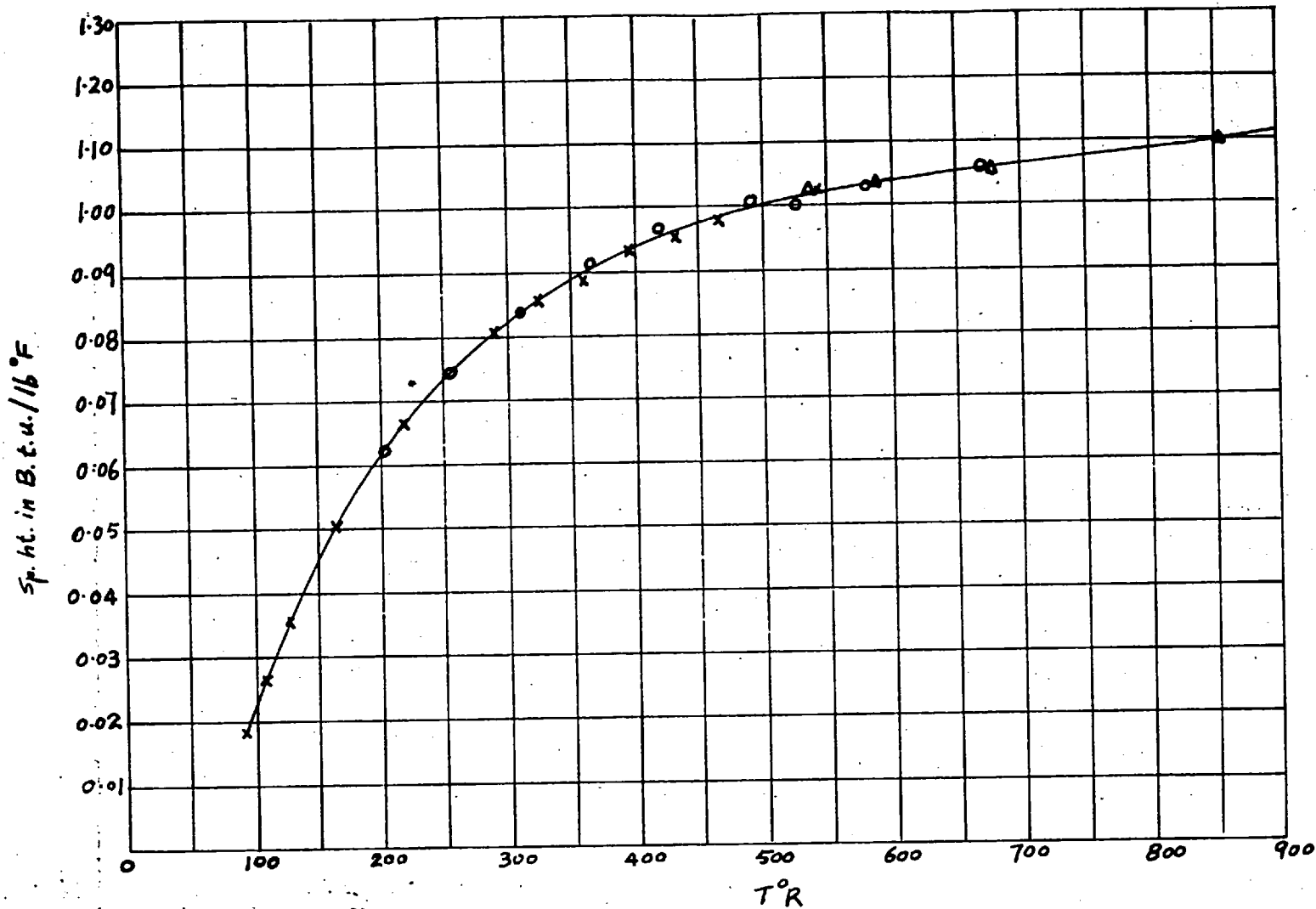
Fig.4.20   Specific heat of Monel 400.
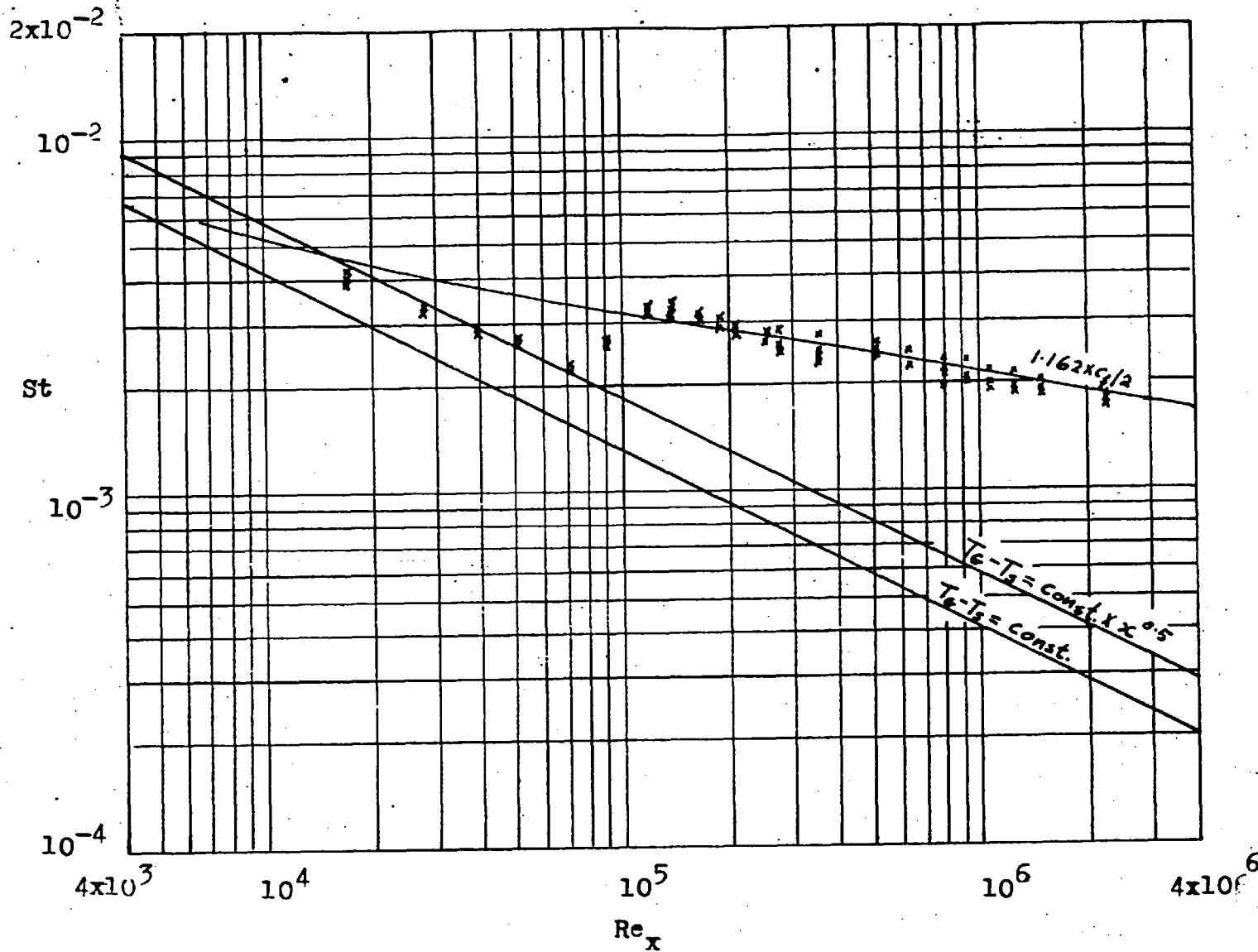
Fig.4.21   St vs Re$_x$ from Tests 1-4,(Tests at small temperature ratios).

Fig. 4.22 Typical wall temperature variations.
x, from test 3 at 100 seconds; o,
from test 4 at 120 seconds.

191
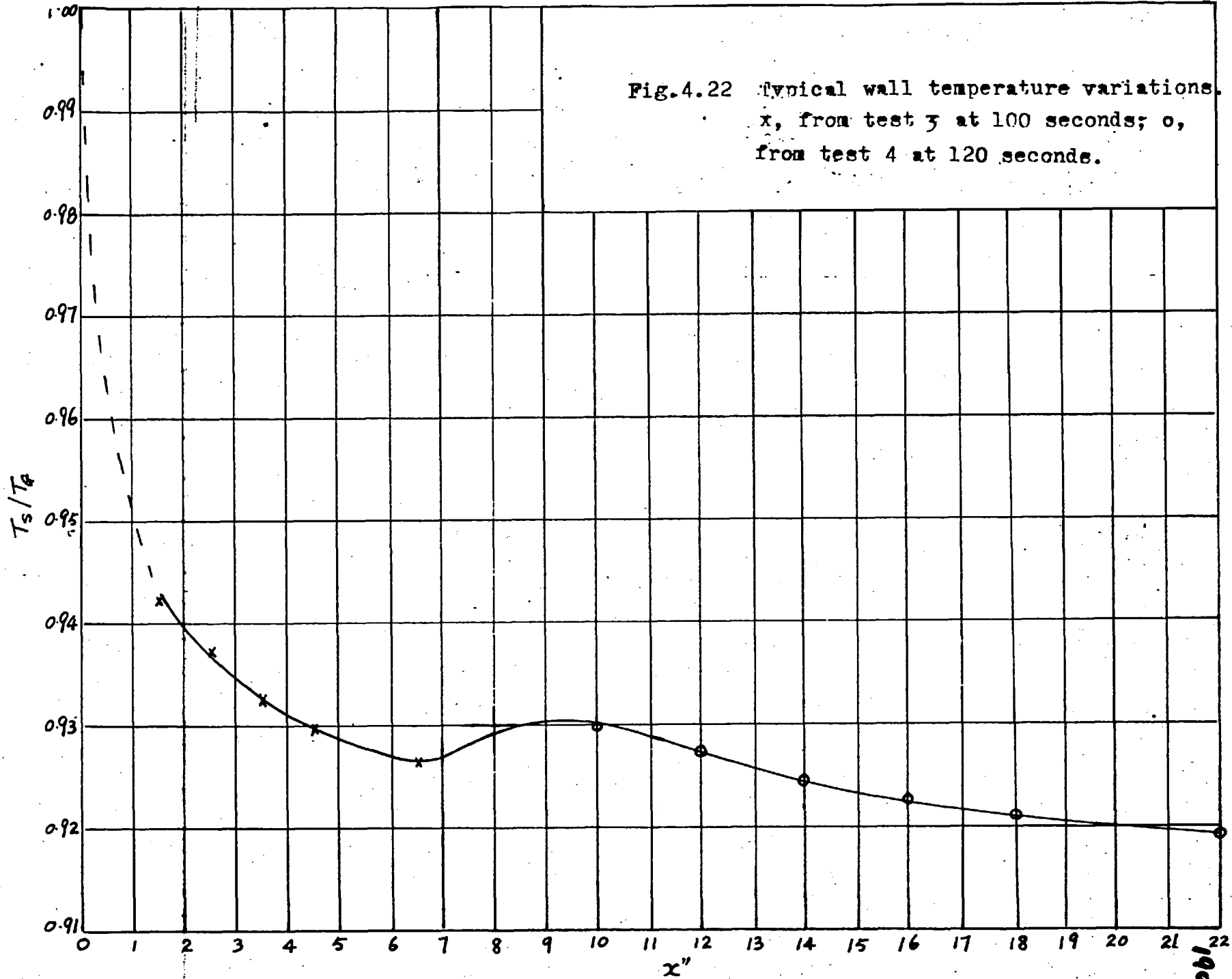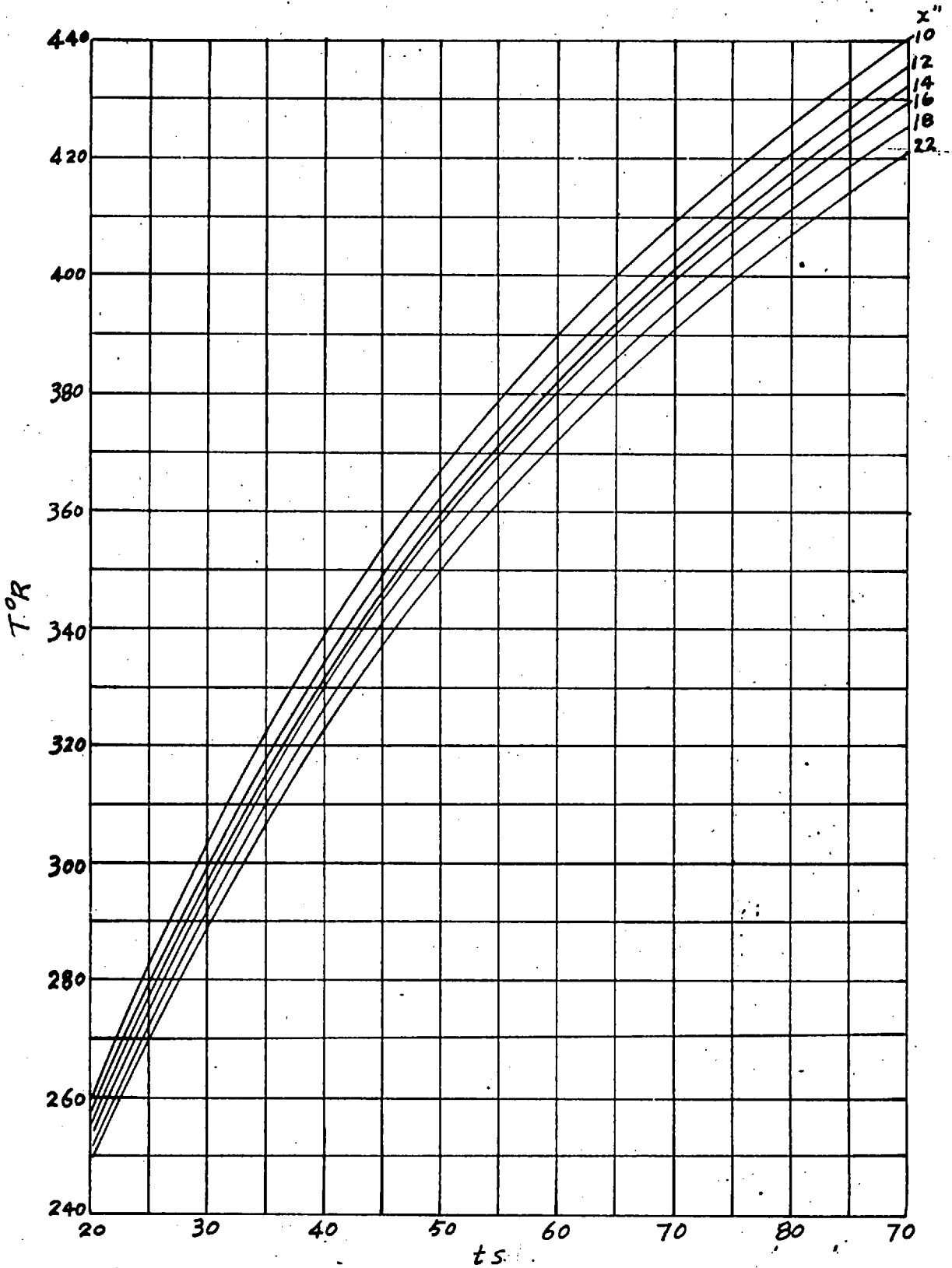
Fig.4.23   T vs t curves from Test 5.
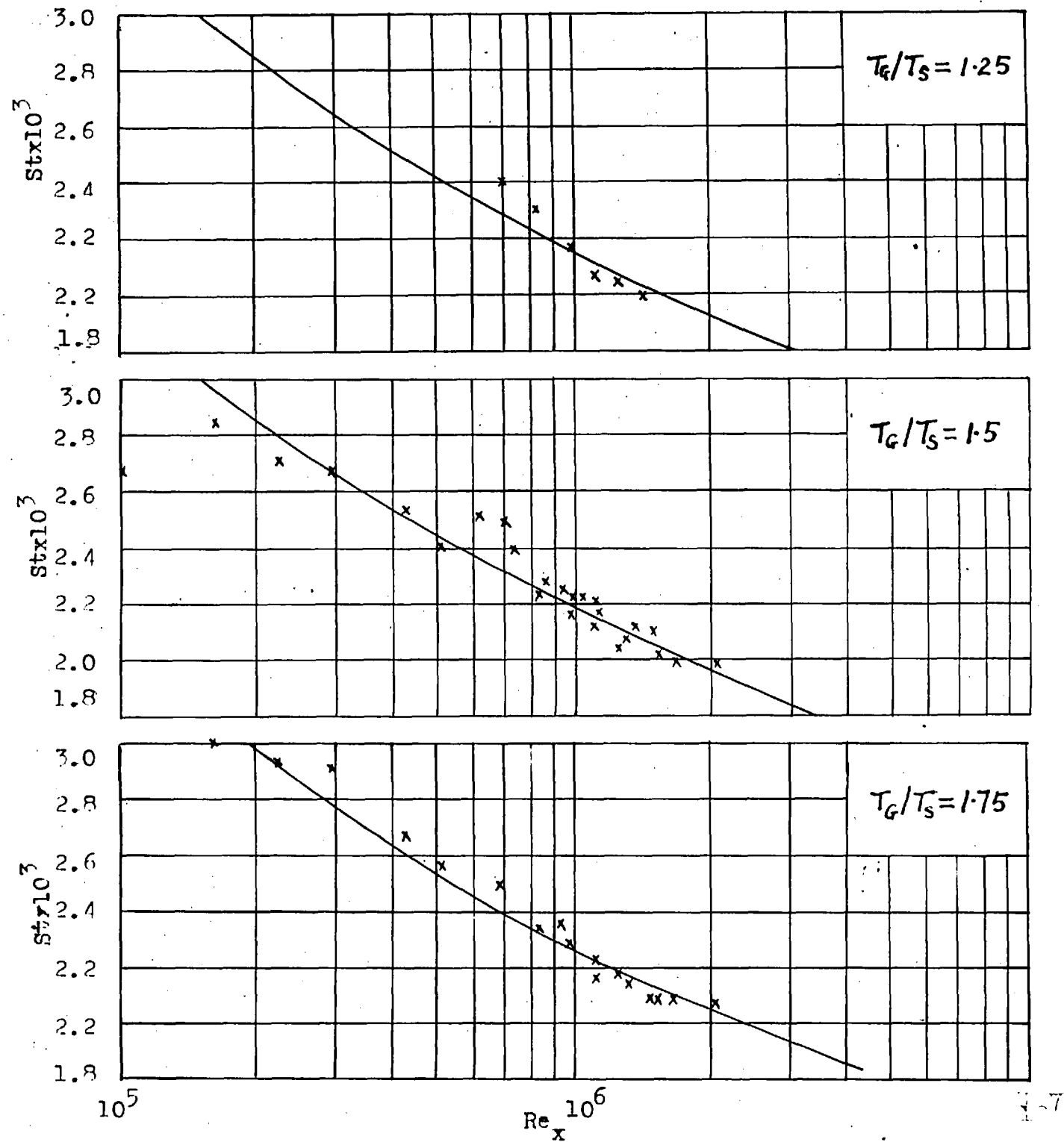
Fig. 4.24 Summary of experimental results, (St vs Re_x at various T_G/T_S)
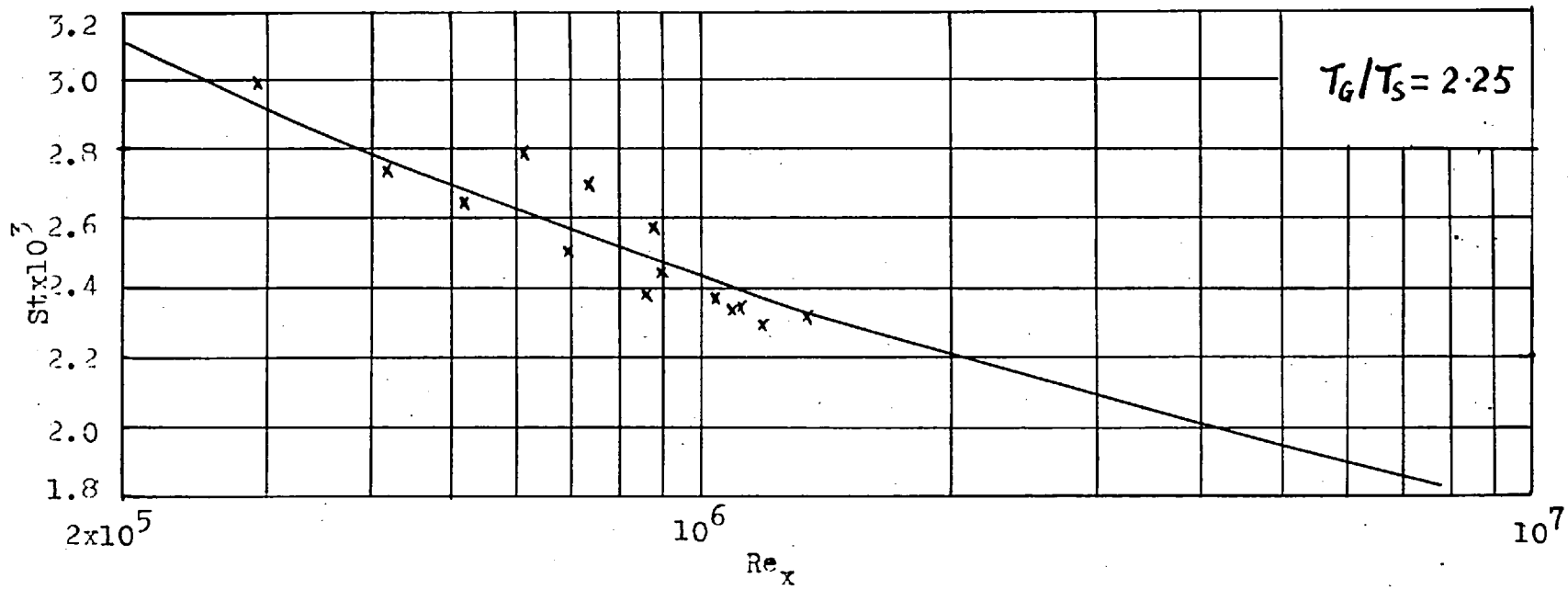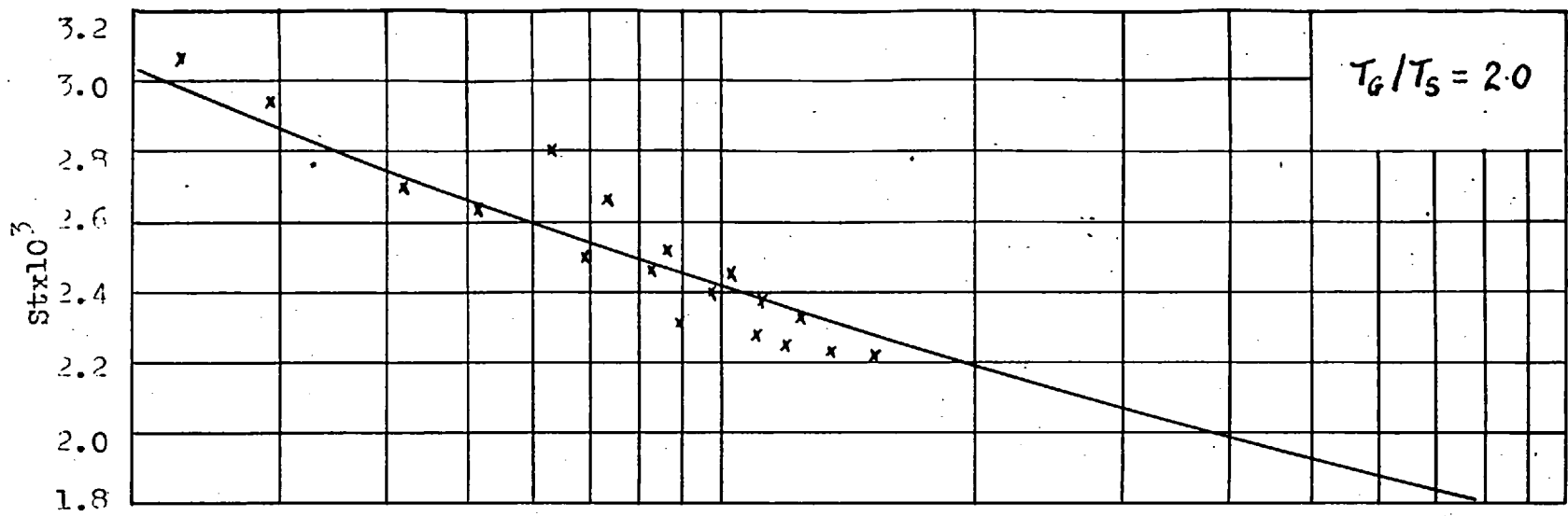
Figure 4.24 (continued).
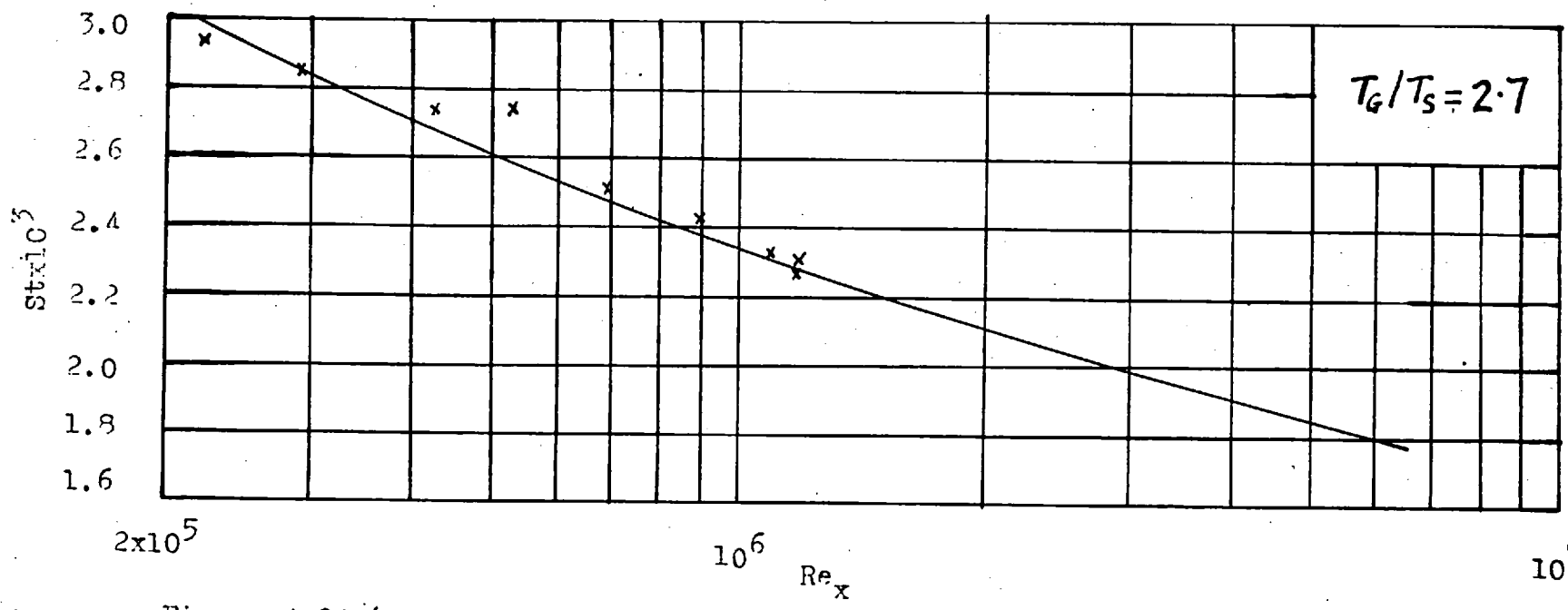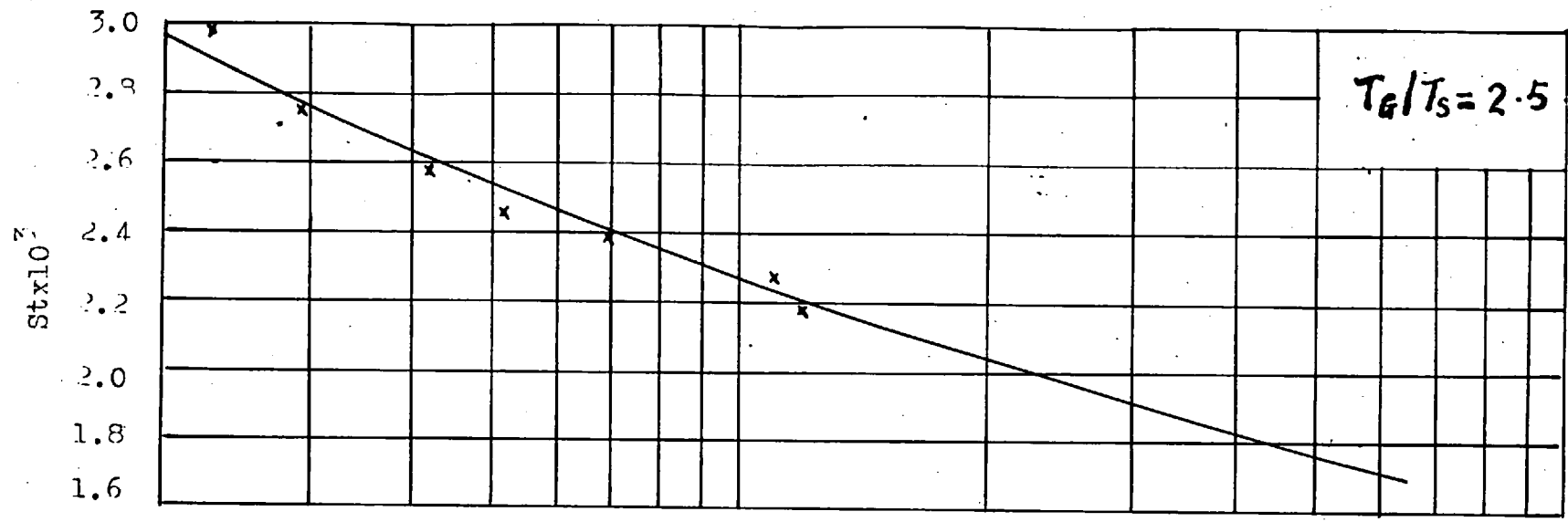
Figure 4.24 (continued).
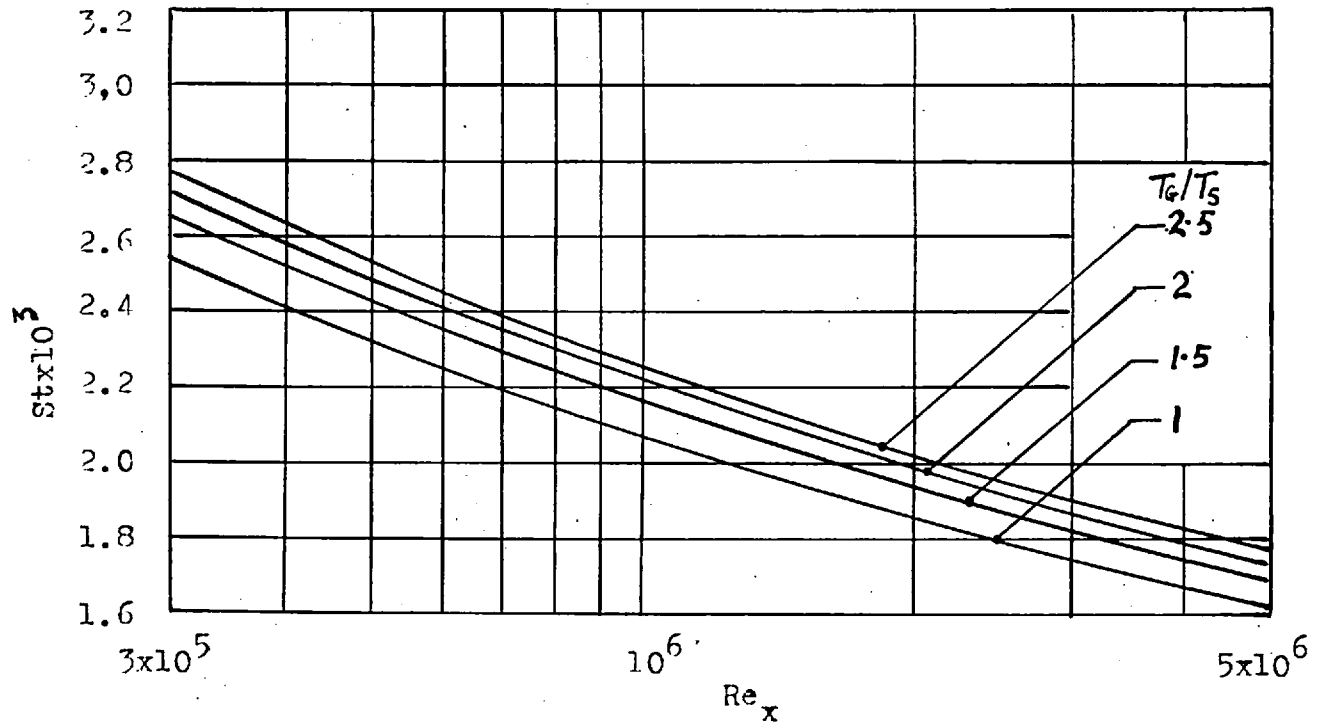
Fig. 4.25 Comparsion of experimental St values at various T_G/T_S.
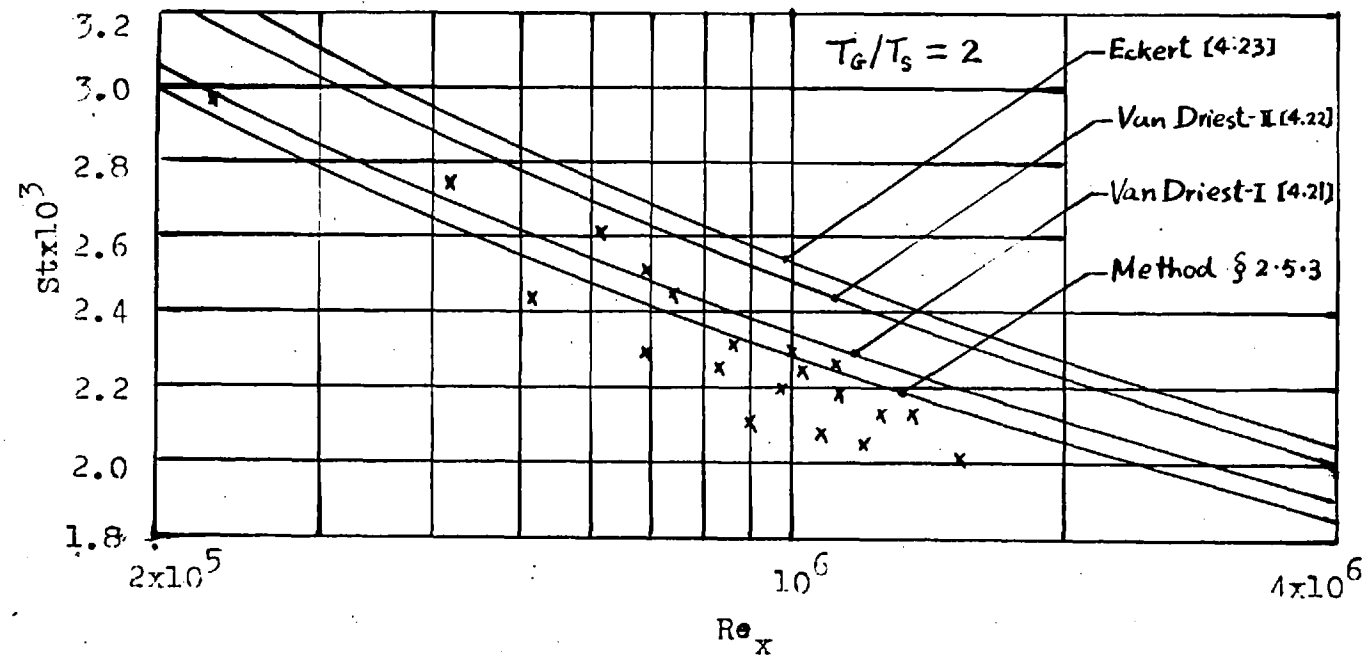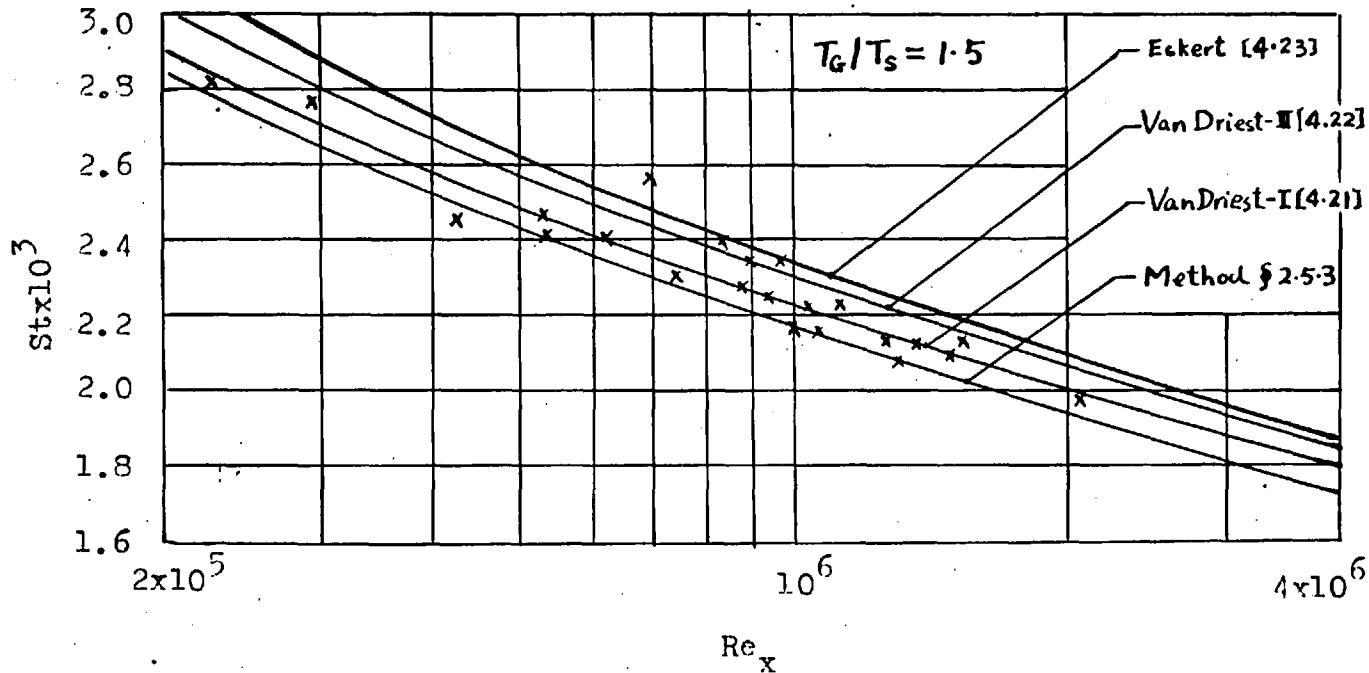
Fig.4.26 Comparison of theoretical St values (based upon a fixed S) with experimental St data.
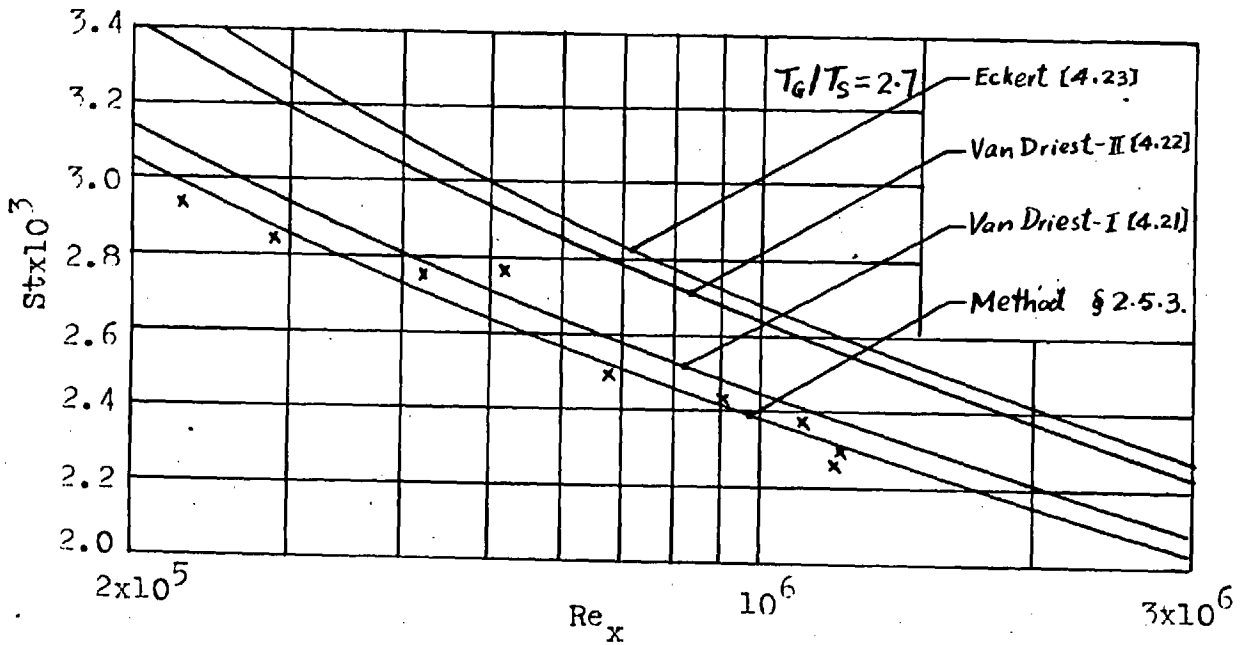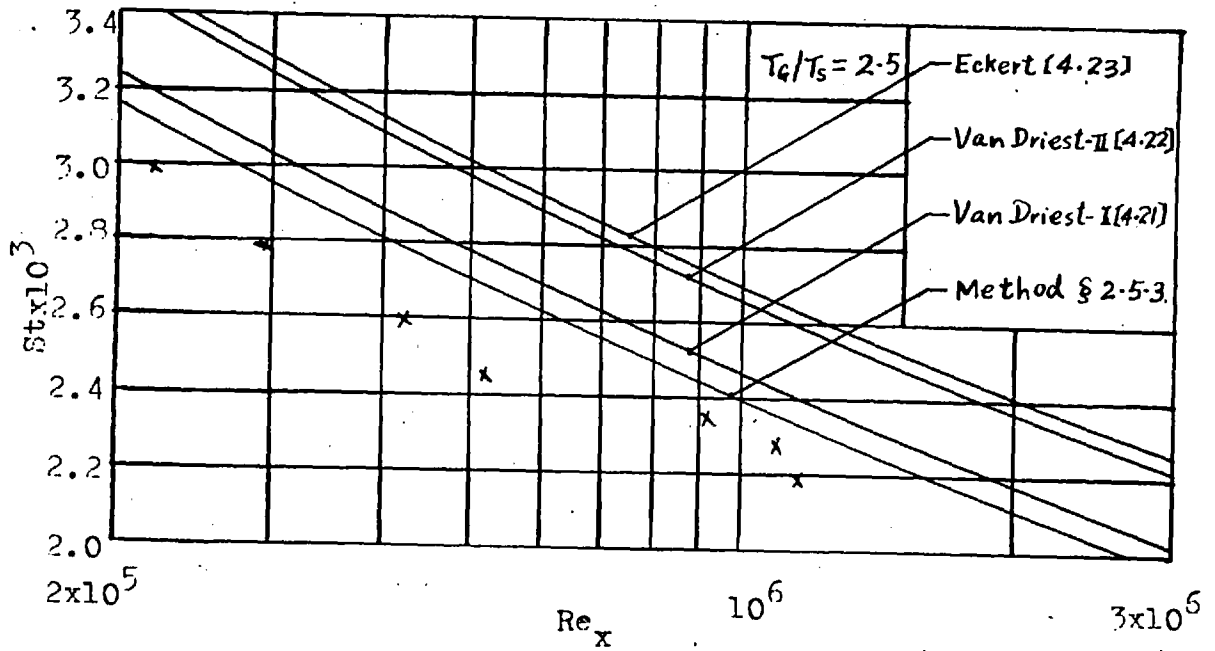
Figure 4.26 (continued).
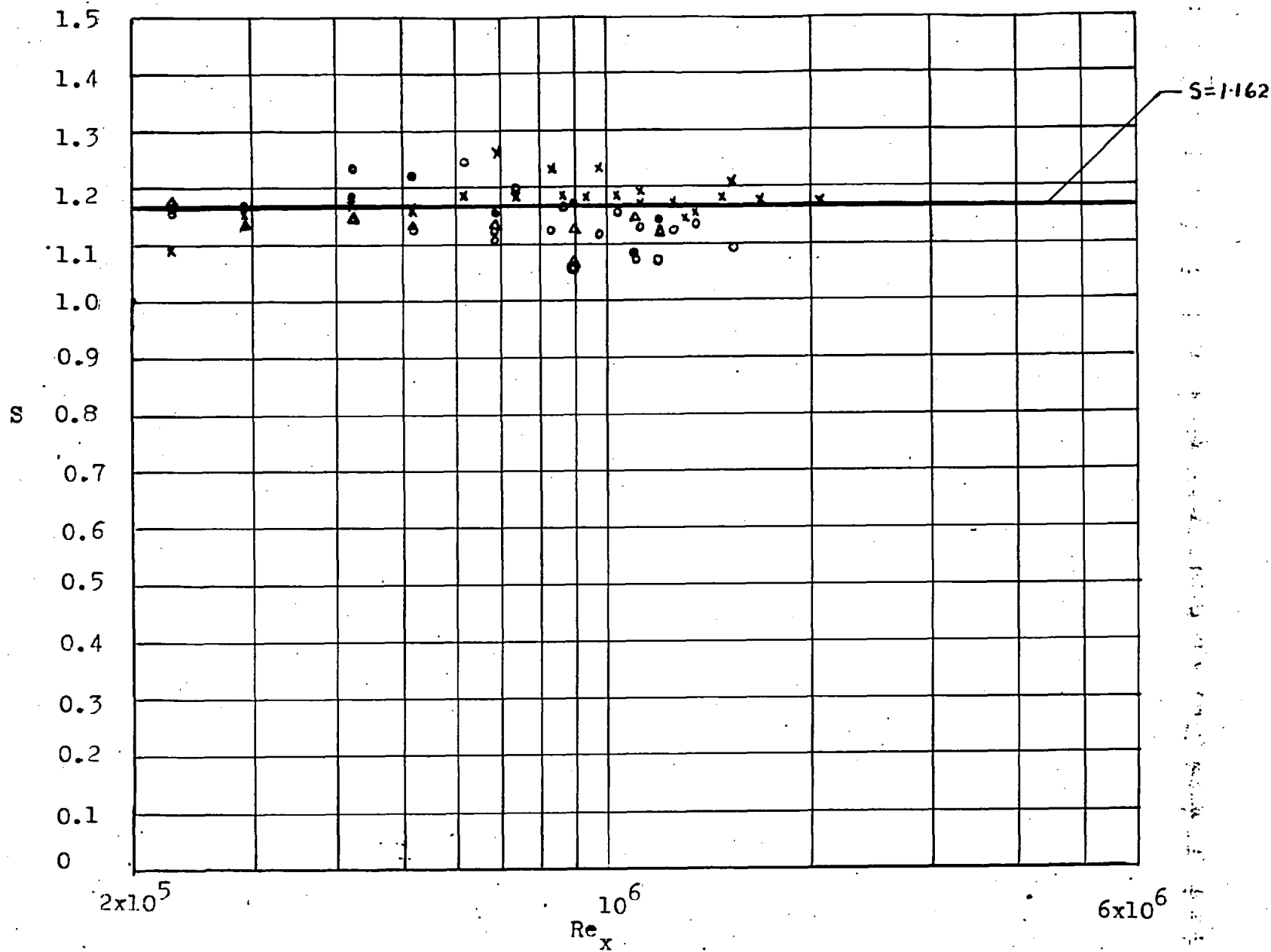
Fig.4.27 S vs Re$_x$ at various T$_G$/T$_S$.. x, T$_G$/T$_S$ = 1.5; o, T$_G$/T$_S$ = 2.0;

△, T$_G$/T$_S$ = 2.5; •, T$_G$/T$_S$ = 2.7.
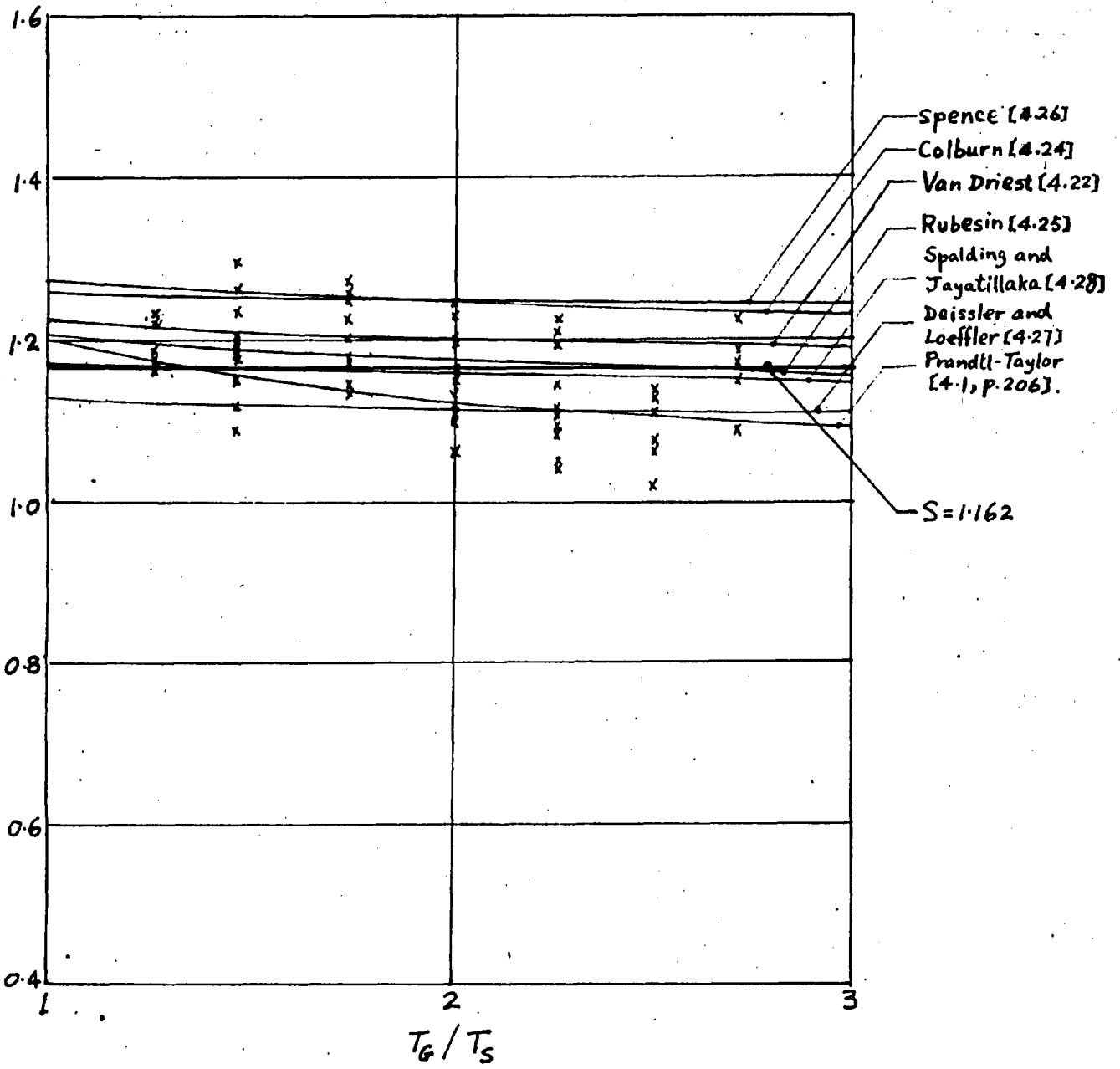
Fig.4.28   Comparison of various theoretical S values with
experimental data.
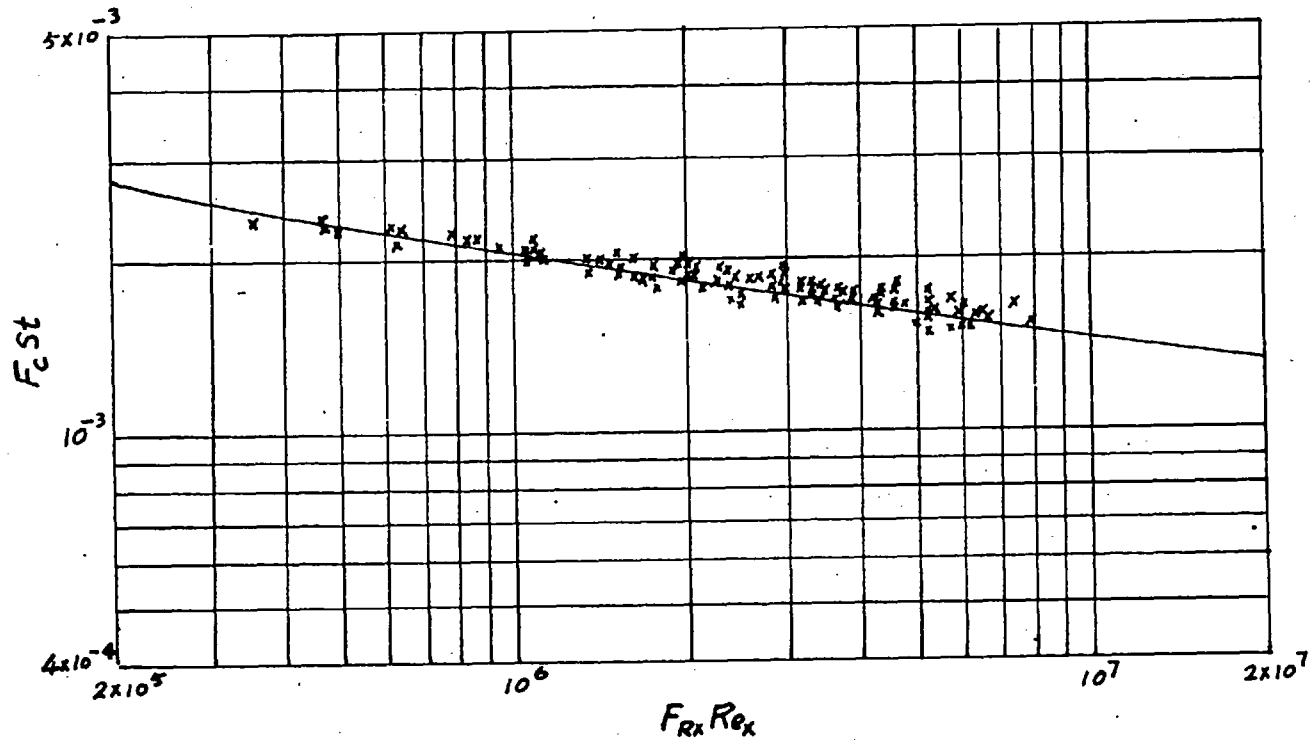
Fig. 4.29 Comparison of theoretical and experimental $F_c St$ vs $F_{Rx} Re_x$.
—————, present theory; x, present experiments.
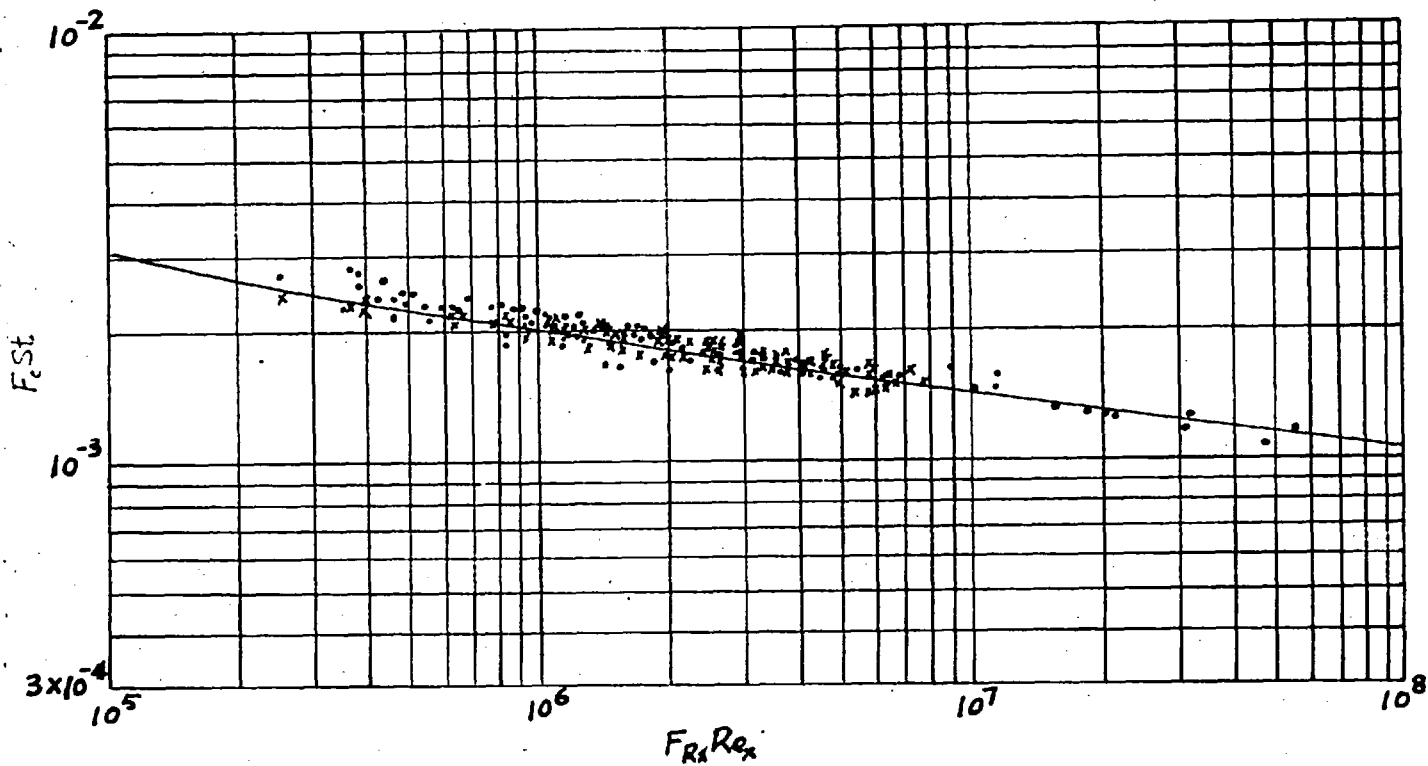
Fig. 4.30 Comparison of theory with the published and the present $F_c St$ vs $F_{Rx} Re_x$ data. ———, present theory; x, present data; at $M_G \approx 0.2$, $T_{ad,S}/T_S = 1.5-2.7$; ·, published data at $M_G = 0.8-10$, $T_{ad,S}/T_S \approx 0.5-1.6$, (Appendix 4B).

Table 2.1 Theories based upon Prandtl differential equation.

Author and year	Hypothesis for E	Nature of ϕ	Method of evaluating Re_{δ_2} Integral.
Smith and Harrop(1846) [2.1]	$E = 11.24$	$\phi = (\rho/\rho_s)^{1/2}$ $= (1 + bz - a^2 z^2)^{-1/2}$	Approximate analytical (a)*
Van Driest-I (1951)[2.2]	$E = 13.1$ (for ψ_x)†	Ditto	Approximate analytical (b) *
Kalikman (1956) [2.3]	$2 y_1 u_{av} \rho_{av} / \mu_{av} = (11.5)^2$ ‡ $y_i^+ = u_G^+ (z_1 + \frac{1}{2} b Pr z_1^2 + \frac{1}{3} a^2 Pr z_1^3)$ Ditto		Exact numerical.
Dorrance (1960) [2.4]	$E = 13.1$ (for ψ_x)	Ditto	Exact numerical (approximate integration used later to yield $c_f (Re_x)$.
Kutateladze and Leont'ev(1961) [2.5]	$y_i^+ = 11.6 (T_G/T_S)^{\omega + \frac{1}{2}}$ $z_1 = 11.6 \times (\frac{1}{2}$ drag coefficient in uniform-property flow at same $Re_{\delta_2})^{1/2}$	$\phi = (\rho/\rho_s)^{1/2}$ $= [1 + (b - 0.1 a^2) z - 0.9 a^2 z^2]^{-1/2}$	Approximate analytical (b). (Remark: Result of this theory can also be obtained without assuming the Prandtl hypothesis for mixing length)

* These methods of evaluating Re_{δ_2} integral are summarized in Appendix 2B

† 'For ψ_x' means that the value of E specified here is for c_f vs Re_x expression.

‡ In this case, the value of E is deduced from u_i^+ and y_i^+ by the equation, $E = \frac{1}{y_i^+} \exp(k \int_0^{u_i^+} \phi \, du^+)$

Table 2.2 Theories based upon von Karman differential equation.

Author and year	Hypothesis for E	Nature of ϕ	Method of evaluating Re_{sz} Integral.
Frankl and Voishel (1937) [2.6]	$u_i^+ = 11.5$ † $(du^+/dy^+)_i = 0.289$	$\phi = (f/f_s)^{1/2}$ $= (1 + bz - a^2 z^2)^{-1/2}$	Approximate analytical — by expanding integrand in series of b and a^2, and neglecting higher terms.
Wilson (1950) [2.7]	$u_i^+ = 11.6$ $(du^+/dy^+)_i = 0.218$	$\phi = (f/f_s)^{1/2}$ $= (1 + bz - a^2 z^2)^{-1/2}$ (adiabatic only)	Approximate analytical (b)*
Rubesin, Maydew and Varga (1951) [2.8]	$u_i^+ = 11.5$ $(du^+/dy^+)_i = 0.218$	$\phi = (f/f_s)^{1/2}$ $= (1 + bz - a^2 z^2)^{-1/2}$	Exact numerical
Van Driest-II (1955) [2.9]	$E = 13.1$ (for ψ_x) †	Ditto	Approximate analytic (b)
Deissler and Loeffler (1959) [2.90]	$y_i^+ = 26$ § For $y^+ \leqslant 26$ $\tau_s = (\mu + 0.01188 \, f u y)(du/dy)$ $q_s = (k + 0.01188 \, f u y)(dT/dy)$	$\phi = (f/f_s)^{1/2}$ $= [\dfrac{T_i}{T_s} - \dfrac{q_s(u^+ - u_i^+)}{c_p T_s \sqrt{(f_s \tau_s)}}$ $- \dfrac{\tau_s(u^{+2} - u_i^{+2})}{2 c_p T_s f_s}]^{-1/2}$	Exact numerical.

Table 2·3   Theories based upon other differential equations.

Author and year	Nature of differential equation	Method of evaluating Re_{δ_2} integral
Clemmow-I (1950) [2·11]	$\gamma_s = \rho k^2 y^2 \left(\frac{du}{dy}\right)^2 + u k^2 y^2 \frac{du}{dy}\frac{d\rho}{dy}$	Approximate analytic (b).*
Clemmow-II (1950) [2·11]	$\gamma_s = k^2 \frac{(du/dy)^3}{(d^2u/dy^2)^2}\left(\rho\frac{du}{dy} + u\frac{d\rho}{dy}\right)$	Ditto
Ferrari (1950) [2·12]	$\sqrt{\frac{\gamma_s}{\rho_s}} = \frac{\rho k y (du/dy)}{\rho_s\left\{1 + const.\times z\left[1 + \frac{2}{(\gamma-1)M_a^2}\right]^{-1/2}\right\}}$ The value of constant is unknown.	Approximate numerical
Li and Nagamatsu (1951) [2·13]	$\gamma_s = \rho k^2 y^2 (du/dy)^2 + f(M_a) u k^2 y^2 \frac{d\rho}{dy}\frac{du}{dy}$ The function of M_a, $f(M_a)$ is unknown.	Approximate analytic (b).
Kosterin and Koshmarov (1960) [2·14]	$\gamma_s = \rho k^2 y^2 (du/dy)^2 + \int k^2 y^2 \frac{d\rho}{dy}\left(\frac{du}{dy}\right)^2 dy$	Exact numerical.

*   See footnote at the end of Table 2·1.

Table 2.4 Theories based upon fixed velocity profile.

Author and year	Assumed velocity Profile	Expression for ρ/ρ_s	Method of evaluating $Re_{\delta 2}$ integral.
Cope-I (1943) [2.15]	$u^+ = 8.7\, y^{+\frac{1}{7}}$	$\rho/\rho_s = (1-a^2 z^2)^{-1}$ (adiabatic only)	Exact numerical.
Cope-II (1943) [2.15]	$y^+ = E^{-1} \exp(\kappa u^+)$	Ditto	Approximate analytical(b)*
Monaghan (1950) [2.16]	$y^+ = E^{-1} \exp(\kappa u^+)$	$\rho/\rho_s = (1+bz-a^2 z^2)^{-1}$	Ditto.

* See footnote at the end of Table 2.1

Table 2.5 Theories based upon incompressible formulae (ψ_z) with reference properties.

Author and year	Expression of T_R/T_G (or h_R/h_G).
Von Karman (1935) [2.17]	$T_R/T_G = 1 + \frac{1}{2}(\gamma-1)M_G^2$ (adiabatic only).
Tucker (1951) [2.18]	$T_R/T_G = 1 + \frac{1}{4}(\gamma-1)M_G^2$ (adiabatic only).
Young and Janssen (1952) [2.19]	For $M_G < 5.6$: $T_R/T_G = 0.42 + 0.58(T_S/T_G) + 0.035 M_G^2$ For $M_G > 5.6$: $T_R/T_G = 0.42 + 0.58(T_S/T_G) + 0.023 M_G^2$.
Sommer and Short (1955) [2.20]	$T_R/T_G = 0.55 + 0.45(T_S/T_G) + 0.035 M_G^2$
Eckert (1955) [2.21]	$T_R/T_G = 0.5 + 0.5(T_S/T_G) + 0.11 Pr^{1/3}(\gamma-1)M_G^2$ $h_R/h_G = 0.28 + 0.5(h_S/h_G) + 0.22(h_{ad,s}/h_G)$

Table 2·6   Comparison of theories with experimental data.

Principle assumptions	Authors and years	R. M. S. errors (%)		
		For adiabatic wall	For heat transfer	Total
Prandtl differential equation	Smith and Harrop (1946) [2·1]	29·3	37·9	32·3
	Van Driest-I (1951) [2·2]	13·3	17·3	14·7
	Kutateladze and Leont'ev (1961) [2·5]	9·5	16·2	12·0
Von Karman differential equation	Frankl and Voishel (1937) [2·6]	20·3	41·7	28·7
	Wilson (1950) [2·7]	10·4	13·6	11·5
	Van Driest-II (1955) [2·9]	9·7	13·6	11·0
Other differential equations	Clemmow-I (1950) [2·11]	11·5	21·5	15·2
	Clemmow-II (1950) [2·11]	20·7	31·7	24·7
Fixed velocity profile	Cope-I (1943) [2·15]	16·7	24·7	19·1
	Cope-II (1943) [2·15]	12·6	25·0	17·4
	Monaghan (1950) [2·16]	13·5	25·3	18·0
Reference temperature	Von Karman (1935) [2·17]	25·0	38·7	29·9
	Tucker (1951) [2·18]	9·6	22·5	14·9
	Young and Janssen (1952) [2·19]	12·7	22·8	16·5
	Sommer and Short (1955) [2·20]	12·0	17·1	13·8
	Eckert (1955) [2·21]	12·2	20·2	15·1
Miscellaneous other assumptions.	Donaldson (1952) [2·22]	12·4	20·6	15·4
	Spence (1959) [2·24]	12·2	18·2	14·3
	Winkler (1961) [2·23]	14·0	23·7	17·6
	Burggraf (1962) [2·25]	16·1	26·1	19·8
	Present Procedure	8·6	12·5	9·9

Table 2.7 Values of y_i^+ (and u_i^+) at various M_G and $T_{ad,s}/T_s$
(For $Re_x \approx 5 \times 10^5 - 2 \times 10^7$)

M_G	$T_{ad,s}/T_s$	$y_i^+ (= u_i^+)$	E
2.43	1	11.4	8.35
2.5	1	11.6	9.05
2.82	1	11.8	9.5
2.95	1	11.8	9.5
4.2	1	11.4	8.42
4.93	1	11.8	9.5
2.43	0.697	10.3	6.05
2.43	0.597	9.5	4.45
2.81	0.691	10.5	6.4
5.01	1.275	12.5	12.1
5.03	1.577	13.1	14.4
5.06	1.700	14.1	20.0
5.82	1.584	13.5	16.3
5.79	1.306	12.7	12.7
5.75	1.129	11.9	9.75
6.83	1.512	12.8	13.0
6.78	1.836	13.4	15.4
6.83	1.829	14.2	22.3
7.67	1.931	14.0	19.5
8.18	1.956	14.1	21.9
8.99	2.007	13.9	20.5

Table 2·8   Values of $F_c c_f$, $F_c \bar{c}_f$, $F_{R\delta} Re_{\delta 2}$ and $F_{Rx} Re_x$.

$F_c c_f$	$F_c \bar{c}_f$	$F_{R\delta} Re_{\delta 2}$	$F_{Rx} Re_x$	$F_c c_f$	$F_c \bar{c}_f$	$F_{R\delta} Re_{\delta 2}$	$F_{Rx} Re_x$
0.0010	0.001117	2.878×10^7	5.758×10^{10}	0.0060	0.008205	233.0	5.679×10^4
0.0015	0.001716	3.955×10^5	4.610×10^8	0.0065	0.009105	177.6	3.901×10^4
0.0020	0.002333	5.425×10^4	4.651×10^7	0.0070	0.01004	140.4	2.796×10^4
0.0025	0.002967	1.386×10^4	9.340×10^6	0.0075	0.01101	114.4	2.078×10^4
0.0030	0.003621	5030	2.778×10^6	0.0080	0.01202	95.62	1.592×10^4
0.0035	0.004299	2283	1.062×10^6	0.0085	0.01304	92.49	1.251×10^4
0.0040	0.005006	1208	4.828×10^5	0.0090	0.01409	70.91	1.006×10^4
0.0045	0.005747	716.0	2.492×10^5	0.0095	0.01516	62.55	8.253×10^3
0.0050	0.006526	462.3	1.417×10^5	0.0100	0.01624	55.87	6.883×10^3
0.0055	0.007345	319.4	8.697×10^4	0.0105	0.01732	50.46	5.826×10^3

Table 2.9   Values of F_c at various M_G and T_S/T_G.

T_S/T_G \ M_G	0	1	2	3	4	5	6	7
0.05	0.3743	0.4036	0.4884	0.6222	0.7999	1.0184	1.2759	1.5713
0.1	0.4331	0.4626	0.5477	0.6829	0.8628	1.0842	1.3451	1.6444
0.2	0.5236	0.5530	0.6388	0.7756	0.9584	1.1836	1.4491	1.7534
0.3	0.5989	0.6283	0.7145	0.8523	1.0370	1.2649	1.5337	1.8418
0.4	0.6662	0.6957	0.7821	0.9208	1.1069	1.3370	1.6083	1.9194
0.5	0.7286	0.7580	0.8446	0.9839	1.1713	1.4031	1.6767	1.9903
0.6	0.7873	0.8168	0.9036	1.0434	1.2318	1.4651	1.7405	2.0564
0.8	0.8972	0.9267	1.0137	1.1544	1.3445	1.5802	1.8589	2.1785
1	1.0000	1.0295	1.1167	1.2581	1.4494	1.6871	1.9684	2.2913
2	1.4571	1.4867	1.5744	1.7176	1.9130	2.1572	2.4472	2.7809
3	1.8660	1.8956	1.9836	2.1278	2.3254	2.5733	2.8687	3.2092
4	2.2500	2.2796	2.3678	2.5126	2.7117	2.9621	3.2611	3.6066
5	2.6180	2.6477	2.7359	2.8812	3.0813	3.3336	3.6355	3.9847
6	2.9747	3.0044	3.0927	3.2384	3.4393	3.6930	3.9971	4.3493
8	3.6642	3.6938	3.7823	3.9284	4.1305	4.3863	4.6937	5.0505
10	4.3311	4.3608	4.4493	4.5958	4.7986	5.0659	5.3657	5.7259
12	4.9821	5.0117	5.1003	5.2470	5.4504	5.7088	6.0204	6.3832
14	5.6208	5.6505	5.7391	5.8860	6.0898	6.3491	6.6621	7.0271
16	6.2500	6.2797	6.3683	6.5153	6.7196	6.9795	7.2937	7.6603
18	6.8713	6.9010	6.9897	7.1368	7.3413	7.6019	7.9170	8.2851
20	7.4861	7.5157	7.6045	7.7517	7.9564	8.2175	8.5334	8.9027
25	9.0000	9.0297	9.1184	9.2658	9.4711	9.7330	10.0505	10.4222
30	10.4886	10.5183	10.6071	10.7546	10.9602	11.2228	11.5415	11.9149

Table 2.9   Continued.

T_S/T_G \ M_G	8	9	10	11	12	13	14	15
0.05	1.9041	2.3738	2.6803	3.1233	3.6027	4.1186	4.6707	5.2591
0.1	1.9812	2.3552	2.7660	3.2134	3.6976	4.2180	4.7748	5.3680
0.2	2.0958	2.4756	2.8925	3.3462	3.8366	4.3636	4.9269	5.5267
0.3	2.1882	2.5723	2.9937	3.4622	3.9974	4.4792	5.0475	5.6523
0.4	2.2892	2.6569	3.0820	3.5443	4.0435	4.5794	5.1518	5.7608
0.5	2.3429	2.7336	3.1620	3.6276	4.1303	4.6697	5.2458	5.8584
0.6	2.4115	2.8049	3.2362	3.7048	4.2105	4.7531	5.3324	5.9483
0.8	2.5379	2.9360	3.3721	3.8459	4.3570	4.9051	5.4901	6.1117
1	2.6542	3.0562	3.4966	3.9748	4.4905	5.0434	5.6333	6.2599
2	3.1564	3.5725	4.0282	4.5228	5.0556	5.6263	6.2345	6.8801
3	3.5929	4.0184	4.4846	4.9904	5.5353	6.1187	6.7401	7.3993
4	3.9964	4.4290	4.9030	5.4176	5.9719	6.5653	7.1972	7.8673
5	4.3792	4.8174	5.2979	5.8196	6.3817	6.9833	7.6240	8.3033
6	4.7477	5.1905	5.6764	6.2041	6.7727	7.3814	8.0297	8.7169
8	5.4549	5.9050	6.3994	6.9368	7.5161	8.1365	8.7972	9.4944
10	6.1347	6.5904	7.0913	7.6363	8.2241	8.8539	9.5247	10.2359
12	6.7955	7.2556	7.7618	8.3129	8.9077	9.5452	10.2245	10.5449
14	7.4422	7.9058	8.4164	8.9727	9.5734	10.2174	10.9040	11.6321
16	8.0778	8.5444	9.0581	9.6194	10.2251	10.6748	11.5676	12.3026
18	8.7045	9.1737	9.6912	10.2556	10.8657	11.5204	12.2187	12.9598
20	9.3238	9.7952	10.3154	10.8832	11.4911	12.1562	12.8595	13.6059
25	10.8467	11.3225	11.8482	12.4227	13.0446	13.7128	14.4263	15.1841
30	12.3418	12.8209	13.3509	13.9305	14.5586	15.2339	15.9556	16.7225

Table 2.10   Values of F_{R8} at various M_G and T_S/T_G.

T_S/T_G \ M_G	0	1	2	3	4	5	6	7
0.05	82.74	93.90	125.3	173.1	234.2	306.4	388.3	478.9
0.1	29.79	33.80	45.11	62.32	84.29	110.3	139.8	172.4
0.2	10.72	12.17	16.24	22.43	30.34	39.70	50.31	62.06
0.3	5.898	6.693	8.933	12.34	16.69	21.84	27.68	34.14
0.4	3.860	4.380	5.846	8.076	10.92	14.29	18.11	22.34
0.5	2.778	3.152	4.207	5.812	7.862	10.29	13.04	16.08
0.6	2.123	2.410	3.216	4.442	6.009	7.862	9.964	12.29
0.8	1.390	1.577	2.104	2.907	3.932	5.145	6.520	8.043
1	1.000	1.135	1.515	2.092	2.830	3.703	4.693	5.788
2	0.3600	0.4085	0.5452	0.7532	1.019	1.333	1.689	2.084
3	0.1980	0.2247	0.2999	0.4143	0.5604	0.7332	0.9292	1.146
4	0.1296	0.1471	0.1963	0.2711	0.3667	0.4798	0.6081	0.7501
5	0.0933	0.1058	0.1412	0.1951	0.2639	0.3453	0.4377	0.5398
6	0.0713	0.0809	0.1080	0.1491	0.2017	0.2639	0.3345	0.4126
8	0.0466	0.0529	0.0706	0.0976	0.1320	0.1727	0.2189	0.2700
10	0.0336	0.0381	0.0508	0.0702	0.0950	0.1243	0.1575	0.1943
12	0.0257	0.0291	0.0389	0.0537	0.0726	0.0950	0.1204	0.1485
14	0.0204	0.0232	0.0310	0.0428	0.0579	0.0757	0.0959	0.1183
16	0.0168	0.0191	0.0254	0.0351	0.0475	0.0622	0.0788	0.0972
18	0.0141	0.0160	0.0214	0.0295	0.0400	0.0523	0.0662	0.0817
20	0.0121	0.0137	0.0183	0.0253	0.0342	0.0447	0.0567	0.0700
25	0.0087	0.0099	0.0132	0.0182	0.0246	0.0322	0.0408	0.0503
30	0.0066	0.0075	0.0101	0.0139	0.0188	0.0246	0.0312	0.0385

Table 2.10   Continued.

T_S/T_G \\ M_G	8	9	10	11	12	13	14	15
0.05	577.6	683.7	796.8	916.6	1043	1175	1312	1456
0.1	207.9	246.1	286.8	330.0	375.3	422.9	472.5	524.2
0.2	74.85	88.60	103.3	118.8	135.1	152.2	170.1	188.7
0.3	41.17	48.74	56.80	65.34	74.33	83.74	93.57	103.8
0.4	26.94	31.89	37.17	42.76	48.64	54.80	61.23	67.93
0.5	19.39	22.95	26.75	30.77	35.01	39.44	44.07	48.89
0.6	14.82	17.54	20.45	23.52	26.76	30.15	33.68	37.37
0.8	9.700	11.48	13.38	15.39	17.51	19.73	22.04	24.45
1	6.981	8.263	9.631	11.08	12.60	14.20	15.86	17.60
2	2.513	2.975	3.467	3.988	4.536	5.111	5.711	6.335
3	1.382	1.636	1.907	2.194	2.498	2.812	3.142	3.485
4	0.9046	1.071	1.248	1.436	1.633	1.840	2.056	2.281
5	0.6511	0.7707	0.8982	1.033	1.175	1.324	1.480	1.641
6	0.4976	0.5891	0.6862	0.7897	0.8983	1.012	1.131	1.255
8	0.3256	0.3855	0.4493	0.5168	0.5878	0.6623	0.7401	0.8210
10	0.2344	0.2774	0.3233	0.3719	0.4231	0.4767	0.5326	0.5909
12	0.1791	0.2121	0.2471	0.2843	0.3234	0.3643	0.4071	0.4876
14	0.1427	0.1690	0.1969	0.2265	0.2576	0.2903	0.3244	0.3598
16	0.1172	0.1388	0.1617	0.1860	0.2116	0.2384	0.2664	0.2955
18	0.0985	0.1167	0.1359	0.1564	0.1779	0.2004	0.2239	0.2484
20	0.0844	0.0999	0.1164	0.1339	0.1523	0.1716	0.1917	0.2127
25	0.0607	0.0719	0.0838	0.0964	0.1096	0.1235	0.1380	0.1531
30	0.0464	0.0549	0.0640	0.0737	0.0838	0.0944	0.1055	0.1170

Table 3:1   Nature of theories of Reynolds-analogy factor

Author and year	Total Prandtl number (Pr_{tot}) and shear stress (τ)*			Value of Pr_t
	Close to wall	Intermediate region	Distant from wall	
Reynolds (1874) [3.1]	$Pr_{tot} = Pr_t$ (across all regions)			1
Prandtl (1910) Taylor (1936) [3.1]	At $u^+ \leq 11.6$ $Pr_{tot} = Pr$	—	At $u^+ \geq 11.6$ $Pr_{tot} = Pr_t$	1
Shirokow (1936) [3.2]	At $u^+/u_c^+ \leq 1/3$ $Pr_{tot} = Pr$	—	At $u^+/u_c^+ \geq 1/3$ $Pr_{tot} = Pr_t$	1
Von Karman (1939) [3.3]	At $u^+ \leq 5$ $Pr_{tot} = Pr$	At $5 \leq y^+ \leq 30$ $y^+ = 5 \exp\left[\int_5^{u^+} (du^+/5)\right]$ Pr_{tot} by Eq. (3.5)	At $y^+ \geq 30$ $Pr_{tot} = Pr_t$	1
Reichardt (1940) [3.4]	At $u^+ \leq 2$ $Pr_{tot} = Pr$	At $2 \leq u^+ \leq 15.5$ $\frac{15.5 - u^+}{13.5} = \exp\frac{2 - y^+}{13.5}$ Pr_{tot} by Eq. (3.5)	At $u^+ \geq 15.5$ $Pr_{tot} = Pr_t$	Pr
Smith and Harrop (1946) [3.5]	At $u^+ \leq 5$ $Pr_{tot} = Pr$	At $5 \leq y^+ \leq 30$ $y^+ = 5 \exp\left[\int_0^{u^+} \frac{du^+}{5(\tau/\tau_s)}\right]$ Pr_{tot} by Eq. (3.4)	At $y^+ \geq 30$ $Pr_{tot} = Pr_t$	1

* τ is equal to τ_s, unless otherwise stated.

Table 3.1   Continued.

Author and year	Pr$_{tot}$- and *γ- distributions			Value of Pr$_t$
	Close to wall	Intermediate region	Distant from wall	
Seban (1948)[3.2]	At $u^+ \leq 5$ $Pr_{tot} = Pr$	At $5 \leq y^+ \leq 30$ $y^+ = 5 \cdot exp(\int_5^{u^+} \frac{du^+}{5})$ Pr_{tot} by Eq. (3.5)	At $y^+ \geq 30$ $Pr_{tot} = Pr_t$	Not specified.
Rubesin (1953) [3.2]	At $u^+ \leq 11.5$ $Pr_{tot} = Pr$	———	At $u^+ \geq 11.5$ $Pr_{tot} = Pr_t$	From the equation: $Pr^{1/3} = Pr_t [1 - (11.5/u_\delta^+) \times$ $\times (1 - \frac{Pr}{Pr_t})]$
Deissler and Loeffler (1959)[3.6]	At $y^+ \leq 26$ $u^+ = \int_0^{y^+} \{ dy^+ / [(T/T_S)^{0.68} + 0.109^2 u^+ y^+ (T_S/T)] \}$ Pr_{tot} by Eq. (3.4)		At $y^+ \geq 26$ $y^+ = \frac{K}{E}\int_0^{u^+} exp[K\int_0^{u^+}(\frac{T_S}{T})^{\frac{3}{2}}$ $\times du^+] du^+$ Pr_{tot} by Eq. (3.4)	1
Spalding and Jayatillaka (1964) [3.7]	Pr_{tot} by Eq. 3.5 with $dy^+/du^+ = 1 + \alpha(u^+)^4$ where $a = [(\pi/4)/(9.24 \sin \frac{\pi}{4})]^{-4}$			0.9

* γ is equal to γ_S, unless otherwise stated.

Table 3·1   Continued

Author and year	Pr$_{tot}$- and r- distributions			Value of Pr$_t$
	Close to wall	Intermediate region	Distant from wall	
Van Driest (1955) [3.8]	At $u^+ \leq 5$ $Pr_{tot} = Pr$	At $5 \leq y^+ \leq 30$, $y^+ = 5 \exp \int_5^{u^+} \frac{du^+}{5}$ Pr_{tot} by Eq.(3·5) $r/r_s = 1 - (y^+/y_G^+)$	At $y^+ \geq 30$ $Pr_{tot} = Pr_t$	0·86
Spence (1959) [3·8]	†At $\eta_R^+ \leq 7·8$ $Pr_{tot} = Pr$ where $\eta_R^+ = \int_0^y \frac{\rho}{\rho_R} dy_R^+$ $u_R^+ = \eta_R^+$	At $\eta_R^+ \geq 7·8$ $\eta_R^+ = 7·8 + \exp [0·4(u_R^+ - 7·8)]$ Pr_{tot} by Eq.(3·5), but using $u_R^+ \sim \eta_R^+$ instead of $u^+ \sim y^+$ $r/r_s = 1 - (u/u_G)^{11}$		0·85

* r is equal to r_s, unless otherwise stated.
† Suffix R stands for the properties being evaluated at the Eckert's reference temperature.

Table 3.2   Variation of S values versus Re_x, (for $P_r = 0.7$).

Author and year	Values of S		Variation of S from mean ($\pm$ %)
	At $Re_x = 1 \times 10^5$	At $Re_x = 1 \times 10^8$	
Reynolds (1874) [3.1]	1.	1	0
Prandtl (1910) Taylor (1936) [3.1]	1.219	1.128	3
Shirokow (1936) [3.2]	1.111	1.111	0
Von Karman (1939) [3.3]	1.179	1.106	3.2
Reichardt (1940) [3.4]	1.170	1.101	3
Smith and Harrop (1946) [3.5]	1.179	1.106	3.2
Seban (1948) [3.2]	1.179	1.101	3.2
Rubesin (1953) [3.2]	1.222	1.195	1.1
Deissler and Loeffler (1959) [3.6]	1.124	1.070	2.5
Spalding and Jaylatillake (1964) [3.7]	1.199	1.165	1.4
Van Driest (1955) [3.8]	1.234	1.207	1.1
Spence (1959) [3.9]	1.274	1.230	1.7
Colburn (1933) [3.10]	1.269	1.269	0

Table 4.1   Copper-Constantan thermocouple reference e.m.f. versus temperature, (From BS 1828, 1962).

°F	0	5	10	15	20	25	30	35	40	45	50	°F
	Millivolts											
−250	−4.748	−4.807	−4.865	−4.921	−4.977	−5.032	−5.086	−5.139	−5.190	−5.241	−5.291	−250
−200	−4.106	−4.175	−4.242	−4.309	−4.374	−4.439	−4.503	−4.566	−4.627	−4.688	−4.748	−200
−150	−3.372	−3.449	−3.526	−3.602	−3.676	−3.750	−3.823	−3.896	−3.967	−4.037	−4.106	−150
−100	−2.550	−2.636	−2.721	−2.805	−2.889	−2.971	−3.053	−3.134	−3.214	−3.293	−3.372	−100
−50	−1.646	−1.740	−1.833	−1.925	−2.017	−2.108	−2.198	−2.287	−2.376	−2.463	−2.550	−50
(−)0	−0.665	−0.767	−0.867	−0.967	−1.067	−1.165	−1.263	−1.360	−1.456	−1.551	−1.646	(−)0
(+)0	−0.665	−0.563	−0.460	−0.357	−0.253	−0.148	−0.042	0.064	0.171	0.279	0.387	0
50	0.387	0.496	0.606	0.717	0.828	0.939	1.052	1.165	1.278	1.393	1.508	50
100	1.508	1.623	1.739	1.856	1.973	2.091	2.210	2.329	2.449	2.570	2.691	100
150	2.691	2.812	2.934	3.057	3.180	3.304	3.429	3.554	3.679	3.806	3.932	150
200	3.932	4.059	4.187	4.316	4.444	4.574	4.704	4.834	4.965	5.097	5.229	200
250	5.229	5.361	5.494	5.628	5.762	5.896	6.031	6.167	6.303	6.439	6.576	250
300	6.576	6.714	6.852	6.990	7.129	7.268	7.408	7.548	7.689	7.830	7.972	300

Table 4.2 Data from calibration of wind tunnel.

(a) Nominal mainstream temperature = 80°F

Observations and results. Test No.	1	2	3	4	5
$P_{atm.}$ mm Hg	761.30	761.30	761.30	767.80	767.80
$T_{atm.}$ °F	75.6	75.6	75.6	75.4	75.4
Fan speed R.P.M.	500	1,000	1,500	2,000	2,500
P_x mm H_2O, G.	0.52	2.64	5.01	9.28	14.91
(P_0-P_x) mm H_2O	7.59	37.59	72.11	137.11	218.76
E_0 mv	0.907	1.012	1.032	0.963	1.067
P_I mm H_2O	0.30	1.50	2.90	5.46	8.46
P_{II} mm H_2O	0.25	1.20	2.32	5.00	6.35
P_{III} mm H_2O	0.21	0.98	1.85	4.09	5.59
P_{IV} mm H_2O	0.17	0.72	1.45	3.05	4.35
ΔP_I mm H_2O	8.50	42.11	81.00	154.21	240.26
ΔP_{II} mm H_2O	8.54	42.39	81.45	154.57	242.26
ΔP_{III} mm H_2O	8.59	42.58	81.82	155.38	242.27
ΔP_{IV} mm H_2O	8.63	42.81	82.24	156.40	242.97
E_I mv	0.905	1.012	1.034	0.962	1.065
E_{II} mv	0.908	1.012	1.035	0.963	1.067
E_{III} mv	0.906	1.012	1.033	0.963	1.066
E_{IV} mv	0.907	1.012	1.031	0.964	1.067
$(P_0-P_x)_c$ mm H_2O	7.77	38.688	74.075	137.95	215.23
u_G ft/s	38.92	86.927	120.45	164.50	205.96
$C (\equiv u_G/\sqrt{(P_0-P_x)_c})$	13.962	13.975	13.995	14.005	14.039

Table 4.2 Continued.

(b) Nominal mainstream temperature = 280°F.

Test No. Observations and results	6	7	8	9	10	11
P_{atm} mm Hg	759.40	759.40	759.08	759.08	765.25	765.25
T_{atm} °F	75.6	75.6	75.2	75.2	76.0	76.0
Fan Speed R.P.M.	300	800	1,250	1,750	2,000	2,500
P_x mm H_2O, G	0.13	1.05	2.35	4.96	6.84	11.28
$(P_0 - P_x)$ mm H_2O	1.78	14.15	35.26	71.11	102.75	169.61
E_0	6.227	6.135	5.660	5.235	6.207	5.612
P_I	0.07	0.83	1.69	3.86	5.12	7.43
P_{II}	0.07	0.73	1.40	3.46	4.43	6.91
P_{III}	0.06	0.65	1.16	2.93	3.82	8.48
P_{IV}	0.05	0.55	1.09	2.51	3.18	5.50
ΔP_I	2.00	15.88	39.52	80.21	115.75	190.88
ΔP_{II}	2.01	15.96	39.72	79.61	116.33	191.83
ΔP_{III}	2.01	16.04	39.92	81.02	116.91	192.79
ΔP_{IV}	2.02	16.12	40.12	81.42	117.49	193.74
E_I	6.217	6.141	5.648	6.221	6.184	5.588
E_{II}	6.215	6.138	5.644	6.220	6.182	5.586
E_{III}	6.210	6.132	5.646	6.214	6.185	5.583
E_{IV}	6.206	6.129	5.638	6.214	6.180	5.580
$(P_0 - P_x)_c$ mm H_2O	2.5576	20.213	49.087	101.53	144.86	230.49
u_G ft/s	22.309	62.836	97.823	141.00	168.28	212.77
$C (\equiv u_G / \sqrt{(P_0 - P_x)_c})$	13.956	13.977	13.962	14.027	13.983	14.015

Table 4.3   Summary of results of tests 1-4, (Test at small temperature ratios).

Test No. 1: $Re_1 = 7.80 \times 10^4$; $T_G = 643.29°R$.

$T_G/T_s = 1.038$		$T_G/T_s = 1.029$		$T_G/T_s = 1.021$	
$Re_x \times 10^{-6}$	$St \times 10^3$	$Re_x \times 10^{-6}$	$St \times 10^3$	$Re_x \times 10^{-6}$	$St \times 10^3$
0.117	3.20	0.117	3.26	0.117	3.09
0.195	2.70	0.195	2.98	0.195	2.88
0.273	2.46	0.273	2.83	0.273	2.56
0.351	2.34	0.351	2.76	0.351	2.42
0.507	2.37	0.507	2.60	0.507	2.40
0.624	2.28	0.624	2.49	0.624	2.25

Test No. 2: $Re_1 = 7.79 \times 10^4$; $T_G = 643.18°R$.

$T_G/T_s = 1.037$		$T_G/T_s = 1.029$		$T_G/T_s = 1.021$	
$Re_x \times 10^{-6}$	$St \times 10^3$	$Re_x \times 10^{-6}$	$St \times 10^3$	$Re_x \times 10^{-6}$	$St \times 10^3$
0.779	2.17	0.779	2.32	0.779	2.35
0.934	2.02	0.934	2.14	0.934	2.18
1.090	1.97	1.090	2.02	1.090	2.16
1.246	1.89	1.246	1.92	1.246	2.07
1.403	1.83	1.403	1.84	1.403	2.04
1.713	1.71	1.713	1.93	1.713	1.80

Test No. 3: $Re_1 = 1.113 \times 10^4$; $T_G = 709.4°R$

$T_G/T_s = 1.083$		$T_G/T_s = 1.075$		$T_G/T_s = 1.067$	
$Re_x \times 10^{-6}$	$St \times 10^3$	$Re_x \times 10^{-6}$	$St \times 10^3$	$Re_x \times 10^{-6}$	$St \times 10^3$
0.0167	4.13	0.0167	4.28	0.0167	4.26
0.0278	3.39	0.0278	3.36	0.0278	3.28
0.0389	3.00	0.0389	2.86	0.0389	2.97
0.0501	2.69	0.0501	2.69	0.0501	2.68
0.0723	2.52	0.0723	2.61	0.0723	2.55
0.0890	2.24	0.0890	2.11	0.0890	1.95

Test No. 4: $Re_1 = 1.154 \times 10^4$; $T_G = 696.64°R$.

$T_G/T_s = 1.089$		$T_G/T_s = 1.075$		$T_G/T_s = 1.056$	
$Re_x \times 10^{-6}$	$St \times 10^3$	$Re_x \times 10^{-6}$	$St \times 10^3$	$Re_x \times 10^{-6}$	$St \times 10^3$
0.115	3.42	0.115	3.20	0.115	3.14
0.139	3.37	0.139	3.14	0.139	3.04
0.165	3.21	0.165	3.05	0.165	2.91
0.185	3.10	0.185	2.93	0.185	2.90
0.208	2.84	0.208	2.85	0.208	2.73
0.254	2.75	0.254	2.73	0.254	2.62

Table 4.4   Summary of results of tests 5-12, (tests at large temperature ratios).

Test 5: $Re_1 = 6.92 \times 10^4$; $T_G = 537.61°R$.

T_G/T_S	1.25		1.5		1.75		2.00	
$Re_x \times 10^{-6}$	$St'\times10^3$	$St\times10^3$	$St'\times10^3$	$St\times10^3$	$St'\times10^3$	$St\times10^3$	$St'\times10^3$	$St\times10^3$
0.692	2.44	2.40	2.57	2.51	2.56	2.51	2.36	2.30
0.830	2.35	2.30	2.48	2.40	2.38	2.34	2.30	2.26
0.968	2.21	2.17	2.38	2.34	2.33	2.29	2.24	2.20
1.11	2.11	2.07	2.25	2.22	2.20	2.17	2.21	2.18
1.25	2.09	2.05	2.16	2.13	2.22	2.19	2.17	2.13
1.53	2.02	1.99	2.16	2.13	2.11	2.09	2.03	2.01

Test 6: $Re_1 = 9.31 \times 10^4$; $T_G = 541.30°R$.   **Test 7:** $Re_1 = 6.46 \times 10^4$; $T_G = 698.57°R$

T_G/T_S	1.5		1.75		T_G/T_S	1.5		1.75	
$Re_x \times 10^{-6}$	$St'\times10^3$	$St\times10^3$	$St'\times10^3$	$St\times10^3$	$Re_x \times 10^{-6}$	$St'\times10^3$	$St\times10^3$	$St'\times10^3$	$St\times10^3$
0.931	2.31	2.16	2.38	2.36	0.097	—	—	—	—
1.12	2.21	2.17	2.25	2.23	0.162	2.98	2.85	3.16	3.01
1.30	2.10	2.08	2.17	2.15	0.226	2.82	2.71	3.06	2.94
1.49	2.13	2.10	2.11	2.09	0.291	2.76	2.67	2.92	2.83
1.68	2.08	2.05	2.11	2.09	0.421	2.59	2.53	2.74	2.67
2.05	2.00	1.96	2.10	2.08	0.517	2.47	2.42	2.63	2.57

Test 7: $Re_1 = 6.46 \times 10^4$; $T_G = 698.57°R$.

T_G/T_S	2.00		2.25		2.7	
$Re_x \times 10^{-6}$						
0.097	—	—	—	—	—	—
0.162	3.10	2.96	3.11	2.96	3.11	2.96
0.226	2.97	2.86	3.00	2.90	3.07	2.96
0.291	2.86	2.78	2.93	2.80	2.95	2.86
0.420	2.81	2.75	2.61	2.55	2.80	2.75
0.517	2.49	2.44	2.50	2.46	2.79	2.76

Table 4.4   Continued.

Test B : $Re_1 = 6.15 \times 10^4$; $T_G = 698.51°R$.

T_G/T_S	1.5		1.75		2.00		2.25	
$Re_x \times 10^{-6}$	$St' \times 10^3$	$St \times 10^3$	$St' \times 10^3$	$St \times 10^3$	$St' \times 10^3$	$St \times 10^3$	$St' \times 10^3$	$St \times 10^3$
0.615	2.45	2.40	2.60	2.55	2.65	2.61	2.64	2.61
0.737	2.30	2.25	2.58	2.54	2.51	2.47	2.54	2.51
0.860	2.33	2.29	2.42	2.39	2.35	2.32	2.41	2.39
1.03	2.27	2.23	2.38	2.35	2.28	2.25	2.20	2.18
1.11	2.24	2.21	2.35	2.42	2.19	2.16	2.17	2.15
1.35	2.15	2.12	2.26	2.24	2.14	2.12	2.14	2.12

Test No.	T_G	T_G/T_S	$Re_x \times 10^{-6}$	$St' \times 10^3$	$St \times 10^3$
9		2.00		2.30	
9		2.25		2.31	
9	688.25°R	2.50	0.688	2.40	
9		2.70		2.50	
10		2.00		2.05	
10		2.25		2.10	
10	696.07°R	2.50	1.188	2.19	
10		2.70		2.27	
11		2.00		2.10	
11		2.25		2.24	
11	705.77°R	2.50	0.898	2.33	
11		2.70		2.43	
12		2.00		2.08	
12		2.25		2.15	
12	700.69°R	2.50	1.098	2.40	
12		2.70		2.48	

APPENDIX 2A

Collected Experimental Data of Frictional-Drag Coefficient in Compressible Turbulent Boundary Layer

(a) For adiabatic-wall case

Data of: H.W. Spivak (1950) [2.31]
Model: Flat wall of a 2-D nozzle
Measurements: Velocity profiles
$M_G = 2.8$

$Re_{\delta_2} \times 10^{-3}$	$Re_x \times 10^{-6}$	$c_f \times 10^3$	$\bar{c}_f \times 10^3$
9.6	7.6	1.87	2.46
9.3	8.0	1.82	2.44
10.8	8.9	1.80	2.37
11.7	10.0	1.77	2.30
12.0	10.0	1.71	2.37
12.3	10.8	1.70	2.26
13.4	12.0	1.69	2.27
13.6	12.5	1.68	2.22

Data of: R.E. Wilson (1950) [2.7]
Model: Flat plate
Measurements: Velocity profiles.

M_G	$Re_x \times 10^{-6}$	$\bar{c}_f \times 10^3$
1.897	3.1	3.30
1.897	5.8	2.60
1.897	11.1	2.38
1.897	13.8	2.42
1.897	16.6	2.30

Data of: R.E. Wilson (1950) [2.7]
Model: Flat plate
Measurements: Velocity profiles
(Continued)

M_G	$Re_x \times 10^{-6}$	$\bar{c}_f \times 10^3$
2.003	2.83	3.10
2.003	5.45	2.58
2.003	10.60	2.34
2.121	0.93	3.50
2.121	8.30	2.40
2.121	11.00	2.20
2.121	13.50	2.18
2.003	13.30	2.30
2.003	16.60	2.20
2.186	8.00	2.40
2.186	10.50	2.19
2.186	12.80	2.18
2.186	15.40	2.72
2.186	0.82	3.90

Data of: W.F. Cope (1952) [2.33]
Model: Flat plate
Measurements: Velocity gradients at the wall.

M_G	$Re_{\delta_2} \times 10^{-3}$	$c_f \times 10^3$
2.5	2.565	2.50
2.5	2.720	2.10
2.5	5.655	2.10

Data of: S. Dahwan (1952) [2.34]
Model: Flat plate
Measurements: Forces on a floating element.

M_G	$Re_x \times 10^{-6}$	$c_f \times 10^3$
0.63	1.00	3.40
0.76	1.00	3.29
1.24	1.00	2.96
1.26	1.00	2.96
1.37	1.00	2.82
1.44	1.00	2.79
1.45	1.00	2.72

Data of: R.J. Monaghan and J.E. Johnson (1952) [2.35]
Model: Flat plate
Measurements: Velocity profiles
M_G: 2.43

$Re_{\delta_1} \times 10^{-3}$	$Re_{\theta} \times 10^{-6}$	$c_f \times 10^3$	$\bar{c}_f \times 10^3$
1.072	0.596	2.95	3.60
1.307	0.772	2.80	3.38

Data of: Monaghan and Johnson (continued).
$M_G = 2.43$

$Re_{\delta_2} \times 10^{-3}$	$Re_x \times 10^{-6}$	$c_f \times 10^3$	$\bar{c}_f \times 10^3$
1.451	0.824	2.72	3.52
1.792	1.187	2.50	3.02
2.521	1.930	2.37	2.98
3.268	2.360	2.27	2.77
3.950	2.930	2.18	2.70

Data of: R.J. Monaghan and J.R. Cooke (1953) [2.36]
Model: Flat plate
Measurements: Velocity profiles
$M_G = 2.82$

$Re_{\delta_2} \times 10^{-3}$	$Re_x \times 10^{-6}$	$c_f \times 10^3$	$\bar{c}_f \times 10^3$
0.886	0.490	2.72	3.59
1.493	0.945	2.43	3.16
1.777	1.346	2.19	2.64
2.180	1.570	2.03	2.78
2.660	1.860	1.96	2.86
2.789	2.178	1.93	2.56

Data of: D.R. Chapman and R.K. Kester (1954) [2.37]
Model: Cylinder (axial flow at the outer surface)
Measurements: Total force on the cylinder

M_G	$Re_x \times 10^{-6}$	$\bar{c}_f \times 10^3$
0.81	4.04	3.08

Data of: Chapman and Kester (Continued)			
$M_G = 0.8$			
$Re_x \times 10^{-6}$	$\bar{c}_f \times 10^3$	$Re_x \times 10^{-6}$	$\bar{c}_f \times 10^3$
4.82	2.93	13.25	2.60
6.20	2.80	13.50	2.61
6.68	2.88	15.00	2.56
7.40	2.82	15.40	2.50
7.78	2.79	17.60	2.50
8.20	2.69	17.30	2.51
9.00	2.76	18.00	2.50
9.80	2.68	20.70	2.43
10.90	2.61	23.30	2.40
11.90	2.63	31.80	2.32
12.00	2.64		

$M_G = 2.5$			
$Re_x \times 10^{-6}$	$\bar{c}_f \times 10^3$	$Re_x \times 10^{-6}$	$\bar{c}_f \times 10^3$
5.78	2.16	16.00	1.82
6.98	2.02	16.00	1.82
7.70	2.02	17.90	1.83
9.00	1.95	18.00	1.79
9.30	1.95	21.00	1.74
11.20	1.91	24.20	1.70
11.30	1.89	26.40	1.68
12.40	1.90	28.30	1.63
14.30	1.90	31.20	1.67
14.40	1.88		

Data of: Chapman and Kester (Continued)			
$M_G = 3.6$			
$Re_x \times 10^{-6}$	$\bar{c}_f \times 10^3$	$Re_x \times 10^{-6}$	$\bar{c}_f \times 10^3$
6.25	1.70	16.20	1.53
9.46	1.63	17.50	1.54
10.00	1.65	18.30	1.51

Data of: D. Coles (1954) [2.38]
Model: Flat plate
Measurements: Forces on a floating element

M_G	$Re_{\delta_2} \times 10^{-3}$	$Re_x \times 10^{-6}$	$c_f \times 10^3$
2.6	6.60	6.08	1.81
2.6	10.20	10.26	1.66
3.7	4.10	3.98	1.62
3.7	7.56	8.63	1.38
4.5	2.90	2.81	1.55
4.5	3.47	3.57	1.48
4.5	5.24	6.20	1.26
4.5	6.59	8.17	1.22

Data of: R.M. O'Donell (1954) [2.39]
Model: Cylinder Coaxial flow at the outer surface
Measurements: Velocity profiles
$M_G = 2.41$

$Re_{\delta_2} \times 10^{-3}$	$c_f \times 10^3$	$Re_x \times 10^{-6}$	$c_f \times 10^3$
1.53	2.40	0.59	3.60
2.14	2.40	0.93	3.26
2.20	2.23	1.42	3.00
3.00	2.36	2.12	3.72
3.60	1.90	2.41	2.91
3.82	2.00	2.90	2.68
4.10	1.80	3.26	2.60
5.36	1.73		

Data of: R.J. Hakkinen (1955) [2.40]
Model: Flat plate
Measurements: Forces on a floating element.

M_G	$Re_x \times 10^{-6}$	$c_f \times 10^3$
0.56	0.90	3.36
0.57	0.90	3.37
0.63	1.00	3.30
0.75	1.03	3.01
0.85	1.12	3.01
0.97	1.20	3.00
1.45	1.04	3.00
1.48	1.04	2.94
1.49	1.04	3.00
1.50	1.02	2.91
1.50	1.04	3.02
1.50	1.02	3.02
1.50	1.03	3.02
1.50	1.03	2.92

Data of: Hakkinen (continued).

M_G	$Re_x \times 10^{-6}$	$c_f \times 10^3$
1.52	1.02	3.09
1.52	1.02	3.07
1.52	1.01	3.09
1.52	1.01	3.07
1.71	0.68	3.24
1.72	0.67	3.21
1.73	0.66	3.21
1.74	0.67	3.23
1.75	0.67	3.23
1.73	0.84	3.13
1.74	0.85	3.19
1.74	0.85	3.19
1.76	0.84	3.10
1.76	0.85	3.12

Data of: R.H. Korkegi (1956) [2.41]
Model: Flat plate
Measurements: Forces on a floating element.

M_G	$Re_{\delta_2} \times 10^{-3}$	$c_f \times 10^3$
5.787	2.477	1.316
5.770	2.780	1.275
5.792	3.429	1.223
5.085	4.040	1.179

Data of: F. E. Goddard (1959) [2.42]
Model: Cylinder (axial flow at the outer surface
Measurements: Total forces on the cylinder

$M_G = 0.7$		$M_G = 3.07$	
$Re_x \times 10^{-6}$	$\bar{c}_f \times 10^3$	$Re_x \times 10^{-6}$	$\bar{c}_f \times 10^3$
1.80	3.40	2.54	1.93
5.71	3.27	2.79	1.89
7.21	3.28	3.41	1.82
1.89	4.12	4.30	1.72
		5.30	1.69

$M_G = 3.7$		$M_G = 4.54$	
$Re_x \times 10^{-6}$	$\bar{c}_f \times 10^3$	$Re_x \times 10^{-6}$	$\bar{c}_f \times 10^3$
3.68	1.69	4.23	1.50
4.40	1.58	4.42	1.40
5.05	1.50	4.45	1.35

$M_G = 4.54$			
$Re_x \times 10^{-6}$	$\bar{c}_f \times 10^3$	$Re_x \times 10^{-6}$	$\bar{c}_f \times 10^3$
4.90	1.42	6.40	1.29
5.20	1.40	7.10	1.40
5.40	1.39	7.40	1.30
6.20	1.40	7.40	1.23
6.40	1.33	7.90	1.27
4.55	1.49	8.20	1.30

Data of: F. W. Matting, D. R. Chapman, J. R. Nyholm, and A. G. Thomas (1961) [2.43]
Model: Flat wall of a 2-D Nozzle
Measurements: Forces on a floating element.

$M_G = 2.95$			
$Re_x \times 10^{-6}$	$c_f \times 10^3$	$Re_x \times 10^{-6}$	$c_f \times 10^3$
6.18	1.60	24.60	1.33
8.30	1.55	26.00	1.30
9.01	1.54	27.50	1.30
10.50	1.50	30.50	1.30
12.00	1.46	34.00	1.26
13.00	1.45	35.50	1.29
14.80	1.42	37.50	1.24
17.20	1.40	42.00	1.23
19.90	1.36	54.00	1.20
21.90	1.34	65.00	1.19

$M_G = 4.2$			
$Re_x \times 10^{-6}$	$c_f \times 10^3$	$Re_x \times 10^{-6}$	$c_f \times 10^3$
4.63	1.32	14.0	1.09
5.90	1.30	15.4	1.07
6.64	1.26	17.5	1.05
7.53	1.25	19.5	1.04
8.00	1.20	22.5	1.01
9.12	1.18	25.0	0.995
9.80	1.15	27.5	0.975
11.20	1.14	30.2	0.960
12.60	1.10	34.8	0.948
37.6	0.928	68.2	0.860
42.0	0.922	75.0	0.855
48.0	0.920	84.0	0.840
55.0	0.898	95.2	0.828
61.0	0.880		

(b) For the case of the presence of heat transfer

Data of: I.H. Abbot (1953) [2.44]
Model: Cylinder
Measurements: Decceleration of the cylinder

M_G	T_s/T_G	$Re_x \times 10^{-6}$	$\bar{q} \times 10^3$
3.90	1.0	5.0	2.39
7.25	1.8	5.0	1.16
7.25	1.8	7.5	1.04

Data of: R.J. Monaghan and J.R. Cooke (1953)[2.36]
Model: Flat plate
Measurements: Velocity profiles.

$M_G = 2.82$, $T_s/T_G = 3.50$

$Re_{\delta_2} \times 10^{-3}$	$Re_x \times 10^6$	$c_f \times 10^3$	$\bar{c}_f \times 10^3$
1.944	1.343	2.21	2.90
2.464	1.731	2.06	2.85
3.107	2.426	1.98	2.56
3.391	2.899	1.96	2.34

Data of: R.J. Monaghan and J.R. Cooke (1952) [2.35]
Model: Flat plate
Measurements: Velocity profiles

$M_G = 2.43$, $T_s/T_G = 2.94$

$Re_{\delta_2} \times 10^{-3}$	$Re_x \times 10^6$	$c_f \times 10^3$	$\bar{c}_f \times 10^3$
1.898	0.98	3.00	3.88
2.278	1.40	2.73	3.26

Data of: Monaghan and Cooke (continued).

$M_G = 2.43$, $T_s/T_G = 2.94$

$Re_{\delta_2} \times 10^{-3}$	$Re_x \times 10^{-6}$	$\bar{c}_f \times 10^3$	$\bar{q} \times 10^3$
3.270	2.10	2.32	3.13
3.516	2.51	2.00	2.79
4.525	3.20	1.88	2.81

$M_G = 2.43$, $T_s/T_G = 3.42$

$Re_{\delta_2} \times 10^{-3}$	$Re_x \times 10^{-6}$	$c_f \times 10^3$	$\bar{q} \times 10^3$
2.239	1.42	2.48	3.15
3.003	2.12	2.32	2.80
3.568	2.71	2.18	2.65
4.556	3.70	2.09	2.45
5.581	4.39	1.95	2.55

Data of: C.C. Pappas (1954) [2.46]
Model: Flat plate
Measurements: Velocity profiles

$M_G = 1.69$, $T_s/T_G = 1.65$

$Re_x \times 10^{-6}$	$\bar{c}_f \times 10^3$	$Re_x \times 10^{-6}$	$\bar{c}_f \times 10^3$
0.807	3.69	1.89	3.36
1.50	3.21	1.92	3.37
2.20	3.16	2.92	3.10
2.89	2.92	3.00	3.16
3.55	2.80	4.01	2.83
2.74	3.18	4.09	2.71
3.80	3.00	5.42	2.79
6.00	2.76		

Data of: Pappas (Continued)

$M_G = 1.69$, $T_S/T_G = 1.65$

$Re_x \times 10^{-6}$	$\bar{c}_f \times 10^3$	$Re_x \times 10^{-6}$	$\bar{c}_f \times 10^3$
3.62	2.73	7.21	2.40
5.45	2.55	8.98	2.35
7.18	2.56		

$M_G = 2.27$, $T_S/T_G = 2.16$

$Re_x \times 10^{-6}$	$\bar{c}_f \times 10^3$	$Re_x \times 10^{-6}$	$\bar{c}_f \times 10^3$
1.95	3.07	4.30	2.68
2.88	2.86	5.50	2.54
3.90	2.70	3.56	2.73
4.80	2.70	4.90	2.50
1.48	3.40	6.40	2.50
2.35	2.90	7.80	2.30

Data of: S.C. Sommer and B.J. Short (1955) [2.20]
Model: Cylinder
Measurements: Decceleration of the cylinder

M_G	T_S/T_G	$Re_x \times 10^{-6}$	$\bar{c}_f \times 10^3$
2.81	1.03	3.00	3.12
3.82	1.05	4.07	2.50
5.63	1.29	4.71	1.87
6.90	1.70	4.06	1.38
6.90	1.70	6.09	1.44
7.00	1.75	6.06	1.26
7.00	1.75	9.92	1.32
3.78	1.05	4.94	2.29
3.67	1.05	3.78	2.51

Data of: F.K. Hill (1956) [2.47]
Model: Axially symmetrical nozzle
Measurements: Velocity gradients at the wall

M_G	T_S/T_G	$Re_{\delta_2} \times 10^{-3}$	$c_f \times 10^3$
8.99	7.67	1.245	0.790
9.04	7.97	1.607	0.891
9.07	8.28	1.908	0.851
9.10	8.69	2.287	0.800
8.22	7.17	2.081	0.924
8.25	7.26	2.498	0.910
8.27	7.34	2.885	0.870
8.29	7.37	3.202	0.820
8.29	7.41	3.451	0.771

Data of: F.K. Hill (1959) [2.48]
Model: Axially symmetrical nozzle
Measurements: Velocity gradients at the wall

M_G	T_S/T_G	$Re_{\delta_2} \times 10^{-3}$	$c_f \times 10^3$
8.25	6.12	2.220	0.910
8.27	6.17	2.505	0.840
8.28	6.25	2.760	0.796
8.29	6.18	2.965	0.754
9.04	8.07	1.936	0.913
9.07	8.30	2.276	0.870
9.10	8.65	2.710	0.805
10.03	9.76	1.300	0.84
10.04	9.31	1.450	0.761
10.05	8.91	1.680	0.696
10.06	8.99	1.700	0.673

Data of: E.M. Winkler (1961) [2.23]
Model: Flat plate
Measurements: Velocity gradients at the wall.

M_d	T_s/T_G	$Re_{\delta_2} \times 10^{-3}$	$Re_x \times 10^{-6}$	$c_f \times 10^3$	$\bar{c}_f \times 10^3$
5.21	5.15	2.099	2.72	1.47	1.54
5.14	5.50	2.936	3.36	1.39	1.75
5.20	5.38	3.173	4.07	1.43	1.56
5.26	5.52	3.880	5.04	1.35	1.54
5.29	5.57	4.300	5.94	1.31	1.45
4.98	4.51	1.900	2.29	1.34	1.66
5.19	4.74	1.782	2.58	1.61	1.38
5.20	4.83	2.960	3.81	1.35	1.55
5.24	5.02	3.455	4.88	1.15	1.52
5.24	4.97	3.799	5.11	1.06	1.48
5.17	3.89	1.055	2.01	1.47	1.33
5.16	3.71	1.652	2.57	1.32	1.29
5.10	3.58	1.735	2.73	1.34	1.27
5.11	3.52	2.488	2.27	1.24	1.53
5.20	3.77	2.482	3.27	1.20	1.37
5.12	3.78	3.256	3.57	1.05	1.82

APPENDIX 2B

Summary of the methods of evaluating Re_{S2} integral, approximations (a) and (b) appearing in tables 2.1 - 2.4

Approximate analytical (a)

Taking Eq.(2.3) of §2.2.2 for example, we have

$$Re_{S2} = \frac{\mu_S K u_G^{+2}}{\mu_G E} \int_0^1 \phi^3 z(1-z) \exp\left[k u_G^+ \int_0^z \phi\, dz\right] dz. \quad \cdots \quad (2.3)$$

As the magnitude of the integrand is small at small z,

$$\int_0^z \phi\, dz$$

is replaced by Nz, where

$$N = \frac{1}{0.9} \int_0^{0.9} \phi\, dz$$

the Eq.(2.3) now becomes

$$Re_{S2} = \frac{\mu_S K u_G^{+2}}{\mu_G E} \int_0^1 \phi^3 z(1-z) \exp(KN u_G^+ z)\, dz \quad \cdots \quad (2B.1)$$

On integrating Eq.(2B.1) by parts twice, there is obtained

$$Re_{S2} = \frac{\mu_S u_G^+}{\mu_G EN} \Big\{ \phi^3 z(1-z) \exp(KN u_G^+ z)$$
$$- \int_0^1 [\phi^3(1-2z) + z(1-z)(d\phi^3/dz)]\exp(KN u_G^+ z)\, dz \Big\}_0^1$$

$$= \frac{\mu_S}{\mu_G EN} [\phi^3 \exp(KN u_G^+ z)]_0^1 + \text{smaller terms}$$

$$\approx \frac{\mu_S \phi_G^3}{\mu_G KEN^2} \exp(KN u_G^+ z). \quad \cdots \quad (2B.2)$$

Hence
$$Re_{s2} = \frac{\mu_s \phi_G^3}{\mu_G N^2 KE} \exp\left[KN\left(\frac{2T_G}{c_f T_s}\right)^{\frac{1}{2}}\right] \quad \cdots \quad (2B.3)$$

Approximate analytical (b)

Taking Eq.(2.3) of §2.2.2, for example, we have

$$Re_{s2} = \frac{\mu_s K u_G^{+2}}{\mu_G E} \int_0^1 \phi^3 z(1-z)\exp\left(Ku_G^+ \int_0^z \phi \, dz\right) dz$$
$$\cdots \quad (2.3)$$

Eq.(2.3) is re-written as

$$Re_{s2} = \frac{\mu_s K u_G^{+2}}{\mu_G E} \exp\left(Ku_G^+ \int_0^1 \phi \, dz\right) \int_0^1 \phi^3 z(1-z)\exp\left(Ku_G^+ \int_1^z \phi \, dz\right)$$
$$dz \quad \cdots \quad (2B.4)$$

Replace $\exp\left(Ku_G^+ \int_1^z \phi \, dz\right)$ by z^n ,

where n is so chosen that the gradient is the same, then, on differentiation, we have $Ku_G^+ \phi = n$. Now Eq.(2B.4) can be re-written as

$$Re_{s2} \approx \frac{\mu_s K u_G^{+2}}{\mu_G E} \exp\left(Ku_G^+ \int_0^1 \phi \, dz\right) \int_0^1 \phi^3 z(1-z)z^n dz$$

$$\approx \frac{\mu_s \phi_G^3 K u_G^{+2}}{\mu_G E} \exp\left(Ku_G^+ \int_0^1 \phi \, dz\right) \int_0^1 (z^{n+1} - z^{n+2}) dz$$

$$= \frac{\mu_s \phi_G^3 K u_G^+ \exp\left(Ku_G^+ \int_0^1 \phi \, dz\right)}{\mu_G \left[E (K\phi_G u_G^+ + 2)(K\phi_G u_G^+ + 3)\right]} \quad \cdots \quad (B2.5)$$

As $Ku_G^+ \phi \gg 3$ in general, Eq. (2B.5) can be approximately written as

$$Re_{S2} = \frac{\mu_S \phi_G}{\mu_G KE} \exp\left(Ku_G^+ \int_0^1 \phi \, dz\right) . \quad \cdots \quad (2B.6)$$

Hence

$$Re_{S2} = \frac{\mu_S \phi_G}{\mu_G KE} \exp\left\{K(\int_0^1 \phi \, dz)\left(\frac{2T_G}{c_f T_S}\right)^{\frac{1}{2}}\right\}. \quad \cdots \quad (2B.7)$$

APPENDIX 3A.

Collected Experimental Data of Heat-Transfer Coefficient

for Incompressible Turbulent Boundary Layer.

Data of: W. C. Reynolds, W. H. Kays and S. J. Kline (1958) [3.11]

Model: Flat Plate.

Measurements: Electrical energy input.

$Re_x \times 10^{-6}$	$St \times 10^3$	S	$Re_x \times 10^{-6}$	$St \times 10^3$	S
0.255	2.73	1.218	0.816	2.12	1.160
0.423	2.41	1.178	0.960	2.03	1.141
0.580	2.13	1.100	1.108	2.01	1.157
0.736	2.11	1.134	1.247	2.05	1.203
0.889	2.06	1.143	1.398	1.84	1.100
1.045	2.02	1.151	1.539	1.95	1.184
1.196	1.97	1.148	1.682	1.85	1.139
1.353	2.01	1.195	1.828	1.83	1.142
1.507	1.85	1.120	1.978	1.81	1.144
1.661	1.79	1.100	2.11	1.77	1.130
1.823	1.84	1.148	2.25	1.78	1.148
1.970	1.78	1.124	2.40	1.74	1.134
2.130	1.79	1.145	2.54	1.72	1.131
2.280	1.73	1.118	2.68	1.71	1.134
2.440	1.74	1.137	2.80	1.72	1.148
2.600	1.75	1.155	2.95	1.66	1.117
2.750	1.72	1.145	3.10	1.53	1.038
2.900	1.68	1.128	3.25	1.58	1.079
3.050	1.73	1.170	0.211	2.87	1.237
3.180	1.67	1.137	0.347	2.51	1.184

$Re_x \times 10^{-6}$	$St \times 10^3$	S	$Re_x \times 10^{-6}$	$St \times 10^3$	S
3.360	1.54	1.058	0.475	2.21	1.160
3.510	1.58	1.092	0.603	2.15	1.117
0.235	2.56	1.126	0.733	2.11	1.133
0.386	2.48	1.192	0.862	2.10	1.159
0.528	2.23	1.132	0.988	1.99	1.124
0.676	2.13	1.128	1.115	2.05	1.181
1.250	1.87	1.098	0.865	2.08	1.149
1.375	1.81	1.079	1.020	2.04	1.158
1.502	1.91	1.155	1.172	1.98	1.150
1.636	1.80	1.104	1.325	1.99	1.179
1.729	1.83	1.132	1.484	1.81	1.098
1.888	1.77	1.110	1.630	1.77	1.085
2.02	1.76	1.116	1.788	1.85	1.151
2.15	1.75	1.121	1.863	1.78	1.114
2.27	1.72	1.111	2.09	1.80	1.148
2.40	1.69	1.101	2.23	1.74	1.121
2.52	1.75	1.140	2.39	1.76	1.146
2.65	1.66	1.099	2.55	1.75	1.151
2.79	1.55	1.034	2.70	1.70	1.128
2.92	1.60	1.075	2.84	1.69	1.131
0.115	3.06	1.168	2.99	1.71	1.153
0.189	3.06	1.193	3.14	1.64	1.115
0.260	2.72	1.218	3.30	1.52	1.041
0.329	2.59	1.218	3.45	1.58	1.051
0.398	2.52	1.210	0.225	2.413	1.051
0.467	2.44	1.213	0.372	2.51	1.140

$Re_x \times 10^{-6}$	$St \times 10^3$	S	$Re_x \times 10^{-6}$	$St \times 10^3$	S
0.541	2.38	1.214	0.507	2.26	1.140
0.609	2.44	1.270	0.648	2.18	1.147
0.680	2.24	1.188	0.788	2.13	1.158
0.750	2.16	1.165	0.924	2.10	1.173
0.824	2.20	1.205	1.064	2.01	1.149
0.890	2.14	1.188	1.203	2.07	1.208
0.960	2.13	1.197	1.344	1.85	1.099
1.033	2.09	1.189	1.481	1.81	1.092
1.104	2.10	1.208	1.613	1.89	1.156
1.169	2.00	1.161	1.759	1.83	1.135
1.236	2.03	1.189	1.891	1.85	1.161
1.310	1.97	1.165	2.03	1.77	1.123
1.440	2.00	1.201	2.17	1.80	1.155
1.382	1.96	1.169	2.29	1.79	1.158
1.518	1.79	1.084	2.45	1.71	1.118
1.589	1.86	1.135	2.58	1.69	1.114
0.249	2.67	1.187	2.69	1.74	1.154
0.410	2.42	1.176	2.83	1.67	1.117
0.562	2.17	1.114	2.98	1.54	1.038
0.712	2.14	1.144	3.12	1.59	1.079
0.177	3.02	1.260	2.44	1.66	1.085
0.289	2.59	1.183	0.092	3.53	1.298
0.396	2.25	1.087	0.151	3.22	1.304
0.506	2.30	1.160	0.206	3.02	1.296
0.611	2.23	1.161	0.264	2.82	1.267
0.721	2.18	1.168	0.319	2.72	1.264

$Re_x \times 10^{-6}$	$St \times 10^3$	S	$Re_x \times 10^{-6}$	$St \times 10^3$	S
0.829	2.09	1.146	0.377	2.64	1.264
0.938	2.11	1.181	0.433	2.56	1.256
1.047	1.99	1.135	0.489	2.62	1.313
1.154	1.91	1.107	0.546	2.34	1.216
1.259	2.00	1.175	0.601	2.34	1.215
1.367	1.93	1.150	0.660	2.42	1.277
1.475	1.90	1.146	0.715	2.32	1.241
1.577	1.87	1.140	0.771	2.23	1.208
1.692	1.86	1.147	0.827	2.34	1.288
1.801	1.83	1.140	0.884	2.31	1.281
1.905	1.79	1.125	0.939	2.26	1.265
2.01	1.81	1.147	0.995	2.19	1.238
2.11	1.80	1.150	1.048	2.13	1.215
2.22	1.76	1.133	1.160	2.19	1.270
2.32	1.64	1.063	1.214	1.98	1.157
1.270	2.07	1.718			

Appendix 3B

Colleted Experimental Data of Heat-Transfer Coefficient for Compressible Turbulent Boundary Layer

Data of: J.H. Johnson and R.J. Monaghan (1951) [3.12] Model: Flat plate Measurements: Rates of steam Condensation.				Data of: R.J. Monaghan and J.R. Cooke (1953) [3.13] Model: Flat plate Measurements: Rates of steam Condensation			
$M_G = 2.5$				$M_G = 2.43$			
T_S/T_G	$Re_x \times 10^{-6}$	$\bar{St} \times 10^3$	$\bar{S}$	T_S/T_G	$Re_x \times 10^{-6}$	$\bar{St} \times 10^3$	$\bar{S}$
3.44	4.35	1.27	1.162	2.78	3.33	1.45	1.202
3.44	4.34	1.23	1.124	2.78	3.34	1.45	1.201
3.71	4.96	1.24	1.181	2.96	3.70	1.34	1.146
3.71	4.96	1.21	1.152	2.97	3.70	1.36	1.164
3.76	5.02	1.20	1.148	2.52	2.96	1.44	1.147
3.76	5.06	1.18	1.131	2.52	2.96	1.48	1.178
3.07	3.73	1.28	1.112	2.49	4.71	1.21	1.118
3.07	3.72	1.27	1.104	3.49	4.71	1.22	1.128
2.93	3.48	1.31	1.115	3.35	4.33	1.30	1.173
2.93	3.47	1.30	1.105	3.36	4.33	1.26	1.137
2.30	3.05	1.38	1.099	3.49	4.60	1.23	1.132
2.23	2.88	1.34	1.050	3.49	4.60	1.24	1.140
2.24	2.90	1.31	1.029	3.09	3.83	1.33	1.153
2.19	2.81	1.35	1.050	3.09	3.83	1.33	1.153
2.18	2.78	1.31	1.016	2.87	3.46	1.38	1.168
2.68	3.66	1.35	1.142	2.87	3.46	1.37	1.150
2.68	3.69	1.36	1.152	2.77	3.31	1.44	1.191
2.59	3.52	1.29	1.076				
2.59	3.52	1.31	1.093				
2.49	3.35	1.37	1.125				
2.49	3.35	1.39	1.141				
2.41	3.19	1.43	1.157				

Data of: R.J. Monaghan and J.R. Cooke (1953) [3.14] Model: Flat plate Measurements: Rates of steam condensation				Data of: C.C. Pappas (1953 & 1954) [3.15 & 3.16] Model: Flat plate Measurements: Electrical energy inputs		
$M_G = 2.82$				$M_G = 1.69$, $T_S/T_G = 1.65$		
T_S/T_G	$Re_\theta \times 10^{-6}$	$\overline{St}\times10^3$	$\overline{S}$	$Re_{\delta_2}\times10^{-3}$	$St\times10^3$	S
3.53	3.12	1.32	1.179	1.950	1.74	1.231
3.98	3.64	1.28	1.205	2.435	1.65	1.224
3.98	3.64	1.30	1.223	3.000	1.52	1.178
4.12	3.83	1.22	1.167	3.450	1.49	1.189
4.53	3.75	1.23	1.191	3.810	1.40	1.140
4.54	3.75	1.23	1.192	4.230	1.40	1.164
3.90	3.55	1.22	1.138	4.600	1.36	1.150
3.89	3.55	1.22	1.138	5.000	1.28	1.100
3.80	3.44	1.29	1.191	4.800	1.40	1.229
3.81	3.44	1.25	1.164	5.700	1.42	1.243
3.74	3.35	1.24	1.134	6.850	1.31	1.188
3.74	3.36	1.24	1.134	7.610	1.35	1.248
3.41	2.93	1.34	1.175	8.100	1.25	1.169
3.41	2.93	1.35	1.184	8.300	1.28	1.203
3.28	2.74	1.41	1.211	2.125	1.58	1.129
3.66	3.21	1.32	1.193	2.125	1.70	1.215
3.66	3.21	1.30	1.174	3.800	1.57	1.265
3.60	3.14	1.33	1.194	4.500	1.45	1.208
3.60	3.14	1.33	1.194	4.500	1.49	1.242
3.36	2.84	1.35	1.174	4.980	1.34	1.139
3.35	2.84	1.36	1.182	4.980	1.40	1.190
3.24	2.70	1.41	1.206	5.360	1.29	1.112
3.24	2.70	1.40	1.197	5.360	1.33	1.147
3.11	2.54	1.43	1.200	5.800	1.30	1.138
3.09	2.54	1.41	1.182	5.800	1.32	1.156
3.91	3.57	1.26	1.175	7.500	1.26	1.158
3.90	3.54	1.28	1.194	7.500	1.30	1.195
4.28	3.99	1.21	1.175	4.850	1.50	1.265
4.28	3.99	1.20	1.165	4.850	1.50	1.265

Data of: Pappas (Continued)
Model: Flat plate
Measurements: Electrical energy inputs

$M_G = 1.69$, $T_S/T_G = 1.70$

$Re_{\delta_2} \times 10^{-3}$	$St \times 10^3$	S
5.60	1.39	1.205
5.60	1.42	1.231
6.45	1.29	1.149
6.45	1.31	1.176
7.50	1.22	1.118
7.50	1.26	1.155
8.80	1.12	1.058
8.80	1.17	1.105
9.78	1.18	1.136
9.78	1.20	1.155
10.20	1.15	1.116
10.20	1.16	1.126
10.65	1.11	1.086
10.65	1.16	1.134

$M_G = 2.27$, $T_S/T_G = 2.16$

$Re_{\delta_2} \times 10^{-3}$	$St \times 10^3$	S
2.27	1.40	1.175
2.95	1.36	1.207
3.53	1.22	1.125
4.13	1.21	1.152
4.67	1.12	1.093
5.25	1.13	1.129
5.90	1.09	1.115
6.45	1.05	1.092
3.00	1.40	1.249
3.54	1.40	1.293
4.19	1.24	1.185
4.75	1.24	1.216

Data of: Pappas (continued)

$M_G = 2.27$, $T_S/T_G = 2.16$

$Re_{\delta_2} \times 10^{-3}$	$St \times 10^3$	S
4.19	1.25	1.185
5.40	1.15	1.157
6.05	1.13	1.163
6.58	1.10	1.150
7.10	1.00	1.061
4.00	1.33	1.250
4.76	1.30	1.265
5.45	1.22	1.235
6.18	1.20	1.234
7.00	1.17	1.241
8.00	1.10	1.198
8.70	1.06	1.172
9.40	1.02	1.145

$M_G = 1.69$, $T_S/T_G = 1.67$

$Re_x \times 10^{-6}$	$St \times 10^3$	S
1.17	1.75	1.251
1.17	1.73	1.237
1.51	1.66	1.240
1.85	1.54	1.190
2.20	1.47	1.169
2.20	1.52	1.209
2.54	1.41	1.149
2.88	1.42	1.181
2.88	1.40	1.164
3.22	1.39	1.117
3.21	1.35	1.143
3.53	1.30	1.117
1.75	1.60	1.218
3.20	1.41	1.186
3.81	1.41	1.219
4.90	1.35	1.215

Data of: Pappas (continued)

$M_G = 1.69$, $T_s/T_G = 1.67$

$Re_x \times 10^{-6}$	$St \times 10^3$	S
5.40	1.26	1.151
1.66	1.60	1.205
2.20	1.59	1.255
2.75	1.46	1.195
3.29	1.40	1.179
3.81	1.32	1.139
3.81	1.30	1.121
4.31	1.31	1.152
4.31	1.25	1.188
4.89	1.30	1.167
4.89	1.26	1.131
3.40	1.51	1.276
4.23	1.46	1.277
4.23	1.39	1.216
5.03	1.32	1.187
5.03	1.35	1.213
5.95	1.28	1.181
5.95	1.21	1.117
6.80	1.18	1.112
6.80	1.13	1.065
7.65	1.20	1.151
8.45	1.16	1.130
9.30	1.12	1.107
9.30	1.17	1.156

$M_G = 2.27$, $T_s/T_G = 2.15$

$Re_x \times 10^{-6}$	$St \times 10^3$	S
1.40	1.40	1.158
1.90	1.36	1.186
2.40	1.24	1.125
2.85	1.20	1.121
3.36	1.13	1.085
3.85	1.12	1.099

Data of: Pappas (continued).

$M_G = 2.27$, $T_s/T_G = 2.15$

$Re_x \times 10^{-6}$	$St \times 10^3$	S
4.32	1.10	1.100
5.00	1.10	1.128
4.79	1.04	1.058
1.95	1.38	1.210
2.45	1.38	1.258
2.99	1.23	1.159
3.50	1.23	1.190
4.00	1.15	1.137
4.52	1.15	1.160
5.50	1.00	1.041
2.77	1.34	1.238
3.50	1.30	1.249
4.20	1.20	1.188
4.92	1.19	1.208
5.61	1.16	1.203
6.30	1.11	1.173
7.05	1.06	1.140
7.80	1.03	1.125

Data of: J. R. Jack and N. S. Diaconis (1956) [3.17]
Model: Cone nosed cylinder
Measurements: Temperature-time history of the model

$M_G = 3.12$, $T_s/T_G = 4$

$Re_x \times 10^{-6}$	$St \times 10^3$	S
1.06	1.26	1.233
1.39	1.21	1.247
2.50	1.09	1.252
4.25	0.96	1.212
4.95	0.94	1.218

Data of: Jack and Diaconis (Continued)

$M_G = 3.12$, $T_S/T_G = 4$

$Re_x \times 10^{-6}$	$St \times 10^3$	S
6.20	0.882	1.188
7.40	0.850	1.180
8.80	0.820	1.171

Data of: M.J. Brevoort and B.D. Arabian (1958)[3.18]
Model: Cylinder (axial flow at the outer surface)
Measurements: Temperature-time history.

$M_G = 0.87$, $T_S/T_G = 1$

$Re_x \times 10^{-6}$	$St \times 10^3$	S
13.9	1.27	1.112
16.6	1.26	1.131
19.6	1.19	1.093
28.3	1.12	1.082
42.7	1.00	1.021

$M_G = 1.62$, $T_S/T_G = 1.6$

$Re_x \times 10^{-6}$	$St \times 10^3$	S
1.94	1.42	1.123
0.95	1.66	1.085
4.85	1.26	1.116
33.6	0.91	1.075
49.0	0.87	1.083
459	0.64	1.065
479	0.615	1.053

Data of: Brevoort and Arabian (continued).

$M_G = 2.06$, $T_S/T_G = 1.8$

$Re_x \times 10^{-6}$	$St \times 10^3$	S
3.30	1.36	1.221
5.20	1.22	1.177
6.60	1.19	1.192
8.35	1.13	1.174
13.7	1.05	1.175
22.4	0.96	1.155
62.0	0.84	1.161
109	0.77	1.154

$M_G = 3.9$, $T_S/T_G = 4.0$

$Re_x \times 10^{-6}$	$St \times 10^3$	S
2.30	0.91	1.128
5.85	0.85	1.240
6.60	0.83	1.235
66.0	0.605	1.289
88.0	0.600	1.019

$M_G = 5.05$, $T_S/T_G = 5.5$

$Re_x \times 10^{-6}$	$St \times 10^3$	S
68	0.390	1.028
72.5	0.395	1.051
115	0.400	1.139

Data of: T. Tendeland (1959)[3.19]
Model: Cone nosed cylinder
Measurements: Temperature-time history

$M_G = 3$, $T_S/T_G = 2$

$Re_x \times 10^{-6}$	$St \times 10^3$	S
1.3	1.20	1.061
1.9	1.15	1.084
3.5	1.15	1.199
4.0	1.18	1.257
4.8	1.10	1.206
2.5	1.10	1.180
3.2	1.06	1.184
3.8	1.04	1.195
4.55	1.07	1.266
5.1	1.06	1.277

$M_G = 4.08$, $T_S/T_G = 3.40$

$Re_x \times 10^{-6}$	$St \times 10^3$	S
2.6	0.94	1.181
3.45	0.87	1.147
4.2	0.76	1.036
4.8	0.80	1.115
5.7	0.76	1.090
2.62	0.85	1.167
3.2	0.83	1.181
3.72	0.76	1.110
4.35	0.77	1.150

$M_G = 5.04$, $T_S/T_G = 4.2$

$Re_x \times 10^{-6}$	$St \times 10^3$	S
2.62	0.83	1.218
2.92	0.86	1.286
3.43	0.80	1.230

Data of: F.K. Hill (1959)[3.20]
Model: Axial symmetrical nozzle
Measurements: Temperature gradients at the wall in the stream

M_G	T_S/T_G	$Re_{\delta_2} \times 10^{-3}$	$St \times 10^3$	S
9.07	8.30	2.276	0.380	1.050
9.10	8.65	2.710	0.352	1.030
10.03	9.76	1.300	0.414	1.148
10.04	9.32	1.450	0.390	1.107
10.05	8.91	1.680	0.362	1.060
10.06	8.99	1.700	0.368	1.083
9.04	8.07	1.936	0.420	1.120

Data of: P.F. Brinich (1961)[3.21]
Model: Cylinder caxial flow at the outer surface
Measurements: Temperature-time history

$M_G = 4.95$

T_S/T_G	$Re_x \times 10^{-6}$	$St \times 10^3$	S
1.83	1.77	1.39	1.696
1.83	2.66	1.28	1.667
1.83	3.52	1.30	1.770
1.83	4.42	1.23	1.735
2.94	1.76	1.16	1.489
2.94	2.65	1.08	1.486
2.94	3.52	1.09	1.573
2.94	4.40	1.02	1.527
2.94	6.15	0.92	1.454
2.94	8.00	0.95	1.565
2.94	9.60	0.88	1.491
2.94	11.30	0.85	1.477
3.60	1.76	1.03	1.454
3.60	2.65	0.98	1.565
3.60	3.56	0.94	1.491
3.60	4.40	0.90	1.477

Data of: E. M. Winkler (1961) [3.22]
Model: Flat plate
Measurements: Temperature gradients in the wall material

M_G	T_S/T_G	$Re_{\delta_2} \times 10^{-3}$	$Re_x \times 10^{-6}$	$St \times 10^3$	S
4.98	4.51	1.900	2.29	0.852	1.226
5.20	4.83	2.960	3.81	0.735	1.202
5.24	5.02	3.455	4.55	0.738	1.260
5.24	4.97	3.799	6.11	0.671	1.166
5.17	3.89	1.055	2.01	0.968	1.170
5.16	3.71	1.652	2.57	0.835	1.215
5.11	3.52	2.488	3.27	0.799	1.297
5.12	3.78	3.256	4.22	0.672	1.062

APPENDIX 4A

Experimental Observations (Tests 1-4)

Test 1   (Date 13/3/64)

P_{atm} 756.80 mm Hg
T_{atm} 73.4 °F

Dew Point Temperature   15 °F
$P_O - P_X$ 196.52 mm H_2O
P_O 204.02 mm H_2O, G
E_O 3.532 mV
E_G 3.523 mV

t sec. \ x''	1.5	2.5	3.5	4.5	6.5	8
	$(E_G - E_S)$ mV					
20	0.705	0.735	0.754	0.766	0.779	0.792
30	0.574	0.607	0.634	0.646	0.666	0.680
40	0.467	0.504	0.530	0.547	0.564	0.581
50	0.383	0.422	0.446	0.464	0.483	0.498
60	0.319	0.354	0.377	0.393	0.414	0.430
70	0.269	0.301	0.325	0.339	0.356	0.372
80	0.231	0.258	0.281	0.305	0.310	0.325
90	0.199	0.226	0.250	0.258	0.272	0.285
100	0.173	0.198	0.217	0.230	0.242	0.252
110	0.152	0.173	0.193	0.206	0.216	0.227
120	0.106	0.152	0.164	0.184	0.193	0.203

Test 2 (13/3/64)

P_{atm}	756.80	mm Hg
T_{atm}	75.4	°F

Dew point temperature	15	°F
$P_0 - P_x$	192.22	mm H_2O
P_0	198.45	mm H_2O, G
E_0	3.530	mV
E_G	3.520	mV

t sec. \ x"	10	12	14	16	18	22
	$(E_G - E_S)$ mV					
20	0.797	0.819	0.839	0.846	0.852	0.860
30	0.678	0.704	0.728	0.737	0.747	0.761
40	0.592	0.605	0.614	0.620	0.627	0.634
50	0.517	0.532	0.539	0.547	0.554	0.561
60	0.448	0.462	0.472	0.478	0.486	0.496
70	0.338	0.393	0.412	0.417	0.427	0.439
80	0.332	0.350	0.359	0.367	0.377	0.388
90	0.282	0.304	0.314	0.323	0.332	0.343
100	0.244	0.260	0.272	0.279	0.293	0.301
110	0.206	0.221	0.233	0.243	0.254	0.263
120	0.171	0.188	0.200	0.210	0.224	0.229
130	0.143	0.156	0.168	0.178	0.189	0.200
140	0.117	0.130	0.140	0.158	0.160	0.175

<u>Test 3</u> (Date 20/3/64)

P_{atm}	747.20	mm Hg
T_{atm}	75.2	°F
Dew point temperature	17	°F
$P_0 - P_x$	5.04	mm H_2O
P_0	5.17	mm H_2O, G
E_0	5.241	mV
E_G	5.226	mV

ts. \ x"	1.5	2.5	3.5	4.5	6.5	8
	— $(E_G - E_s)$ mV					
40	1.597	1.688	1.706	1.719	1.748	1.734
60	1.469	1.569	1.592	1.617	1.666	1.632
80	1.346	1.458	1.485	1.512	1.592	1.541
100	1.235	1.360	1.391	1.446	1.514	1.455
120	1.125	1.268	1.319	1.338	1.451	1.378
140	1.029	1.179	1.229	1.281	1.388	1.307
160	0.947	1.101	1.155	1.207	1.325	1.233
180	0.872	1.026	1.084	1.142	1.270	1.167
200	0.807	0.958	1.016	1.077	1.212	1.105
220	0.748	0.891	0.940	1.020	1.161	1.051
240	0.718	0.834	0.896	0.962	1.111	0.995
260	0.644	0.777	0.845	0.912	1.066	0.947
280	0.595	0.730	0.794	0.762	1.008	0.895

Test 4   (Date 20/3/64)

P_{atm}	747.20	mm Hg
T_{atm}	75.2	°F
Dew point temperature	17	°F
$P_0 - P_x$	5.12	mm H_2O
P_0	5.21	mm H_2O , G
E_0	4.903	mv
E_G	4.890	mv

t sec. \ x"	10	12	14	16	18	22
	$(E_G - E_S)$ mV					
40	1.605	1.626	1.649	1.656	1.664	1.670
60	1.487	1.517	1.544	1.560	1.574	1.587
80	1.383	1.413	1.442	1.469	1.484	1.502
100	1.289	1.322	1.352	1.377	1.395	1.415
120	1.202	1.242	1.274	1.295	1.313	1.335
140	1.124	1.160	1.193	1.217	1.239	1.268
160	1.041	1.085	1.119	1.151	1.169	1.200
180	0.968	1.017	1.050	1.082	1.104	1.137
200	0.899	0.947	0.989	1.019	1.044	1.073
220	0.836	0.887	0.930	0.959	0.986	1.010
240	0.780	0.831	0.870	0.902	0.929	0.957
260	0.731	0.780	0.818	0.846	0.873	0.902

APPENDIX 4B

Experimental Observations (Tests 5-12)

__Test 5__   (Date 12/6/64)

P_{atm}	760.10	mm Hg
T_{atm}	77	°F
Dew point temperature	14	°F
$P_0 - P_1$	98.32	mm H_2O
P_0	103.23	mm H_2O, G
E_0	0.999	mV
E_G	0.999	mV

t sec \ x''	10	12	14	16	18	22
			$(E_G - E_s)$ mV			
10	5.141	5.171	5.186	5.213	5.254	5.284
20	4.485	4.549	4.579	4.613	4.650	4.695
30	3.941	4.013	4.050	4.076	4.133	4.196
40	3.450	3.548	3.593	3.619	3.679	3.750
50	3.045	3.135	3.169	3.221	3.278	3.353
60	2.681	2.768	2.813	2.854	2.921	3.023
70	2.351	2.434	2.498	2.589	2.610	2.700
80	2.066	2.168	2.224	2.269	2.348	2.434
90	1.691	1.759	1.830	1.916	1.98	2.070

Test 6   (Date 12/6/64)

P_{atm} 7 60.10   mm Hg
T_{atm} 77   °F

Dew point temperature   14   °F
$P_0 - P_x$ 1 89.20   mm H_2O
P_0 199.88   mm H_2O, G
E_0 1.083   mV
E_G 1.083   mV

t sec. \ x"	10	12	14	16	18	22
	$(E_G - E_S)$ mV					
10	5.059	5.089	5.111	5.141	5.168	5.213
15	4.838	4.605	4.643	4.688	4.721	4.766
20	4.219	4.269	4.313	4.343	4.399	4.451
25	3.795	3.855	3.904	3.986	4.039	4.088
30	3.495	3.593	3.641	3.713	3.754	3.806
35	3.176	3.266	3.323	3.375	3.450	3.510
40	2.925	3.034	3.083	3.143	3.199	3.270
45	2.666	2.771	2.843	2.914	2.963	3.023
50	2.460	2.584	2.621	2.693	2.738	2.813
55	2.254	2.351	2.404	2.479	2.546	2.595
60	2.066	2.172	2.228	2.310	2.348	2.430
65	1.856	1.961	2.048	2.093	2.134	2.220

Test 7   (Date 24/6/64)

P_{atm}	769.65	mm Hg
T_{atm}	73.4	°F

Dew point temperature	.13	°F
$P_0 - P_x$	136.88	mm H_2O
P_0	142.90	mm H_2O, G
E_0	4.958	mv
E_G	4.941	mv

t sec. \ x''	1.5	2.5	3.5	4.5	6.5	8
	$-E_S$ mv					
10	4.590	4.481	4.530	4.556	4.601	4.631
15	3.893	3.679	3.784	3.833	3.934	3.968
20	3.221	2.959	3.075	3.154	3.296	3.341
25	2.625	2.295	2.441	2.554	2.693	2.798
30	2.059	1.691	1.841	1.973	2.130	2.246
35	1.549	1.163	1.339	1.453	1.658	1.781
40	1.084	0.660	0.848	0.983	1.193	1.339
45	0.656	0.195	0.416	0.529	0.788	0.941

Test 8   (24/6/64)

P_{atm}	769.65	mm Hg
T_{atm}	73.4	°F
Dew point temperature	13	°F
$P_0 - P_x$	123.23	mm H_2O
P_0	128.39	mm H_2O, G
E_0	4.952	mV
E_G	4.939	mV

t sec. \ x''	10	12	14	16	18	22
			$-E_s$ mV			
10	3.881	3.930	3964	3.990	4.001	4.039
15	3.326	3.375	3413	3.450	3.491	3.555
20	2.810	2.884	2.910	2.948	3.004	3.064
25	2.291	2.359	2.408	2.471	2.543	2.584
30	1.763	1.909	1.929	2.021	2.081	2.169
35	1.403	1.481	1.549	1.613	1.650	1.736
40	0.986	1.061	1.148	1.215	1.268	1.339
45	0.608	0.720	0.799	0.859	0.911	0.979
50	0.253	0.334	0.458	0.506	0.593	0.668

Tests 9-12   (Dates 1/7/64 and 17/7/64)

Test No.	9	9	10	11	12
P_{atm} mm Hg	769.47	769.47	769.47	767.60	767.60
T_{atm} °F	74.2	74.2	74.2	82.4	82.4
Dew point temperature °F	13	13	13	15	15
$P_0 - P_x$ mm H_2O	53.65	53.65	164.73	97.32	142.56
P_0 mm H_2O, G	56.05	56.05	171.81	101.41	148.98
E_0 mV	4.689	4.689	4.893	5.150	5.012
E_G mV	4.678	4.678	4.876	5.136	4.997

t sec.		$-E_s$ mV			
5		4.373	4.527	4.652	4.528
10		3.976	3.858	4.087	3.885
15		3.595	3.287	2.581	3.316
20		3.245	3.755	3.138	2.793
25		2.910	2.374	2.714	2.320
30		2.597	1.821	2.314	1.912
35		2.298	1.425	1.929	1.502

APPENDIX 4C

Correction of Experimental Errors.

(a) Radiation error

The radiation heat addition to the test plate (at temperature T_S) from tunnel wall (at temperature T_G) in the present case is the intermediate between a small enclosed body and a large enclosed body. The emissivity of the test plate (polished Monel), ε_S, is 0.06 and that of the Cadmium-plated-steel tunnel-wall, ε_G, is 0.5 [4.17, pp. 472-478].

For a small enclosed body, the equation for the radiation-heat addition is:

$$q_{r,1} = \varepsilon_G \sigma (T_G^4 - T_S^4)$$

$$= 0.06 \, \sigma \, (T_G^4 - T_S^4) \qquad \ldots \qquad (4C.1);$$

whilst for a large enclosed body, it is:

$$q_{r,2} = \frac{\sigma (T_G^4 - T_S^4)}{(1/\varepsilon_G) + (1/\varepsilon_S) + 1}$$

$$= 0.0566 \, \sigma \, (T_G^4 - T_S^4) \qquad \ldots \qquad (4C.2).$$

The difference between Eqs. (4C.1) and (4C.2) is small, so the intermediate value of $q_{r,1}$ and $q_{r,2}$ can be used to estimate the radiation-heat addition, i.e.,

$$q_r = 0.058 \, \sigma (T_G^4 - T_S^4) \qquad \ldots \qquad (4C.3),$$

where the unit of q_r is in Btu/ft^{2}h, the unit of T is in $^\circ$R, the value of σ (Stefan Boltzman constant) is equal to 0.117×10^{-8}. The correction due to radiation by Eq. (4C.3) was made and its magnitude
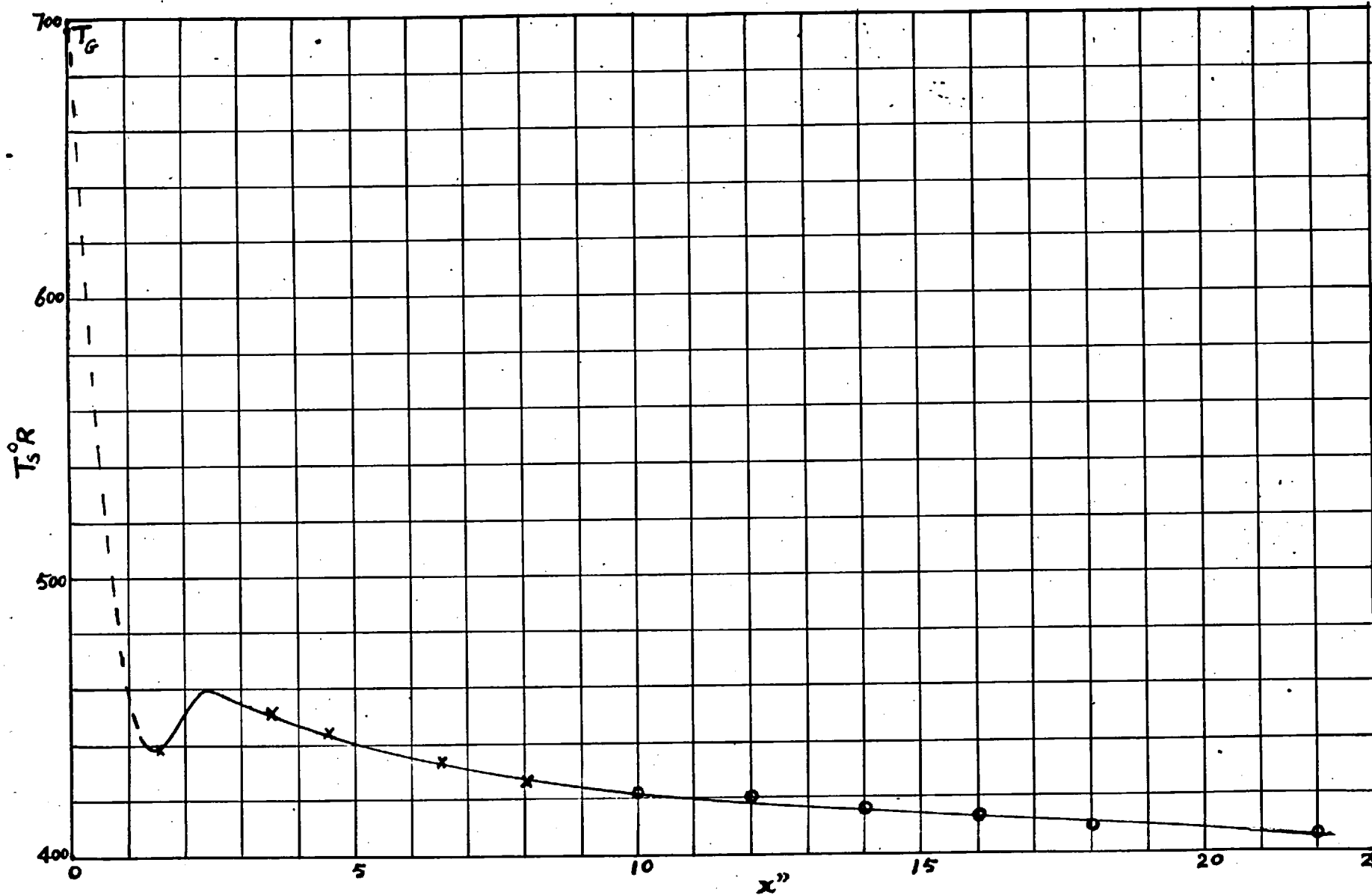
Fig. 4C.1 Typical wall temperature variation in x-direction. x, test 7, 40 sec.; o, test 6, 60 sec.

was found to be from 0.1 to 0.2%.

(b) Non-uniform wall-temperature correction.

Implicit in the calculation of the theoretical heat-transfer coefficient is the assumption that the wall is at a uniform temperature at each instant of time. That this is not the case is evident from the experimental temperature distribution shown in Fig. 4C.1. A theoretical relationship between heat-transfer coefficient on a flat plate with uniform wall temperature (St) and non-uniform wall temperature (St') was derived by Eckert et. al. [4.11, pp. 182-183]. For the turbulent flow, they used Seban's stepwise temperature variation formula and the method of superposition [4.11]. The result was:

$$St'/St = \left\{ \Delta T_0 + 0.991(\Delta T_n - \Delta T_0) + 0.117(\Delta x/x) \left[(2n-1) \Delta T_n - \Delta T_0 - 2(\Delta T_1 + \Delta T_2 + \Delta T_3 + \ldots + \Delta T_{n-1}) \right] \right\} / \Delta T_n$$

$$\ldots \quad (4C.4),$$

where ΔT is the difference between the wall and the mainstream temperatures, St' is the local Stanton number for non-uniform wall temperature and St is that for the uniform wall temperature, meanings of other symbols are shown in the following figure:
Eq. (4C.4) together with the experimental temperature distribution curves, e.g. Fig. 4C.1, was used to correct the error due to the wall temperature variation. The correction was found to be from 1 to 6% dependent mainly on the position (x).
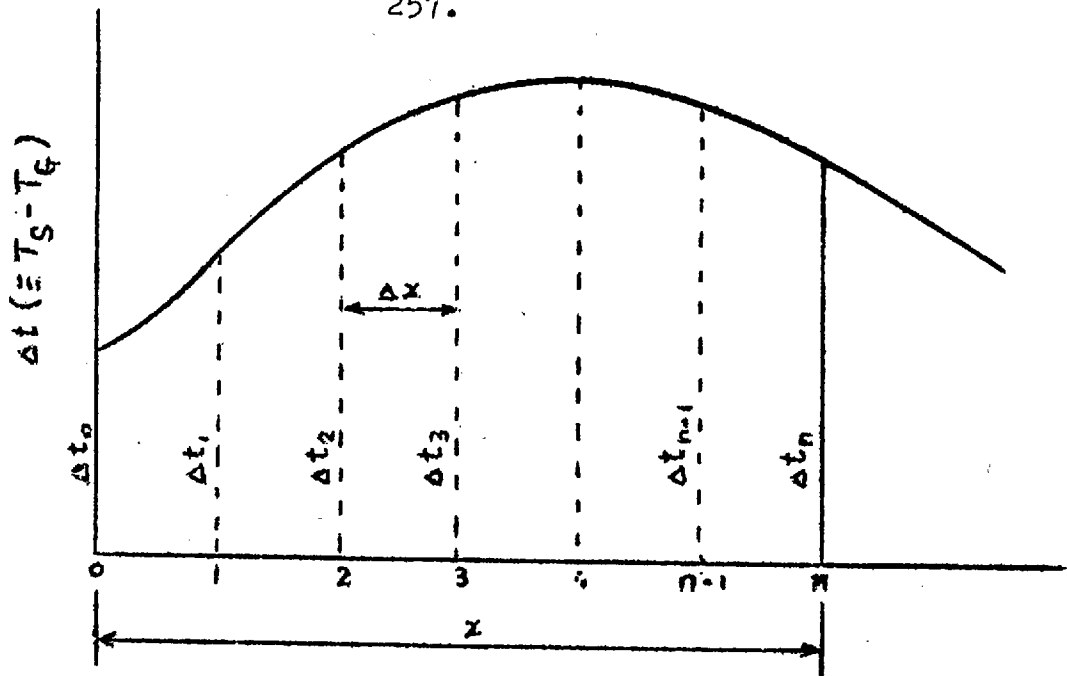
(c) Condensation Correction.

The formation of frost on the surface of a cooled plate
influences the heat transfer to the plate in two different ways,
namely; first, as the water vapour is tranferred toward the test
plate to form the frost, the latent heat of sublimation is added
to the plate; and second, the frost deposited on the surface
of the plate increases the effective thickness of the plate
and/or the roughness of the surface.

For the first named influence, its magnitude can be
predicted quite accurately, so a correction for this influence
will be made below. For the 2nd named influence, its magnitude
is less certain and its contribution to the uncertainty of the
measured Stanton number will be estimated in Appendix 4D.

The deposition of frost on the surface of a cooled plate
is a process of mass transfer. In an equilibrium state, the

258.

rate of frost formation depends on the mainstream dewpoint temperature and the plate surface temperature. Using the method of Ref. 4.18,

$$\dot{m}'' = gB \qquad \ldots \qquad (4C.5).$$

where $B \equiv m_{H_2O,G} - m_{H_2O,S}$, $g \equiv St/\rho_G u_G$, (the mass fractions of water vapour at the mainstream $(m_{H_2O,G})$ and at the surface $(m_{H_2O,S})$ corresponding to the mainstream dewpoint temperature and the surface temperature can be obtained from table 22 of Ref. 4.19, and the values of St and $\rho_G u_G$ are known), we can compute the rate of frost formation $(\dot{m}'')$.

Knowing the rate of frost formation $(\dot{m}'')$ from Eq. (4C.5) and the latent heat of sublimation (H) from Ref. 4.19, we can calculate the heat addition by the equation:

$$q_m = H.\dot{m}'' \qquad \ldots \qquad (4C.6).$$

Eqs. (4C.5) and (4C.6) were used to make correction for the frost formation. The magnitude of correction was about 0.1-0.2%.

Corrections (a), (b) and (c) described above have been made to the Stanton Number (St') of Table 4.4. The corrected Stanton numbers are entered into the Table 4.4 as St.

APPENDIX 4D

Estimation of Experimental Uncertainties.

Besides those errors described in Appendix 4C, there are further possible experimental errors whose magnitude cannot be accurately calculated. Those errors contribute to the uncertainty of the experimental data; their orders of magnitude are estimated below:

(a) Effective Reynolds number.

The Reynolds number (Re_x) in Table 4.4 has been based upon the distance from the leading edge of the plate. In Para. (iii) of §4.4.1, it was shown that the transition did not complete until Re_x got to about 1.2×10^5. Although the exact effective starting position from which the distance should be measured is not known; for the purpose of estimation, we assume that the transition started somewhere between the leading edge of the plate and the position of transition, say, at Reynolds number equal to $6 \times 10^4 (Re'_x)$. Hence at Re_x equal to 1×10^6, the effective Reynolds number would be about 9.4×10^5 $(=Re_x - Re'_x)$. As St is approximately proportional to $Re_x^{1/5}$, the uncertainty due to the unknown effective start of turbulence is about 1.2%.

(b) Temperature Potential.

The temperature potential $(T_G - T_S)$ was required to calculate the experimental St (Eq. 4.10), where T_G was measured by a total temperature probe placed at $x=12"$. In §4.3.3, it was pointed out that the accuracy of the measured mainstream total

temperature is $\pm 0.3^{\circ}$F;   in addition, the adiabatic wall

temperature instead of the total temperature should have been

used for calculating the Stanton number. At Mach number number

equal to 0.2, recovery factor being equal to 0.89 and T_G

equal to 600°R, the difference between the total temperature

and the adiabatic wall temperature is less than 0.5°F.;   so

the uncertainty in the temperature potential is about $\pm 0.8^{\circ}$F

which contributes to an error of about $\pm 1\%$ in St data.

(c) Temperature-time slope.

Care has been taken to measure the slope (dT/dt) accurately

by the method of "mirror and image";   an uncertainty of about 5% may

however still be present.

(d) Heat conduction.

The conduction has two components: they are the chord-wise

component and the x-component. For the former, it was found to

be negligible;   because we have placed the test-plate thermo-

couples in the centre-line of the plate or 1" away from the

centre-line (Fig. 4.3), and Fig. (4C.1) does not reveal the effect

of the chord-wise positions of the thermocouples on the value of

T. For the latter, the conduction can theoretically be calculated

from T vs x curves (e.g., Fig. 4C.1). The variation of T against

x in the turbulent region is, however, small (Fig. 4C.1);   and the

conduction is believed to be still smaller, because it is pro-
portional to the 2nd derivative of T vs x (i.e., d^2T/dx^2).
Hence, the error due to conduction is small in the present experi-

ments, say, it does not exceed 0.5%.

(e) <u>Frost Deposition.</u>

The heat addition to the plate due to latent heat of sublimation has been described in Appendix 4C. The effects of the increased effective thickness and roughness of the plate due to the frost are estimated below. For this purpose, the total frost deposited on unit area at time (t) is first calculated.

The method for calculating the frost formed on a unit surface area per unit time ($\dot{m}''$) has been described in Appendix 4C (Eq. 4C.5); the total frost deposited on the unit area at time t is then

$$m'' = \int_{0}^{t} \dot{m}'' dt \qquad \ldots \qquad (4D.1).$$

On the assumption that the frost deposited on the plate forms a smooth surface, part of the convective heat transferred to the surface is then absorbed by the frost instead of the plate. The ratio of the heat absorbed by the frost to the total convective heat (E_f) represents the possible error of the measured Stanton number and is expressible by the equation,

$$E_f = \frac{m'' c_i}{(\rho \tau c)_S + m'' c_i} \qquad \ldots \qquad (4D.2),$$

where m'' is calculated by Eq. (4D.1), c_i is the specific heat of ice and $(\rho \tau c)_S$ is the thermal capacity of the test plate per unit area. It was found that the average error represented by Eq. (4D.2) for the present experiments is only 0.02%.

Now, if we assume that the frost deposited to the surface of the plate is in the form of spheres at 10-spherical diameters apart, the relation between the spherical diameter (d) and m" can then be expressed by the equation:

$$d = 300 \, m''/(4 \pi \rho_i) \qquad \cdots \qquad (4D.3).$$

where ρ_i is the density of ice. The average value of d (by Eq. 4D.3) for the present experiments was found to be 4.5×10^{-5} ft.

Now, the average value of x and Re_x for the present experiments are 1 ft and 1×10^{6}, respectively. Hence the average roughness parameter ($\equiv d/x$) for the present experiments is 4.5×10^{-5} at Re_x equal to 1×10^{6}. In Ref. 4.20 [4.20, p.558], it is stated that the surface is aerodynamically smooth if d/x is less than 1×10^{-4} at Re_x equal to 1×10^{6}. The roughness effect of the frost formation is therefore negligible for the present experiments.

The total uncertainty accounted above amounts to about 7.7%; so the accuracy of the present data (St) is believed to be well within $\pm 10\%$.